Coastal and Hydraulics Laboratory

US Army Corps
of Engineers®
Engineer Research and
Development Center

Navigation Systems Research Program

Longshore Sediment Transport Rate Calculated Incorporating Wave Orbital Velocity Fluctuations

Ernest R. Smith   September 2006

Longshore Sediment Transport Rate Calculated Incorporating Wave Orbital Velocity Fluctuations

Ernest R. Smith

Coastal and Hydraulics Laboratory
U.S. Army Engineer Research and Development Center
3919 Halls Freey Road
Vicksburg, MS 39180-6199

Final report

Abstract: Laboratory experiments were performed to study and improve longshore sediment transport rate predictions. Measured total longshore transport in the laboratory was approximately three times greater for plunging breakers than spilling breakers. Three distinct zones of longshore transport were observed across the surf zone: incipient breaker zone, inner surf zone, and swash zone. Transport at incipient breaking was influenced by breaker type; inner surf zone transport was dominated by wave height, independent of wave period; and swash zone transport was dependent on wave period.

Selected predictive formulas to compute total load and distributed load transport were compared to laboratory and field data. Equations by Kamphuis (1991) and Madsen et al. (2003) gave consistent total sediment transport estimates for both laboratory and field data. Additionally, the CERC formula predicted measurements well if calibrated and applied to similar breaker types. Each of the distributed load models had shortcomings. The energetics model of Bodge and Dean (1987) was sensitive to fluctuations in energy dissipation and often predicted transport peaks that were not present in the data. The Watanabe (1992) equation, based on time-averaged bottom stress, predicted no transport at most laboratory locations. The Van Rijn (1993) model was comprehensive and required hydrodynamic, bedform, and sediment data. The model estimated the laboratory cross-shore distribution well, but greatly overestimated field transport.

Seven models were developed in this study based on the principle that transported sediment is mobilized by the total shear stress acting on the bottom and transported by the current at that location. Shear stress, including the turbulent component, was calculated from the wave orbital velocity. Models 1 through 3 gave good estimates of the transport distribution, but underpredicted the transport peak near the plunging wave breakpoint. A suspension term was included in Models 4 through 7, which improved estimates near breaking for plunging breakers. Models 4, 5, and 7 also compared well to the field measurements.

It was concluded that breaker type is an important variable in determining the amount of transport that occurs at a location. Lastly, inclusion of the turbulent component of the orbital velocity is vital in predictive sediment transport equations.

TABLE OF CONTENTS

LIST OF FIGURES

LIST OF TABLES

Preface

CHAPTER I

INTRODUCTION

Background

Longshore sediment transport is defined as the movement of sediment, which can be sand or other beach material such as gravel and shell, along the shore. Waves breaking at an oblique angle to the coast generate a current in the surf zone that flows parallel to the shore. Breaking waves and the longshore current they generate are capable of transporting hundreds of thousands of cubic meters of sand along the coast during a typical year. Gradients in longshore sediment transport play a dominant role in the long-term response of a shoreline to waves and currents, particularly at engineering structures. Significant erosion or accretion can be caused by disruption of longshore sediment transport, producing gradients in the transport rate. A portion of the sediment transported by the longshore current also is deposited in navigation channels issuing from coastal inlets and harbor entrances.

Accurate prediction of the total longshore sediment transport rate is central to many coastal engineering studies. Examples of practical engineering applications include beach response in the vicinity of coastal structures, beach fill evolution and renourishment requirements, and sedimentation rates in navigation channels.

This dissertation follows the style and format of Coastal Engineering

Additionally, knowledge of the cross-shore distribution of longshore sediment transport in the surf zone is necessary in the design and planning of groins, jetties, weirs and pipeline landfalls. Accurate estimates of the longshore sediment transport distribution aids in understanding spit development, migration of sediments, natural or artificial, and the development of other coastal morphologic features.

To maintain navigable waterways along the coasts of the United States, engineers and scientists routinely apply analytical and numerical models to estimate the total longshore sediment transport rate. Engineers require both the total longshore transport rate and the cross-shore distribution of the longshore transport rate for project planning and the development of predictive numerical simulation models. Despite many studies that have been performed worldwide to develop accurate estimates for the longshore sediment transport rate, this field is still deficient in adequate quantitative predictive capabilities.

Description of Processes

It has been generally accepted that, in the surf zone, waves are the primary mechanism for mobilizing sediment, and the wave-induced quasi-steady longshore current is the primary mechanism for transport of this sediment. For this research, longshore sediment transport generated by wave-driven currents is considered, although wind, tide, and other forcing mechanisms also may drive currents that will move sediment alongshore. Almost all longshore sediment transport occurs in the surf zone

because of the great intensity of turbulence generated by breaking and broken waves. The surf zone can be divided into three zones: the breaker zone, inner surf zone, and swash zone.

The breaker zone is characterized by waves, which have shoaled from offshore, becoming unstable, and dissipating their energy through breaking. Turbulence from breaking waves contributes greatly to mobilizing sand, which can be transported by any current. Breaker height is defined as the vertical distance between the wave crest and the preceding wave trough at incipient breaking, and it is controlled by wave period, water depth, and local bottom slope (Weggel 1972; Smith and Kraus 1991). In addition, the manner in which waves break, i.e., the breaker type, has been found to be controlled by wave height, period, water depth, and local beach slope (Galvin 1968; Battjes 1974). Numerous laboratory and field studies have found that suspended sediment concentration at the breaker line is strongly influenced by breaker type (e.g., Kana 1977; Van Rijn 1993). Four types of breakers have been distinguished largely based on visual observations (Patrick and Wiegel 1957; Galvin 1968; Dean and Dalrymple 1991; Komar 1998); spilling, plunging, surging, and collapsing. Galvin (1968) defined the following terminology; spilling breakers occur if the wave crest becomes unstable and flows down the front face of the wave producing a foamy water surface; plunging breakers occur if the crest curls over the front face and falls into the base of the wave, resulting in a high splash; collapsing breakers occur if the crest remains unbroken while the lower part of the front face steepens and then falls, producing an irregular turbulent water surface; surging breakers occur if the crest remains unbroken and the front face of the wave

advances up the beach with minor breaking. Spilling and plunging breakers are more common at incipient breaking. Sediment concentrations measured under plunging breakers are significantly greater than concentrations measured under spilling breakers of similar wave height (Kana 1977; Wang et al. 2002). Because longshore sediment flux is the product of sediment concentration and longshore current velocity, greater concentration would result in greater sediment transport given similar longshore current velocities.

Broken waves continue to decay in height through the inner surf zone, and turbulence is primarily contained in a surface roller. Research has shown that wave height through the surf zone decays linearly with water depth (Battjes and Janssen 1978; Dally et al. 1984). In the swash zone, waves run up and down the foreshore slope in a thin turbulent water layer. In most predictive models of longshore sediment transport, the swash transport contribution is either ignored or merely accounted for as part of the total sediment transport budget (Van Wellen et al. 2000). However, significant swash zone transport rates have been observed in the field (Sawaragi and Deguchi 1978; Kraus et al. 1982; Bodge and Dean 1987), and swash zone transport can account for up to 50 percent of the total longshore transport (Elfrink and Baldock 2002). Little research has been conducted on longshore currents in the swash zone because of the difficulty of obtaining reliable measurements. Recent methods have allowed accurate swash zone velocity measurements (Puleo et al. 2000), but data are limited. Swash zone velocity is influenced by wave runup, which has been studied historically and is better understood

(Ahrens and Titus 1985; Hughes 2004). Runup is successfully parameterized in terms of wave height, period, and foreshore slope.

Nearshore hydrodynamics of wave breaking, decay through the surf zone, and runup are understood and can be modeled reasonably well. Additionally, models have been developed that estimate longshore currents sufficiently (e.g., Kraus and Larson 1991; Putrevu and Svendsen 1999; Johnson 2003) for engineering applications. However, methods to predict the longshore sediment transport rate have not been as successful. Although breaking waves are responsible both for driving currents and mobilizing sand, their effect on hydrodynamics and sediment transport are not the same. Improved understanding of how waves mobilize sand is necessary in the development of predictive equations for the cross-shore distribution of the longshore sediment transport rate.

Longshore Transport Data Collection Methods

One of the challenges in predicting the longshore sediment transport rate is the difficulty in obtaining accurate data. Present predictive tools have largely been developed based on field studies (e.g. Watts 1953; Komar and Inman 1970; Inman et al. 1980; Kraus et al. 1982; Bodge and Dean 1987; Dean 1989; Schoonees and Theron 1993; Wang et al. 1998; Wang 1998). Fluorescent-dyed sand distributed across the surf zone can measure the short-term (order of hours) longshore sand transport rate (Komar and Inman 1970), and deployment of as many as four sand tracer colors in distinct

regions of the surf zone can reveal information on the cross-shore distribution of the longshore sand transport rate (Kraus et al. 1982).

Total longshore transport in the field often is estimated indirectly by impoundment of sand at a jetty, breakwater or groin, or by deposition of sand in an inlet or harbor. Measurement accuracy is a function of the coastal structure's efficiency at trapping the sediment, and this method sometimes produces a long-term average by integrating over many wave and water level conditions that occur over weeks, months, and years, depending on the surveys made (Johnson 1952; Bruno and Gable 1976; Bruno et al. 1980; Dean et al. 1982). More recent experiments have focused on short-term impoundment methods (Bodge and Dean 1987; Wang and Kraus 1999). Sand bypassing is not accounted for in surveys and dredging records, which may lead to an under estimate of longshore transport. Conversely, deposition may occur from other sources, i.e., bi-directional transport, resulting in an overestimate of transport.

Another method to estimate a local longshore sediment transport in the field is the use of Optical Backscatter Sensors (OBS) in conjunction with a current meter (Downing et al. 1981). The instrument records backscattered light, and requires calibration to the native sediment to estimate sediment concentration. The product of the concentration and longshore current gives an estimate of longshore sediment transport rate. Concentration estimates from an OBS are made at a point; therefore, several OBS's placed vertically would be required to obtain accurate estimates of transport over the entire water column. Additionally, an OBS measures only suspended sediment concentration, i.e., bedload transport is omitted. Operational concerns with OBS are

adequate calibration with the in-situ sediment and changing light conditions between direct sunshine and passage of clouds.

Sand traps of various types have also been deployed across the surf zone to obtain instantaneous measurements of the sediment flux in the water column (Kana 1976) or integrated flux over several minutes (Kraus 1987; Kraus and Dean 1987; Wang et al. 1998; Wang 1998). Manual deployment of traps limits operational wave height to less than about 1 m.

Wave data necessary to correlate with measured impoundments are usually lacking or limited in field data collection, and the extremely dynamic and non-repeatable nature of the surf zone can introduce considerable uncertainties in field measurements (Wang and Kraus 1999). The non-controllable nature of field conditions increases the difficulties of isolating and examining the contributions of, and interactions among, individual parameters.

In contrast to field measurements, laboratory studies are controllable and repeatable, allowing contributions of individual parameters to be isolated. The convenience of laboratory instrumentation enables precise measurement of many parameters such as wave height, current velocity, sediment concentration, and their spatial and temporal distribution patterns. The main difficulties of laboratory studies have historically been their substantially reduced temporal and spatial scales and their unproven capability for replicating field conditions.

Laboratory data have not been broadly incorporated in the calibration of longshore sediment transport formulas because typically small scales are involved. Scaling

distortion enters in at least three ways for small scale and even mid-scale lab
experiments: (1) the flows may only seldom exceed the critical threshold for sediment
motion, (2) the suspended sediment concentration may not approach that generated
under large waves and turbulence in the field, including possible saturation of maximum
possible concentration, and (3) bed load transport may occur more as saltation, rather
than sheet flow, and form ripples, which rarely appear in the surf zone in the field.

Despite the shortcomings associated with both field and laboratory data collection,
each provides value to the understanding of longshore sediment processes.
Improvements to sediment transport relationships should result from the complimentary
aspects of both field and laboratory data with an understanding of the limitations of each.

Purpose of Study and Approach

The objective of this research is to develop and verify an improved method to
determine the cross-shore distribution of the longshore sediment (sand) transport rate
and its integral quantity – the total longshore sediment transport rate. It is anticipated
that if the cross-shore distribution of longshore sediment transport can be reliably
predicted, the total transport rate can be obtained by integrating the transport rate
through the cross-shore.

Based on the findings of Kamphuis (2002), mid-scale laboratory experiments were
performed to measure the longshore sediment transport and nearshore hydrodynamics in
a controlled environment. Mid-scale denotes wave and current conditions that can be

found commonly on some coasts in the field, such as the Gulf of Mexico (for example, west coast of Florida) and in the Great Lakes. "Mid-scale" contrasts with much smaller wave heights and shorter wave periods normally available in three-dimensional laboratory basin facilities. For example, mid-scale wave height and period might be on order of 0.25 m and 3-sec, respectively, as opposed to small-scale laboratory conditions on the order of 0.1-m wave height and 1-sec wave period. Because wave energy is proportional to the square of wave height and energy flux to the 5/2 power of wave height, more than doubling the wave height capable in mid-scale experiments as compared to traditional small-scale laboratory experiments greatly increases mean energy and associated turbulence in the surf zone.

The magnitude of longshore sediment transport can vary significantly by breaker type. Therefore, experiments performed in the present study were designed to include spilling and plunging breaker types of similar incident wave energy. Results of the experiments are compared to commonly applied prediction methods, and a new approach is developed for calculating the local longshore sand transport rate. In addition to laboratory data, field measurements are incorporated in testing of selected existing longshore transport predictors and in development of new transport rate relationships.

CHAPTER II

PRESENT ENGINEERING PREDICTION METHODS

Introduction

Many studies have been conducted to relate the total longshore sediment transport rate to wave and current processes for the purpose of developing predictive capability in terms of variables that are relatively easy to measure or hindcast. This chapter reviews selected predictive equations for the total load longshore transport rate and cross-shore distribution of longshore transport. Total, or bulk, load transport refers to the total amount of sediment transported along the coast in the surf zone. Distributed transport refers to the cross-shore distribution of longshore transport with a varying local rate at different locations across the surf zone.

Total Transport Equations

The most widely used model for estimating total longshore sediment transport rate is the "CERC" formula (Shore Protection Manual (SPM), 1984). The original form of the equation was derived from laboratory data of Krumbein (1944) and field data of Watts (1953) and Caldwell (1956):

$$I_y = KP_y \qquad (2\text{-}1)$$

where I_y is the immersed weight transport rate (force/time), K is a dimensional

coefficient, and

$$P_y = EC_g \sin\theta \cos\theta \qquad (2\text{-}2)$$

in which θ is the angle between the wave crest and shoreline, E is the average wave

energy per unit surface area and C_g is the wave group celerity. Average wave energy per

unit surface area is defined as

$$E = \frac{\rho g H^2}{8} \qquad (2\text{-}3)$$

where ρ is fluid density, g is acceleration due to gravity, and H is a statistical wave

height. Wave group celerity is the velocity at which waves carry energy, which is

related to the wave celerity, the velocity of an individual wave, by

$$C_g = nC \qquad (2\text{-}4)$$

in which C is the wave celerity, defined as the ratio of wavelength, L, to wave period, T,

and n is given as

$$n = \frac{1}{2}\left(1 + \frac{2kh}{\sinh(2kh)}\right) \qquad (2\text{-}5)$$

where h is water depth and k is the wave number defined as

$$k = \frac{2\pi}{L} \qquad (2\text{-}6)$$

In linear wave theory, wavelength is given by

$$L = \frac{gT^2}{2\pi}\tanh\frac{2\pi h}{L} \qquad (2\text{-}7)$$

In shallow water, such as in the surf zone, $n = 1$; therefore, Equations 2-4 and 2-7 result in

$$C_g = C = \sqrt{gh} \qquad (2\text{-}8)$$

Longshore sediment transport is normally calculated using the wave height at the wave breakpoint, and Equation 2-1 can be re-written in the form

$$I_y = \frac{K}{16\sqrt{\gamma_b}} \rho g^{\frac{3}{2}} H_b^{\frac{5}{2}} \sin(2\theta_b) \qquad (2\text{-}9)$$

in which the subscript b indicates quantities evaluated at breaking, γ_b is the breaker index (the ratio of breaking wave height, H_b to water depth at breaking, h_b, typically taken to have the value $\gamma_b = 0.78$), and K is a dimensionless coefficient. Equation 2-9 is known as the CERC formula in engineering applications. The CERC formula can be expressed as a volumetric rate:

$$Q_y = \frac{I_y}{(\rho_s - \rho) ga'} \qquad (2\text{-}10)$$

where ρ_s is the density of sediment, and a' is the ratio of volume of solids to total volume.

The coefficient K was originally determined to be 0.42 using the root-mean-square wave height, H_{rms}, in Equation 2-9 (USACE 1966). Data analyzed for the calibration included the aforementioned data of Krumbein (1944), Watts (1953) and Caldwell (1956), and additional laboratory data of Saville (1950), Shay and Johnson (1951), Sauvage de Saint Marc and Vincent (1954), and Savage (1962). A subsequent calibration excluded all laboratory data and was performed with the field data of Watts

(1953) and Caldwell (1956) and additional field data of Komar and Inman (1970). The re-calibration gave $K = 0.77$, also based on H_{rmsb}, and is presently the recommended value of the Shore Protection Manual (SPM) (1984) and Coastal Engineering Manual (CEM) (2002). The SPM recommends a K-value of 0.39 if significant breaker height, H_{sb}, is used in Equation 2-9.

Although recommended K-values are provided in the SPM and CEM, Equation 2-9 is best applied if the coefficient is calibrated using historical data for a particular site. For design applications with adequate field measurements, the CERC formula can be applied to estimate total longshore sediment transport rates with reasonable confidence (± 50 percent). However, many sites do not have historical data available to calibrate K, and the CERC formula provides only order-of-magnitude accuracy.

One shortcoming of the CERC formula is that it has no dependence on wave period. Miller (1999) measured longshore transport rates during storms, and compared the measured rates to CERC formula predictions. Miller found the CERC formula sometimes over and sometimes under predicted longshore transport rate. Miller suggests that additional terms are required for an accurate prediction of longshore sediment transport rates for storm conditions. As part of the present study, Wang et al. (2002) examined laboratory transport rates of waves having similar wave heights, but differing breaker types. The difference in transport rate between spilling and plunging waves was nearly a factor of three. The CERC formula over-predicted both cases – by 700 percent for spilling waves, and by 250 percent for plunging waves. They also stated that the total rate of longshore sediment transport based solely on longshore wave-energy flux

might not be complete. Other shortcomings of the CERC formula are that it has no

grain-size dependence and gives only the bulk transport rate. It should be thought of as

pertaining to typical sand grain sizes in the approximate range of 0.2 to 0.4 mm. On the

other hand, the CERC formula requires a minimum amount of data – namely wave

height and wave direction, and so it is convenient for engineering studies.

Inman and Bagnold (1963) gave an alternative to the CERC formula based on the

energetics approach presented by Bagnold (1963), which is discussed in the Distributed

Transport Equations section. Inman and Bagnold related the longshore sediment

transport rate to the longshore current:

$$I_y = K'(EC_g)_b \left(\frac{\cos\theta}{u_{mb}} \right) V_l \tag{2-11}$$

where K' is a dimensionless coefficient, V_l is the mean longshore current velocity near

the mid-surf position, and u_{mb} is the maximum horizontal orbital velocity of the waves

evaluated at the breaker zone. Komar and Inman (1970) determined $K' = 0.28$ from sand

tracer experiments. Later, Kraus et al. (1982) performed sand tracer experiments and

determined a value $K' = 0.21$.

Equation 2-11 can be simplified by assuming shallow-water conditions. The root-

mean-square horizontal wave orbital velocity from linear theory is

$$u_{rms} = \frac{H_{rms}\sigma}{2} \frac{\cosh k(h+z)}{\sinh kh} \cos(kx - \sigma t) \tag{2-12}$$

where z is elevation from the free water surface (positive upward), x is cross-shore

position, and σ is the angular frequency:

$$\sigma = \frac{2\pi}{T} \tag{2-13}$$

The maximum values of u_{rms} occur under the crest and trough at phase positions $(kx - \sigma t) = 0$, π, etc. At breaking, and using the shallow water assumption, maximum horizontal orbital velocity becomes

$$u_{mb} = \frac{1}{2}\frac{H_b}{h_b}\sqrt{gh_b} = \frac{1}{2}\gamma_b C_{gb} \tag{2-14}$$

Breaker index is a function of incident wave height, wave period, and beach slope (Weggel 1972, Smith and Kraus 1991, Rattanapitikon and Shibayama 2000); however it often is assumed as either unity or the theoretical value of a solitary wave on a horizontal bottom, $\gamma_b = 0.78$ (McCowan 1891). Assuming the waves are Rayleigh-distributed, significant wave height, H_s is related to H_{rms} by

$$H_s = \sqrt{2}H_{rms} \tag{2-15}$$

Therefore, substituting Equations 2-14 and 2-15 into Equation 11 results in

$$I_y = 0.026\rho\, gH_{sb}^2 V_l \tag{2-16}$$

if $K' = 0.21$

Based on their laboratory study, Kamphuis and Readshaw (1978) found that the accuracy of the recommended CERC formula K-value depended on breaker type. Kamphuis and Readshaw used the Iribarren number (commonly known as the surf similarity parameter) to determine breaker type. The Iribarren number is given as:

$$\xi_b = \frac{m}{\sqrt{\dfrac{H_{sb}}{L_o}}} \tag{2-17}$$

where ξ_b is the Iribarren number at wave breaking, m is beach slope, and L_o is deepwater wavelength. Kamphuis and Readshaw found that:

$$K = 0.7\xi_b \tag{2-18}$$

Battjes (1974) reanalyzed the work of Galvin (1968) and determined that spilling breakers occurred for $\xi_b < 0.4$ and plunging breakers occurred for $0.4 < \xi_b < 2.0$. According to Equation 2-18, $K = 0.39$ would only be valid for Iribarren numbers associated with plunging breakers, and K-values for spilling breakers would be less.

Bailard and Inman (1981) and Bailard (1984) developed an energy-based model that determines the CERC K as a function of breaker angle and the ratio of wave orbital velocity magnitude to sediment fall speed, and based on H_{rmsb}. The model of Bailard (1984) was calibrated using field and laboratory data and is similar to a relationship developed based on limited laboratory data by Walton (1979) and Walton and Chiu (1979). The Bailard equation is given as:

$$K = 0.05 + 2.6\sin^2(2\theta_b) + 0.007\frac{u_{mb}}{w_f} \tag{2-19}$$

where w_f is the fall speed of the sediment. The relationship was developed based on sand fall speeds ranging between 0.025 and 0.205 m/s, breaker angles ranging between 0.2 and 15 deg, and u_{mb} ranging between 0.33 and 2.83 m/s.

Ozhan (1982) performed a laboratory study and found that the CERC formula K was a function of wave steepness (ratio of wave height and wavelength) in deep water:

$$K \cong \frac{0.007}{\left(\dfrac{H_o'}{L_o}\right)} \tag{2-20}$$

where $H_o^{'}$ is the unrefracted deepwater wave height. Ozhan's findings support the observations of Saville (1950). Saville found that for waves of identical energy levels, greater longshore transport rates occurred in his laboratory experiments for lower steepness waves (longer periods).

Kamphuis et al. (1986) developed an empirical formula from field data similar to that used to develop the CERC formula. In addition to breaker height and angle, the Kamphuis et al. equation included beach slope and sediment grain size. The equation for SI units and saltwater yields longshore transport in kg/s and is given as:

$$Q_y = 1.28 \frac{H_{sb}^{3.5} m}{d_{50}} \sin(2\theta_b) \qquad (2\text{-}21)$$

where d_{50} is median sediment grain size expressed in meters.

After reanalysis of existing field data and collection of data from a comprehensive series of small-scale laboratory experiments, Kamphuis (1991) modified the 1986 equation by including wave period. The modified equation for SI units and saltwater becomes:

$$Q_y = 2.27 H_{sb}^2 T_p^{1.5} m^{0.75} d_{50}^{-0.25} \sin^{0.6}(2\theta_b) \qquad (2\text{-}22)$$

where T_p is wave period and d_{50} is again expressed in meters and Q_y in kg/s. Wave height in the Kamphuis (1991) laboratory tests ranged from $H_s = 0.05$ to 0.14 m. The smallest waves encountered in field measurements are much higher than the highest waves in the laboratory measurements, and the applicability of the predictive relations to field conditions has been questioned. Wang et al. (1998) found that the Kamphuis (1991) formula predicted consistently lower total longshore transport rates than those

predicted by the CERC formula. Also, Miller (1998) found that the Kamphuis model

gave predictions an order of magnitude lower than the CERC formula for storm

conditions with breaker height of nearly 4 m.

However, Schoones and Theron (1996) ranked 52 longshore transport equations

according to predictive performance against a large data assemblage and found the most

accurate to be the Kamphuis (1991) formula. Schoones and Theron also recalibrated the

equation with the following guidance for its use:

$$Q_y = 3.51 H_{sb}^2 T_p^{1.5} m^{0.75} d_{50}^{-0.25} \sin^{0.6}(2\theta_b) \qquad (2\text{-}23)$$

if H_{sb} normally exceeds 0.3 m and $d_{50} < 1$ mm. If a site has calm wave conditions or has

coarse sediment, the following equation was recommended:

$$Q_y = 2.77 H_{sb}^2 T_p^{1.5} m^{0.75} d_{50}^{-0.25} \sin^{0.6}(2\theta_b) \qquad (2\text{-}24)$$

Kraus et al. (1988) assumed that the total rate of longshore sediment transport in the

surf zone is proportional to the longshore discharge of water:

$$Q \propto K_d(R - R_c) \qquad (2\text{-}25)$$

where K_d is an empirical coefficient that may relate to sediment suspension, R_c a

threshold value for significant longshore sand transport, and R a discharge parameter is

proportional to the average discharge of water moving alongshore:

$$R = V_l X_b H_{sb} \qquad (2\text{-}26)$$

in which X_b is surf zone width and V_l is the mean longshore current velocity in the surf

zone. Based on their field data collected using streamer sediment traps at Duck, North

Carolina, Kraus et al. (1988) suggested $K_d = 2.7$ and $R_c = 3.9$ m^3/s.

del Valle et al. (1993) developed an empirically based relationship for K, which also shows decreasing values of K with larger grain sizes. The equation was based on data presented by Komar (1988) and data obtained from the Adra River Delta, Spain. The equation, applied with H_{rmsb} is given as:

$$K = 1.4e^{(-2.5d_{50})} \tag{2-27}$$

in which d_{50} is expressed in mm. The relationship is based on limited data and is strongly dependent on the relatively larger median sand grain sizes from the Adra River Delta, ($d_{50} = 0.44$ to 1.5 mm).

Madsen et al. (2003) presented an order of magnitude equation to compute total load longshore sediment transport. The equation was based on physically realistic, but simple, numerical models of surf zone hydrodynamic and sediment transport processes. Madsen et al. derived expressions for these processes, which resulted in the equation:

$$I_y = \left(\frac{\rho_s}{\rho} - 1 \right) \rho g Q_y = K_B P_y + K_s P_y^{3/2} \tag{2-28}$$

where K_B and K_S are constants of proportionality for bed load and suspended load transport, respectively. Using representative values for various coefficients, Madsen et al. found $K_B = 0.16$ and $K_S = 0.08$ $(N/s)^{-1/2}$ for a quartz sand of $d_{50} = 0.18$ mm. The equation agreed well to laboratory and field data. Madsen et al. stated that it appears justified to accept with confidence the qualitative features of the formula, but it is premature to accept the quantitative validity of the equation based on comparison to the single sediment grain size. It is interesting to note that the suspended transport term is

raised to the 3/2-power, which indicates that suspended load transport becomes increasingly important during storm conditions.

Distributed Transport Equations

Several models, with varying degrees of complexity, have been developed to predict the cross-shore distribution of longshore transport. Bodge (1989) noted that the majority of existing models shared a central concept of a mechanism that mobilizes sediment and a longshore current that transports the sediment. The models generally fall into one of two categories; "energetics" models, which assume the mobilizing mechanism is a function of wave energy dissipation, and "stress" models, in which shear stress exerted on the bottom by waves and currents mobilize sediment. This section provides a summary of pertinent cross-shore distribution of longshore transport studies.

Bagnold (1963) proposed that wave orbital motion mobilizes beach sand and expended wave power maintains sand in motion, while a mean longshore current transports the sand. Bagnold suggested a suspended and bedload model written as:

$$i_y = k_B \frac{d}{dx}\left(EC_g\right)\frac{V}{u_o} \tag{2-29}$$

where i_y is the local immersed weight sediment transport rate per unit offshore length, k_B is a dimensionless constant, u_o is the near-bottom wave orbital velocity, V is the mean local longshore current, and the x-axis is directed offshore.

Bijker (1967) was among the first investigators to develop a longshore transport model based upon river-borne sediment transport studies. This formula is significant in

the literature because it is the first to consider micro-scale processes, such as the shear

stress exerted by waves, and the combined wave and current shear stress, in a practical

coastal engineering formula. Bijker modified the Kalinske-Frijlink formula (Frijlink

1952) to compute a bedload component, which was combined with a suspended load

component calculated using the method of Einstein (1950). Volumetric bed load

transport, q_{yb} in units of m^3/s/m, is calculated from:

$$q_{yb} = Ad_{50} \frac{V}{C} \sqrt{g} \, \exp\left[\frac{-0.27\left(\frac{\rho_s}{\rho}-1\right)d_{50}\rho g}{\mu\tau_{b,wc}}\right]$$

(2-30)

where A is an empirical coefficient (1.0 for non-breaking waves, and 5.0 for breaking

waves), C the Chezy coefficient based on d_{50}, μ a ripple factor, and $\tau_{b,wc}$ the bottom

shear stress due to waves and currents. The first part of the expression represents a

transport parameter, and the exponent is a stirring parameter. The influence of the form

of the bottom roughness on bed load transport is indicated in the ripple factor defined as:

$$\mu = \left(\frac{C}{C_{90}}\right)^{1.5}$$

(2-31)

where C_{90} is the Chezy coefficient based on d_{90}, which is the sediment particle diameter

exceeded by 10 percent of the distribution by weight. The combined shear stress at the

bed induced by waves and currents is:

$$\tau_{b,wc} = \tau_{b,c}\left[1+\frac{1}{2}\left(\xi\frac{u_o}{V}\right)^2\right]$$

(2-32)

in which $\tau_{b,c}$ is the bed shear stress de to current only, and the coefficient ξ is defined as:

$$\xi = C\sqrt{\frac{f_w}{2g}} \qquad (2\text{-}33)$$

where f_w is the wave friction factor (Jonsson 1966).

Bijker (1967) assumed that the bedload transport occurred in a bottom layer having a thickness equal to the bottom roughness, r. The concentration of material in the bed load layer, c_b was assumed to be constant over the thickness and was defined as:

$$c_b = \frac{q_b}{6.34\sqrt{\frac{\tau_{b,c}}{\rho}}r} \qquad (2\text{-}34)$$

The concentration distribution for the suspended load is obtained by:

$$c(z) = c_b \left[\frac{r}{h-r}\frac{h-z}{z} \right]^{\frac{w_f\sqrt{\rho}}{\kappa\sqrt{\tau_{b,wc}}}} \qquad (2\text{-}35)$$

where z is elevation, w_f the sediment fall speed, and κ the von Karman constant. The total volumetric suspended sediment load, q_{ys}, is determined by integrating vertically from the reference height to the water surface:

$$q_{ys} = 1.83 q_{yb}\left[I_1 \ln\left(\frac{33h}{r}\right) + I_2 \right] \qquad (2\text{-}36)$$

where I_1 and I_2 are Einstein integrals. The total local volumetric sediment transport rate, q_y, is computed by:

$$q_y = q_{yb} + q_{ys} \qquad (2\text{-}37)$$

Komar (1971, 1975, 1977) determined that local longshore transport is related to the product of breaking wave related stress and longshore current. The model, often called a stress model, is given is:

$$i_y = \frac{\pi k_1 f_b}{8} \rho g \kappa^2 h V \qquad (2\text{-}38)$$

where k_1 is a proportionality constant, and f_b is a bed drag coefficient for wave motions.

For the case where the stress exerted on the bed by the longshore current also contributes

as a sediment mobilizing factor, Komar gave:

$$i_y = k_2 V \left(\rho C_f V^2 + \frac{\rho g f_b}{8} \kappa^2 h \right) \qquad (2\text{-}39)$$

in which k_2 is a proportionality constant, and C_f is a frictional drag coefficient for

longshore current.

   Madsen (1978) developed a distributed longshore transport model based on an

experimentally verified expression for sediment transport under oscillatory flow after

Brown (1950), Einstein (1972), and Madsen and Grant (1976):

$$\vec{\phi}(t) = 40\vec{\psi}^3(t) \qquad (2\text{-}40)$$

where $\vec{\phi}(t)$ is the non-dimensional transport function and $\vec{\psi}(t)$ is the Shields parameter

and the over arrow denotes a vector quality. The terms are defined as:

$$\vec{\phi}(t) = \frac{\vec{q}(t)}{w_f d} \qquad (2\text{-}41)$$

and

$$\vec{\psi}(t) = \frac{\vec{\tau}_b(t)}{g(\rho_s - \rho)d} \qquad (2\text{-}42)$$

where $\vec{q}(t)$ is the instantaneous volumetric sediment transport rate per unit width, d is the

grain size, and $\vec{\tau}_b(t)$ is the instantaneous bottom shear stress given by:

$$\vec{\tau}_b(t) = \frac{1}{2}\rho C_{f,wc}\left|\vec{u}_w(t)+\vec{V}\right|\left[\vec{u}_w(t)+\vec{V}\right] \qquad (2\text{-}43)$$

where $\vec{u}_w$ is the unsteady velocity associated with waves, and $\vec{V}$ is the steady velocity

associated with longshore current, $C_{f,wc}$ is a bed friction factor due to combined waves

and currents. Using linear shallow water wave theory and time averaging in the

longshore direction, Madsen found the local volumetric longshore transport rates as:

$$q_y = 8.5\frac{w_f}{d^2}\left(\frac{C_{f,wc}}{g\left(\frac{\rho_s}{\rho}-1\right)}\right)^3 u_o V \qquad (2\text{-}44)$$

Walton and Chiu (1979) gave the following expression for calculated distributed

longshore sediment transport:

$$q_y = K_w P_l X(x) \qquad (2\text{-}45)$$

where K_w is a dimensionless constant, and P_l is calculated from Equation 2-2. The

variable $X(x)$ is a local modifying function specifying the bedload and suspended load

components of transport independently as functions of the longshore current and water

depth; however, selection of the separate bedload and suspended load components is not

straightforward.

Bailard and Inman (1981) extended the Bagnold (1963) equation to oscillatory flow

combined with a steady current over a plane-sloping bottom. The instantaneous bed

load transport rate vector, $\vec{q}_b(t)$, is expressed as:

$$\vec{q}_{yb}(t) = \frac{0.5 C_{f,w}\rho e_b}{(\rho_s - \rho) g \tan\gamma}\left[\left|\vec{U}(t)\right|^2 \vec{U}(t) - \frac{\tan\beta}{\tan\gamma}\left|\vec{U}(t)\right|^3 i_\beta\right] \qquad (2\text{-}46)$$

and the instantaneous suspended load transport rate vector, $\vec{q}_s(t)$, is given as:

$$\vec{q}_{ys}(t) = \frac{0.5 C_{f,w} \rho e_s}{(\rho_s - \rho) g w_s \left[\left| \vec{U}(t) \right|^3 \vec{U}(t) - \frac{e_s}{w_s} \tan\beta \left| \vec{U}(t) \right|^5 i_\beta \right]}$$

(2-47)

in which $\tan\beta$ is the local bottom slope, $\tan\gamma$ is a dynamic friction factor, U_t' is the

instantaneous velocity vector near the bed for combined waves and currents, i_β is a unit

vector in the direction of the bed slope, and e_b and e_s are efficiency factors. The total

transport rate and direction containing the contributions of both the wave and current

related contributions can be obtained by averaging Equations 2-46 and 2-47 over a wave

period.

Assuming that a weak longshore current prevails and neglecting effects of the slope

term on the total transport rate for near-normal incident waves, Bailard (1984) found that

the local time-averaged longshore transport rate of Bailard and Inman (1981) can be

written as:

$$\begin{aligned}
q_y &= 0.5 \rho f_b u_o^3 \frac{e_b}{(\rho_s - \rho) g \tan\gamma} \left(\frac{\delta_v}{2} + \delta_v^3 \right) \\
&\quad + 0.5 \rho f_b u_o^4 \frac{e_s}{(\rho_s - \rho) g w_f} \left(\delta_v u_3^* \right)
\end{aligned}$$

(2-48)

where:

$$\delta_v = \frac{V}{u_o}$$

(2-49)

and

$$u_3^* = \frac{\left\langle \left| \vec{U}(t) \right|^3 \right\rangle}{u_o} \tag{2-50}$$

Bailard (1984) calibrated the efficiency factors e_b and e_s with laboratory and field data and found that $e_b = 0.13$ and $e_s = 0.032$. However, values of $e_b = 0.1$ and $e_s = 0.02$ are typically used, but other work has suggested that the efficiency factors are related to bed shear stress and grain size diameter. The typical value used for $\tan\gamma$ is 0.63.

Bodge and Dean (1987) examined forms of energetics and stress models and developed several alternative models based on laboratory experiments and short-term impoundment of sand under moderate wave conditions in the field. The recommended equation from their study, which predicts longshore transport based on wave energy dissipation and is valid only inside the surf zone where wave energy is expected to dissipate, is given as:

$$i_y = \frac{k_q}{h} \frac{\partial}{\partial x} \left(EC_g \right) V \left[\frac{dh}{dx} \right]^r \tag{2-51}$$

k_q is a dimensional constant equal to 0.057 for laboratory data and 0.48 s for field data, and r is a dimensionless constant between 0 and 0.5. An r-value of 0.5 gave the best agreement with their data; however, Bodge (1989) stated that scaling effects in the Bodge and Dean movable-bed laboratory experiments may have exaggerated the apparent relationship between local transport and bottom slope, and that r probably should equal 0. For $r = 0$, Equation 2-51 becomes:

$$i_y = \frac{k_q}{h} \frac{\partial}{\partial x} \left(EC_g \right) V \tag{2-52}$$

Miller (1998) used this form of the equation in a comparison of predictive models to field data. Miller found that the equation modeled the cross-shore sediment flux distribution reasonably well; however, the model overpredicted the magnitude. Reducing k_q by a factor of four improved the agreement with sediment transport measurements in storms. As part of the present research, Smith and Wang (2001) found that cross-shore locations having high wave energy dissipation did not necessarily produce increased transport rates with spilling breakers. They suggested that the influence of breaker type should be included in predictions of cross-shore distribution of longshore sediment transport.

Bodge (1989) reviewed several distribution models of longshore transport including the above-cited models. He found that models that do not include bottom stress due to the longshore current or non-breaking wave orbital motion exhibit discontinuities in transport at the breaker line, with no transport seaward of breaking. Most of the models did not predict transport landward of the shoreline where considerable transport has been observed, for example, by Saville (1950), Sawaragi and Deguchi (1978), Kraus et al. (1982), and Bodge and Dean (1987). Bodge (1989) stated that the Madsen (1976) and Komar (1971, 1975, 1977) models could predict longshore transport landward of the shoreline, but the method was not straightforward. With inclusion of wave-induced set-up, the Bodge and Dean (1987) model predicted transport landward of the shoreline.

Watanabe (1992) proposed an equation to calculate longshore sediment transport as combined bed and suspended load of the form:

$$q_y = A \left[\frac{\left(\tau_{b,wc} - \tau_{cr} \right) V}{\rho g} \right] \tag{2-53}$$

where τ_{cr} is the critical shear stress for inception of sediment motion and A is an

empirical coefficient, which is approximately 0.5 for monochromatic waves and 2.0 for

irregular waves. The difference in shear stresses represents a stirring function, and the

velocity term represents a transport function. This formula has received wide-spread

application for its simplicity, while incorporating several physical factors. However,

breaker type is not represented, nor is turbulence in the surf zone.

Van Rijn (1993) presented comprehensive formulas for calculating bed load and

suspended load. A synopsis of his work is presented here. Van Rijn used the approach

of Bagnold (1963) and assumed that sediment particles saltating under the influence of

hydrodynamic fluid forces and gravity forces dominate motion of bed load particles.

Saltation characteristics were determined by solving the equation of motion for an

individual sediment particle. Bed load was defined as the product of particle

concentration in the bed, c_b, the particle velocity, u_b, and layer thickness, δ_b:

$$q_b = c_b u_b \delta_b \tag{2-54}$$

where c_b is defined as:

$$\frac{c_b}{c_o} = 0.18 \frac{T}{D_*} \tag{2-55}$$

in which T is the excess bed shear stress parameter:

$$T = \frac{\vec{\tau}_{b,wc} - \tau_{cr}}{\tau_{cr}} \tag{2-56}$$

where D_* is the dimensionless grain diameter defined as:

$$D_* = d_{50} \left[\frac{\left(\frac{\rho_s}{\rho} - 1 \right) g}{v^2} \right]^{1/3} \qquad (2\text{-}57)$$

where v is the kinematic viscosity of the fluid. Combining these relationships into Equation 2-54 along with other relationships defined by Van Rijn (1993) results in:

$$q_b = 0.25 \gamma \rho_s d_{50} D_*^{-0.3} \sqrt{\frac{\vec{\tau}_{b,wc}}{\rho}} \left[\frac{\vec{\tau}_{b,wc} - \tau_{cr}}{\tau_{cr}} \right]^{1.5} \qquad (2\text{-}58)$$

where

$$\gamma = 1 - \sqrt{\frac{H_s}{h}} \qquad (2\text{-}59)$$

Van Rijn (1993) defined the depth-integrated suspended load transport in the presence of current and waves as the integration of the product of velocity, v, and concentration, c, from the edge of the bed-load layer, a, to the water surface:

$$q_s = \int_a^h vc \, dz \qquad (2\text{-}60)$$

Substituting the longshore current into the equation and integrating gives:

$$q_s = c_a V h \frac{1}{h} \int_a^h \frac{v}{V} \frac{c}{c_a} \, dz = c_a V h F \qquad (2\text{-}61)$$

where V is the mean longshore current, and:

$$c_a = 0.015 \frac{d_{50}}{a} \frac{T^{1.5}}{D_*^{0.3}} \qquad (2\text{-}62)$$

$$F = \frac{V_*}{\kappa V} \left(\frac{a}{h-a}\right)^Z \left(\int_{a/h}^{0.5} \left(\frac{h-z}{z}\right)^{Z'} \ln\left(\frac{z}{z_o}\right) d\left(\frac{z}{h}\right) + \int_{0.5}^{1} e^{-4Z'\left(z/h-0.5\right)} \ln\left(\frac{z}{z_o}\right) d\left(\frac{z}{h}\right) \right) \quad (2\text{-}63)$$

where

$$Z' + \psi \quad (2\text{-}64)$$

$$Z = \frac{w_f}{\beta \kappa V_*} \quad (2\text{-}65)$$

$$\psi = 2.5\left(\frac{w_f}{V_*}\right)^{0.8} \left(\frac{c_a}{c_o}\right)^{0.4} \quad (2\text{-}66)$$

$$\beta = 1 + 2\left(\frac{w_f}{V}\right)^2 \quad (2\text{-}67)$$

in which Z is a suspension parameter reflecting the ratio of downward gravity forces and upward fluid forces acting on a suspended sediment particle in a current, ψ is a correction factor representing damping and reduction in particle fall speed due to turbulence, and β is a coefficient quantifying the influence of the centrifugal forces on suspended particles.

Van Rijn (1993) calculated the concentration distribution in three separate layers; from the reference level, a, to the end of a near bed mixing layer of thickness, δ_s, from the top of the δ_s-layer to the lower half of the water depth, $h/2$, and from $h/2$ to h. Different exponential or power functions are employed in these regions with empirical expressions depending on mixing characteristics in each layer.

Although the model is complex, Van Rijn (1993) incorporated the equations into a computer program. The program is simple to use, but requires hydrodynamic, bedform, and grain size information at each cross-shore location.

Although not expressed as a simple formula or group of formulas as in the preceding, a recent calculation procedure is that of Tajima and Madsen (2005), who developed a process-based theoretical model to predict nearshore hydrodynamics and local sediment transport rates applicable for long, straight beaches. The model consists of two computer programs that run sequentially; a hydrodynamic model and a sediment transport model. The hydrodynamic model calculates forcing functions required to drive the longshore sediment transport model at each specified cross-shore location. In addition to calculating transport rates in the cross shore, the sediment transport model includes bedload and suspended load modules, and it can predict the vertical sediment concentration. The model does not include adjustable calibration coefficients.

Summary

Total Load Models

Several approaches have been attempted to estimate the total load of longshore sediment transport, but most of the methods are a form of the CERC formula, which is based on energy flux at wave breaking. A reason for the widespread use of the CERC formula is that it is simple to apply, as the equation requires only two quantities typically available to engineering studies, H_b, and θ_b. If the CERC coefficient K is calibrated to

historical data, total longshore sediment transport rate can be estimated with reasonable confidence. However, if it is not calibrated the equation provides only an order of magnitude accuracy. Researchers have developed methods to estimate K by incorporating fall speed (Bailard 1981, 1984), wave steepness (Ozhan 1982), and grain size (del Valle et al. 1993). These methods are still relatively easy to use, but require additional data to apply. Inman and Bagnold (1963) kept the basic form of the CERC formula, but included maximum horizontal orbital velocity and the mean longshore current. The Inman and Bagnold equation can be reduced to two terms, breaker height and longshore current, if shallow water conditions are assumed.

A criticism of the CERC formula includes omission of wave period, beach slope, and grain size, which are variables that contribute to sediment transport. Kamphuis (1991) included these additional terms and developed an empirical equation through analysis of laboratory data and limited field data. The Kamphuis equation has had mixed results when applied to the field. Wang et al. (1998) found that it consistently predicted lower estimates than the CERC formula and Miller (1999) found the equation underestimated measurements by an order of magnitude for storm conditions. However, Schoones and Theron (1996) found the Kamphuis equation to be the most accurate of 52 equations ranked.

Kraus et al. (1988) related longshore transport to average discharge of water moving alongshore. The equation requires only three terms, breaker height, longshore current, and surf zone width. Additionally, of the total load models discussed, the Kraus et al. equation is the only one that explicitly includes a threshold of motion term.

Madsen et al. (2003) developed an equation based on energy flux and includes terms for bed load transport and suspended load transport. The equation was simplified from complex equations by scaling physical processes and choosing reasonable values for different coefficients. The model does not include a threshold of motion term, but the model assumes that the bed shear stress must exceed a critical shear for transport to occur. The equation is simple to apply, requiring the same information as the CERC formula; however, it has not been fully calibrated to a wide range of conditions.

Distributed Load Models

The majority of distributed longshore sediment transport models are energetics models or stress models. Energetics models assume that sediment is mobilized by dissipation of waves, which is related to turbulence. Stress models assume that mobilization of sediment is caused by a wave- and current-induced shear stress acting on the bottom.

Although range in complexity varies with both methods, the energetics models are generally simpler to apply. For example, the models of Bagnold (1963) and Bodge and Dean (1987) are straightforward and consist of a few basic engineering terms. Conversely, the basic equation of Walton and Chiu (1979) has a simple appearance; however, the equation contains a local modifying function that is more difficult to determine. None of the energetics models discussed includes a threshold of motion term explicitly and none distinguished dissipation by breaker type.

The stress models of Komar (1971, 1975, 1977) and Watanabe (1992) rely on averaged terms and estimates can be calculated with basic data; however, the Watanabe equation includes a critical shear term for inception of sediment motion, whereas the Komar equation does not. The Madsen (1978) model does not include a term for critical shear stress, but is dependent on fall velocity and grain size, which implies that longshore transport decreases with increasing grain size. The models of Bijker (1967), Bailard and Inman (1981), Van Rijn (1993) and Tajima and Madsen (2005) include more physical processes, hence more terms, and are more complex and difficult to apply. Only the Van Rijn model and Tajima and Madsen model include critical shear stress.

CHAPTER III

DESCRIPTION OF THE LABORATORY FACILITY

Introduction

Physical model experiments were conducted in the Large-Scale Sediment Transport Facility (LSTF) (Figure 3-1). The U.S. Army Engineer Research and Development Center constructed the LSTF in an effort to overcome the limitations of small-scale facilities and to bridge the gap between field and previous laboratory measurements. The intent for the facility is to reproduce certain surf zone processes found on a long straight natural beach in a finite-length wave basin. The LSTF simulates nearshore hydrodynamic and sediment transport processes at a relatively large geometric scale, including situations where considerable sand is mobilized and transported in suspension. The LSTF is specifically designed for studies on longshore sediment transport (Fowler et al. 1995). The facility has the capability of simulating wave height and period that are almost directly comparable to annual averages along many low-wave energy coasts, for example, a majority of estuary beaches (Nordstrom, 1992), and many beaches along the Gulf of Mexico and the Great Lakes in the U.S. Detailed design considerations, capabilities, and initial testing of the LSTF are described in Hamilton et al. (2001). This section describes the facility, instrumentation and laboratory procedures.
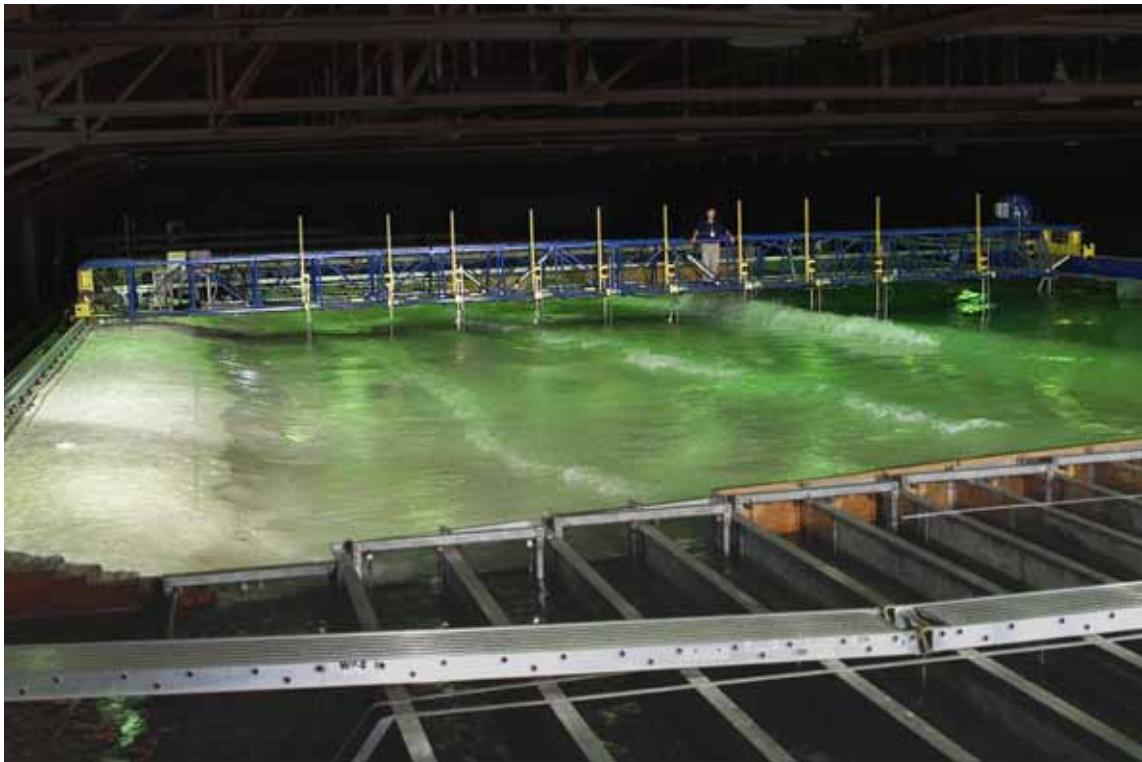
Figure 3-1. Photograph of the Large-Scale Sediment Transport Facility (LSTF)

LSTF Features

The LSTF consists of a 30-m wide, 50-m long, 1.4-m deep basin (Figure 3-2), and includes wave generators, a sand beach, a recirculation system, sand traps, and an instrumentation bridge. The origin for the LSTF coordinate system is the corner of the two basin walls shown in the lower right of Figure 3-2. Hence, positive "X" is offshore and positive "Y" is to the left. Although the longshore current produced in the facility is typically in the negative direction, it is presented as positive for simplicity. Common alongshore measurement transects (Y14 to Y38) also are shown in the figure to provide
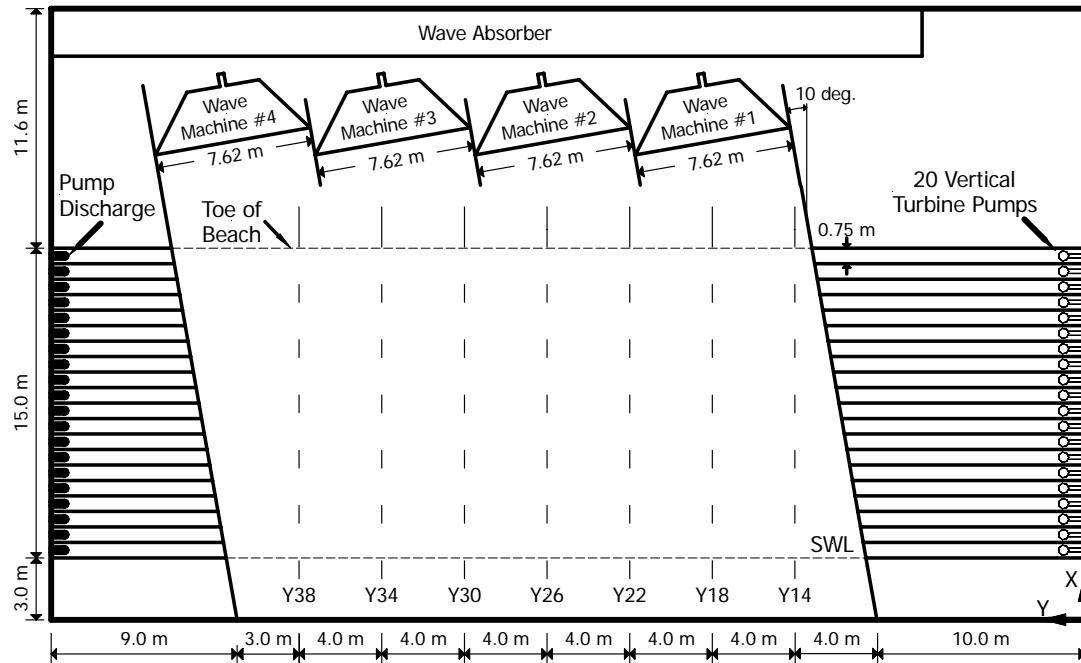
Figure 3-2. Layout of LSTF

a perspective of sampling locations with respect to the basin. The transect name

indicates its location based on its distance in meters from the origin.

Wave Makers

The LSTF is equipped with four wave generators operated simultaneously

(Figure 3-3). Each generator has a board length of 7.62 m and is synchronized with the

other generators to produce 30.5-m unidirectional long-crested waves. A digitally

controlled drive servo electric system controls the position of the piston-type wave board

and produces waves with the periodic motion of the board. The system allows a variety

of regular and irregular wave types to be produced. The generators can be positioned to

Figure 3-3. LSTF wave generators

produce waves from 0 to 20 deg from shore normal, and they were positioned at 10 deg from shore normal for the present experiment. A TMA shallow-water wave spectrum (Bouws, et al. 1985) was used to define the spectral shape for all wave conditions in the present study.

Model Beach

The sand beach consists of approximately 150 m^3 of fine quartz sand having a mean grain diameter, d_{50}, of 0.15 mm with a narrow distribution (Figure 3-4). The sand beach was constructed on top of a concrete fixed-bed having a slope of 1:30 over the main section of the beach and a 1:18 slope at the toe, which slopes down to the basin floor.
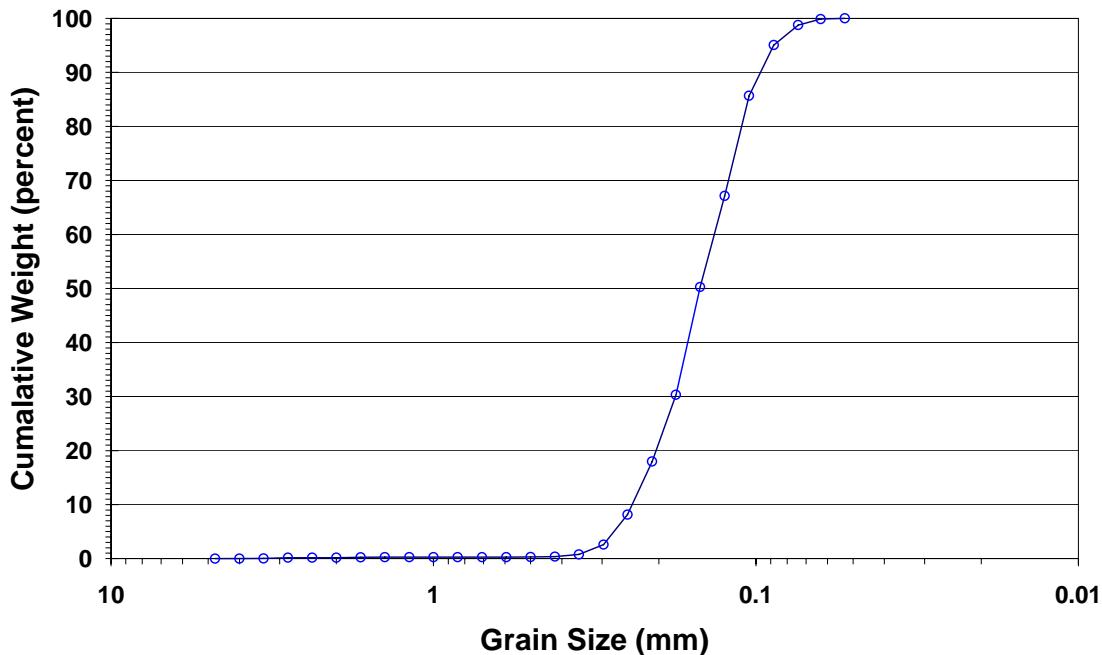
Figure 3-4. Grain size distribution of LSTF sand

The lateral boundaries of the beach were bounded by stacked 19.5-cm long by 9-cm wide mortar bricks having heights ranging from 1.4 to 5.6 cm. The use of bricks of varying height allowed flexibility in constructing the boundaries similar to the average beach profile. Additionally, because of their density, they are less likely to be displaced under waves and currents than other materials. Maintaining brick elevations at the downdrift boundary to match the average beach profile was found to be important. Lower brick elevations in relation to the beach may induce sand to enter the traps and cause an overestimate of sediment transport. Conversely, if the brick elevation is higher than the beach elevation, the bricks act as a barrier and transport into the traps is restricted and results in underestimation of sediment transport. Additionally, excess or deficient sand near the downdrift boundary alters the local profile and uniformity of

longshore currents. For these reasons, the downdrift boundary was observed carefully during each experiment and, if necessary, bricks were removed or installed so that the boundary profile matched the average beach profile.

The goal was to obtain an accurate rate of longshore sediment transport and its cross-shore distribution with minimal longshore variation and boundary influences. To achieve this goal, it was necessary to maintain straight and parallel contours throughout the model to maximize the length of beach over which longshore uniformity of waves and currents exist in the basin. Beaches having "three-dimensionality" affect incident waves and the longshore currents and sediment transport associated with the waves.

Recirculation System

The model beach is of finite length and bounded at the upstream and downstream ends. To minimize adverse laboratory effects created by the boundaries and to produce uniform longshore currents across the beach, wave-driven currents are supplemented by an external recirculation system discussed by Hamilton, et al 2001, Hamilton and Ebersole 2001, and Visser 1991. The recirculation system consisted of 20 independent vertical turbine pumps placed in the cross-shore direction at the downdrift boundary (Figure 3-5). Flow channels placed upstream of each pump are used to direct flow to the pump, which externally re-circulates water to the upstream end of the facility where it is discharged through flow channels onto the beach. The objective of this system is to maximize the length of beach over which waves and wave-driven longshore currents are

Figure 3-5. Recirculation pumps

uniform by continually re-circulating currents of the same magnitude as the wave-driven

longshore current through the lateral boundaries of the facility. Each pump includes a

variable speed motor to control discharge rates. The variable speed motors are

controlled remotely to produce a cross-shore distribution of longshore current.

Without the external circulation system, the longshore current would be forced to

circulate within the test basin, which would influence the measurement accuracy, and

potentially negate the experiment. Visser (1991) found that if the pumped currents

either exceed or were less than the wave-driven currents, an undesired internal current would develop and recirculate within the offshore portion of the basin. Visser also found that as pumped currents approached the "proper" wave-driven current distribution, the internally recirculated current was minimized. Hamilton and Ebersole (2001) found the criterion proposed by Visser to be valid for the LSTF, and it was used in part to determine the distribution of pumped longshore currents.

Instrumentation Bridge

The facility includes a 21-m instrumentation bridge (Figure 3-6) that spans the entire cross-shore length of the beach. The bridge serves as a rigid platform to mount instruments and observe experiments. Each end of the bridge is independently driven on support rails by drive motors, which allows it to travel the entire alongshore length of the wave basin.

Instrumentation

Wave Gauges

Time series of water surface elevations were measured using single-wire capacitance-type wave gauges. Ten gauges mounted on the instrumentation bridge provided wave height measurements as the waves transformed from offshore to nearshore (Figure 3-7). The cross-shore location of the gauges can be repositioned on the bridge; however, the cross-shore locations remained the same for this study. In

Figure 3-6. Instrumentation bridge

addition to the bridge-mounted gauges, a gauge was placed in front of each wave

generator to measure offshore wave characteristics. The locations are given in

Table 3-1, as are cross-shore locations of the acoustic Doppler velocimeters (ADVs)

used to measure wave orbital velocities and currents (discussed in the following section).
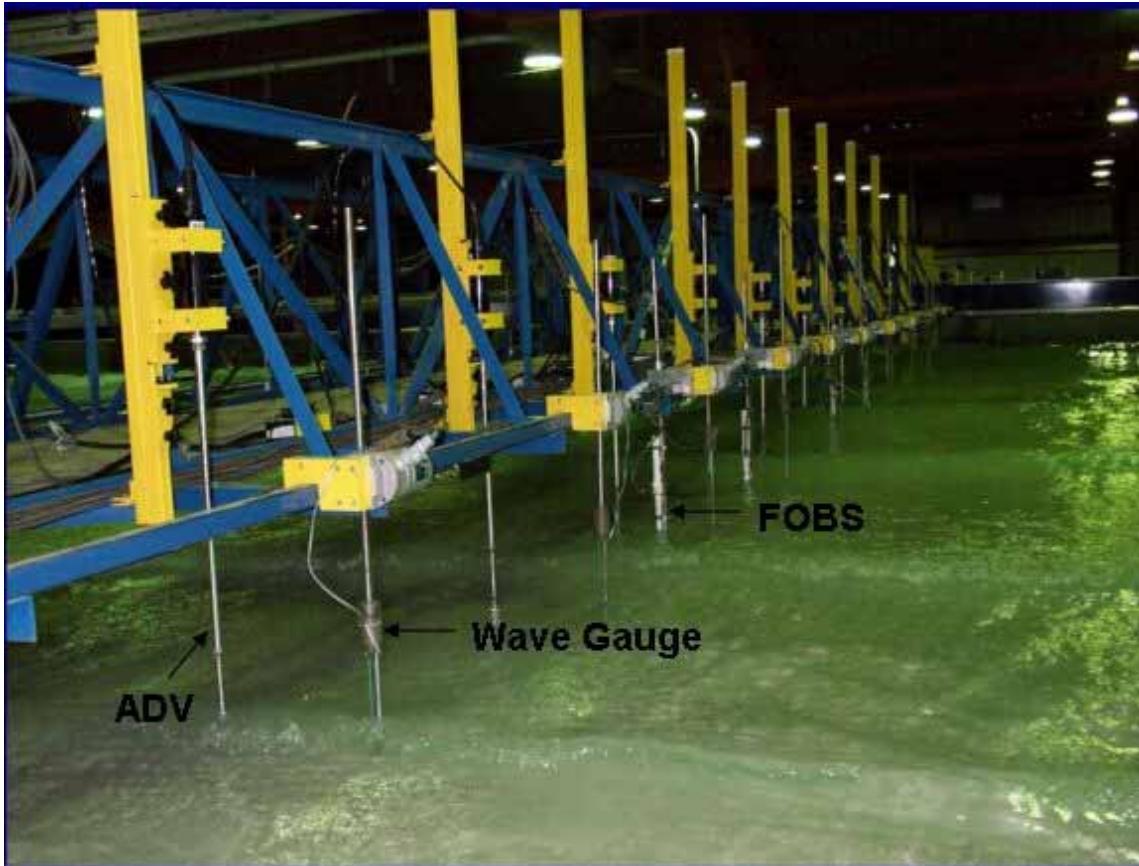
Figure 3-7. Wave gauges, ADVS, and FOBS

Calibration of the wave gauges was performed at least twice during an experiment series; at the beginning of the experiment series, and after the iteration phase (defined below) of an experiment was completed. Additionally, the gauges were calibrated if the ambient temperature during the course of the experiment changed significantly from the ambient temperature during the calibration.

Wave gauge calibration was performed in the flow channels of the recirculation system. The flow channels provided sufficient depth to perform the calibration, which the sloping sand beach did not. The procedure involved raising or removing all

Table 3-1. Cross-shore sampling locations of wave gauges and ADVs

Wave Gauge	ADV	Cross-shore Location (m)
1	1	4.13
2	2	5.73
3	3	7.13
4	4	8.73
5	5	10.13
6	6	11.53
7	7	13.13
8	8	14.63
9	9	16.13
10	10	18.60
12[*]	-	21.43 (Y = 21.0 m)
13[*]	-	21.43 (Y = 24.5 m)
14[*]	-	21.43 (Y = 32.0 m)
15*	-	21.43 (Y = 39.5 m)

[*] During Test 1, cross-shore location of wave gauges 12 through 15 was 18.0 m

instruments from the bridge to allow the bridge to clear the flow channels, positioning the bridge over the flow channels, and re-mounting the wave gauges. After re-attaching the gauges, the middle of each rod was positioned at the still-water level. Calibration was computer-controlled and involved raising and lowering each rod to 11 known elevations at which voltages were recorded. A least-square fit of measurements using 21 voltage samples per gauge minimized the errors of slack in the gear drives and hysteresis in the sensors. Typical calibration errors were less than one percent of full scale for the capacitance wave gauges.

Acoustic Doppler Velocimeters

Ten acoustic Doppler velocimeters (ADVs) were deployed to measure orbital wave velocities and unidirectional longshore current (Kraus et al. 1994). The ADVs were positioned at the same cross-shore position on the bridge with the wave gauges (Table 3-1), but separated by approximately 40 cm in the longshore direction to prevent electrical interference between the two instrument types (Figure 3-7). As with the wave gauges, the ADV cross-shore location can be repositioned on the bridge, but were located in the same position for the experiments in this study. The ADVs make sample point measurements, but were mounted on vertical supports that allow the vertical position of the sampling volume to be adjusted. Typically, the ADVs were positioned vertically to sample at a location that gives the average velocity in the water column (an elevation equal to one third of the water depth from the bottom (Hamilton, et al. 2001)). However, some runs were conducted in which the vertical positions of the ADVs were continually adjusted to obtain the velocity distribution through the water column.

Calibration of the ADVs is based on the geometry of the acoustic transmitter and receiver, as well as the speed of sound in water. The ADVs are calibrated by the manufacturer and do not need to be calibrated on a regular basis if the acoustic transmitter and receivers are not damaged, and if the geometry of the unit remains unchanged. Speed of sound in water is the only parameter that influences ADV calibration, and the instruments were adjusted daily.

Beach Profiler

Surveys of the beach were accomplished by three methods over the course of the experiments. An automated beach profiler mounted to the instrumentation bridge was used for the first two experiment series (Figure 3-8). The profiling system is amphibious to allow both the dry and submerged portions of the beach to be surveyed without draining the basin. Horizontal positioning of the profiler is controlled by the bridge position and a cross-shore motor mounted on the bridge. The vertical resolution of the system was ± 1 mm. Survey data were obtained every 0.005 m in the cross-shore direction and every

Figure 3-8. Mechanical beach profiler

0.5 or 1.0 m in the longshore direction. Initially, the entire beach was surveyed every 0.5 m in the longshore; however, it was found that the middle portion of the beach remained uniform and the higher resolution was not required. Higher irregularity in the bathymetry occurred near the upstream and downstream boundaries, and denser profile lines were required. The system recorded cross-shore and alongshore positions and associated elevations referenced to the model floor.

After the second experiment was completed, the beach profiler failed. Rod surveys were performed to obtain bathymetric data for the last two experiments. A minimum of twenty subaqueous elevations and 4 to 5 subaerial elevations was obtained in the cross-shore at 12 longshore locations.

During the fourth wave experiment, an ultrasonic profiler was installed to conduct underwater beach surveys. The instrument operated solely underwater, and beach profiles above the still water level (swl) were obtained using a rod. Cross-shore measurements were obtained every 0.02 m with the ultrasonic profiler.

Sediment Traps

Eighteen traps are installed in the downdrift flow channels of the LSTF to collect sand transported through the downdrift boundary. Two additional traps are located landward of the first flow channel to quantify longshore sediment transport rate near the still-water shoreline and in the swash zone. Each sand trap is equipped with three load cells to weigh the amount of trapped sand, allowing the cross-shore distribution of longshore sediment transport to be determined.

Because the total amount of longshore sediment transport during individual wave runs was only a small fraction, less than 1 percent, of the total amount of sand on the artificial beach, it was judged that continuous sand recharging during wave runs was not necessary (Hamilton et al. 2001). The traps were emptied when they were full or if observations indicated the beach had become non-uniform in the longshore direction. Each trap was dredged and the material was placed back on the beach. After the traps were emptied, the beach was rebuilt to uniform contours.

The downdrift traps consist of rectangle aluminum boxes sealed to the flow channels and the test beach with rubble neoprene, and a certain amount of sand deposits on the rubber seal. Generally, the total quantity that accumulates on all rubber seals is 3 to 12 percent of the total that actually settles into the trap. However, the percentage of sand accumulating on the seals can approach 15 to 20 percent in individual traps. To account for this error, accumulated sand was washed off the rubber seals into the individual traps following each test segment and incorporated in the total measured sand weight.

Fiber Optic Backscatter Sensors

Profiles of sediment concentration were measured, but not used, in this study with Fiber Optic Backscatter (FOBS) sensors (Figure 3-7). The FOBS simultaneously measure suspended sediment concentration at 19 elevations in the water column. Elevations of the FOBS sensors were determined by deploying the bottom sensor directly on the bottom and using it as a reference for the upper sensors.

Laboratory Procedures

   To measure longshore sediment transport accurately and efficiently as well as the

hydrodynamics that produce the transport, a set of procedures was followed for each

wave condition generated. To help explain the procedures discussed in this section,

some of the terminology is defined. Each *test*, or *experiment*, consisted of a single wave

condition having a given incident wave height, period, wave angle and water depth.

Data collected at a longshore (Y) location was defined as a *transect*, and a *run* consisted

of a series of transects performed during a continuous generation of waves and current.

Each test consisted of two *phases*, the *iteration phase* to determine proper pump settings,

and the *measurement phase* to collect sediment transport and hydrodynamic data. Each

run conducted during the iteration phase was termed an *iteration*, and each run during

the measurement phase was defined as a *case*.

   At the onset of a test series of a particular wave condition, the initial beach was

constructed based on the equilibrium profile shape described by Bruun (1954) and Dean

(1977) in the form of

$$h = Ax^m \qquad\qquad (3\text{-}1)$$

where h is the still-water depth, x is the horizontal distance from the shoreline, A is a

dimensional scale parameter related to sediment grain size, and the empirical shape

coefficient, m, was found to be equal to 2/3. For the present experiments, $A = 0.084$,

which was determined using the 0.15-mm median grain size of the very well sorted

quartz sand. The beach profile calculated using Equation 3-1 was approximated with 3

planar beach segments for the convenience of construction. Following construction of the beach, the basin was filled with water to 0.9 m at the wave makers, which was the swl of all the experiments.

The first goal of a test was to obtain the proper pump distribution settings and allow the beach to reach an equilibrium condition. As waves and currents were generated, the beach responded towards an equilibrium profile. Likewise, the waves responded to changes in bathymetry, altering shoaling and breaking, and the cross-shore distribution of longshore current. Therefore, it was necessary to adjust the pump distribution continually during the beach-evolution process. This part of the test was named the iteration phase as mentioned above. After a series of runs, or iterations, a reasonably uniform longshore current pattern was achieved.

Initial estimates of the cross-shore distribution of longshore current for the iterative process were calculated using NMLONG (Kraus and Larson 1991) and Nearhyds (Johnson 2003). The first attempt followed the method of Hamilton and Ebersole (2001), in which the predicted longshore current distribution was significantly reduced, and longshore currents were under-pumped across the entire surf zone. The bridge was positioned at a longshore measurement location, or transect, and waves were generated for approximately 10 min prior to data collection to allow the basin to reach a steady state (Hamilton, et al. 2001). Measurements of wave height and longshore velocities were collected at a 20-Hz rate for 600 sec. After data collection was completed at the initial transect, the bridge was then moved to a new longshore location, and the

procedure was repeated. Typically, current data from four to six transects were compared to pumped fluxes during the iteration phase.

Following completion of each iteration, the beach was surveyed, and the pumps were adjusted based on measured longshore velocities and fluxes. The measurement procedure was repeated until the pump settings required little further adjustment

After completion of the iteration phase, the measurement phase of the experiment began. Three goals during the measurement phase were to obtain sufficient horizontal spatial coverage, obtain sufficient vertical spatial coverage, and repeat key measurements to ensure data quality and reproducibility. Horizontal spatial coverage was achieved by collecting data at several transects over the length of the facility. Vertical spatial coverage was achieved by collecting data at one transect (normally Y=22 m), and adjusting the vertical position of the ADVs after each 600-sec run. A minimum of 10 locations was sampled to provide the vertical velocity profile for defining cross-shore and longshore velocities.

Sediment flux measurements were obtained during the iterative process and the measurement phase. However, only sediment fluxes obtained during the measurement phase were analyzed in this study. Prior to each run during quiescent conditions, the traps were sampled to obtain an initial weight. Another sample was taken during quiescent conditions following each wave run. Sediment flux was calculated as the difference between the post- and pre-run weights divided by the wave run time.

In principle, the sediment traps situated at the downdrift end of the beach should be 100 percent efficient, i.e., completely trap the sand that the waves and currents transport

alongshore. However, the physical boundaries of the facility, and imperfections in the systems and scheme used to control wave, current, and sediment transport processes at the lateral boundaries, influence the degree to which alongshore uniformity can be achieved. Along the downdrift boundary, slight changes in contour orientation are evident within a few meters of the boundary. This is evidence that there is some anomalous erosion and/or accretion along this lateral boundary. These anomalies must be accounted for in estimates of LST rates that are derived from the trap weight measurements. The extent and magnitude of the anomalies change with cross-shore position; therefore, the magnitude of the corrections varies with cross-shore position. In general, anomalies were restricted to the region of beach within 1 to 3 m of the downdrift boundary. At the downdrift end of the beach, between alongshore coordinates of 11 and 16 m, larger volume changes are evident. Volume changes in this zone are assumed to be anomalous and caused by lateral boundary imperfections. These volume changes are used to develop corrections to the quantities of sand that accumulate in the traps.

Within each 0.75-m cross-shore section of beach in this anomalous zone (0.75 m is the width of each flow channel), the measured trap volume for that channel was adjusted to reflect the anomalous volume change within that section of beach. Trap weights were converted to volume by incorporating the porosity of wet sand that accumulates in the traps (porosity of 0.40 is assumed). Generally, volume changes between the downdrift boundary and the alongshore coordinate of 15 m were considered. Where anomalous erosion occurred, the correction was subtracted from the volume that accumulated in the

trap; where accretion occurred, the correction was added to the volume in the trap. All

trapped quantities were corrected in this manner.

CHAPTER IV

LSTF RESULTS AND ANALYSIS

Introduction

Four irregular wave signals with a relatively broad spectral shape, representing typical sea conditions, were generated in the LSTF. The wave conditions were designed to obtain and compare LST rates for different breaker types by varying incident wave height and period. Four conditions generated in the LSTF are listed in Table 4-1, where H_{mo} is energy-based significant wave height measured near the wave makers, H_{sb} is energy-based significant wave height at breaking, T_p is peak wave period, h is water depth at the wave generators, θ_b is incident wave angle at the wave generators, and m is the slope of the beach from the breaker line to the shoreline. Furthermore, the wave conditions were grouped by energy level; Tests 1 and 3 had similar incident wave heights and are referred to as higher energy conditions, and Tests 5 and 6 are referred as lower energy conditions. Each test was conducted with an $h = 0.9$ m and $\theta = 10$ deg at the wave generators.

Table 4-1. LSTF test wave conditions

Test Number	Breaker Type	H_{mo} m	H_{sb} m	T_p s	h m	θ_b deg	m
1	Spilling	0.25	0.26	1.5	0.9	6.5	0.031
3	Plunging	0.23	0.27	3.0	0.9	6.4	0.024
5	Spilling	0.16	0.18	1.5	0.9	6.7	0.025
6	Plunging	0.19	0.21	3.0	0.9	6.4	0.020

Test 1

The initial test condition consisted of waves having $T_p = 1.5$-s, $H_{mo} = 0.25$-m, which produced spilling waves ($\xi_b = 0.34$). The wave spectra measured at Gauge 10 (X = 18.6 m) is shown in Figure 4-1, and the quasi-equilibrium beach profile developed after 14 hr of waves is shown in Figure 4-2. Elevations are referenced relative to the basin floor, and the heavy horizontal line represents the swl elevation of 0.9 m. The profile shown in Figure 4-2 represents an average of 16 profiles measured in the middle section of the test beach, and the profile slope is nearly planar inside the surf zone from cross-shore locations X = 4.9 m to X = 12.6 m. Three cases were performed for Test 1 wave conditions and are described in the following paragraphs
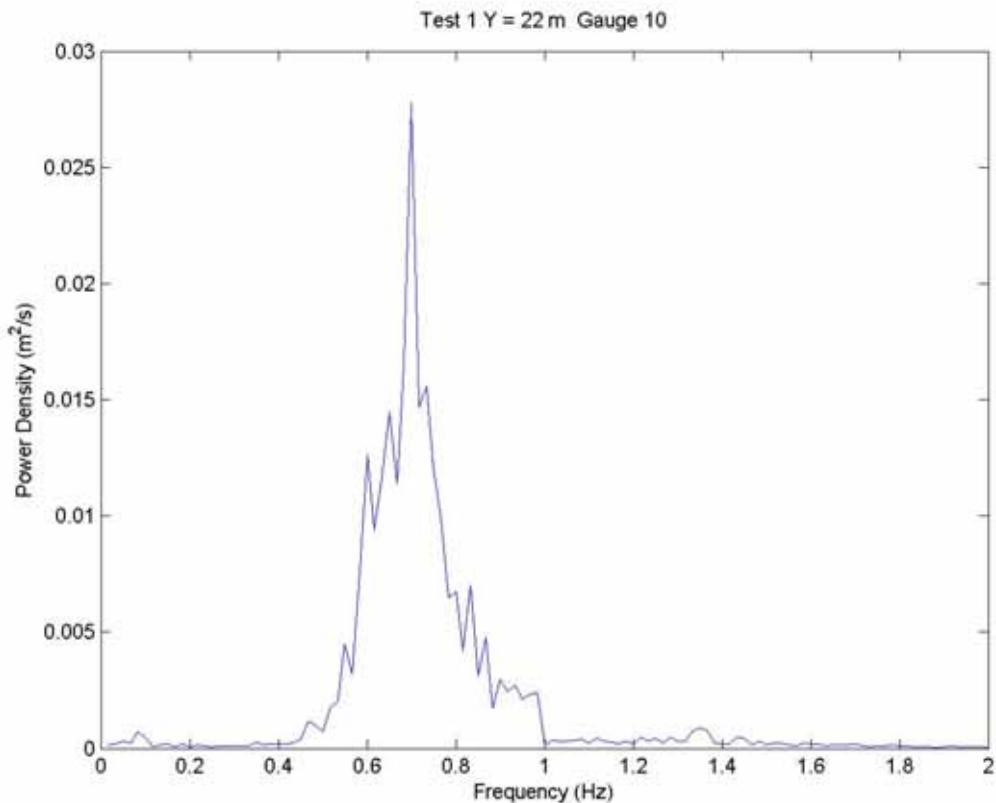
Figure 4-1. Measured incident wave spectra, Test 1

Test 1, Case 1

The purpose of Test 1, Case 1, was to measure uniformity of the longshore current. Measurements were made at eleven transects spaced at 2-m intervals in the longshore direction between Y=14 m to Y=34 m. Duration of the Test 1, Case 1, was 3.0 hr. The distribution of mean longshore currents measured during Test 1, Case 1, is shown in Figure 4-3. The heavy line denoted as LB's represents the pumped currents at the lateral boundaries (LB's). Erroneous measurements were observed with ADV 8 at
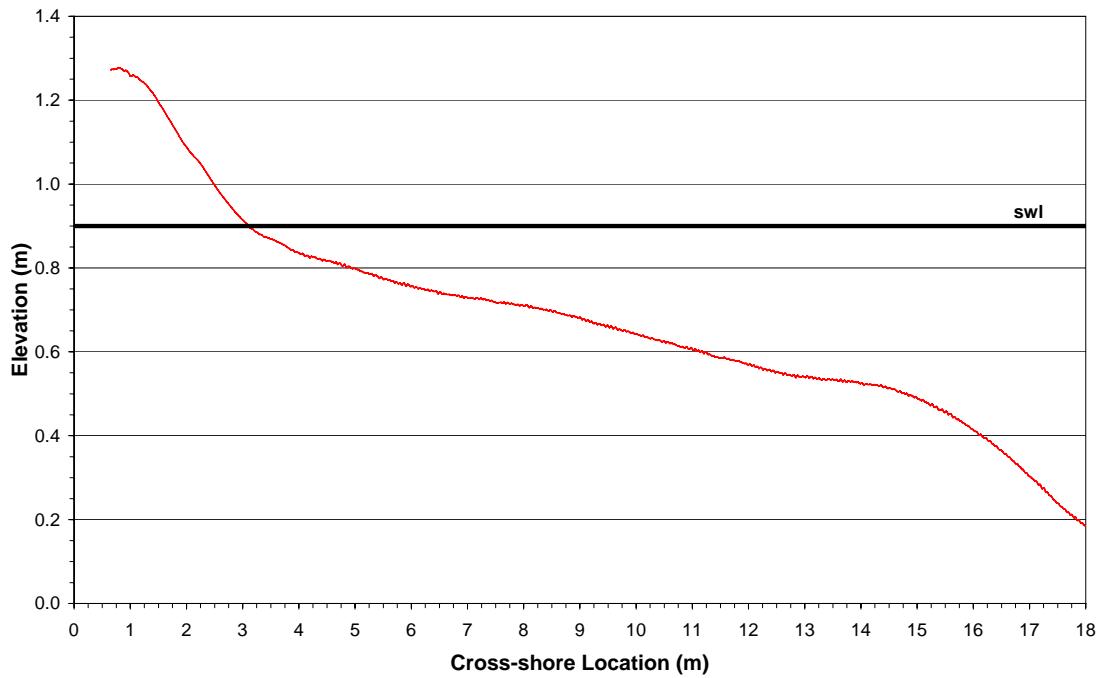
Figure 4-2. Quasi-equilibrium beach profile formed from Test 1 waves
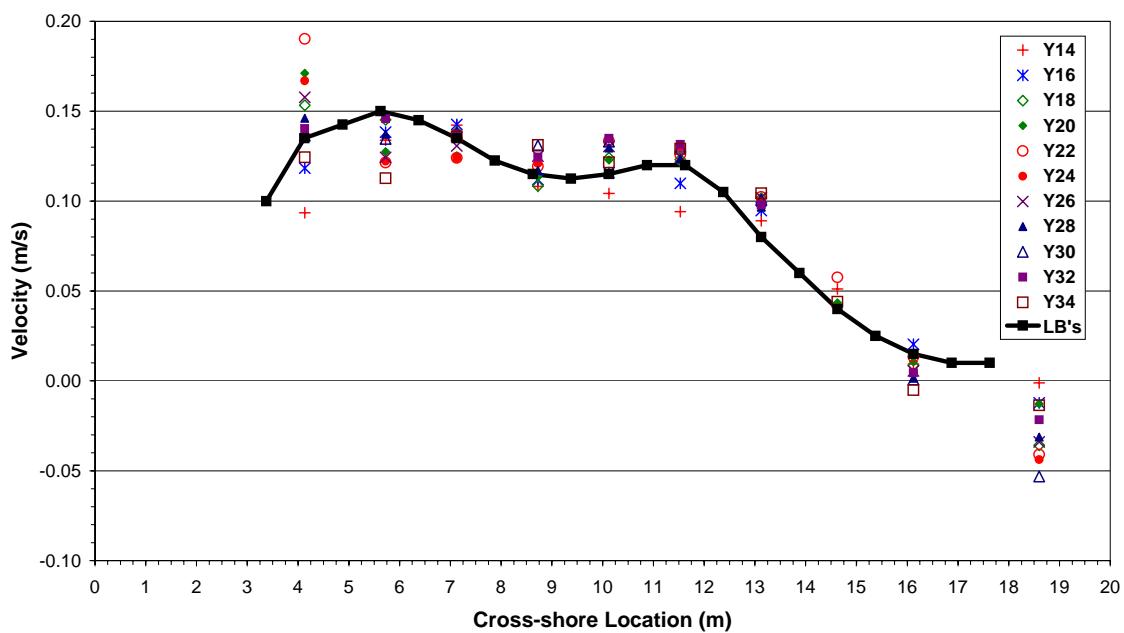
Figure 4-3. Cross-shore distribution of longshore currents, Test 1, Case 1

Y=16, 18, 24, 26, 28, 30, and 32 m, and the suspect points were removed from the figure. Considering this condition was the inaugural test with a movable bed in the LSTF, measurements overall agreed well with the pumped values, especially between transects Y=18 m and Y=30 m. Longshore currents varied greatly at the most shoreward location, and the current appeared to be under-pumped in this region if transects only in the middle of the test beach were considered. Slight recirculation due to the lateral boundaries was observed at the most offshore measurement location (X = 18.6 m) where longshore current is negative.

All of the wave gauges on the bridge were operating during Test 1, Case 1. However, the gauges positioned in front of each wave generator (X=18.0 m) gave lower than expected results. Wave height distribution and mean water surface elevations are shown in Figure 4-4. Wave heights show uniformity in the longshore direction and a gradual decay in wave height typical of spilling-type breakers.

The distribution of longshore sediment flux, corrected for trap inefficiency, is shown in Figure 4-5. Each point represents the longshore transport rate at a particular trap. Longshore transport showed a slightly increasing trend through the surf zone. Transport rates fluctuated shoreward of 10 m, with three spikes in transport occurring at X ~ 9 m, X ~ 6 m, and X ~ 4 m. No explanation can be given for these spikes, and they appear to be anomalous data.
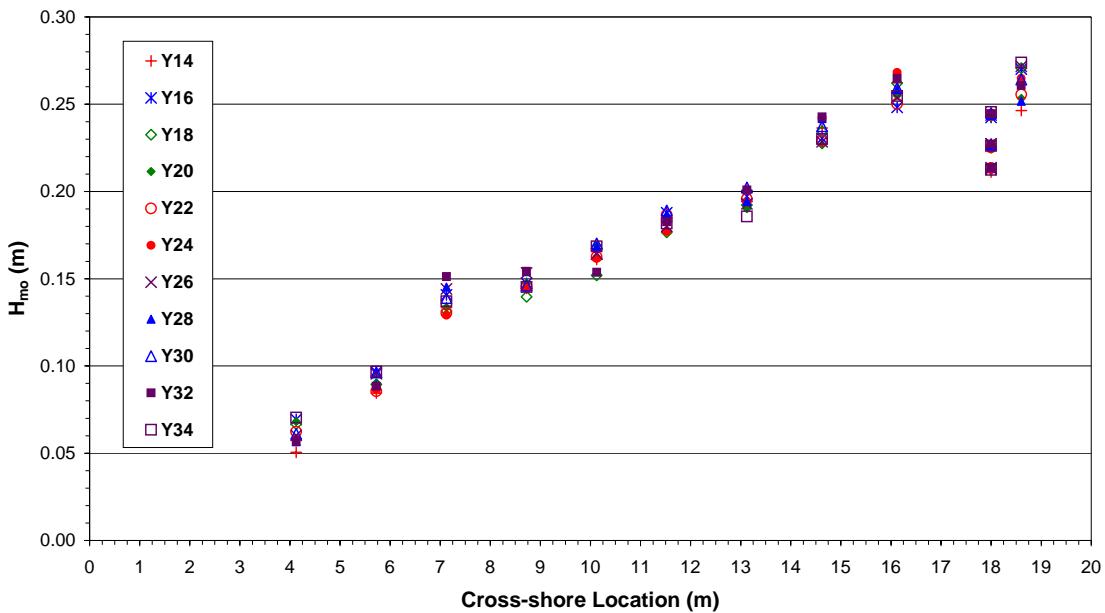
Figure 4-4. Cross-shore distribution of wave heights, Test 1, Case 1
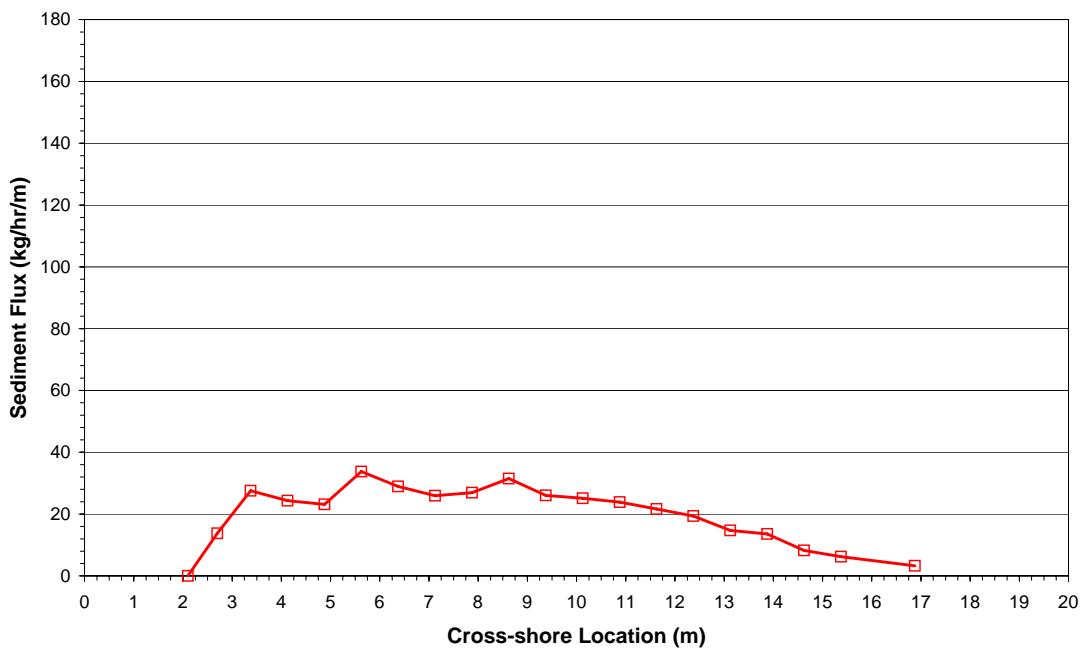
Figure 4-5. Cross-shore distribution of longshore sediment flux, Test 1, Case 1

Test 1, Case 2

The purpose of Test 1, Case 2, was to measure steadiness of the longshore current. Measurements were made at four transects between Y=14 m to Y=30 m, and repeated twice for a total of three sets of measurements at each transect. The temporal spacing between the sets was approximately one hour. The total duration of Test 1, Case 2, was 3.33 hr.

ADVs 2, 7, and 8 malfunctioned throughout the test (see Table 3-1 for cross-shore locations). The cross-shore distribution of the longshore current obtained at the one-third water depth is shown in Figure 4-6 with suspect points removed. The letters A, B, and C define the first, second, and third sets of transect measurements, respectively.
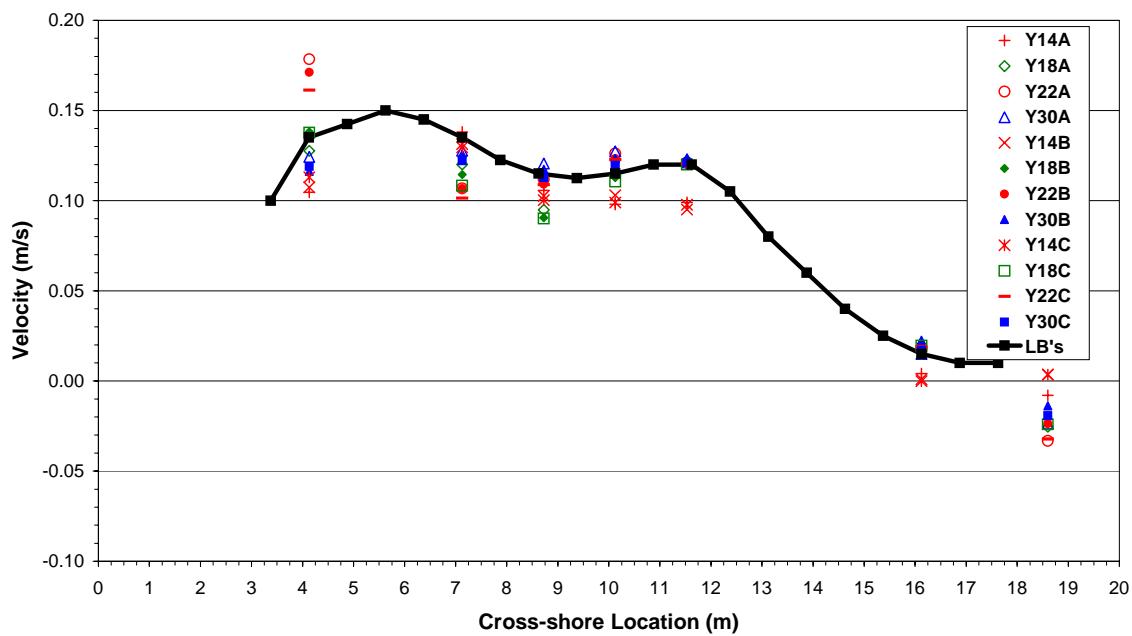
Figure 4-6. Cross-shore distribution of longshore currents, Test 1, Case 2

Values were similar to those of Test 1, Case 1, although longshore currents were slightly lower for Test 1, Case 2, between X = 7.0 and X = 10.m. The longshore current is plotted by transect in Figures 4-7 through 4-10, which show consistency at each location throughout the test, demonstrating that conditions were steady in the basin.

Wave height distribution through the surf zone is shown in Figure 4-11. Gauges on the bridge were operating, but as with Test 1, Case1, the gauges in front of each wave maker gave questionable results and are omitted from the figure. The figure shows that wave heights were both steady and longshore uniform.

Longshore sediment flux distribution with trap corrections is plotted in Figure 4-12. Transport was similar through the surf zone as in Test 1, Case 1, showing a slightly increasing trend; however, the transport rate increased substantially in the swash zone for Test 1, Case 2, where maximum sediment flux occurred. The difference in swash zone sediment flux between the two cases may have resulted from the swash zone downdrift boundary being observed and adjusted according to the adjacent beach profile during Test 1, Case 2.

Test 1, Case 3

Test 1, Case 3, was performed to measure the vertical distribution of the longshore current through the water column. All measurements were obtained at Y = 22 m, and the duration of Test 1, Case 3, was 3.33 hr. Velocities were obtained at each ADV for eleven depths given in Table 4-2. The ADVs only record measurements if submerged; therefore, all measurements depths were targeted below the expected wave trough level
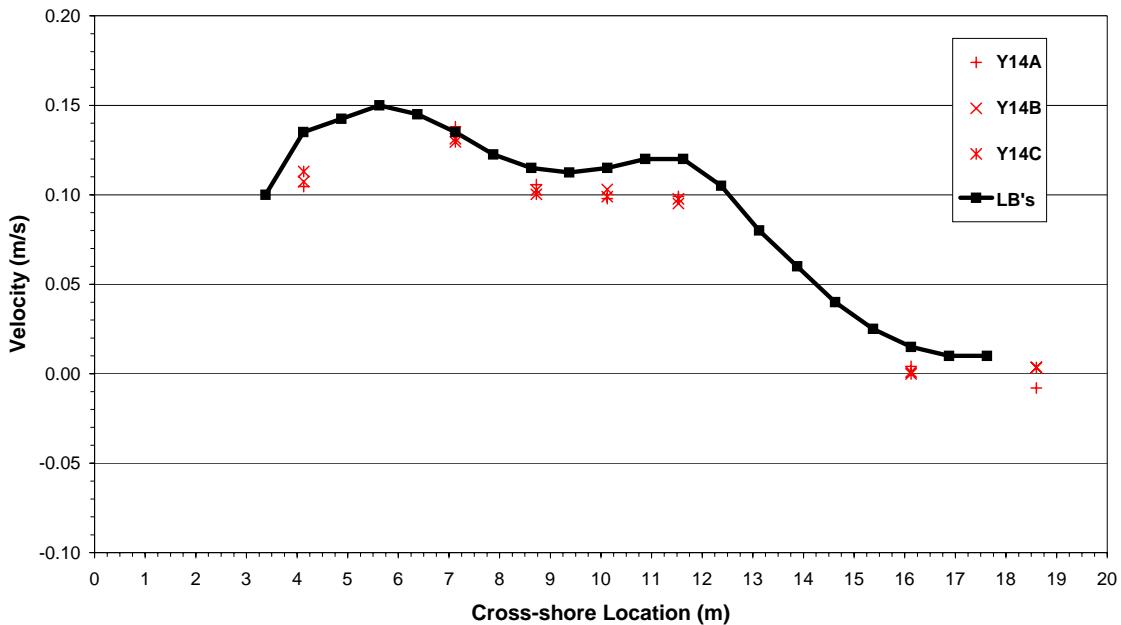
Figure 4-7. Cross-shore distribution of longshore currents, Test 1, Case 2, Y = 14 m
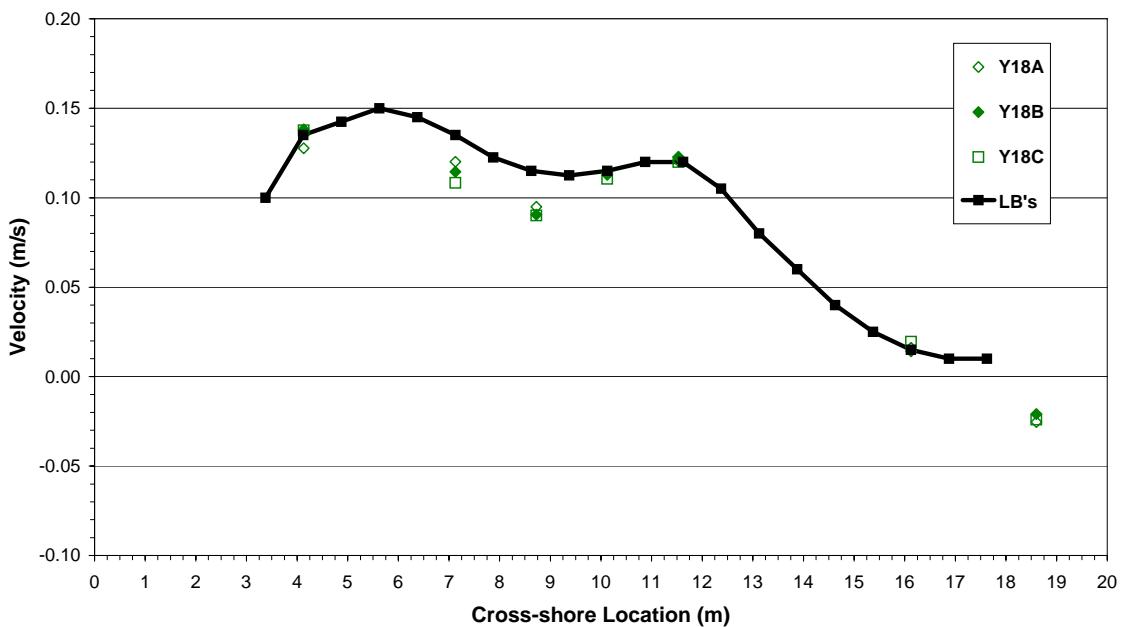
Figure 4-8. Cross-shore distribution of longshore currents, Test 1, Case 2, Y = 18 m
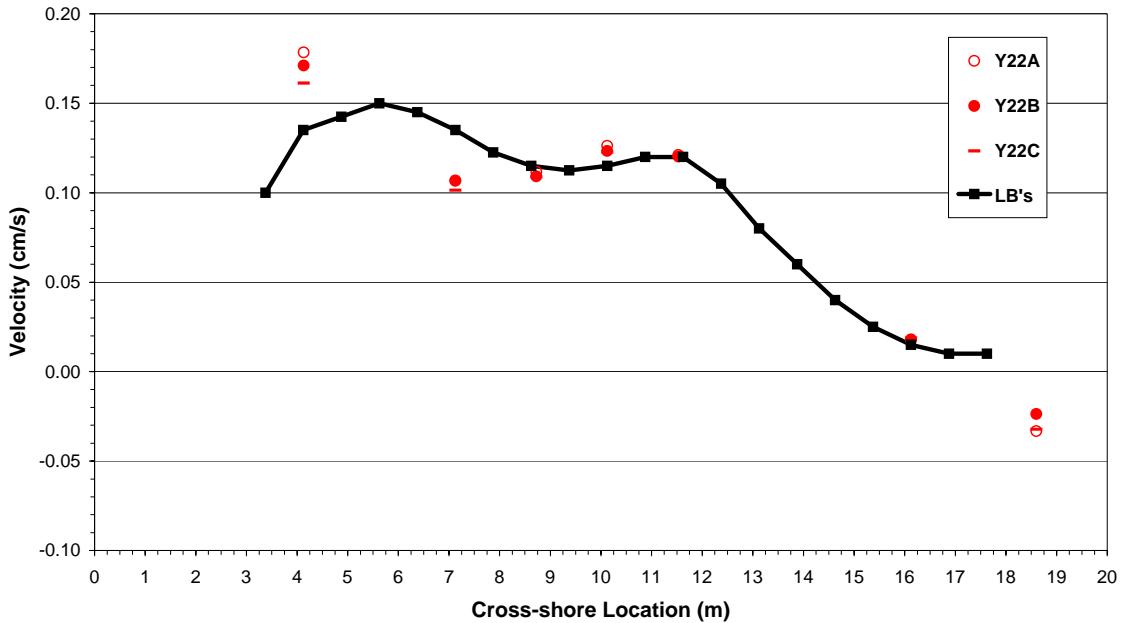
Figure 4-9. Cross-shore distribution of longshore currents, Test 1, Case 2, Y = 22 m
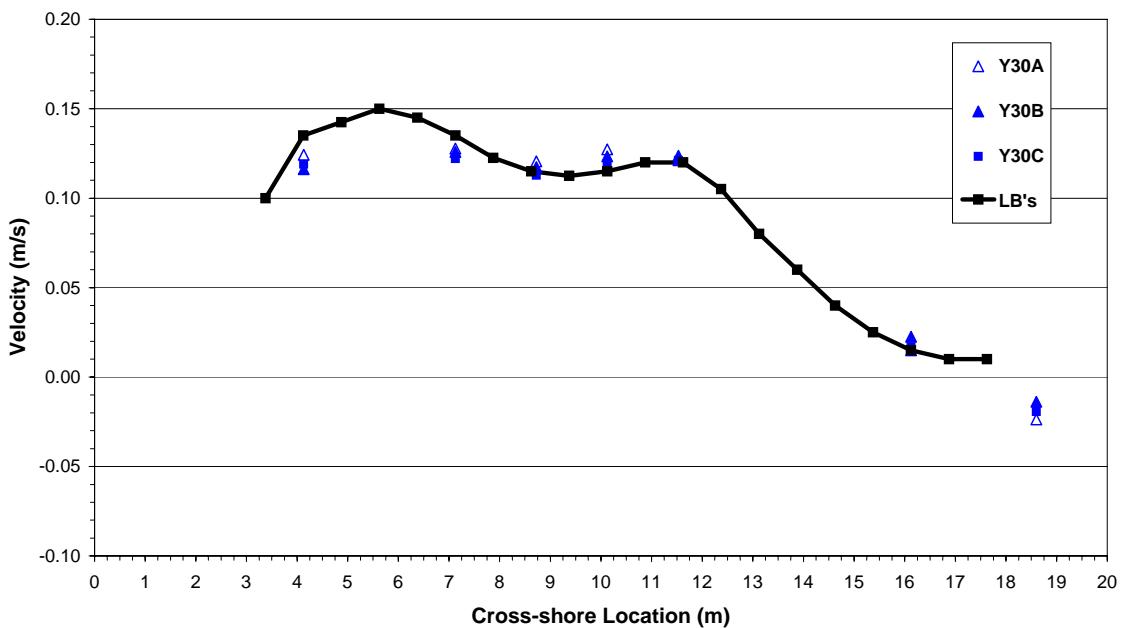
Figure 4-10. Cross-shore distribution of longshore currents, Test 1, Case 2, Y = 30 m
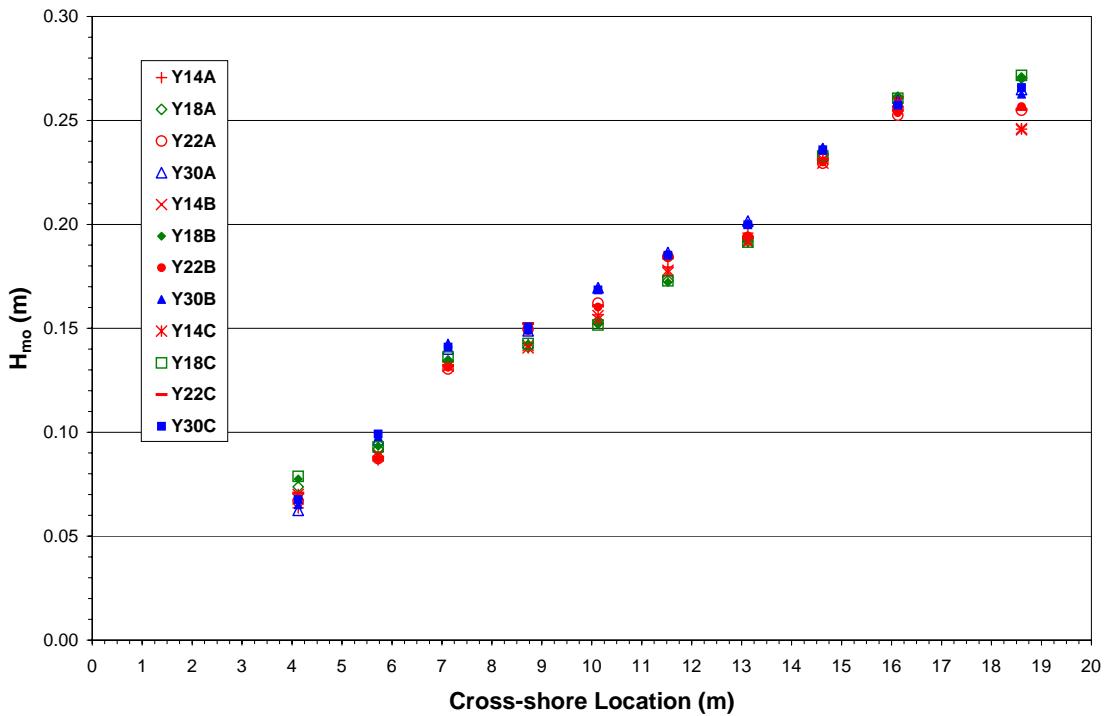
Figure 4-11. Cross-shore distribution of wave heights, Test 1, Case 2
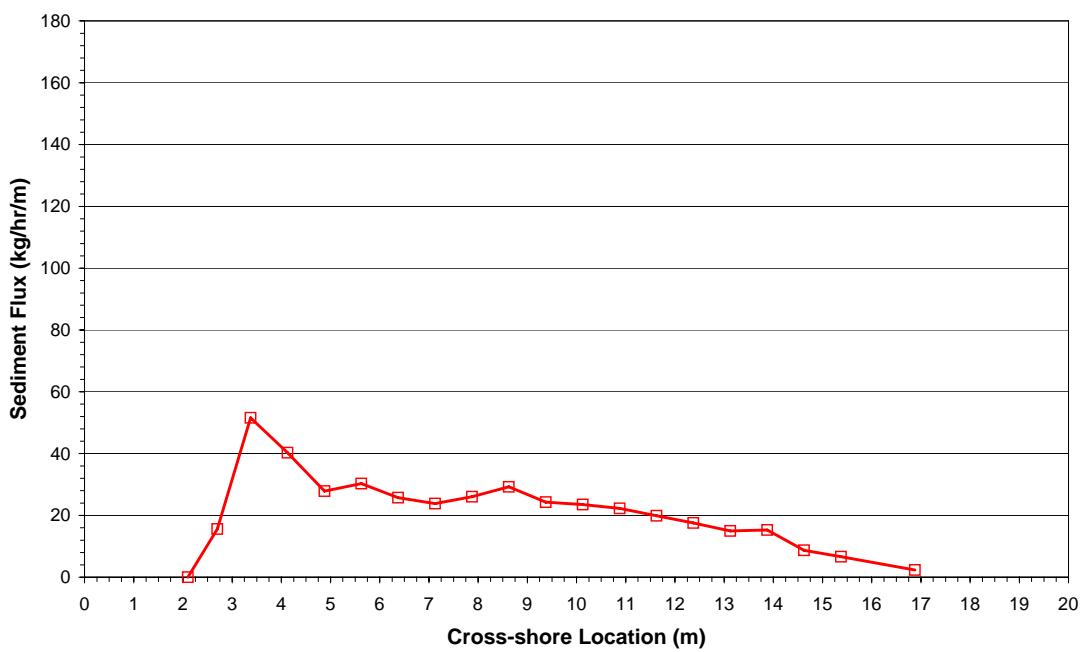
Figure 4-12. Cross-shore distribution of longshore sediment flux, Test 1, Case 2

Table 4-2. Test 1, Case 3, ADV sampling depths

	Sampling Depth (m)										
ADV	Y22A	Y22B	Y22C	Y22D	Y22E	Y22F	Y22G	Y22H	Y22I	Y22J	Y22K
1	0.09	0.08	0.08	0.07	0.07	0.06	0.05	0.04	0.03	0.02	0.05
2	0.15	0.14	0.14	0.14	0.13	0.12	0.11	0.09	0.07	0.05	0.11
3	0.17	0.17	0.16	0.15	0.14	0.13	0.12	0.10	0.07	0.04	0.11
4	0.20	0.20	0.19	0.18	0.17	0.16	0.14	0.11	0.08	0.07	0.15
5	0.26	0.25	0.25	0.24	0.23	0.22	0.20	0.16	0.12	0.09	0.19
6	0.32	0.31	0.31	0.30	0.29	0.27	0.25	0.22	0.17	0.12	0.23
7	0.36	0.36	0.35	0.34	0.33	0.31	0.27	0.21	0.15	0.11	0.25
8	0.36	0.35	0.35	0.34	0.33	0.31	0.27	0.21	0.15	0.12	0.28
9	0.46	0.46	0.46	0.44	0.44	0.42	0.38	0.32	0.24	0.18	0.36
10	0.77	0.76	0.76	0.71	0.65	0.57	0.47	0.37	0.27	0.20	0.63

of the waves. Cross-shore directed velocities are shown in Figure 4-13 in which positive velocity is offshore, and the thick horizontal black bars represent the bottom at each ADV location. Maximum offshore velocities occurred in the lower water column, indicating undertow. Although most of the data were directed offshore, the velocity profiles indicate that velocities were directed onshore near the surface. The figure shows a boundary layer present at each location. The vertical profile of longshore velocity is plotted in Figure 4-14, which also shows the presence of a boundary layer. The presence of a boundary layer has been observed in the field (Garcez Faria et al. 1998). Hamilton and Ebersole (2001) found the mean longshore current to be generally uniform with depth; however, their tests were conducted on a fixed bed with a smooth concrete bottom with minimal effects of bottom roughness. The present tests were conducted on a movable bed with sand (with a higher friction coefficient than smooth concrete), which
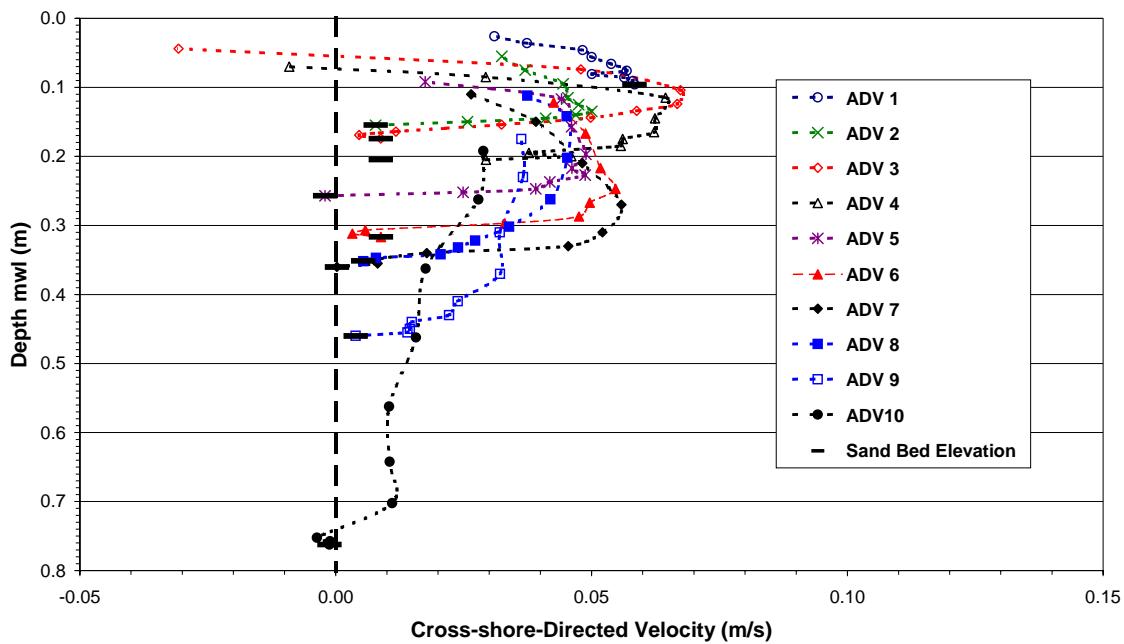
Figure 4-13. Cross-shore directed velocities as a function of depth, Test 1, Case 3
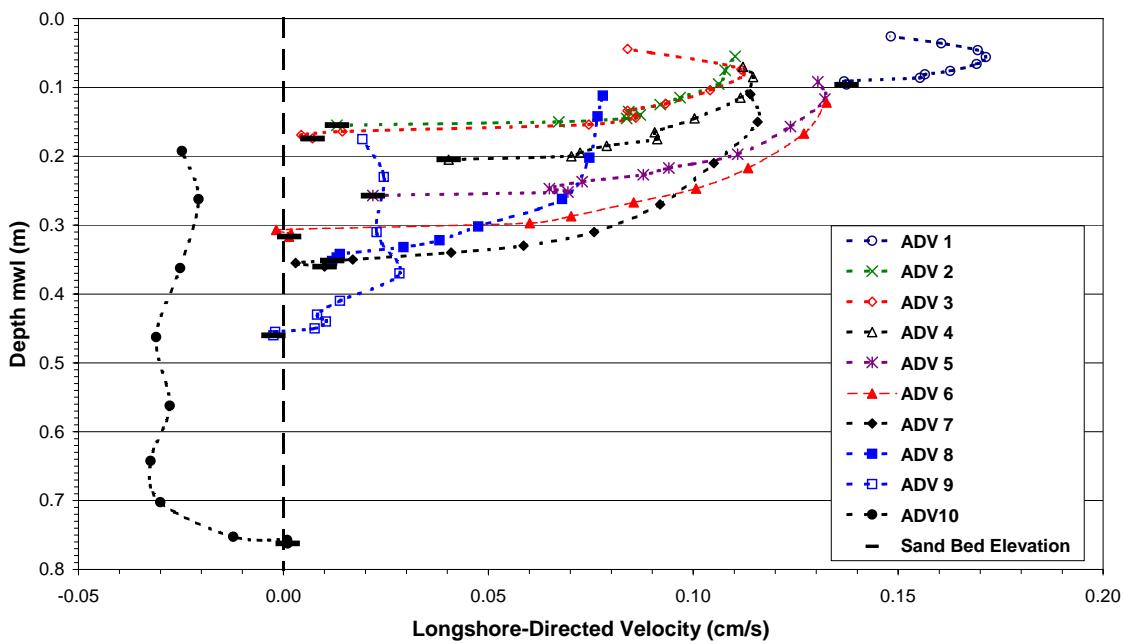
Figure 4-14. Longshore directed velocities as a function of depth, Test 1, Case 3

formed ripples that contributed to higher bottom roughness. Outside the surf zone, the vertical profiles were nearly invariant, a trend which also was observed by Hamilton and Ebersole (2001) for an irregular wave case on a fixed bed, but not for regular waves. Additionally, a theoretical model of Putrevu and Svendsen (1999) predicts a slight decrease of current speed with increasing distance from the bottom outside the surf zone. An increase in longshore velocity with distance from the bed occurred in the inner surf, which also was observed by Hamilton and Ebersole and agrees with the model of Putrevu and Svendsen.

All of the longshore current profiles in Figure 4-14 show positive directed flow with the exception of measurements at ADV10. The recirculated current at ADV 10 was due to the laboratory effect of the lateral boundaries.

The cross-shore distribution of the longshore current obtained at the one-third-water depth for Test 1, Case 3, is plotted in Figure 4-15. The current was slightly weaker in the inner surf zone than in the previous cases, but had the same distribution pattern.

Test 1, Case 3, wave height distribution through the surf zone is plotted in Figure 4-16. Gauges on the bridge were operating, but the gauges in front of each wave maker gave questionable results and were omitted from the figure. As with the previous cases, wave height was both steady and uniform alongshore.

Longshore sediment flux distribution with trap corrections is shown in Figure 4-17. Longshore sediment transport distribution increased slightly through the surf zone, but increased substantially to a maximum rate in the swash zone. Sediment flux distribution was nearly identical to Test 1, Case 2.
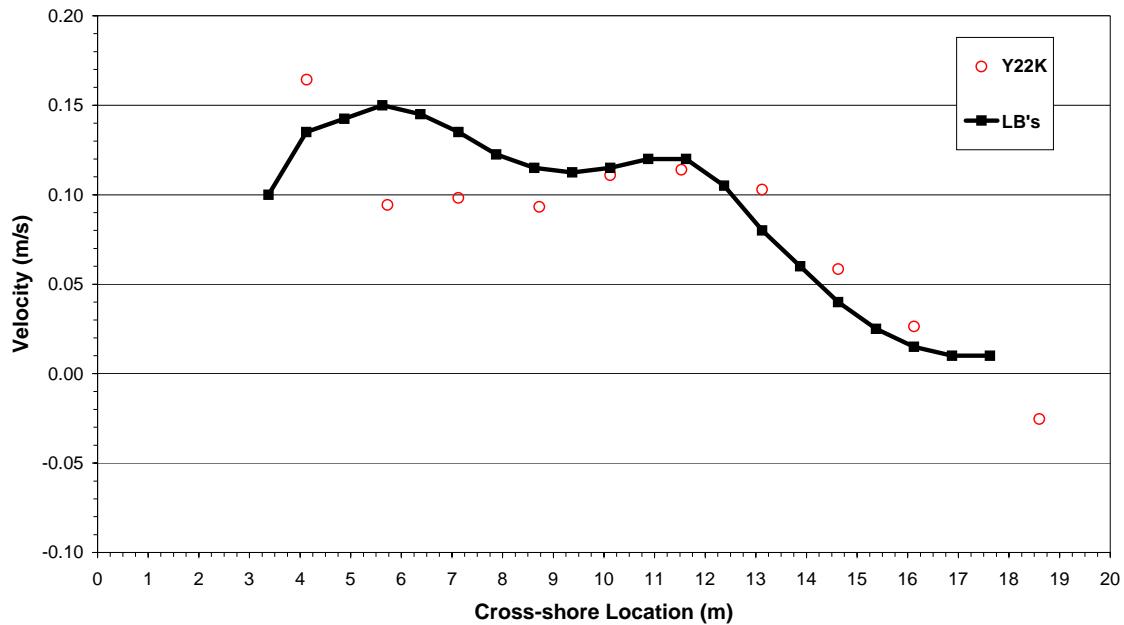
Figure 4-15. Cross-shore distribution of longshore currents, Test 1, Case 3
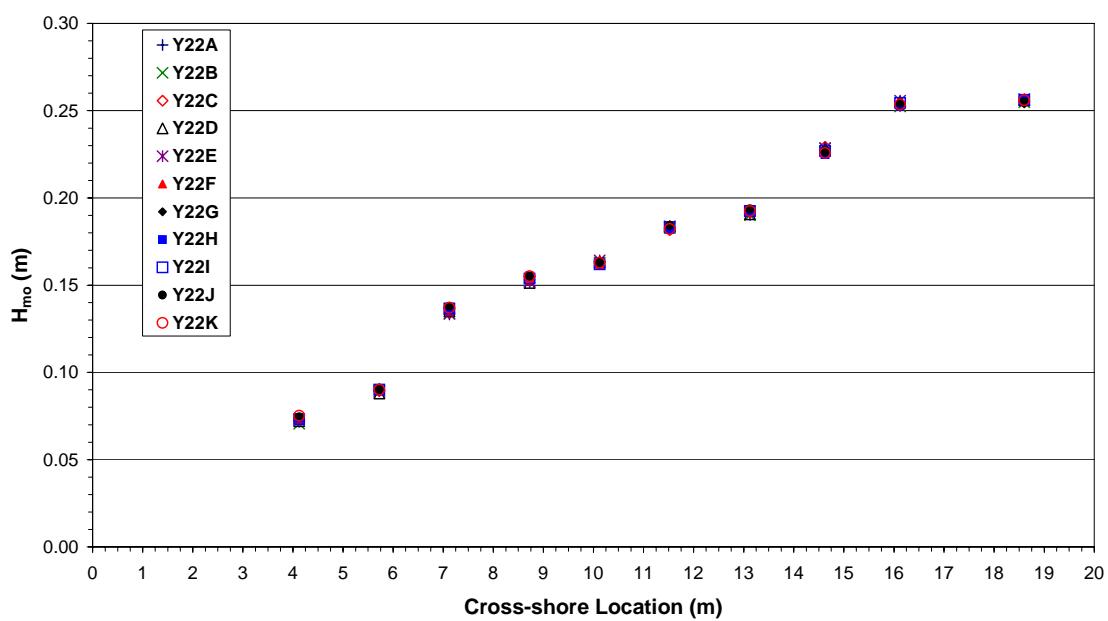

Figure 4-16. Cross-shore distribution of wave heights, Test 1, Case 3
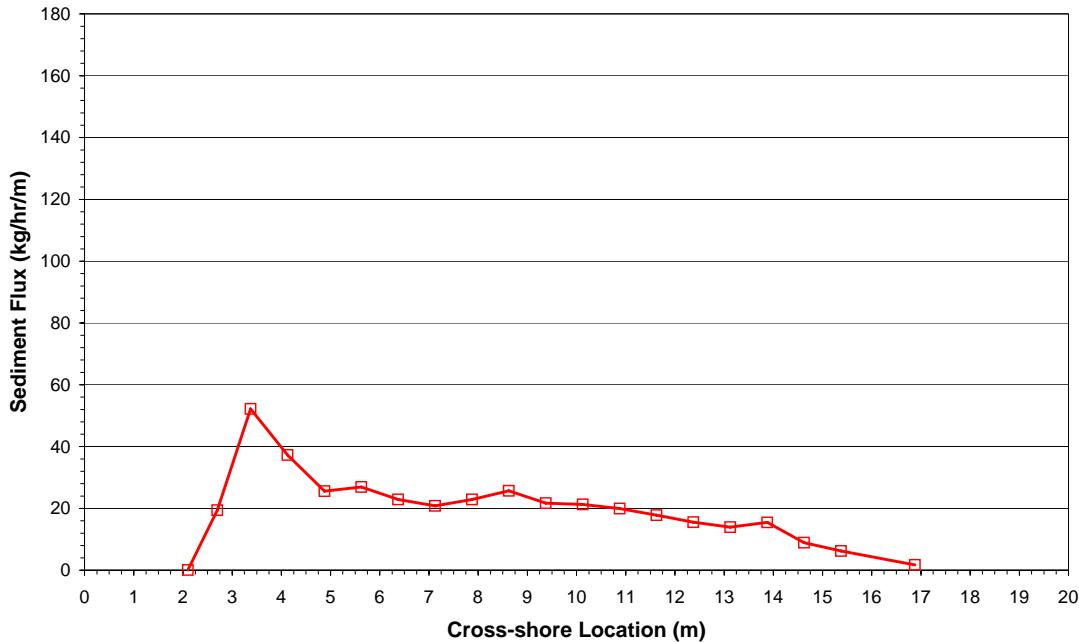
Figure 4-17. Cross-shore distribution of longshore sediment flux, Test 1, Case 3

Test 3

Test 3 consisted of waves having T_p = 3.0-sec and H_{mo} = 0.23-m wave that produced plunging-type breakers (ξ_b = 0.51). The wave spectrum measured directly in front of the wave generators (X = 21.4 m) is shown in Figure 4-18. The quasi-equilibrium beach profile developed after only 4 hr of wave action is plotted in Figure 4-19, which is an average of 16 profiles measured in the middle section of the test beach. Test 3 featured a breakpoint bar, which is associated with plunging breakers. The wave condition of Test 3 was dynamic, and it was difficult to maintain longshore uniformity. As a result, the beach required more frequent rebuilding than during Test 1, and test cases were
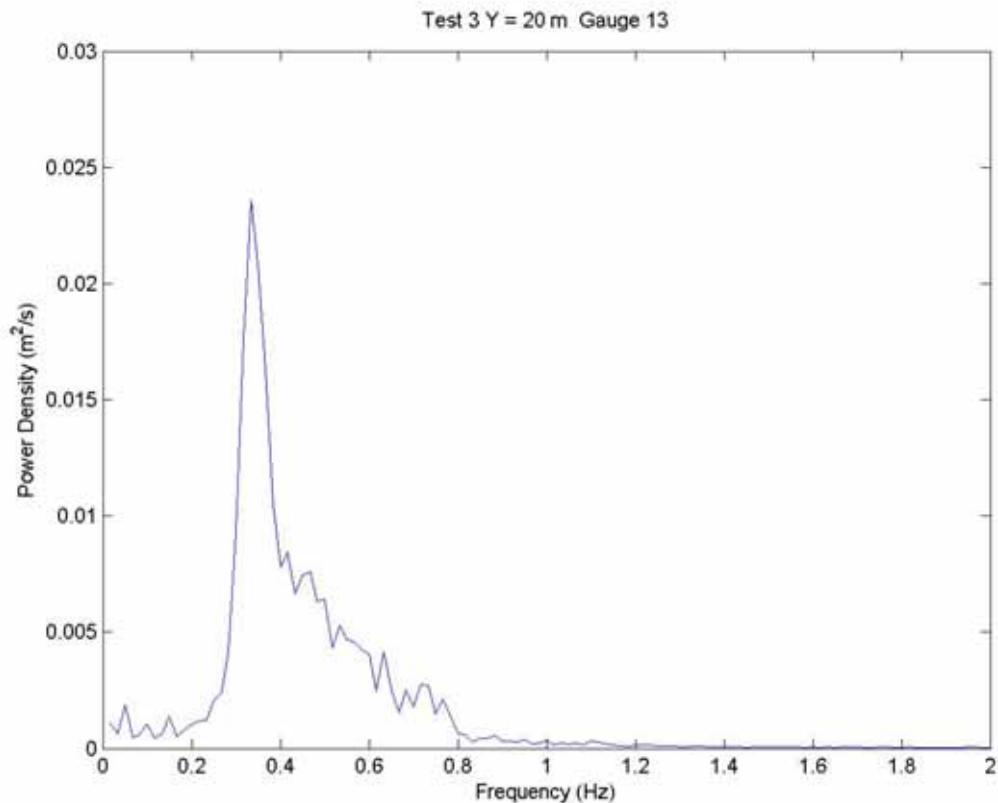
Figure 4-18. Measured incident wave spectra, Test 3

performed for shorter durations. Three cases were conducted for Test 3 wave conditions

and are described in the following paragraphs.

Test 3, Case 1

   The purpose of Test 3, Case 1, was to measure uniformity of the longshore current.

Measurements were made at four transects between $Y = 16$ to $Y = 30$ m. Duration of

Test 3, Case 1, was 0.87 hr.
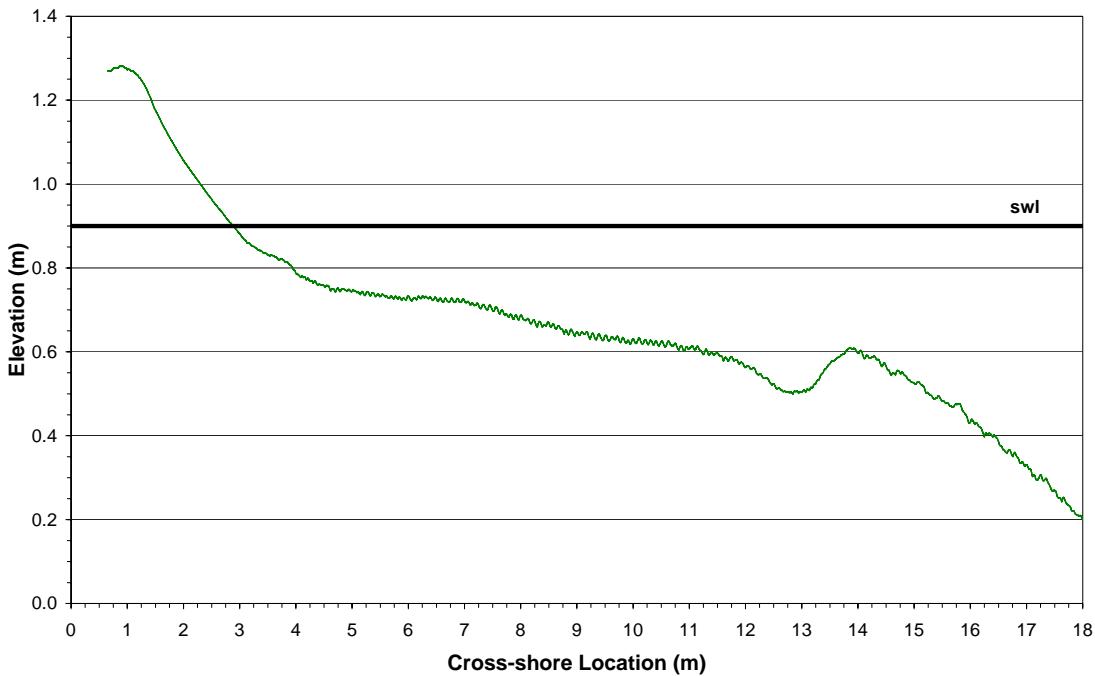
Figure 4-19. Quasi-equilibrium beach profile formed from Test 3 waves

Cross-shore distribution of longshore currents for Test 3, Case 1, is plotted in

Figure 4-20. Longshore current uniformity was reasonable in the mid-surf zone with the

exception of measurements at Y = 16 m.

All wave gauges were operating during the experiment with the exception Gauge 9.

The gauges fronting each wave generator were moved from the beach to the rail directly

in front of each wave machine, with cross-shore location of X = 21.4. The distribution

of wave height is plotted in Figure 4-21, which shows waves shoaling offshore of the

breakpoint and decreasing sharply directly shoreward of breaking. Wave heights were

similar to those of Test 1 in the inner surf zone. Wave heights were uniform except in

the region of the breakpoint bar and trough. Deviations in elevation of the breakpoint
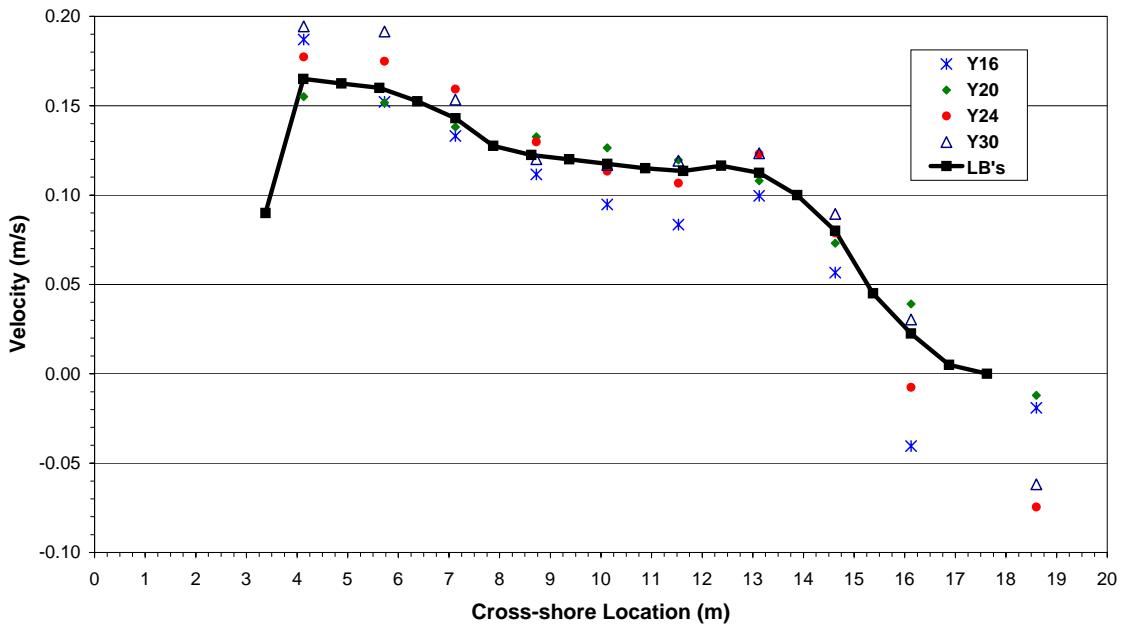
Figure 4-20. Cross-shore distribution of longshore currents, Test 3, Case 1
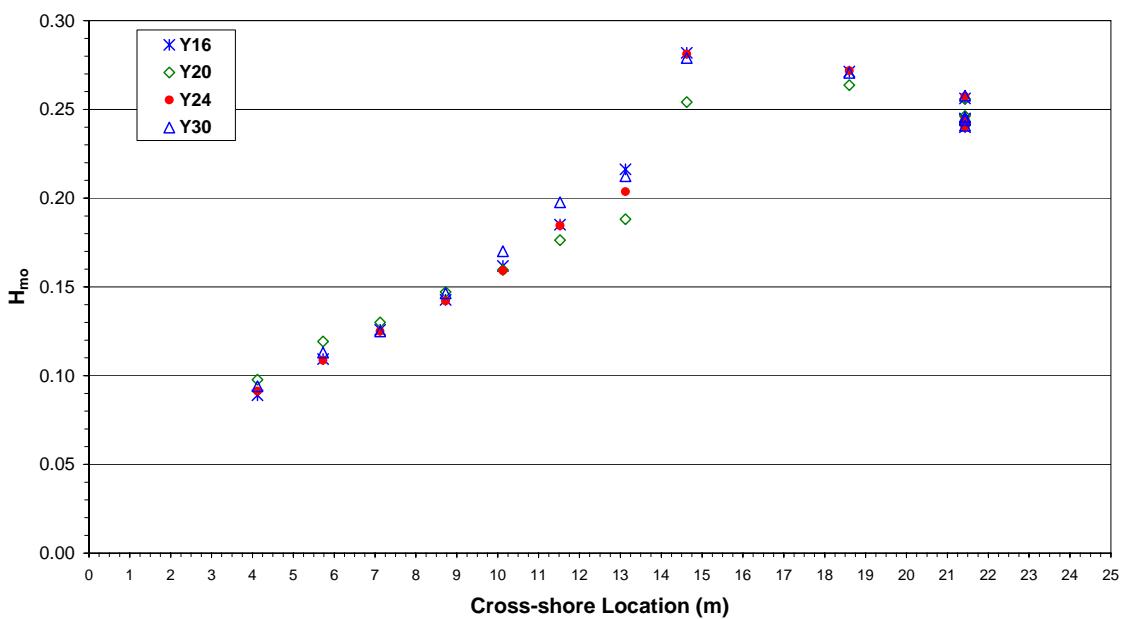
Figure 4-21. Cross-shore distribution of wave heights, Test 3, Case 1

bar were noted during the test, and the irregularities in bar height contributed to wave height variation in this vicinity.

Distribution of longshore sediment transport for Test 3, Case 1, is given in Figure 4-22. Unlike the sediment flux distributions of Test 1, a definitive peak in transport occurred near breaking with Test 3 waves. Shoreward of breaking and through the inner surf zone, longshore sediment flux was similar to Test 1 sediment flux in the same region. Sediment flux increased greatly in the swash zone, as it did for Test 1 waves; however, swash zone sediment flux for Test 3, Case 1, was greater than three times the flux measured during Test 1 conditions. The increasing trend in the swash
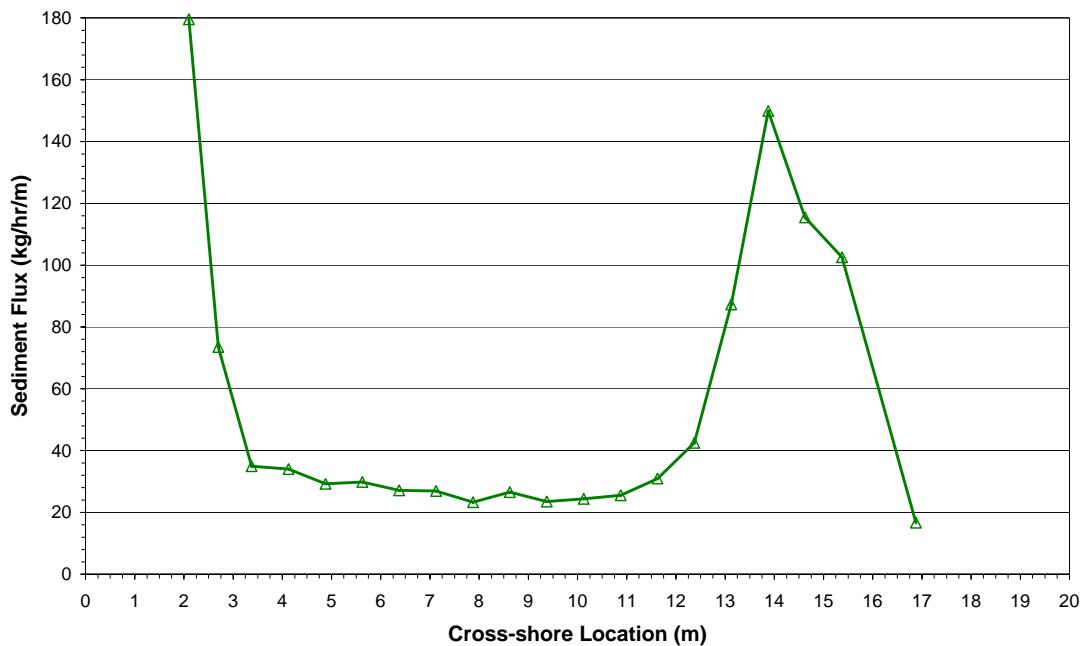
Figure 4-22. Cross-shore distribution of longshore sediment flux, Test 3, Case 1

zone raised a concern of potential bypassing of sediment around the landward end of the

traps. Observations during the test indicated that all of the sediment was trapped, and no

bypassing occurred.

Test 3, Case 2

Test 3, Case 2, was performed to measure the vertical distribution of longshore

currents through the water column. All measurements were obtained at Y = 20 m. The

velocity distribution was obtained at each ADV for eight vertical locations given in

Table 4-3. Duration of Test 3 Case 2 was 1.68 hr.

All ADVs were operational during the test except at ADV 4 at the highest

measurement location. Vertical distributions of the cross-shore and longshore directed

velocities are plotted in Figures 4-23 and 4-24, respectively. Measurements did not

extend to the bottom at ADV 10 for this test. The plots are similar to those of Test 1,

Table 4-3. Test 3, Case 2, ADV sampling depths

ADV				Sampling Depth (m)				
	Y20A	Y20B	Y20C	Y20D	Y20E	Y20F	Y20G	Y20H
1	0.150	0.140	0.130	0.120	0.110	0.080	0.050	0.010
2	0.188	0.178	0.168	0.158	0.148	0.108	0.058	0.008
3	0.216	0.206	0.196	0.186	0.166	0.116	0.066	0.006
4	0.254	0.244	0.234	0.214	0.184	0.134	0.074	0.004
5	0.267	0.257	0.247	0.227	0.187	0.137	0.077	-0.003
6	0.307	0.297	0.277	0.257	0.207	0.157	0.087	-0.003
7	0.395	0.385	0.355	0.325	0.275	0.195	0.095	-0.005
8	0.272	0.262	0.252	0.232	0.192	0.142	0.072	-0.008
9	0.403	0.393	0.363	0.333	0.283	0.203	0.103	-0.007
10	0.494	0.484	0.434	0.374	0.294	0.194	0.094	-0.006
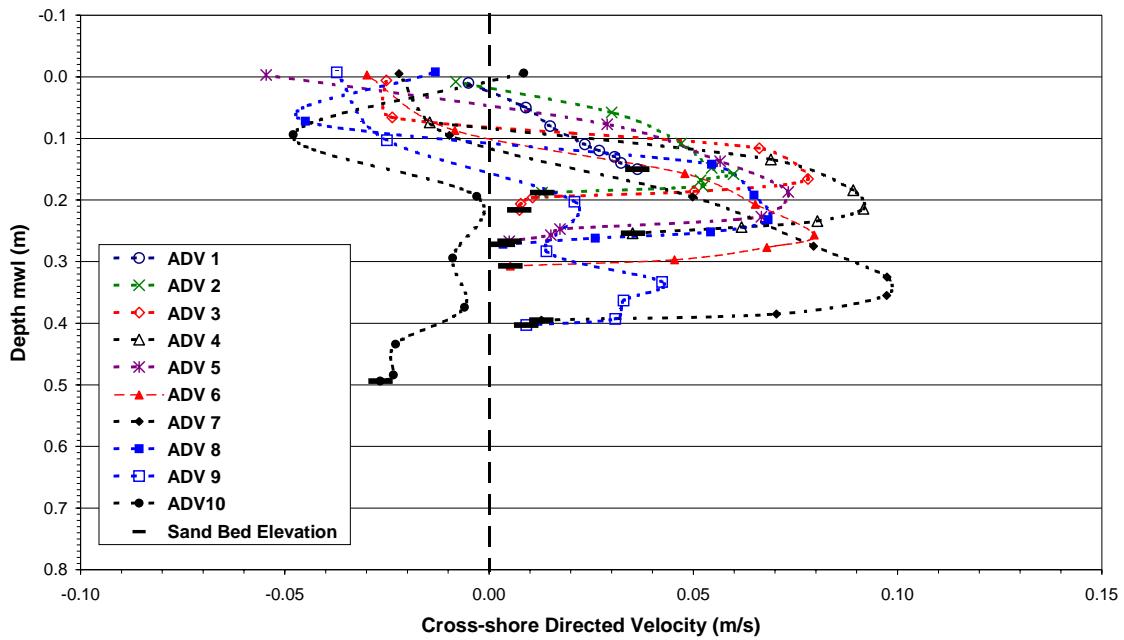
Figure 4-23. Cross-shore directed velocities as a function of depth, Test 3, Case 2
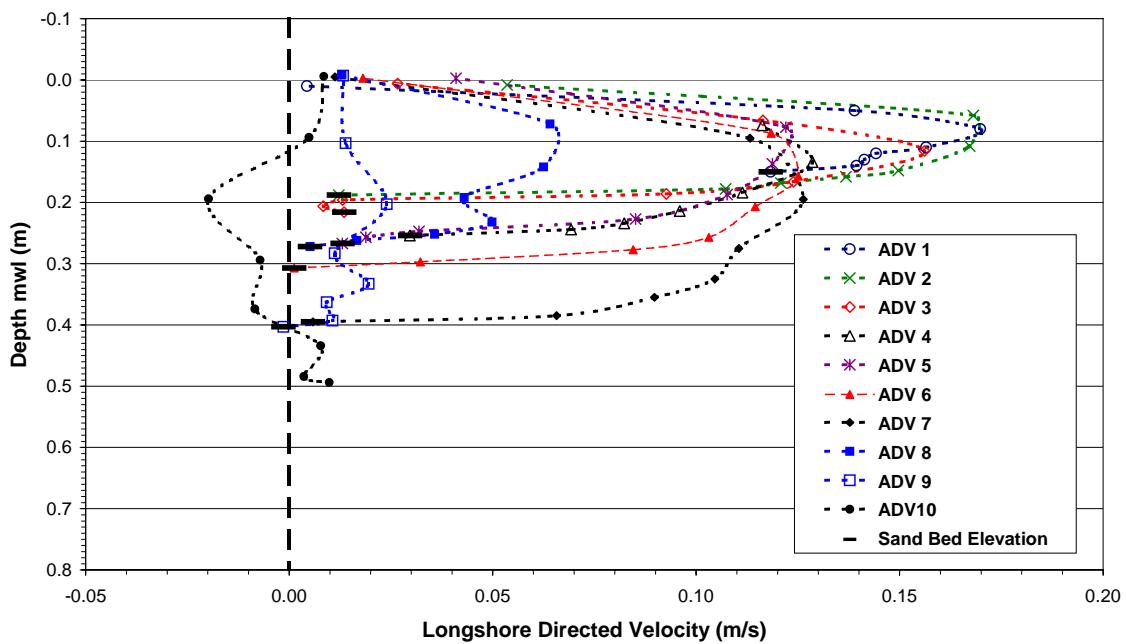
Figure 4-24. Longshore directed velocities as a function of depth, Test 3, Case 2

Case 3; a boundary layer was present in both the cross-shore and longshore directions, cross-shore velocities were directed onshore in the upper column and offshore in the lower water column, longshore velocities were generally invariant outside the surf zone, and longshore velocity increased with distance from the bed in the inner surf. No measurements were taken at the one-third depth; therefore, no plot is provided for the cross-shore distribution of longshore velocities.

Wave Gauges 2, 5, and 9 malfunctioned during the entire test; however, measurements at Gauge 5 during runs Y20c and Y20d were considered reliable. The cross-shore distribution of wave height for Test 3, Case 2, is plotted in Figure 4-25 with erroneous points omitted. The figure shows that waves were steady at $Y = 20$ m throughout the test.
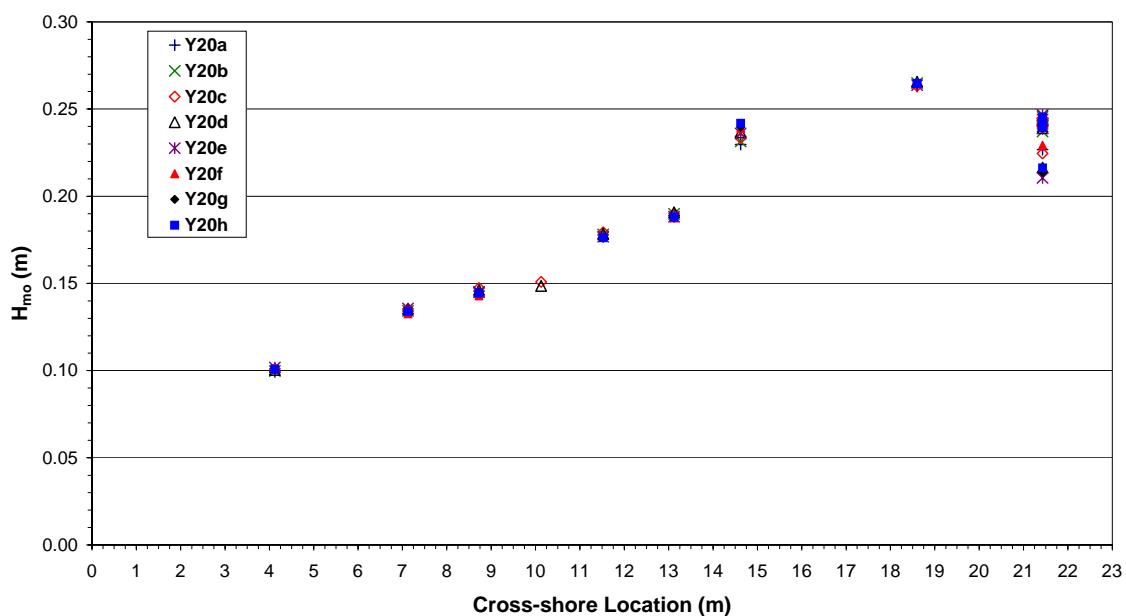
Figure 4-25. Cross-shore distribution of wave heights, Test 3, Case 2

Figure 4-26 plots the distribution of longshore sediment flux for Test 3, Case 2, exhibiting two peaks in transport that were similarly observed for Test 3, Case 1. The distribution was similar to that of Test 3, Case 1, except in the swash zone where a decrease in sediment flux occurred at the first sediment trap (X = 2.1 m).
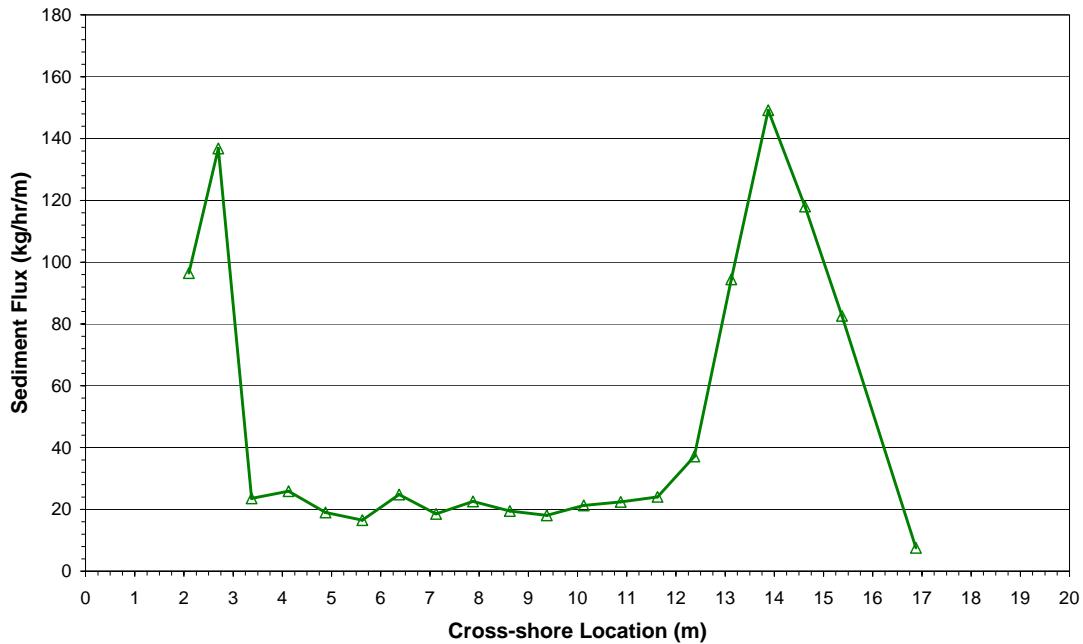
Figure 4-26. Cross-shore distribution of longshore sediment flux, Test 3, Case 2

Test 3, Case 3

The purpose of Test 3, Case 3, was to measure uniformity of the longshore current at locations not occupied during Test 3, Case 1. Measurements were made at four transects between Y = 18 and Y = 34 m. Duration of Test 3, Case 3, was 0.98 hr.

The distribution of the mean longshore current measured during Test 3, Case 3, is plotted in Figure 4-27. Measurements at Y = 34 m, which is near the upstream boundary, deviated greatly from pumped values. Measurements in the middle section of the test beach between Y = 18 and Y = 26 m exhibited more longshore uniformity. However, the longshore current was not as uniform as observed in Test 3, Case 1.
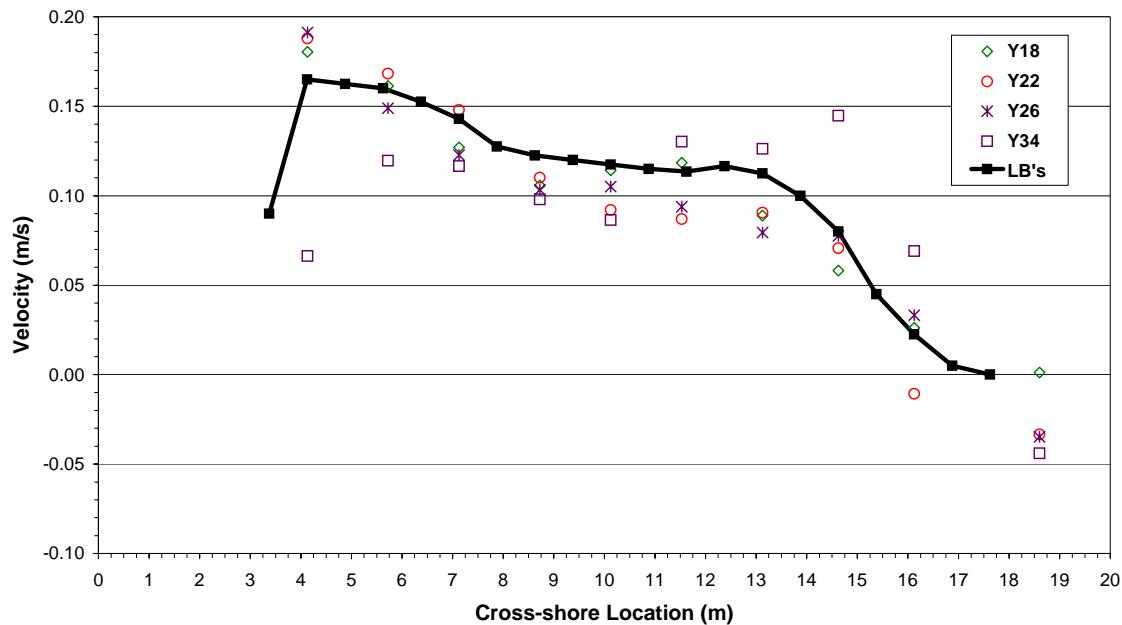
Figure 4-27. Cross-shore distribution of longshore currents, Test 3, Case 3

Wave Gauges 5 and 9 were not operating during the test. Wave height distribution and mean water surface elevations are plotted in Figure 4-28. Waves shoaled offshore of breaking, and decayed sharply shoreward of the break point. Wave height varied alongshore and was not as uniform as in Test 3, Case 1.
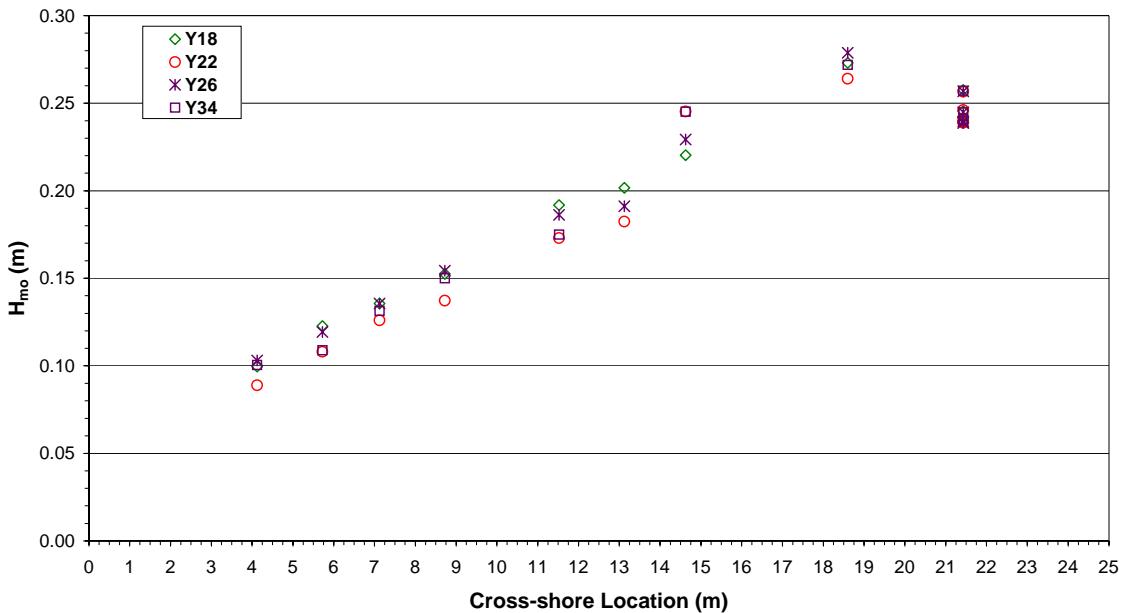
Figure 4-28. Cross-shore distribution of wave heights, Test 3, Case 3

Figure 4-29 plots the distribution of longshore sediment flux for Test 3, Case 3. The distribution was similar to the previous two Test 3 cases, with a peak in transport near breaking and a peak in the swash zone. Similar to Test 3, Case 1, and unlike Test 3, Case 2, swash zone transport does not decrease at the first sediment trap at X = 2.1 m.
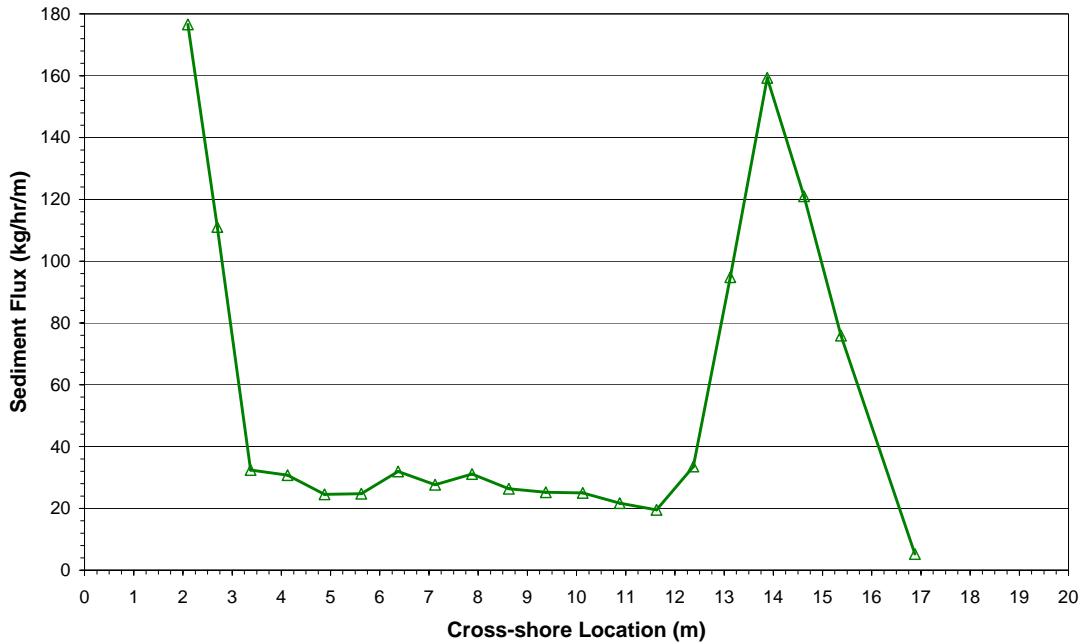
Figure 4-29. Cross-shore distribution of longshore sediment flux, Test 3, Case 3

Test 5

Test 5 consisted of waves having T_p = 1.5-sec and H_{mo} = 0.16-m waves, which

produced spilling breakers (ξ_b = 0.38). The wave spectrum measured directly in front of

the wave generators (X = 21.4 m) is plotted in Figure 4-30. The quasi-equilibrium beach

profile after 17 hr of wave action is plotted in Figure 4-31, which is an average of four

profiles measured in the middle section of the test beach. The survey was performed

with a graduated rod, and the points represent measurement locations. Three cases were

performed for Test 5 wave conditions and are described in the following paragraphs.
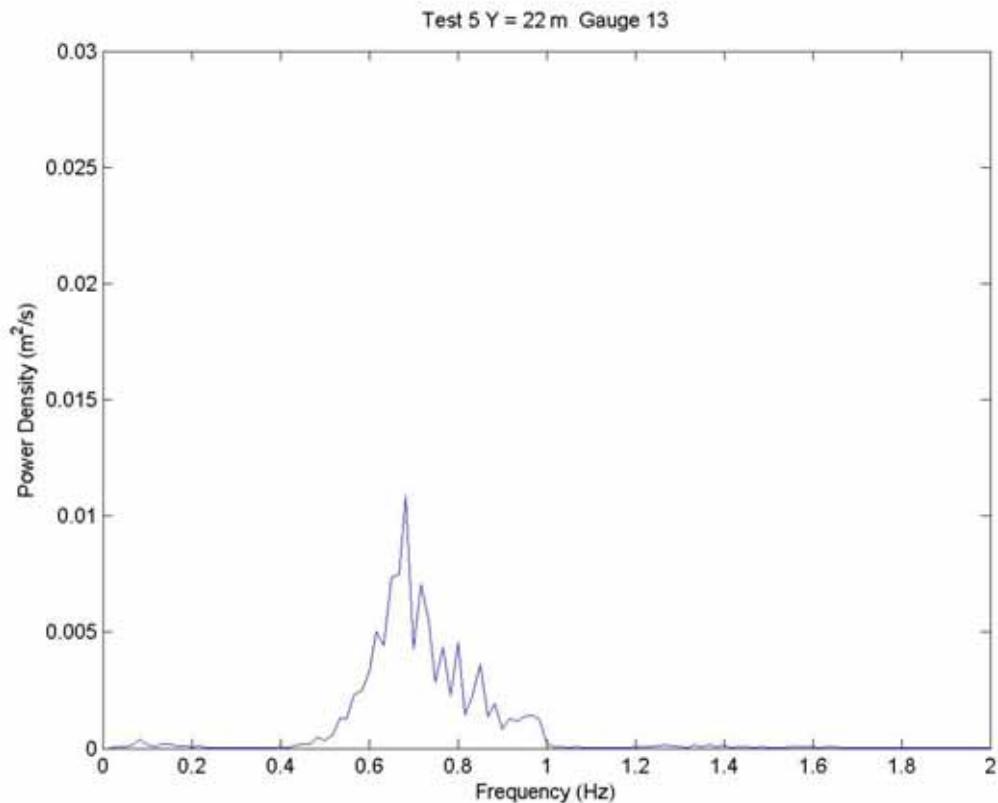
Figure 4-30. Measured incident wave spectra, Test 5

Test 5, Case 1

The purpose of Test 5, Case 1, was to measure uniformity of the longshore current. Measurements were made at 11 transects spaced at 2-m alongshore between $Y = 16$ and $Y = 34$ m. Duration of Test 5, Case 1, was 2.67 hr.

The cross-shore distribution of the longshore current is plotted in Figure 4-32. Uniformity was generally good in the middle section of the beach between $Y = 18$ m and $Y = 30$ m, with exception in the inner surf zone where the current at $Y = 18$, 20, and 30 m deviated from pumped values.
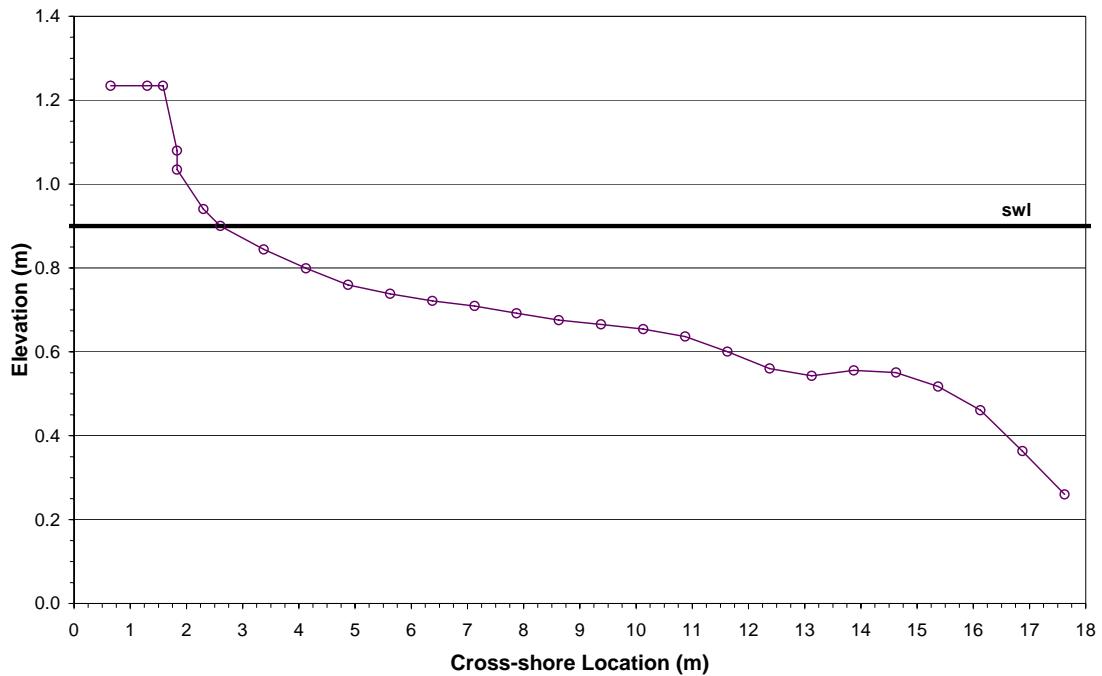
Figure 4-31. Quasi-equilibrium beach profile formed from Test 5 waves
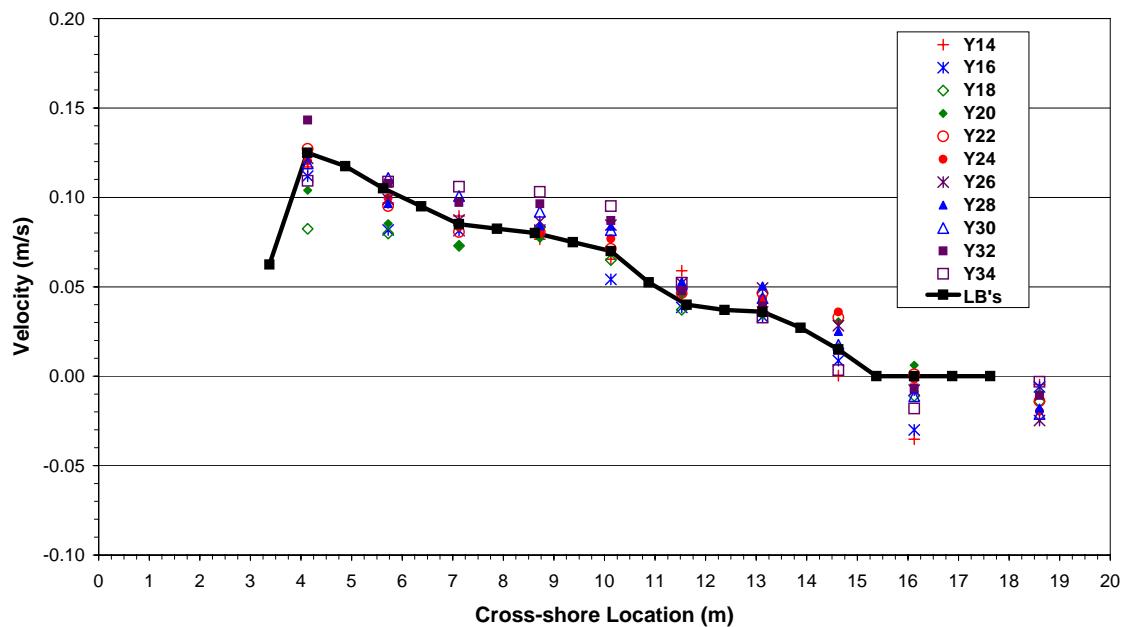
Figure 4-32. Cross-shore distribution of longshore currents, Test 5, Case 1

Cross-shore wave height distribution for Test 5, Case 1, is plotted in Figure 4-33. Wave height gradually decreased across the surf zone. All gauges were operational during the test. Heights recorded at Gauge 3 were lower than expected and the cause is not known.

Longshore sediment flux distribution is plotted in Figure 4-34. Sediment flux increased gradually through the surf zone and peaked in the swash zone. The trend was similar to the Test 1 longshore sediment flux, but with much lower values in the surf zone. The transport rate was greatest in the swash zone and was essentially the same rate observed for Test 1, Cases 2 and Case 3, but with a different cross-shore location.
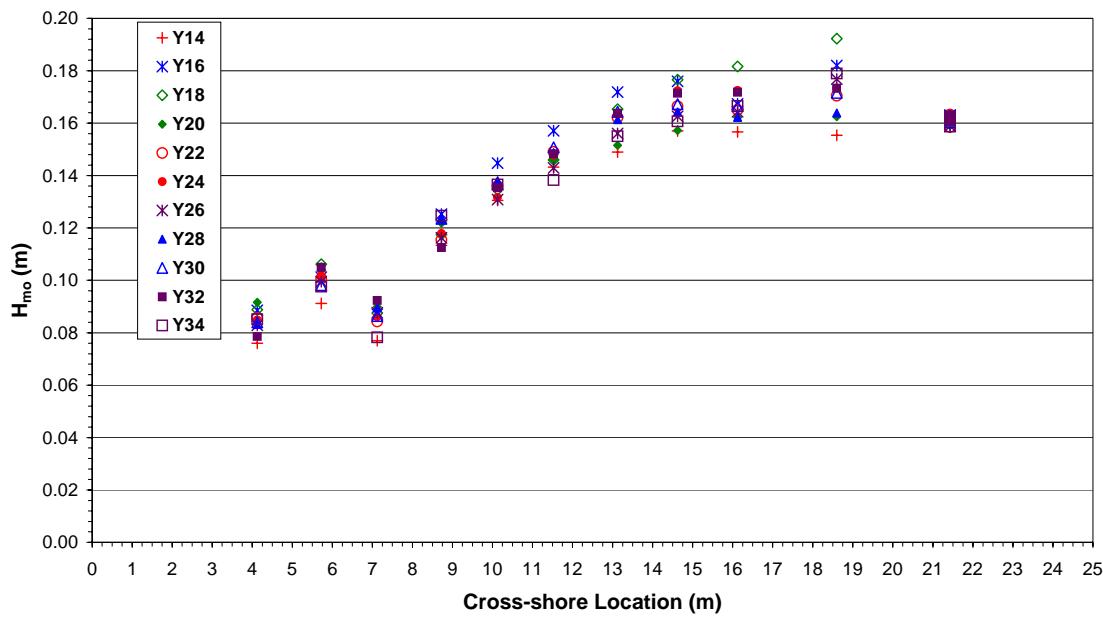

Figure 4-33. Cross-shore distribution of wave heights, Test 5, Case 1
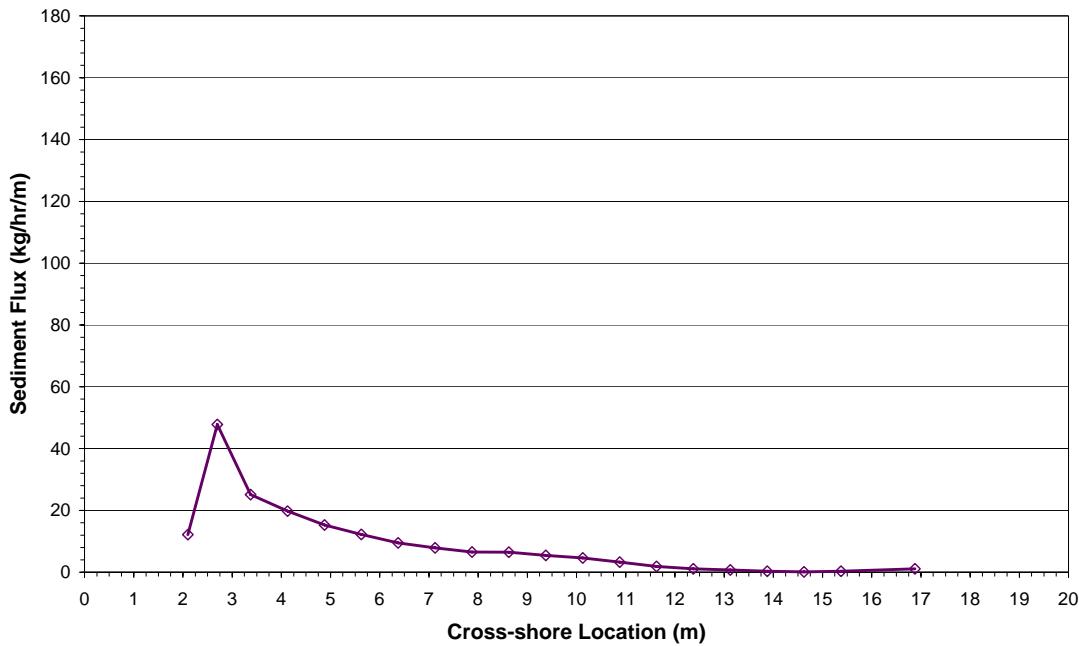
Figure 4-34. Cross-shore distribution of longshore sediment flux, Test 5, Case 1

Test 5, Case 2

The purpose of Test 5, Case 2, was to measure steadiness of the longshore current. Three different measurements with an approximate temporal spacing of 1 hr were made at four transects between Y18 and Y30. Duration of Test 5, Case 2, was 2.75 hr.

Velocity measurements at ADV 7 gave erroneous values for transects Y22A through Y30B. The cross-shore distribution of the longshore current obtained at the one-third-water depth show magnitudes similar to those of Test 5, Case 1 (Figure 4-35). Measurements were constant at each location throughout the test, indicating a steady condition (Figures 4-36 through 39).
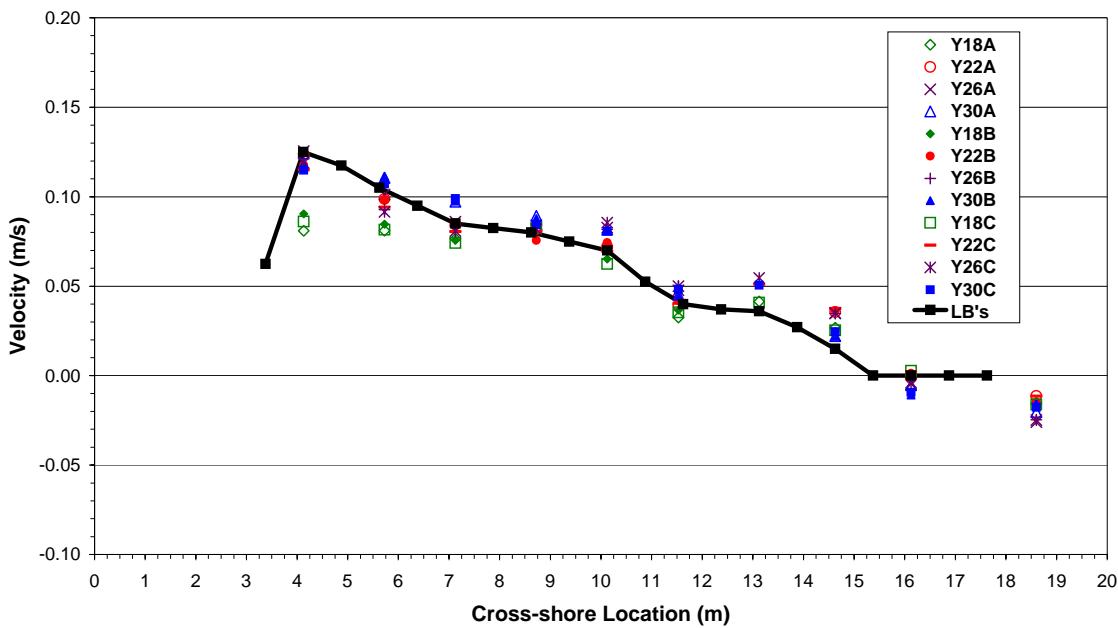
Figure 4-35. Cross-shore distribution of longshore currents, Test 5, Case 2
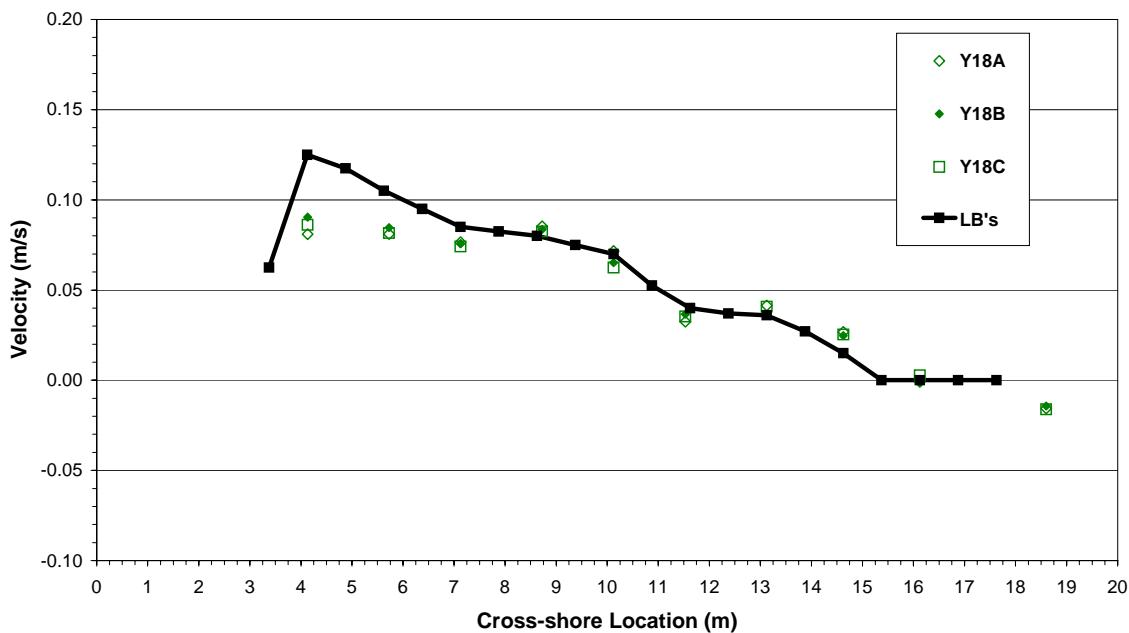
Figure 4-36. Cross-shore distribution of longshore currents, Test 5, Case 2, Y = 18 m
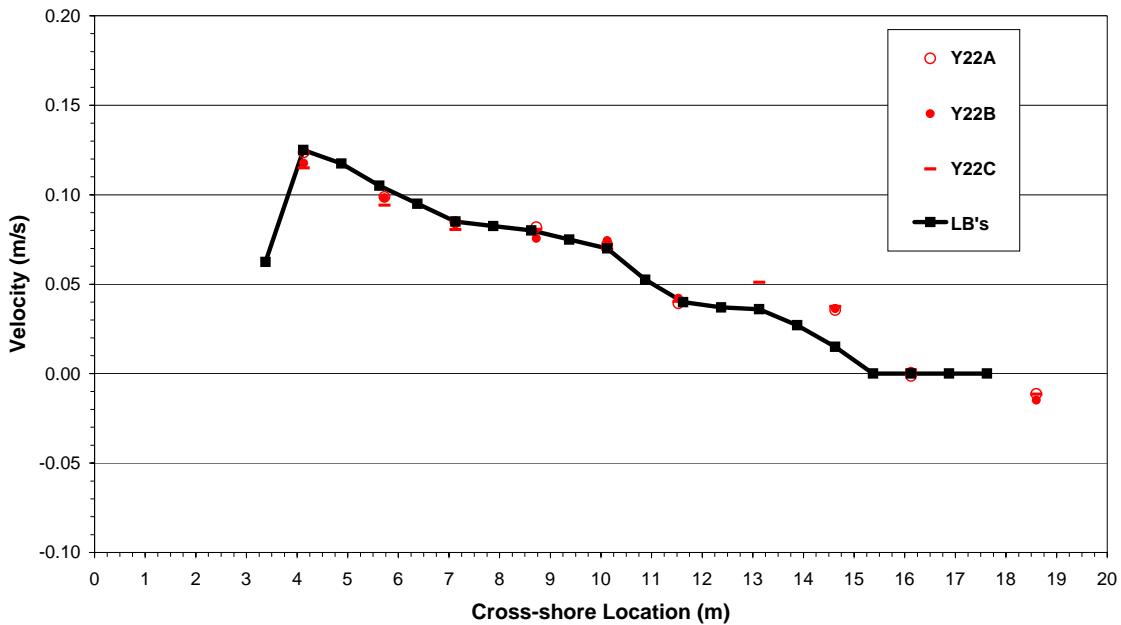
Figure 4-37. Cross-shore distribution of longshore currents, Test 5, Case 2, Y = 22 m
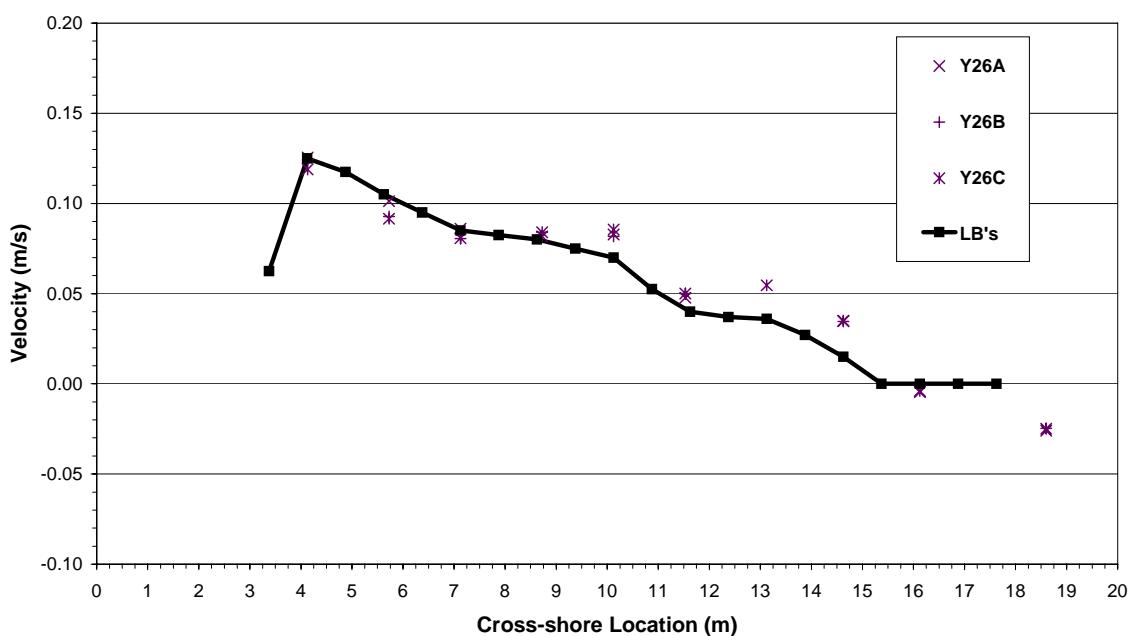
Figure 4-38. Cross-shore distribution of longshore currents, Test 5, Case 2, Y = 26 m
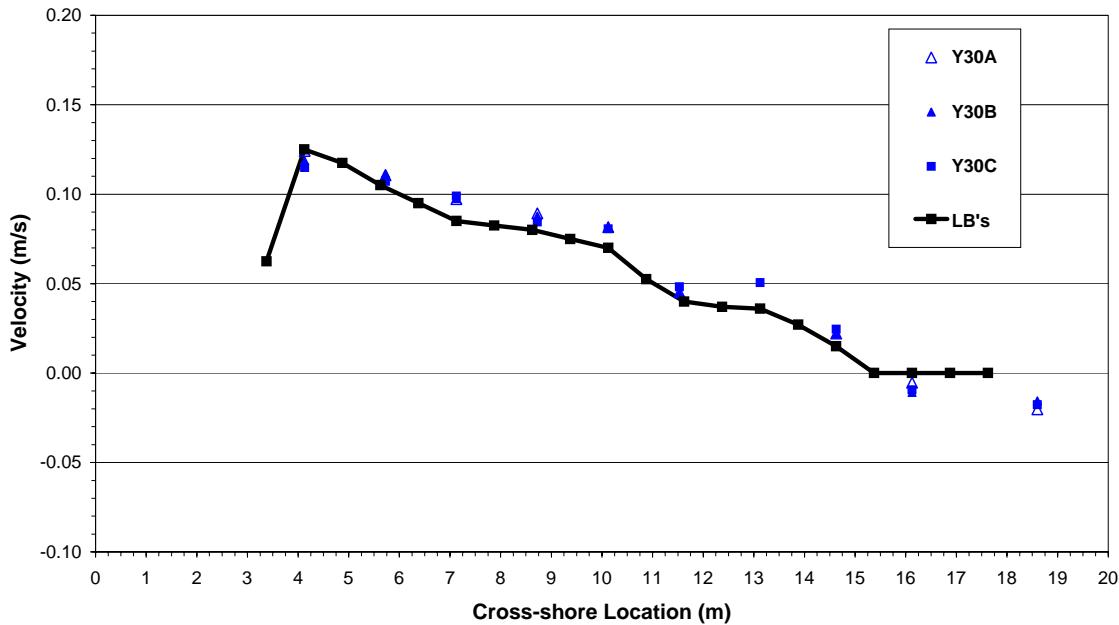
Figure 4-39. Cross-shore distribution of longshore currents, Test 5, Case 2, Y = 30 m

Wave height distribution through the surf zone is plotted in Figure 4-40. The figure shows that waves were steady with longshore location and, with the exception of measurements at Y = 18 m, wave height was generally uniform.

Longshore sediment flux distribution with trap corrections is plotted in Figure 4-41. The distribution was similar to that of Test 5, Case 1, flux gradually increased through the surf zone and a peaked in the swash zone. However, the peak sediment flux of Test 5, Case, 2 was approximately 80 percent of the peak measured during Test 5, Case 1.
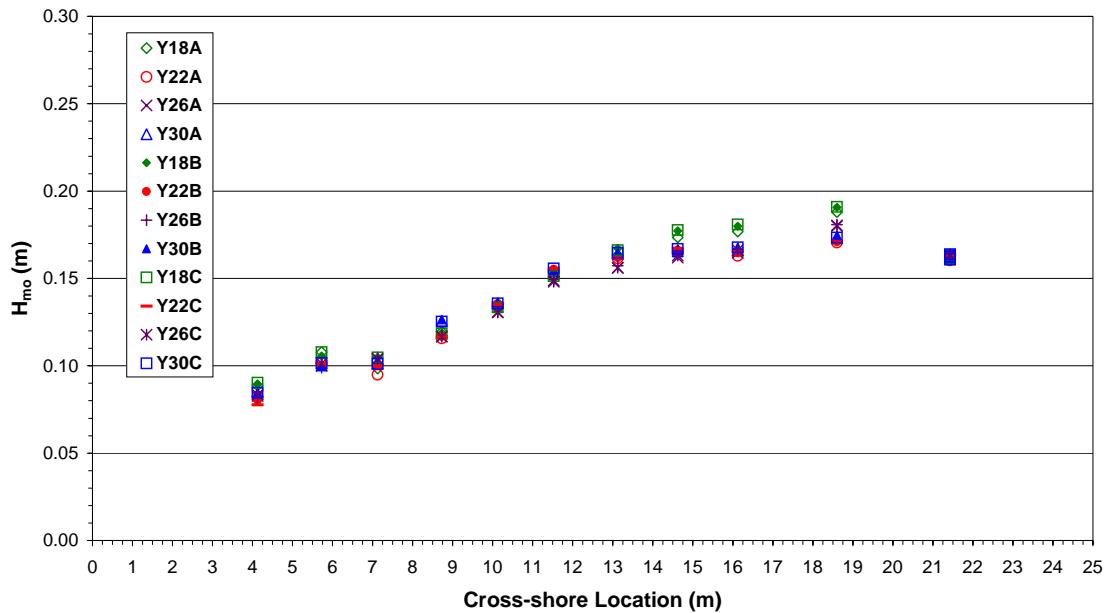
Figure 4-40. Cross-shore distribution of wave heights, Test 5, Case 2
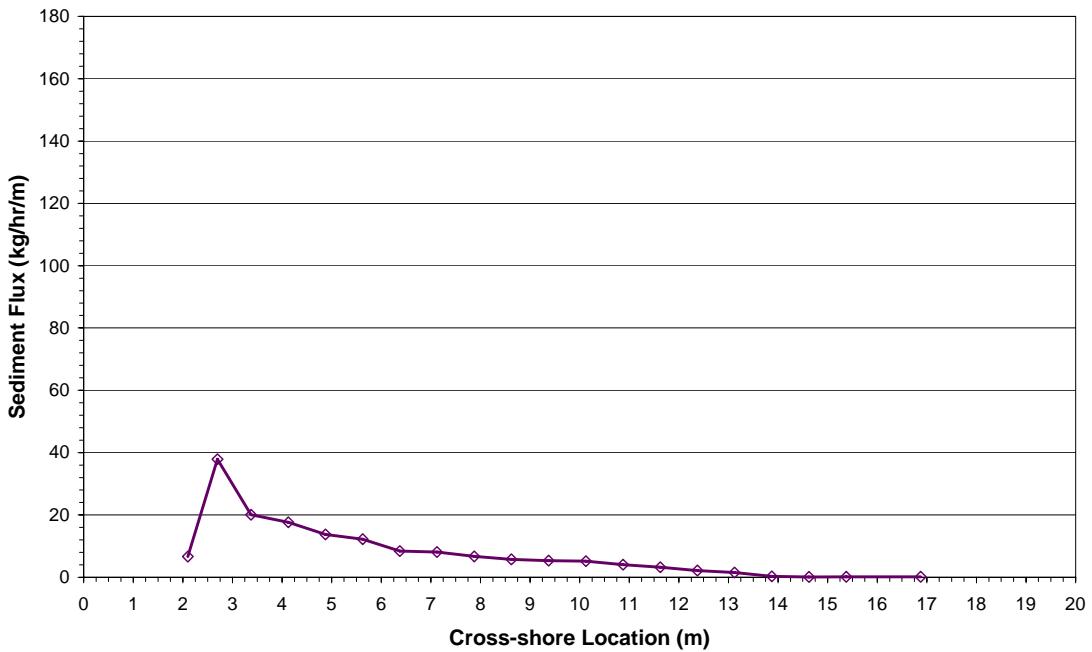
Figure 4-41. Cross-shore distribution of longshore sediment flux, Test 5, Case 2

Test 5, Case 3

The purpose of Test 5, Case 3, was to measure the vertical distribution of the

longshore current through the water column. All measurements were obtained at

Y = 22 m. Measurements were made at eleven vertical positions with all gauges.

Table 4-4 gives the vertical location of the ADV sampling volume for each. Duration of

Test 5, Case 3, was 2.42 hr.

Table 4-4. Test 5, Case 3, ADV sampling depths

ADV	Sampling Depth (m)										
	Y22A	Y22B	Y22C	Y22D	Y22E	Y22F	Y22G	Y22H	Y22I	Y22J	Y22K
1	0.07	0.06	0.06	0.06	0.05	0.04	0.04	0.03	0.02	0.01	0.04
2	0.16	0.16	0.15	0.14	0.14	0.13	0.12	0.10	0.08	0.06	0.10
3	0.18	0.18	0.17	0.17	0.15	0.14	0.13	0.11	0.08	0.05	0.12
4	0.23	0.22	0.22	0.21	0.20	0.19	0.17	0.14	0.11	0.09	0.15
5	0.24	0.23	0.23	0.22	0.21	0.2	0.18	0.14	0.10	0.07	0.16
6	0.29	0.28	0.28	0.27	0.26	0.24	0.22	0.19	0.14	0.09	0.19
7	0.35	0.34	0.34	0.33	0.32	0.30	0.26	0.20	0.14	0.10	0.23
8	0.35	0.34	0.34	0.33	0.32	0.30	0.26	0.20	0.14	0.11	0.24
9	0.44	0.44	0.43	0.42	0.41	0.39	0.35	0.29	0.21	0.16	0.29
10	0.76	0.75	0.70	0.58	0.47	0.41	0.35	0.27	0.17	0.61	0.50

All ADVs were operational during the test.   Vertical distributions of the cross-shore

and longshore-directed velocities are plotted in Figures 4-42 and 4-43, respectively.

Measurements did not extend to the bottom at ADV 10 for this test. A boundary layer

was present in both the cross-shore and longshore directions, similar to the previous

tests. The cross-shore velocity measurements indicate a current directed onshore near

the surface and offshore lower in the water column. In the longshore direction, ADVs 9
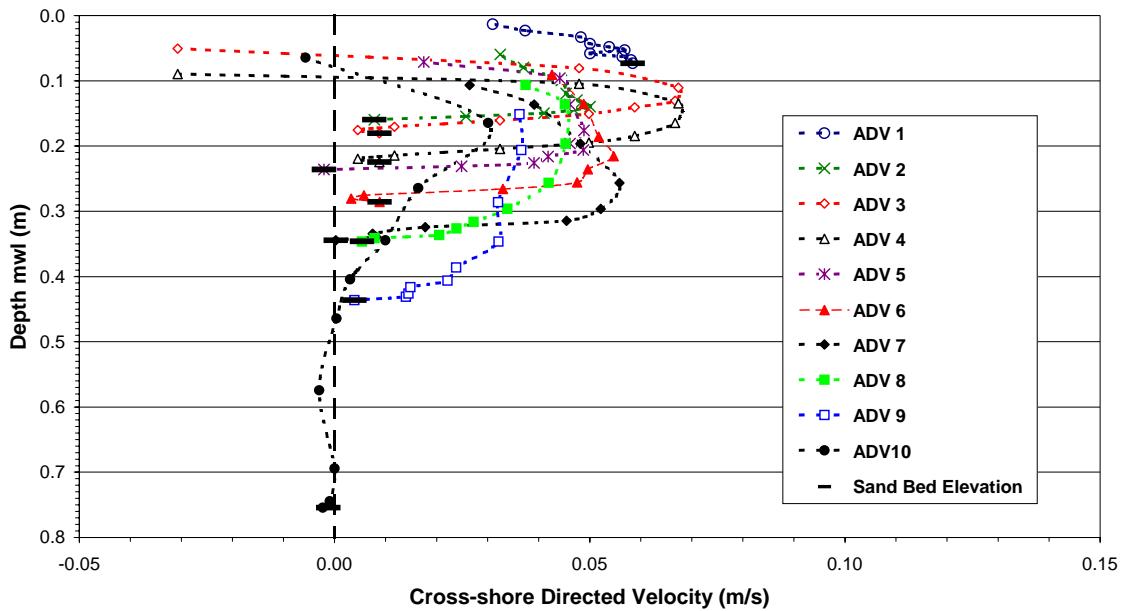
Figure 4-42. Cross-shore directed velocities as a function of depth, Test 5, Case 3
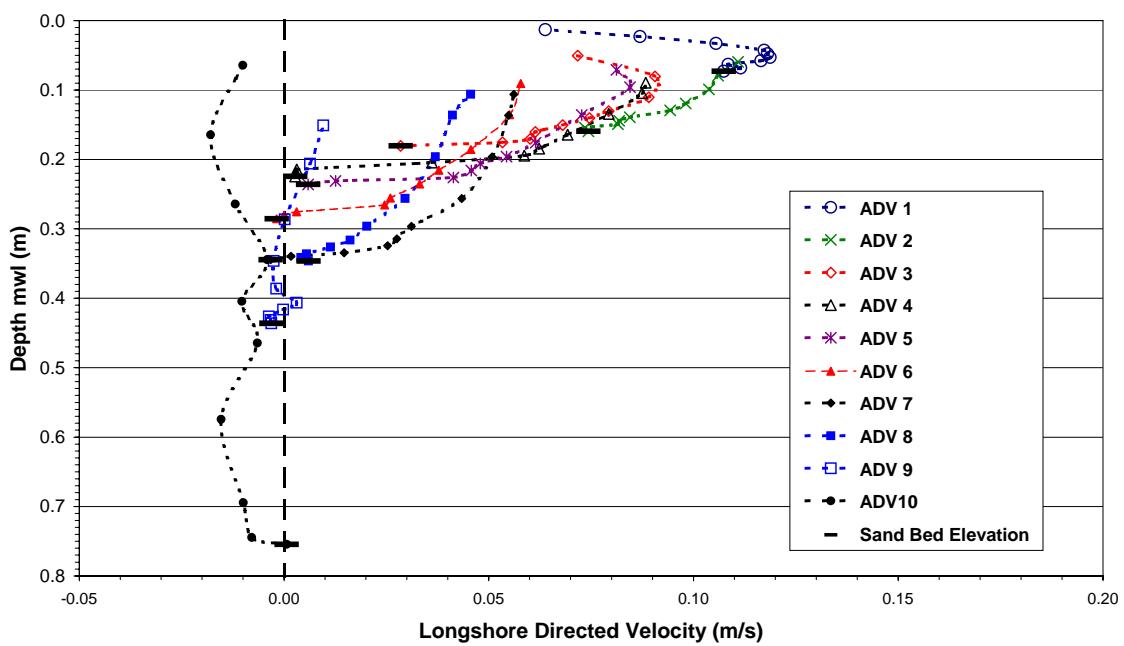
Figure 4-43. Longshore directed velocities as a function of depth, Test 5, Case 3

and 10, which were located outside the surf zone, showed invariant profiles with depth. Additionally, longshore velocity increased with distance from the bed in the inner surf zone. The cross-shore distribution of the longshore current obtained at the one-third water depth for Test 5, Case 3, was similar to Test 5, Case 1 and Case 2 (Figure 4-44).

The cross-shore distribution of wave heights for Test 5, Case 3, is plotted in Figure 4-45. Wave height was consistent throughout the test at Y = 22 m and was similar to the previous cases of Test 5, with the exception of Gauges 2 and 3; heights at Gauge 2 were smaller than observed in the earlier cases, and heights at Gauge 3 were greater than previously observed.
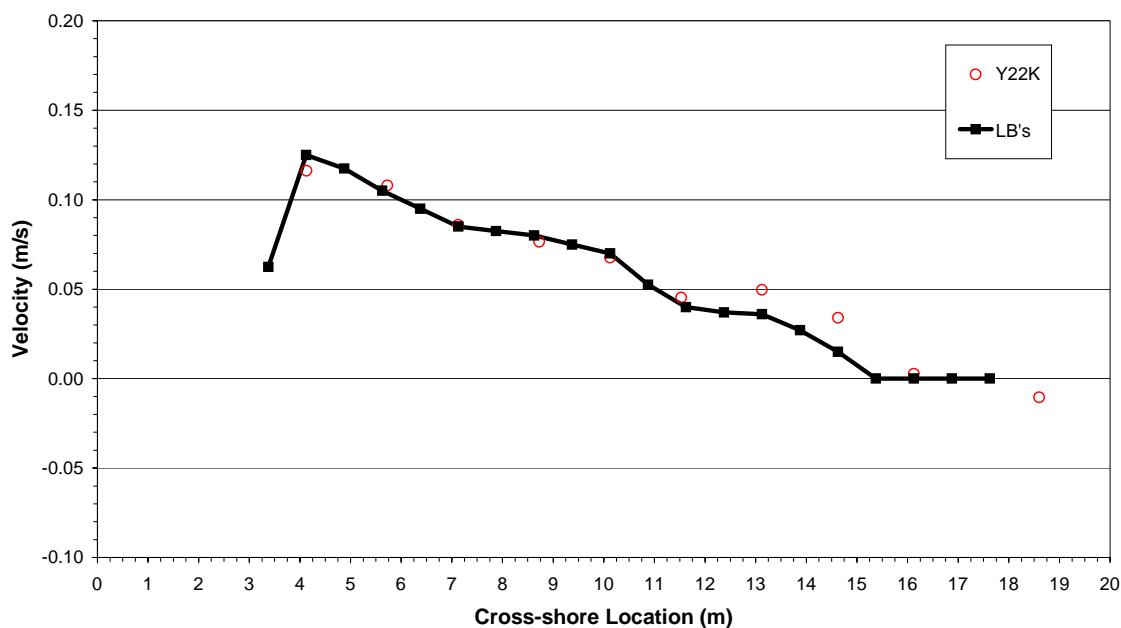

Figure 4-44. Cross-shore distribution of longshore currents, Test 5, Case 3
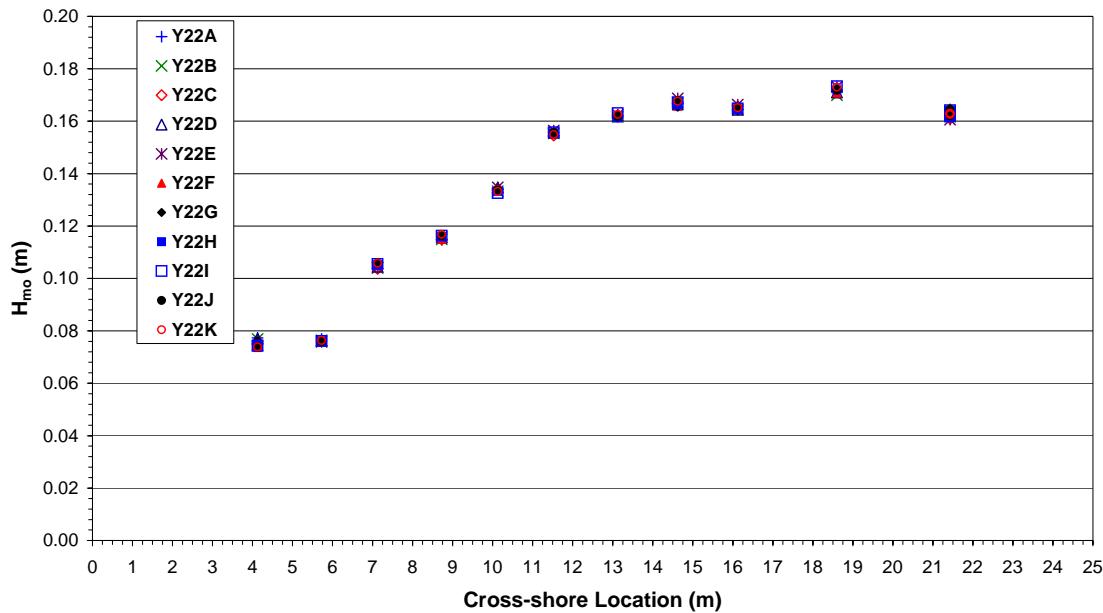
Figure 4-45. Cross-shore distribution of wave heights, Test 5, Case 3

Figure 4-46 shows the cross-shore distribution of sediment flux for Test 5, Case 3. The longshore transport rate was similar to the previous Test 5 cases, but the peak in the swash zone was less, almost half of the measured peak of Test 5, Case 1.
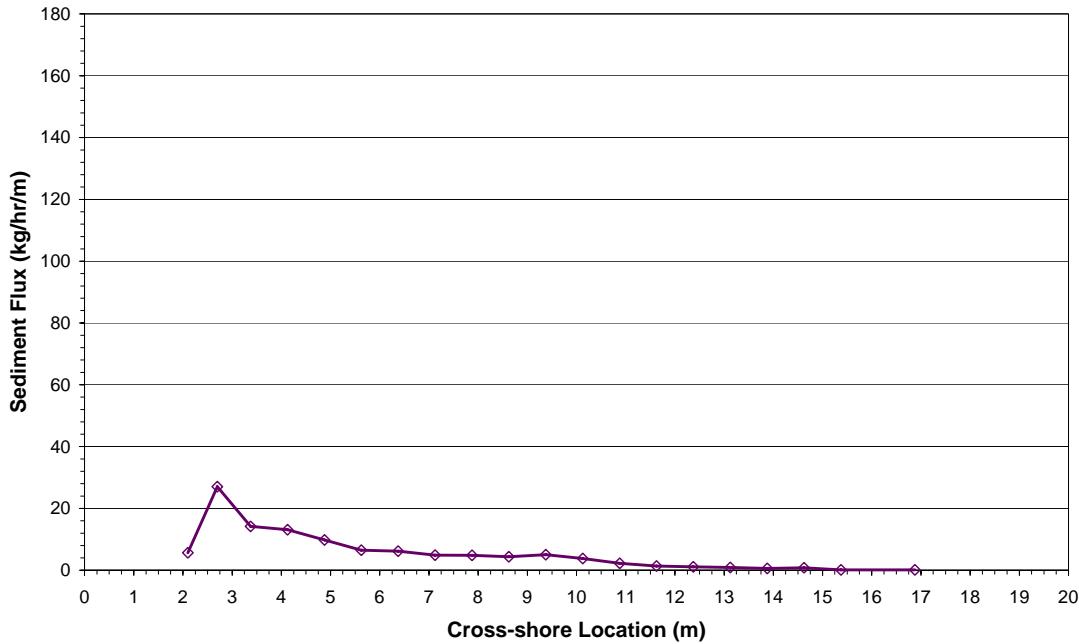
Figure 4-46. Cross-shore distribution of longshore sediment flux, Test 5, Case 3

Test 6

Waves having $T_p = 3.0$ sec and $H_{mo} = 0.19$ m, which produced plunging breakers

($\xi_b = 0.50$), were generated for Test 6. The measured wave spectrum directly in front of

the wave generators (X = 21.4 m) is plotted in Figure 4-47. The quasi-equilibrium beach

profile obtained at Y = 22 m using an ultra-sonic profile for the underwater portion of

the beach and a rod above the swl is shown in Figure 4-48 after 23 hr of wave action.

The points in the figure represent rod measurement locations. Only one case is

presented for Test 6. It was difficult to maintain beach uniformity during the iterative

process, and the proper pump settings were not determined. However, the longshore
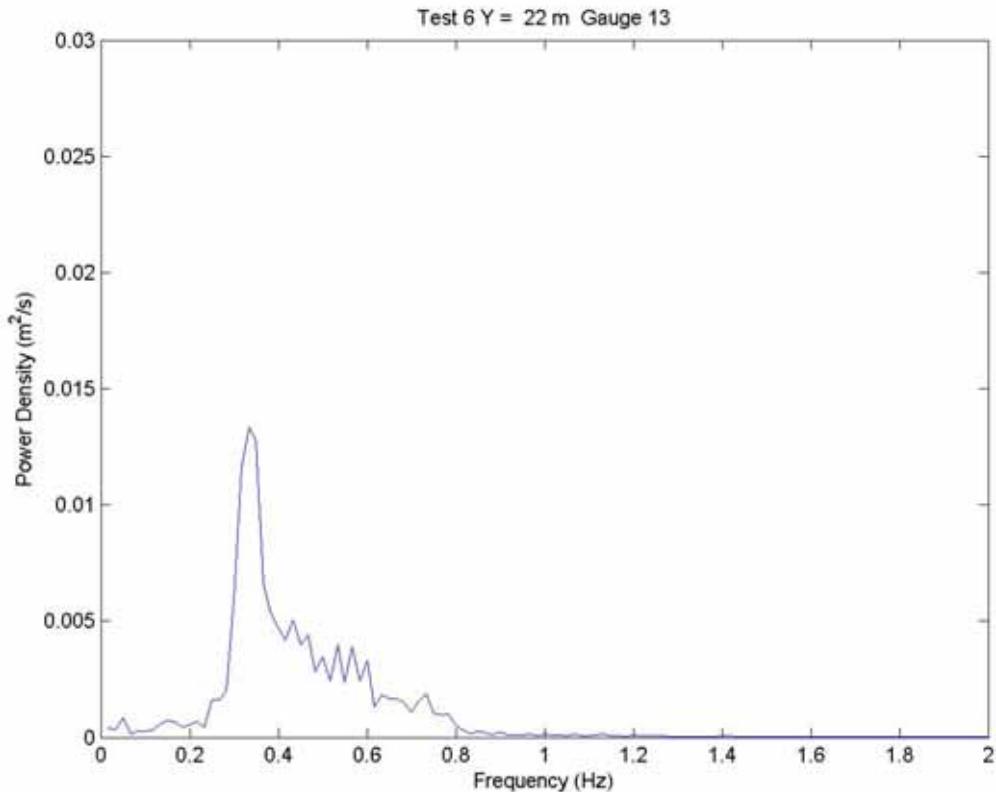
Figure 4-47. Measured incident wave spectra, Test 6

current, wave height, and longshore sediment flux were similar between many of the iterations. One of the iterative cases is presented here in which data were collected at five longshore transects between $Y = 18$ and $Y = 34$ m. The duration of the test was 1.27 hr.

The cross-shore distribution of the longshore current is plotted in Figure 4-49. The current varied over the measured transects between $X = 9.0$ and $X = 11.0$ m; however, the current was more uniform for other cross-shore locations. The recirculated current within the basin was observed at $X = 16.0$ m, which contributed to non-uniform
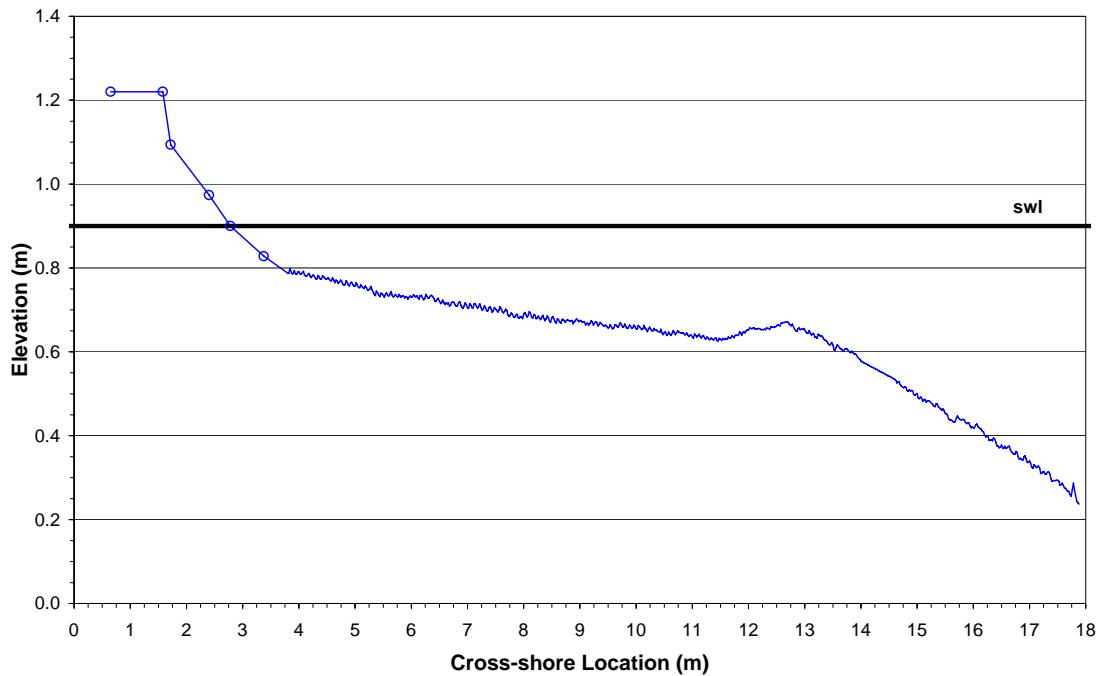
Figure 4-48. Quasi-equilibrium beach profile formed from Test 6 waves
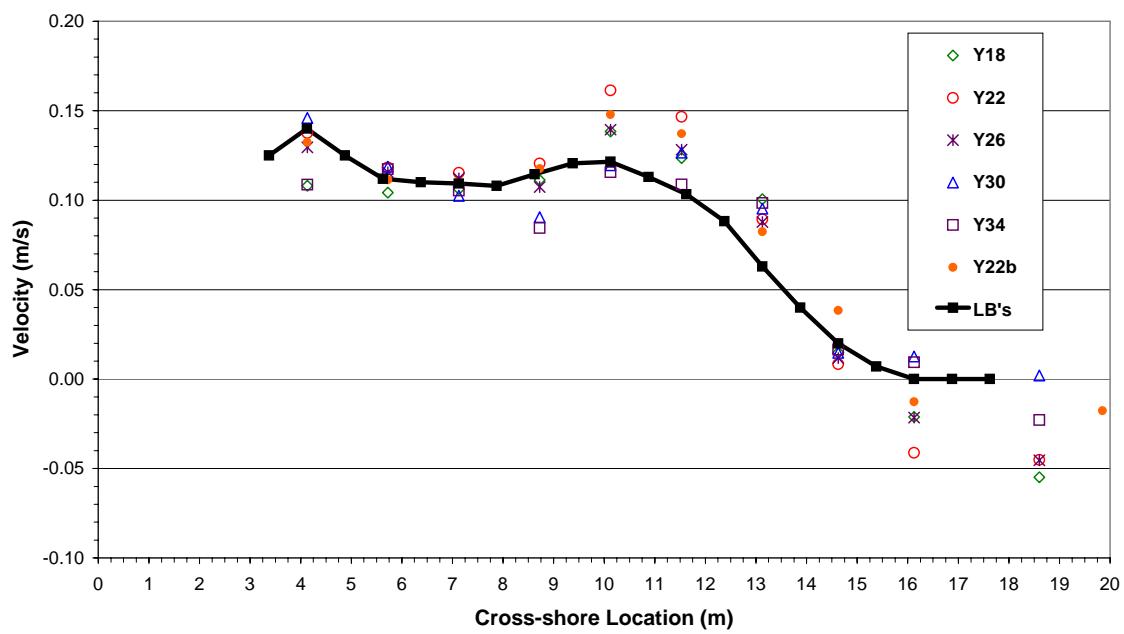
Figure 4-49. Cross-shore distribution of longshore currents, Test 6

conditions. Wave heights for Test 6 were smaller than those of Test 1 and Test 3, which resulted in breaking closer to the shoreline and a narrower surf zone. Consequently, a greater percentage of the basin resided outside the surf zone, where the longshore current was weak. The recirculation pumps in this region were either pumping low flows or shut off. The same situation was experienced with the Test 5 waves, but the longshore current produced with Test 5 waves was much weaker than the current of Test 6. It is believed that the difficulty in obtaining proper pump settings was due to the strong longshore current produced in the surf zone in combination with the larger, non-pumped region outside the surf zone. Although alongshore variation in the current was greater than desired, uniformity was not considered unreasonable, and longshore sediment flux measurements were consistent over several iterations.

The cross-shore distribution of wave height for Test 6 is plotted in Figure 4-50. Gauge 8 gave erroneous measurements for all transects except Y = 18 m, and Gauges 3 and 10 were not functioning, and values for these instruments are not included in the figure. Waves shoaled from offshore and peaked at X = 13 m, where breaking occurred. A steep decay in height occurred directly shoreward, indicating a plunging wave condition, and wave decay was gradual throughout the remainder of the surf zone.

Figure 4-51 plots the cross-shore distribution of sediment flux for Test 6. The distribution exhibited two peaks in transport (one near breaking and one in the swash zone), which was the same pattern observed for the plunging wave condition of Test 3. The swash zone peak was much greater than the peak near the break point in Figure 4-51, whereas the peaks observed for Test 3 condition were closer in magnitude.
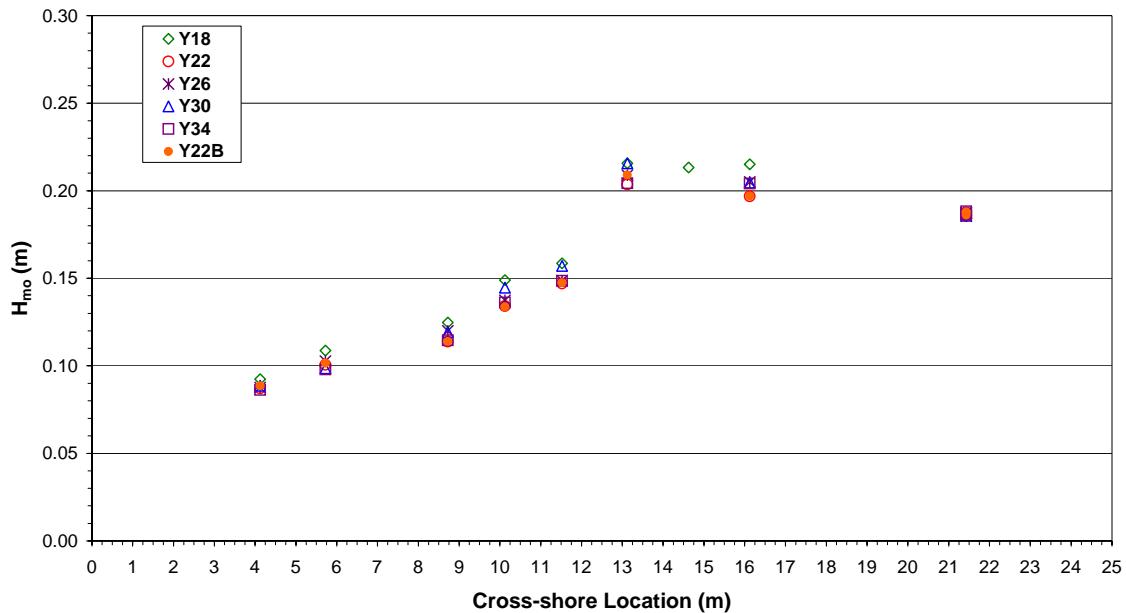
Figure 4-50. Cross-shore distribution of wave heights, Test 6
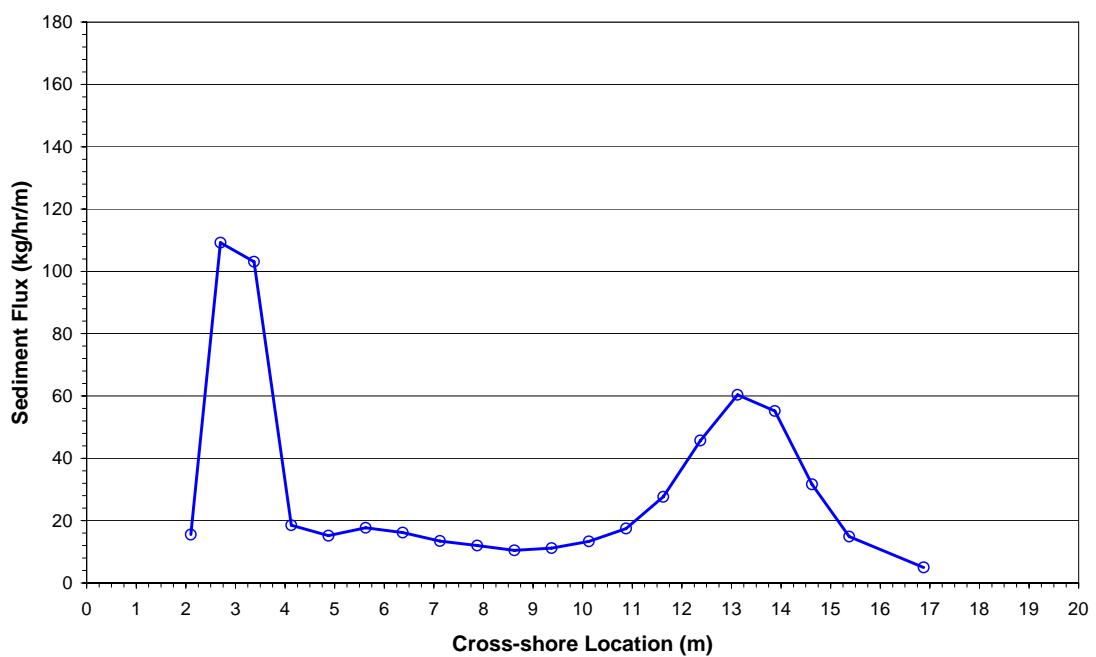
Figure 4-51. Cross-shore distribution of longshore sediment flux, Test 6

Summary

Measurements of waves, currents, and longshore sand transport rates were performed in a large-scale physical model for four incident wave conditions that were designed to vary by breaker type and incident energy. Waves and currents were generally steady and uniform during the tests. Two wave conditions produced spilling breakers (Test 1 and Test 5) and two produced plunging breakers (Test 3 and Test 6). The wave conditions were grouped by energy level; Test 1 and Test 3 had similar incident wave height and were referred to as higher energy conditions, and Tests 5 and 6 were referred to as lower energy conditions. Wave heights were averaged from the cases for each wave condition and plotted in Figure 4-52. The figure shows that Test 3 and Test 6 waves shoaled prior to breaking and decreased sharply directly shoreward of the break point, typical of plunging waves. Test 1, a spilling case, also showed a sharp decrease in height directly shoreward of breaking. Test 1 had a surf similarity parameter on the upper end of spilling waves, 0.34, and some plunging waves were observed within the time series; however, waves were observed to break predominately by spilling. Test 5 showed a gentle decay in wave height throughout the surf zone, typical of spilling breakers.

Longshore sediment flux was averaged for each test, and plotted as a function of cross-shore location in Figure 4-53. The figure indicates that there are three distinct zones of longshore sand transport; the incipient breaking zone, inner surf zone, and swash zone. Transport in each zone is described in the following paragraphs.
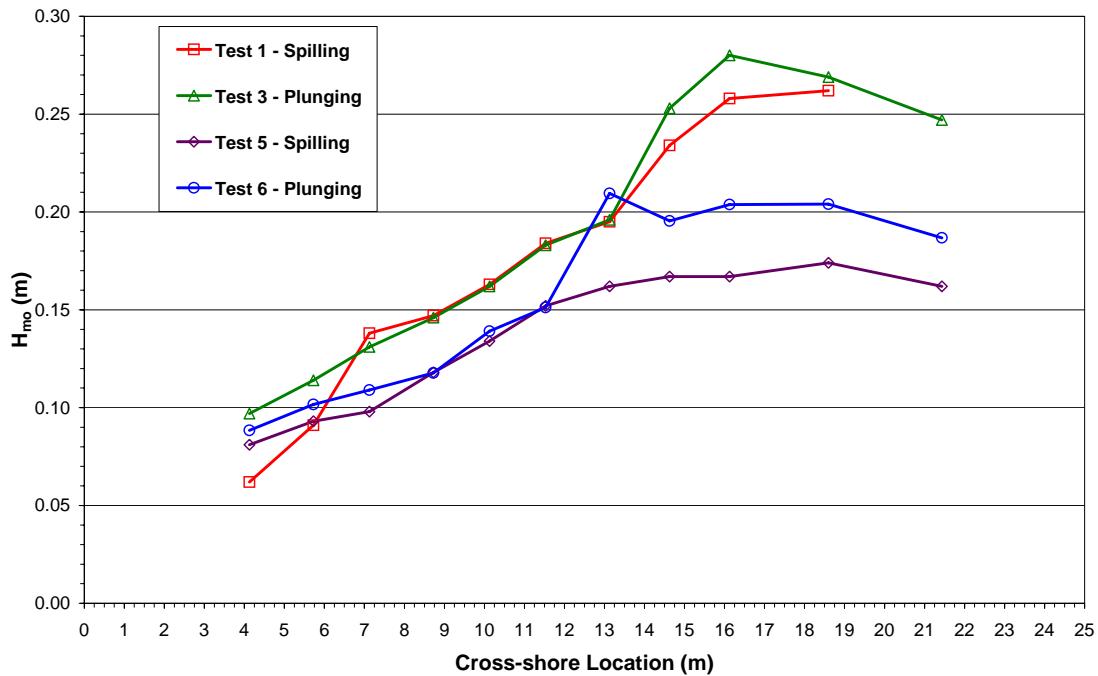
Figure 4-52. Cross-shore distribution of wave heights, all tests

Figure 4-53. Cross-shore distribution of longshore sediment flux, all tests
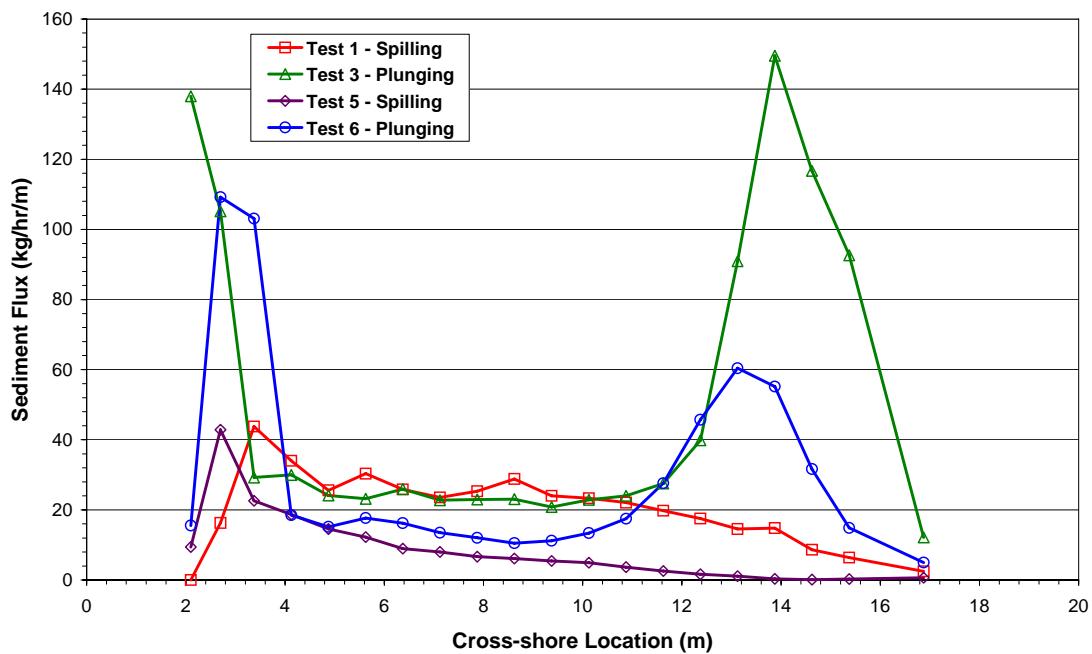
Incipient Breaking Zone

At incipient breaking, a substantial peak in transport occurred for the plunging-waves of Test 3 and Test 6. However, a similar increase in transport was not observed in the spilling-wave tests (Test 1 and Test 5) . The absence of a peak in transport for the spilling tests can be explained as a function of breaker type. Turbulence associated with spilling breakers remains close to the surface in the bore. The jet associated with the large plunging waves penetrated deep into the water column, impacted the bed, and caused sand to be suspended and transported by the longshore current (Kana 1977; Wang et al. 2002).

Inner Surf Zone

Figure 4-52 shows the wave height distribution for the four tests. Test 1 and Test 3 have similar wave height (energies) and similar sediment flux in the inner surf zone. Wave height and sediment flux for Test 5 and Test 6 were smaller in the inner surf zone than for the higher energy cases. However, wave height and sediment flux distributions for Test 6 had similar shape and were slightly greater than those of Test 5. In the inner surf, wave energy is saturated, and wave height is strongly controlled by depth, independent of wave period. The results imply that sediment flux in the inner surf zone is dominated by wave height and independent of period.

Swash Zone

The swash zone was defined as the region where an increase in foreshore slope was observed, which was within 2 m from the shoreline. There was a peak in transport in the swash zone for all tests, and Figure 4-53 shows that swash zone transport has a dependence on wave period. For waves having similar incident wave height, but different period, i.e., Test 1 and Test 3, and Tests 5 and Test 6, swash zone transport is much greater for the longer period tests. This result is consistent with the Hunt (1959) formula for wave runup, in which runup is directly proportional to wave period.

In all practical longshore sediment transport models, the swash transport contribution is either ignored or merely accounted for as part of the total sediment transport budget (Van Wellen et al., 2000). However, significant swash zone transport rates have been observed in field and laboratory studies (Sawaragi and Deguchi 1978, Kraus et al. 1982; Bodge and Dean 1987), and swash zone transport can account for as much as 50 percent of the total longshore sediment transport (Elfrink and Baldock 2002; Van Wellen et al. 2000). For the higher energy tests (Test 1 and Test 3), swash zone transport accounts for a third of the total transport. However, for the lower energy experiments (Test 5 and Test 6), swash zone transport accounts for 40 to 60 percent of the total transport. Additionally, the reduction in total transport between the higher and lower wave energy spilling tests (Test 1 and Test 5) was a factor of 2.3, but the reduction in swash transport was only a factor of 1.2. The reduction in total transport between higher and lower energy plunging tests (Test 3 and Test 6) was 1.7, but the reduction in swash zone transport was 1.3. Although data are limited, the results presented here imply that swash

zone transport contributes a higher percentage of the total transport rate for lower energy beaches, and conversely, as incident wave height increases the contribution of swash transport to total transport is less. This observation agrees with findings of Elfrink and Baldock (2002), who found that the relative contribution of swash zone transport was greater during calm conditions than during storms. The results indicate that the role of swash zone transport can be significant, especially in lower energy environments, which would include small-scale physical models.

In addition, results from the present study have implications for field measurement of longshore sediment transport. Although swash zone transport measurements are difficult to obtain in the field, the results indicate that the swash zone contribution is significant, and it is necessary to include swash zone transport to obtain accurate measurements of the total longshore sediment transport.

CHAPTER V

DESCRIPTION OF THE FIELD STUDY

Introduction

Many studies have been conducted in the field to measure longshore sediment transport; however, there are few field studies that include direct measurements during storms. One factor is the expense of procurement, calibration, and operation of the many instruments required to adequately define hydrodynamics and sediment transport at the large spatial scale of the surf zone during severe wave conditions. Another factor is the robustness of the instruments for storm deployment. A system was developed at the US Army Corps of Engineers Field Research Facility (FRF) to operate during severe storms. Data obtained from this system, the Sensor Insertion System (SIS) was selected for comparison to the predictive models.

The Field Research Facility

The FRF is located at Duck, North Carolina, near the center of a 140-km-long barrier island on the Atlantic Ocean. A 561-m-long, 6-m-wide steel and concrete research pier provides access across the surf zone (Figure 5-1). The FRF routinely measures environmental conditions with a suite of instruments including permanent current meters

Figure 5-1. The Field Research Facility (FRF), Duck, NC

and directional wave gauges located at an 8-m depth offshore. Additionally, the

bathymetry around the FRF is surveyed monthly.

The SIS (Miller 1998) was developed at the FRF to make direct measurements of

longshore sediment transport during storm conditions (Figure 5-2). The SIS employs a

70,000-kg crane, on which an array of instruments can be mounted. The crane can be

moved along the length of the research pier to measure waves, current, and sediment

transport at different positions across the surf zone. To minimize the influence of the

pier, the SIS can place instruments on the ocean bottom in 9 m depth as far as 22 m from

the pier centerline. The SIS can reposition sensors as the beach profile evolves during a

storm. A disadvantage of the system is that spatial measurements across the shore are

not simultaneous, but occur over a 3-hr period (tide, wind, and waves may change).

Figure 5-2. The Sensor Insertion System (SIS)

The SIS contains several instruments mounted on a frame at the end of the crane's boom (Figure 5-3). Optical backscattering concentration sensors in combination with electromagnetic current meters (EMCMs) are used to calculate sediment flux throughout the water column. The SIS deploys eight OBS and four EMCMs positioned through the water column. Measurements have shown that most of the sediment is transported near the bottom (less than 1 m); therefore, the sensors are placed more densely lower in the water column. In addition to OBS and EMCMs, a pressure sensor was mounted on the frame to measure water surface elevation.

During October 1997, the SIS measured longshore sediment transport daily during the SandyDuck '97 field experiment (Miller 1998). During the experiment, a low-pressure system developed along a front, strengthened, and moved north along the Atlantic coast. The storm produced peak conditions at the FRF of $T_p = 9.8$ sec and $H_{mo} = 3.3$ m at the 8-m water depth. The SIS operated continuously during the storm.
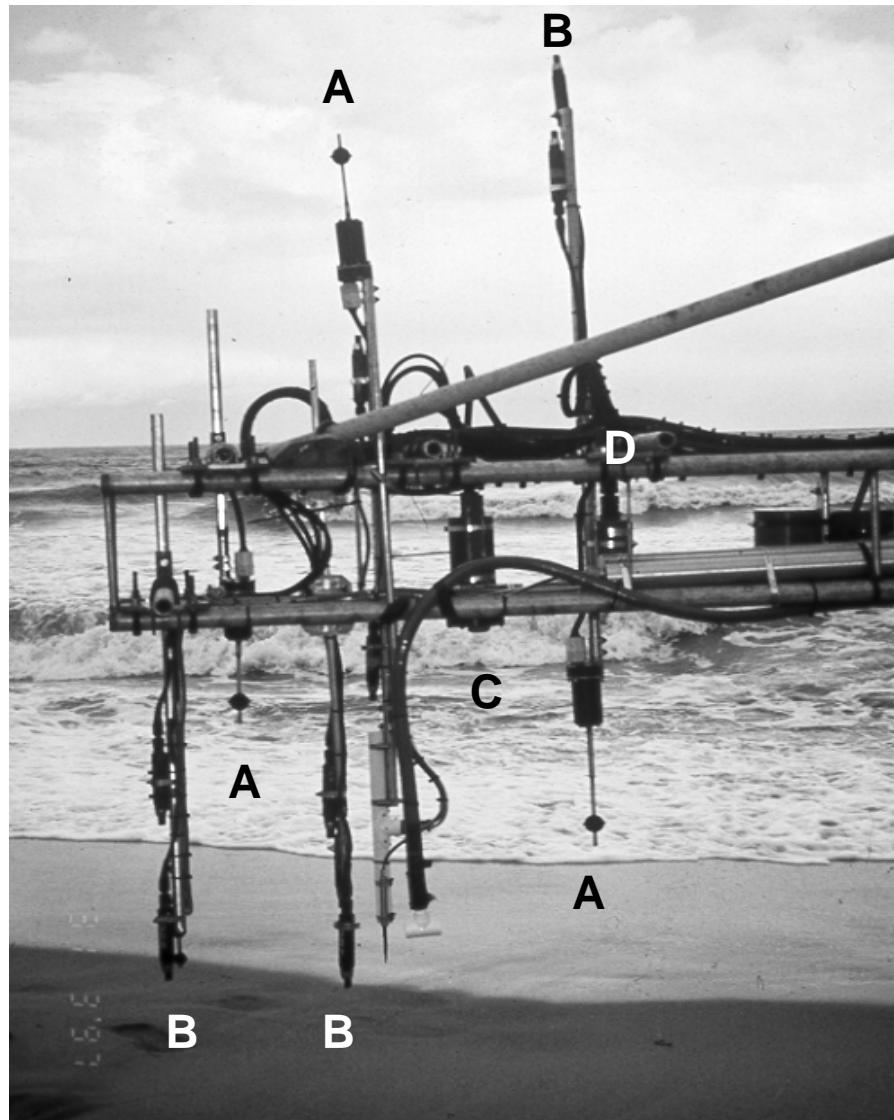
Figure 5-3. SIS instrument array: A – EMCM, B – OBS, C – Down-looking
sonar, D – Pressure sensor

The SIS data are similar to LSTF data in that measurements of wave height, current,

and sediment transport were made at several cross-shore locations. The data were

collected at 16 Hz and are ideal for comparing cross-shore distribution of longshore

sediment transport models. Additionally, the sediment d_{50} was similar to the LSTF sand.

Stauble (1992) performed analysis on sediment samples collected at the FRF from March 1984 to September 1985. For locations where SIS measurements were made the mean grain size ranged from 0.12 mm to 0.20 mm. For computations of τ_{cr}, a d_{50} of 0.15 mm was used.

A difference in the field and laboratory data was the relative position of the velocity measurements. The LSTF ADVs were positioned to the one-third water depth at each cross-shore location. The SIS EMCMs were mounted to a frame and their vertical position relative to the bottom remained the same for all cross-shore stations, i.e., their position relative to water depth differed between stations. Two methods were considered for selecting velocity measurements for comparison to the predictive models. The first method would use measurements from an EMCM that was positioned in the lower half of the water column for all cross-shore locations. An alternate method is to calculate the relative depth of each EMCM at each cross-shore location and select measurements from the instrument closest to the one-third depth from the bottom for each station. Neither method would necessarily use measurements at the one-third depth. It was preferred to select a single EMCM for all cross-shore measurements, and data using the first method were chosen for analysis and comparison to predictive transport models.

SIS Data

   Two transects recorded from the SIS SandyDuck experiments, Transects 15 and 19

covered on 18 and 19 Oct 1997, respectively, were selected to compare to predictive

models. The wave conditions for transects SIS 15 and SIS 19 are listed in Table 5-1.

The wave height distribution and bathymetry for transect SIS 15 are shown in

Figure 5-4. Waves gradually shoaled to a peak of 0.97 m at Station X = 271 m and

remained relatively constant to X = 198 m (H_{rms} = 0.95 m). Wave height decreased

significantly shoreward of this point to 0.76 m at X = 162 m. Wave heights that

occurred over with transect SIS 19 were much higher than those of SIS 15 and the

heights vary across shore (Figure 5-5). From the most offshore station of X = 540 m to

X = 238 m, wave height varied from 1.65 m to 1.36 m. Wave breaking occurred at

X = 238 m, where height decreased from 1.56 m to 0.76 m at X = 162.

Table 5-1. SIS experiment wave conditions

Transect Number	Breaker Type	H_o m	H_{sb} m	T_p sec	h_b m	θ_b deg	m
15	Spilling	0.99	0.97	6.4	4.2	13.8	0.029
19	Spilling	1.49	1.56	7.1	3.4	14.9	0.037

   The average longshore current measured during SIS 15 is shown in Figure 5-6,

where positive values indicate currents directed south. Currents increased gradually

from X = 518 m to X = 198 m. The longshore current direction reversed to the north at
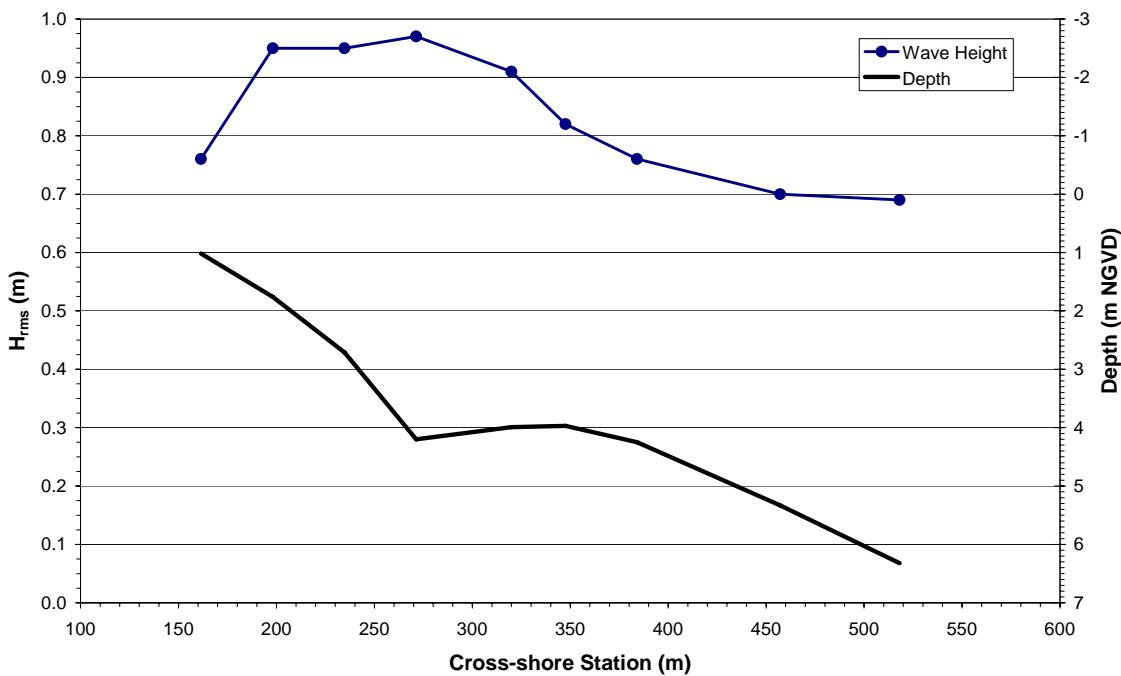
Figure 5-4. Wave height distribution and beach profile associated with SIS Transect 15
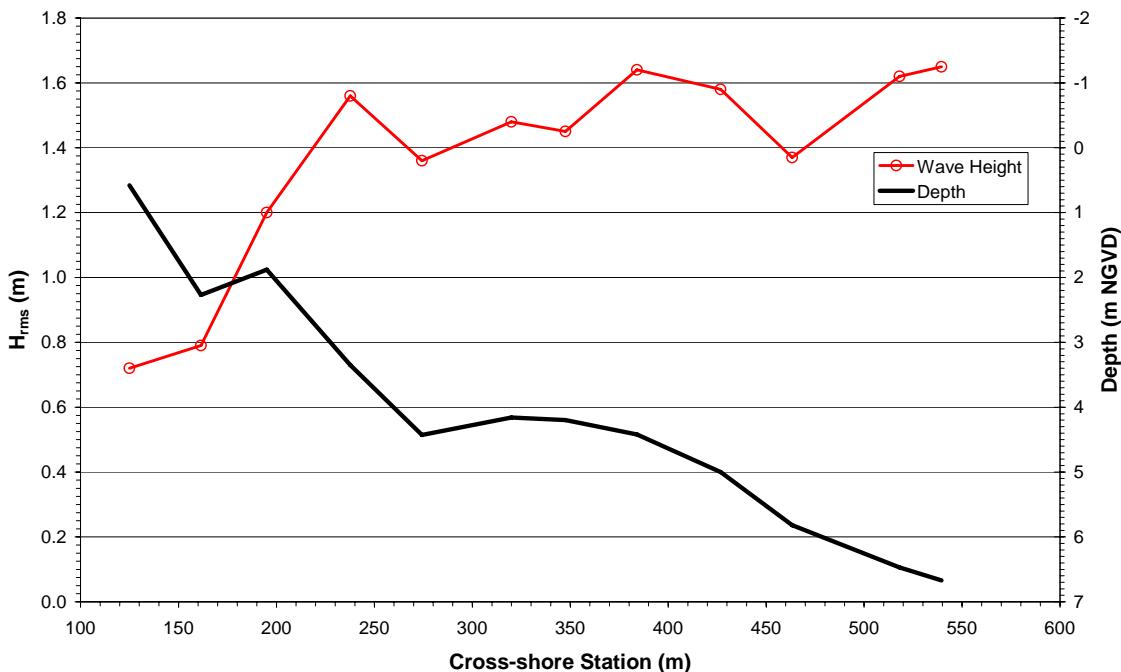
Figure 5-5. Wave height distribution and beach profile associated with SIS Transect 19
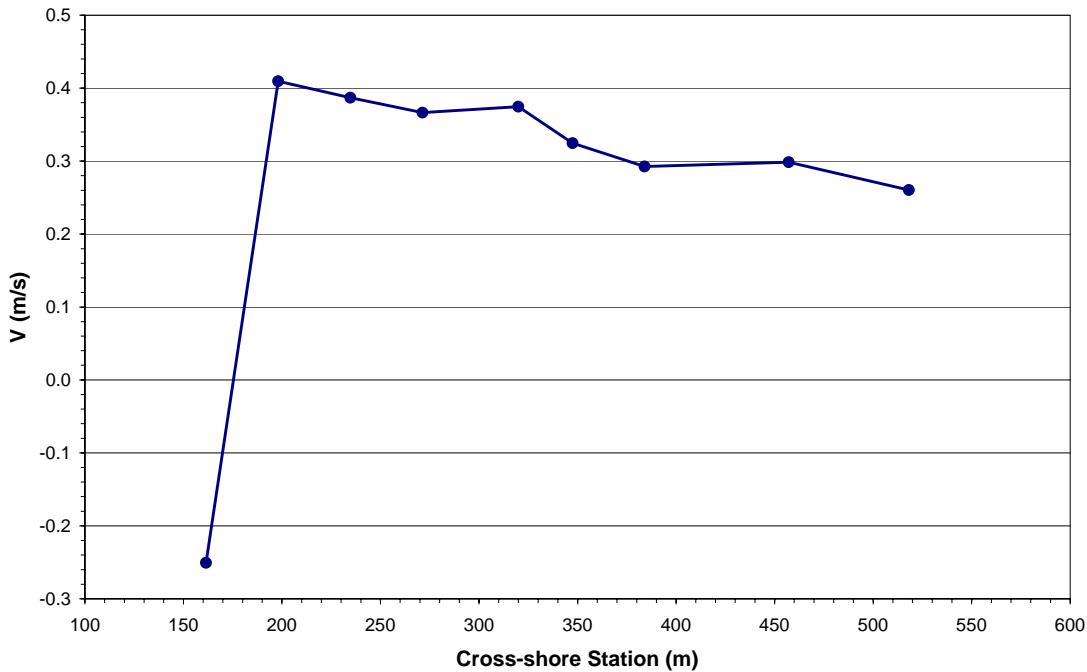
Figure 5-6. Cross-shore distribution of longshore currents, SIS Transect 15

X = 162 m. Figure 5-7 shows average longshore current for SIS 19, which had

significantly higher velocities. The increase in longshore current was more dramatic

across the surf zone than shown for SIS 15, especially between X = 540 m and

X = 320 m. A less severe increase was observed between X = 320 m and X = 238 m.

The current decreased sharply shoreward of this station, but remained southerly directed.

Figure 5-8 shows a shoreward increasing trend of longshore sediment flux for

SIS 15, with maximum transport occurring at X = 198 m. No sediment transport

measurement was made at X = 162 m where currents were to the north. The peak in

transport at X = 320 m cannot be readily explained and may be considered a suspect

point. Transport was an order magnitude or greater for SIS 19 (Figure 5-9). Sediment
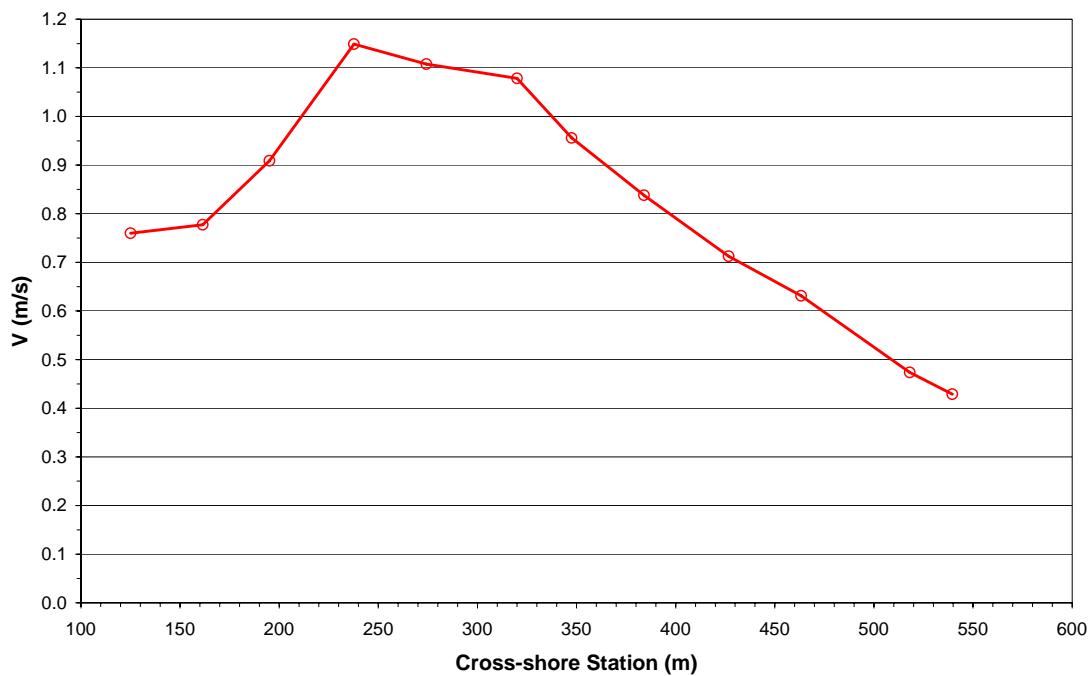
Figure 5-7. Cross-shore distribution of longshore currents, SIS Transect 19
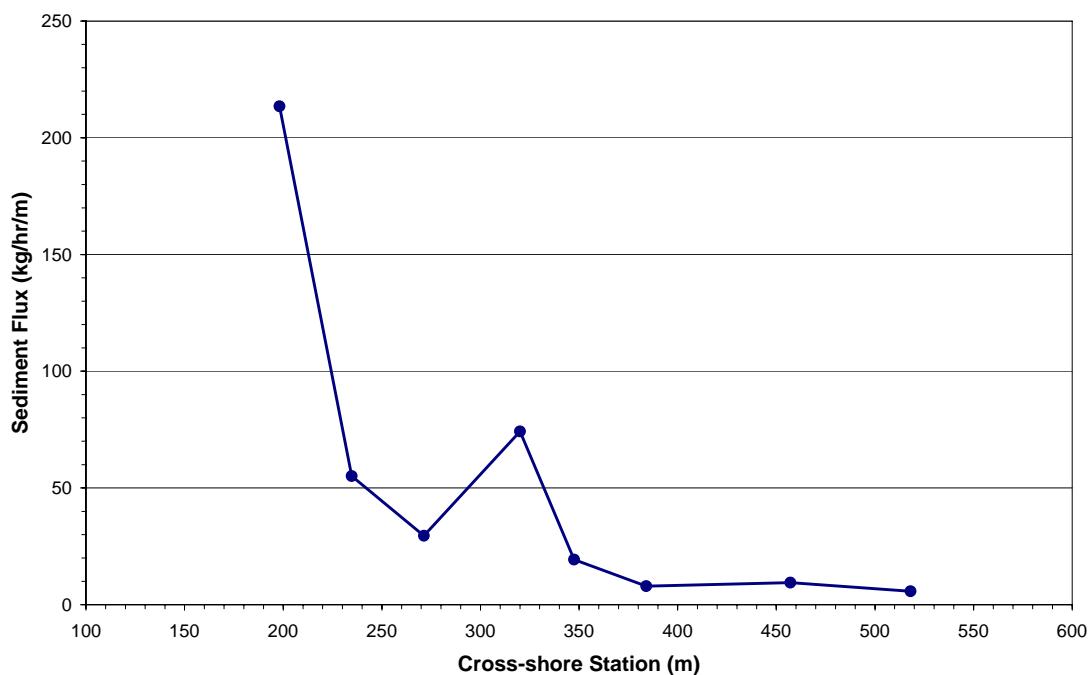
Figure 5-8. Cross-shore distribution of longshore sediment flux, SIS Transect 15
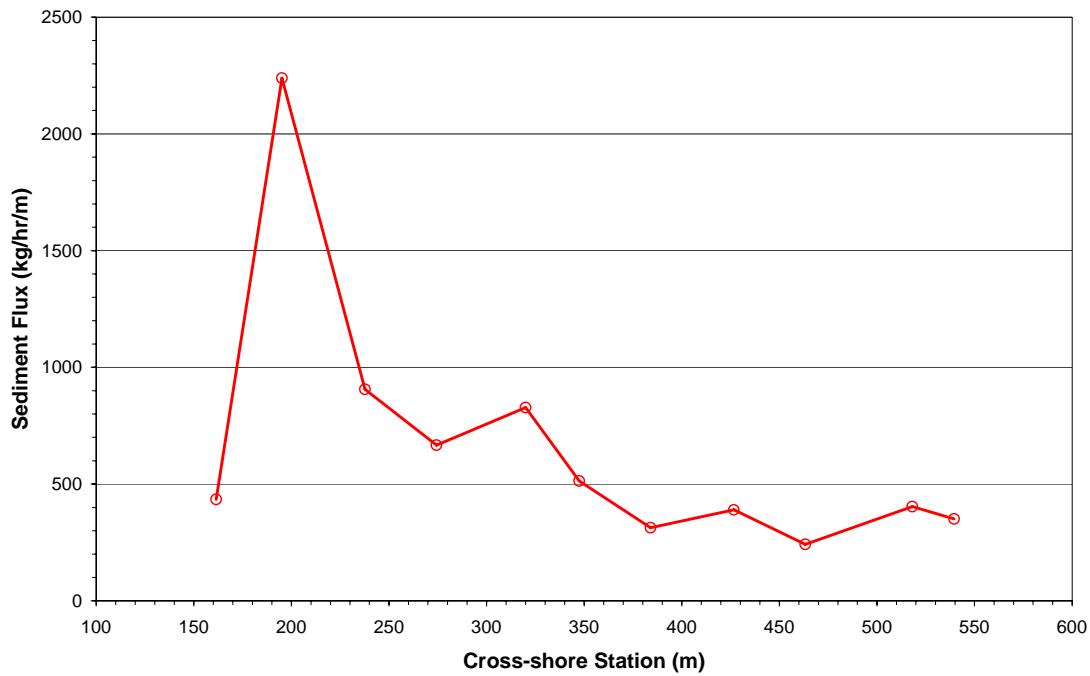
Figure 5-9. Cross-shore distribution of longshore sediment flux, SIS Transect 19

flux increased steadily with some variation from X = 540 m to X = 238 m. A sharp

increase in longshore transport occurred at X = 195 m (directly shoreward of the break

point), and transport decreased shoreward of this location. No transport measurement

was obtained at X = 125.0 m.

CHAPTER VI

COMPARISON OF SELECTED AVAILABLE TRANSPORT MODELS TO LABORATORY AND FIELD DATA

Total Load Transport Models

Total longshore sediment transport rates from the LSTF and SIS were compared to the CERC formula, and to the models of Bailard (1984), Ozhan (1982), Kamphuis (1991), and Madsen et al. (2003). The CERC formula estimates sediment transport based on energy flux at wave breaking. Bailard (1984) and Ozhan (1982) each developed a method to compute the K-coefficient in the CERC formula. Kamphuis (1991) developed an empirical formula based on small-scale laboratory and field data. Madsen et al. (2003) separately estimated bed load and suspended load transport based on energy flux with a coupled hydrodynamic and sediment transport model.

LSTF Data Comparison

Longshore sediment transport measurements obtained from the four LSTF tests (Chapter IV) were compared to selected existing total load models. Input parameters for these equations are listed in Table 4-1. The values in the table represent averages of the individual cases of each test condition.

For the LSTF tests, the main breaker line was determined as the location at which a significantly steep rate of wave-height decay initiated. This criterion was based on the

comprehension that a significant wave-energy loss, and, consequently, a significant wave height decrease, should follow dominant wave breaking. Visual observations during the LSTF tests supported the above determination. Therefore, H_{sb} and h_b were obtained from the gauge located at the onset of significant wave-energy loss.

Breaker angle was measured visually using the digital compass in an electronic total station transit, which was positioned on the data-collection bridge and located over the mean breaker line. Approximately 20 breaker angles were measured during each transect of a wave case. An overall average, for all the wave runs for each wave condition, was computed to represent the breaker angle. Wave angles can be calculated from the orbital velocities of ADVs; however, the small oscillatory longshore component relative to the steady longshore current and the precision required in positioning the instruments make it difficult to obtain accurate wave angles directly from these instruments (Johnson and Smith 2005).

Kamphuis (2002) redefined the beach slope entering the Kamphuis (1991) equation as the slope that causes breaking, i.e., the slope over one or two wavelengths offshore of the breaker line. However, the slope offshore of breaking in the LSTF is somewhat artificial because of the physical model limits. Therefore, in the present study, m is defined as the slope from the breaker line to the shoreline originally proposed by Kamphuis (1991).

Total longshore transport rate was computed by summing the sediment flux measured in all of the traps, and averaging the rates of the cases performed for each test. The values presented are given in immersed deposited sand volume assuming a porosity

of 40 percent. Measured transport rates are given in Table 6-1 along with the predicted

values of the selected models.

Table 6-1. Measured and predicted LSTF total longshore transport rates

Experiment Number	Measured m^3/yr	CERC Formula (K=0.39) m^3/yr	Bailard m^3/yr	Ozhan m^3/yr	Kamphuis m^3/yr	Madsen m^3/yr
1	2,660	21,350	10,660	4,470	2,390	6,630
3	7,040	23,100	14,570	25,830	6,060	8,350
5	1,130	8,400	4,500	3,010	1,010	2,090
6	4,040	12,040	5,250	15,430	3,160	5,000

If the recommended K-value of 0.39 is used, the CERC formula over-predicted

measured values from the spilling cases by a factor of 8 for Test 1 and nearly 7 for

Test 5. Overestimates were greater than a factor of 3 for both plunging wave tests. The

CERC formula produced similar estimates for Test 1 and Test 3 because they have

similar breaking wave heights, although the breaker type differed. Measured transport

rates were nearly 3 times greater for Test 3 (plunging) than Test 1 (spilling) and more

than 3 times greater for Test 6 (plunging) than Test 5 (spilling).

Predictions using the method of Bailard (1984), which includes grain size in the

computation of K, gave better estimates than the CERC formula. However, differences

ranged from 30 percent (Test 6) to 300 percent (Tests 1 and 5). It should be noted that

the relationship of Bailard (1984) was developed based on sediment fall speeds between

0.025 and 0.205 m/s, breaker angles between 0.2 and 15 deg, and maximum horizontal

orbital velocities between 0.33 and 2.83 m/s. The LSTF parameters of θ_b and u_{mb} are

within the ranges given by Bailard. The fall speed was obtained by a formula of

Hallermeier (1981) for the LSTF grain size of 0.15 mm and was calculated to be

0.018 m/s, which is lower than the minimum valid value given by Bailard (1984).

However, estimates of longshore sediment transport were made with the CERC formula

with K estimated by Bailard for the purpose of comparison.

The Ozhan (1982) equation produced better agreement with the spilling tests than the

CERC formula and the Bailard (1984) equation, although it overestimated Test 1 by

68 percent and Test 5 by 167 percent. The equation gave the largest estimates for the

plunging cases for the models examined; an overprediction of 267 percent for Test 3

measurements and 282 percent for Test 6 measurements. The Ozhan equation's

dependence on wave steepness yielded correct results for the higher transport rates for

plunging waves, but it appears to be overly sensitive to the parameter.

Results using the Kamphuis (1991) formula produced more consistent estimates with

the LSTF measurements; differences ranged between 10 percent for Test 1 to 22 percent

for Test 6. The improved estimates of Kamphuis (1991) can in part be attributed to the

incorporation of wave period, which influences breaker type.

The Madsen et al. (2003) equation greatly overpredicts Test 1 measurements and

slightly overpredicts measurements for the remaining tests. The coefficients Madsen et

al. provided were based on a limited comparison, and they stated that it is premature to

accept its quantitative validity.

Influence of Breaker Type on Total Load Transport

Saville (1950) observed that for laboratory waves of identical energy levels, greater

longshore transport rates occurred for waves having lower wave steepness. Ozhan

(1982) found similar results in a laboratory study. Breaker type is a function of wave

steepness, and lower steepnesses indicate plunging breakers. In summarizing a review

of longshore sediment transport literature, Bodge and Dean (1987) stated that longshore

sediment transport should somehow depend upon the breaker type, as concluded, for

example by Kana (1977) and Kamphuis and Readshaw (1978). The results shown in

Table 6-1 support these conclusions and indicate that in addition to wave height, breaker

type is a factor that determines the longshore sediment transport rate.

Smith et al. (2003) evaluated the CERC formula based on breaker type for LSTF

data. If measured transport rates from Test 1 were used to calibrate the CERC formula,

then $K = 0.05$. Applying this coefficient to the wave conditions of the lower energy

spilling case (Test 5) gave a transport rate of 1,080 m^3/yr, or a 5 percent difference from

the measured rates. Likewise, if the CERC formula was calibrated with transport rates

from Test 3, then $K = 0.13$. Applying this coefficient with wave conditions of the lower

energy plunging case (Test 6), a transport rate of 3,700 m^3/yr was calculated, or an

8 percent difference compared to measured rates. The improved rates are illustrated in

Figure 6-1, which shows calculated CERC formula predictions with calibrated K-values

versus measured transport rates. The solid line in the figure represents perfect prediction.

Additionally, CERC formula estimates with $K = 0.39$ and estimates from Kamphuis
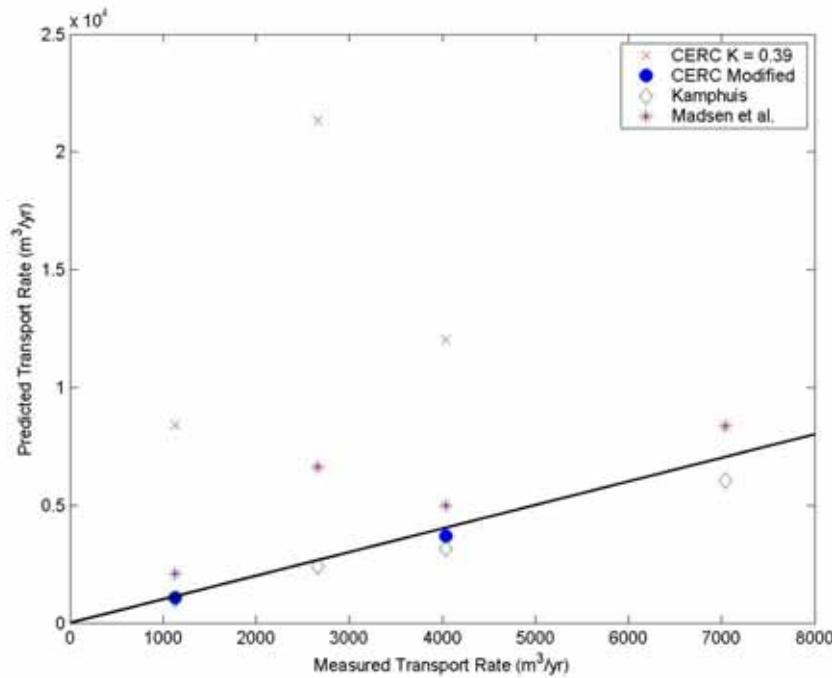
Figure 6-1. Comparison of calculated to measured transport rates

(1991) and Madsen et al. (2003) are included. The figure indicates that the CERC

formula gives reasonable estimates if *K* is calibrated to a lower value, and it is applied to

similar breaker types. Wang and Kraus (1999) measured longshore transport rate in the

surf zone of a low energy beach and found *K*-values ranging from 0.044 to 0.541 for low

energy conditions (0.14 m < H_{rmsb} < 0.38 m). The *K*-values calculated for the LSTF test

conditions are within the range of values found by Wang and Kraus.

For most engineering projects, reliable historical data are not usually available to

calibrate *K*. An alternative solution to estimate *K* at these locations is to use shoreline

change data to estimate the LST rate for such a calibration. Also, if historical transport

data are available at another site that has similar wave conditions, sediment grain sizes,

and bathymetry it may be applicable for calibration, although this introduces greater uncertainty.

The Kamphuis (1991) equation, which includes wave period, a factor that influences breaker type, predicted measured rates well for the LSTF tests. The Kamphuis equation gives transport rate as a function of H^2, whereas transport rate using the CERC formula is a function of $H^{5/2}$. For higher waves, the Kamphuis equation will give significantly lower values than the CERC formula, and it is unclear if the Kamphuis formula will give accurate results for high-energy conditions – for which the longshore transport rate will be greatest during the year.

The Madsen et al. (2003) equation overpredicted the Test 1 measurements, but transport estimates for the other tests have the same slope as measurements for increasing longshore transport (Figure 6-1). This consistency in slope supports their conclusion that the form of their equation is valid.

SIS Field Data Comparison

Longshore sediment transport measurements obtained from SIS 15 and SIS 19 were compared to the selected models. The input variables used in the models are given in Table 5-1. It should be noted that neither of the cases presented have plunging breaker types. During this particular storm, only spilling-type breakers occurred.

Breaker height and depth were determined in the same manner as for the LSTF data; the location at the onset of a significant loss in wave energy. Data from the FRF directional wave gauge at the 8-m depth were transformed with Snell's law to calculate

the wave angle at the cross-shore station where significant wave energy was lost. Total

longshore transport rate was obtained by summing the cross-shore contributions. It

should be noted that measured transport rates were calculated between the measurements

stations, and did not include contributions of the entire swash zone.

Measured and predicted transport rates are shown in Table 6-2. The CERC formula,

Bailard (1984) model, and Ozhan (1982) model overestimated SIS 15 measurements by

an order of magnitude. The Kamphuis (1991) equation overpredicted measurements by

a factor of 4, and Madsen et al. (2003) overestimated by a factor of 2.4. The CERC

formula and Ozhan estimates gave better estimates for SIS 19 measurements, but both

overpredicted by a factor of nearly 2. The Bailard model overestimated measurements by

a factor of 6.5. The Kamphuis and Madsen et al. gave the closest predictions; however,

both underestimated measurements, Kamphuis by 25 percent and Madsen et al. by 40

percent.

Table 6-2. Measured and predicted SIS total longshore transport rates

Transect Number	Measured $x10^6$ m^3/yr	CERC Formula (K=0.39) $x10^6$ m^3/yr	Bailard $x10^6$ m^3/yr	Ozhan $x10^6$ m^3/yr	Kamphuis $x10^6$ m^3/yr	Madsen $x10^6$ m^3/yr
15	0.11	1.23	4.17	1.42	0.44	0.26
19	2.25	4.33	14.58	4.11	1.67	1.33

Summary of Total Load Transport Model Comparison

Models based on energy flux at breaking, the CERC formula with recommended

K-value, the Bailard (1984) model, and Ozhan (1982) model, yielded overpredictions for

both laboratory and field data. It was found that if K was calibrated and applied to

similar breaker types, the CERC formula gave excellent results. Bailard and Ozhan each

developed a method based on laboratory data to estimate the CERC formula K

coefficient. These models gave better estimates than the CERC formula for the LSTF

data. However, both the Bailard and Ozhan models produced similar (Ozhan) or greater

overpredictions (Bailard) than the CERC formula in comparisons to the field data.

The Kamphuis (1991) and Madsen et al. (2003) models gave more consistent results

for both the laboratory and field data. One of the common criticisms of the Kamphuis

equation is that it greatly underpredicts field measurements; however, that was not

observed in the present comparison. Madsen et al. indicated that the coefficients for

their equation are preliminary and still being developed, although the coefficients used

gave acceptable results.

Distributed Transport Models

Cross-shore distribution models of Bodge and Dean (1987), Watanabe (1992), and

Van Rijn (1993) were selected to compare to the laboratory and field data. The selected

models represent different approaches and degrees of difficulty. The Bodge and Dean

model, a wave-energetics model, and the Watanabe model, a stress model, are

straightforward and can be applied with ease. The Van Rijn equations are

comprehensive and more complicated to use. Van Rijn provided a program to compute

sediment transport rates; however, an adequate understanding of littoral processes and

Van Rijn's model are necessary in applying the model appropriately.

Bodge and Dean (1987) Model

The Bodge and Dean (1987) model is a function of energy dissipation and the

original form of the equation, Equation 2-51, includes the bottom slope term as

$(dh/dx)^{0.5}$. The model was applied to LSTF sediment transport data with the

recommended laboratory value of k_q of 0.057. Figure 6-2 shows the equation followed

the general trend of the Test 1 measurements. However, predictions fluctuated greatly

for the spilling wave case. Predictions were underestimated for the Test 3 measurements

(Figure 6-3), and no transport was reported in the trough of the breakpoint bar. The

model is based on energy dissipated and will predict no transport where no dissipation

occurs, i.e., increasing depths or increasing wave height. The model predicted the

spilling wave results of Test 5 well (Figure 6-4). Estimates were slightly high in the

outer portion of the surf zone and slightly low in the inner portion. The model

underpredicted Test 6 measurements and did not capture the peak in transport near

breaking because the slope term was negative (Figure 6-5).

Inclusion of the slope term in the Bodge and Dean (1987) model predicted the trend

of distributed longshore transport well for the laboratory spilling waves. The model was

sensitive to changes in energy flux, which caused fluctuations in the transport estimates
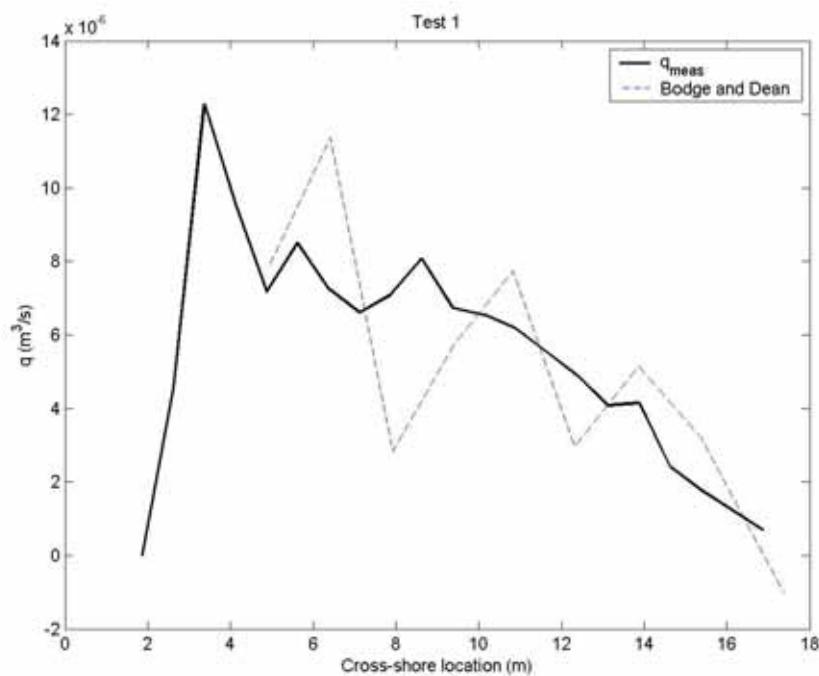
Figure 6-2. Bodge and Dean (1987) estimates (with slope term)
compared to Test 1 measurements
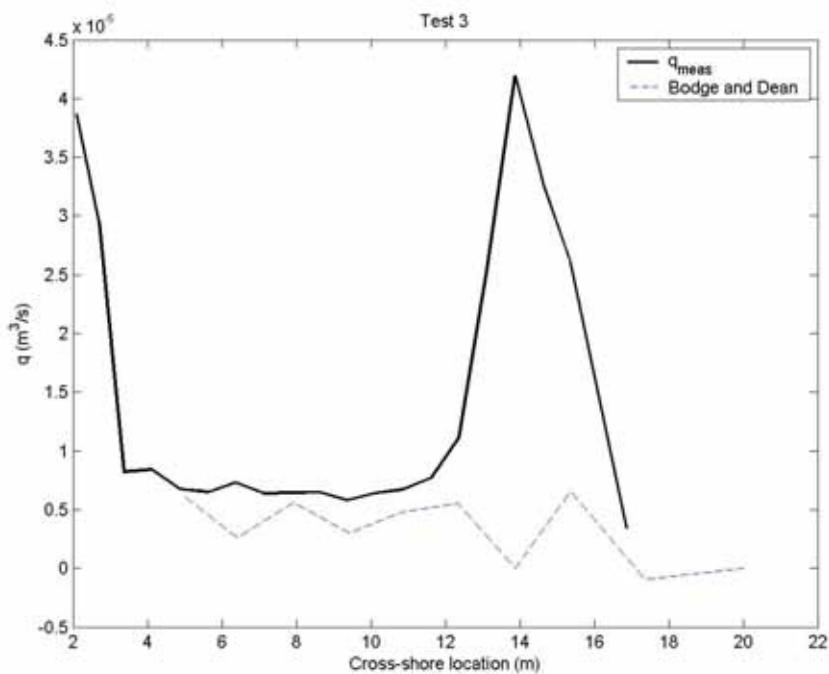
Figure 6-3. Bodge and Dean (1987) estimates (with slope term)
compared to Test 3 measurements
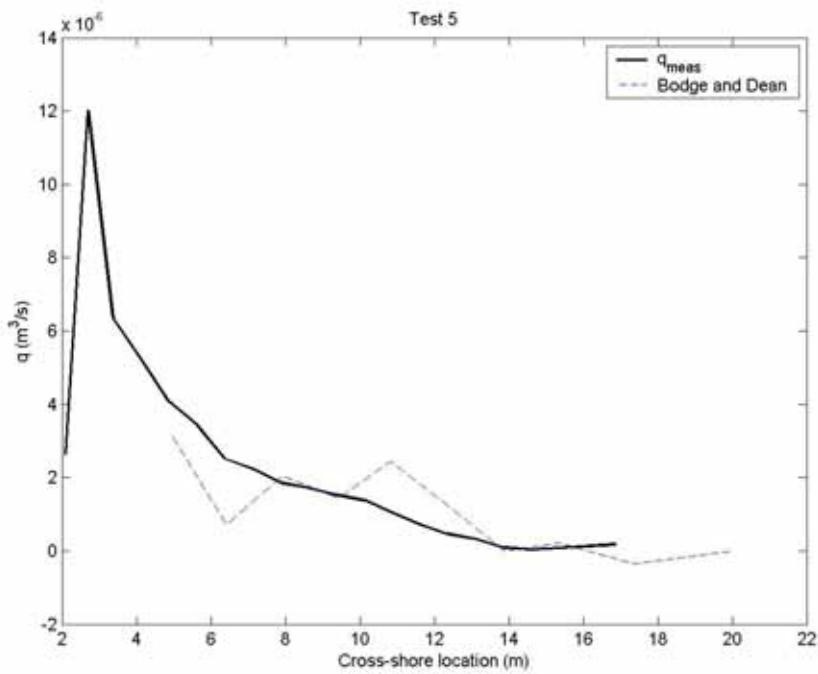
Figure 6-4. Bodge and Dean (1987) estimates (with slope term)
compared to Test 5 measurements
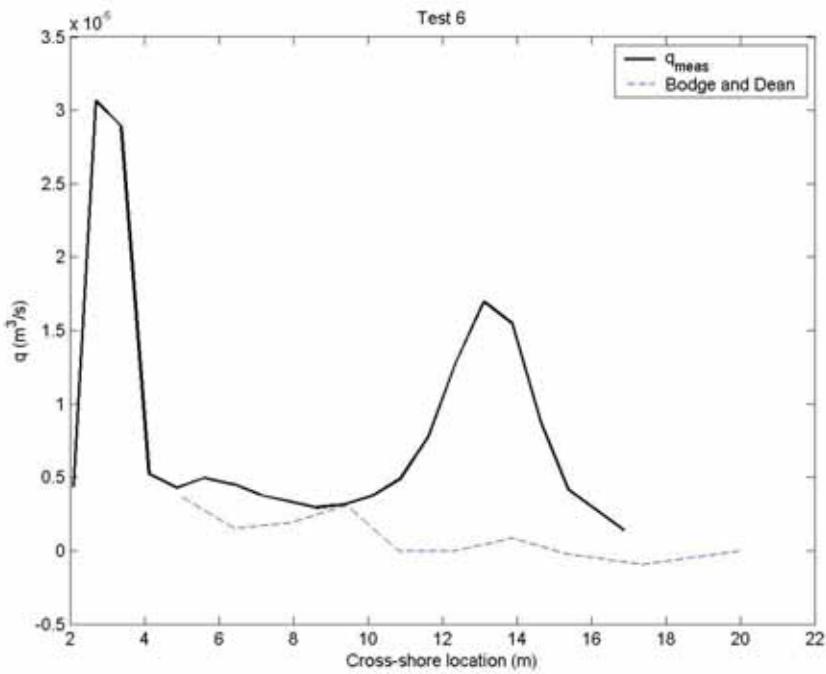
Figure 6-5. Bodge and Dean (1987) estimates (with slope term)
compared to Test 6 measurements

that were not measured. The model underpredicted transport with plunging waves. Breakpoint bars are associated with plunging waves, and longshore transport is large in the trough of the bar. However, the slope is negative from the bar crest to bar trough, and the Bodge and Dean (1987) model with the slope term does not estimate transport if bottom slope is negative.

Bodge (1989) later suggested omitting the slope term of Bodge and Dean (1987) because scaling effects in the laboratory may have exaggerated the relationship between beach slope and sediment transport, Equation 2-52. This version of the model was compared to longshore sediment flux measurements of the LSTF with $k_q = 0.057$. The resultant model significantly overpredicted Test 1 measurements (Figure 6-6). The model estimated the trend of the Test 3 sediment distribution, but slightly overestimated the peak near breaking and greatly overpredicted transport shoreward of breaking (Figure 6-7). Test 5 measured transport rates were greatly overpredicted and did not follow the trend well (Figure 6-8). Measurements of Test 6 were overpredicted, although the model estimated a peak near breaking (Figure 6-9).

The suggested form of the Bodge and Dean (1987) overestimated longshore sediment transport rates for all of the LSTF tests. However, exclusion of the slope term produced a peak near breaking of the plunging wave cases. The coefficient k_q was reduced to 0.01 and compared to the LSTF tests. Figure 6-10 shows the Bodge and Dean equation results with the reduced coefficient compared to Test 1 measurements. Predictions were similar to those obtained with the model including the slope term; the model estimated the general trend of the distribution, but yielded fluctuations in
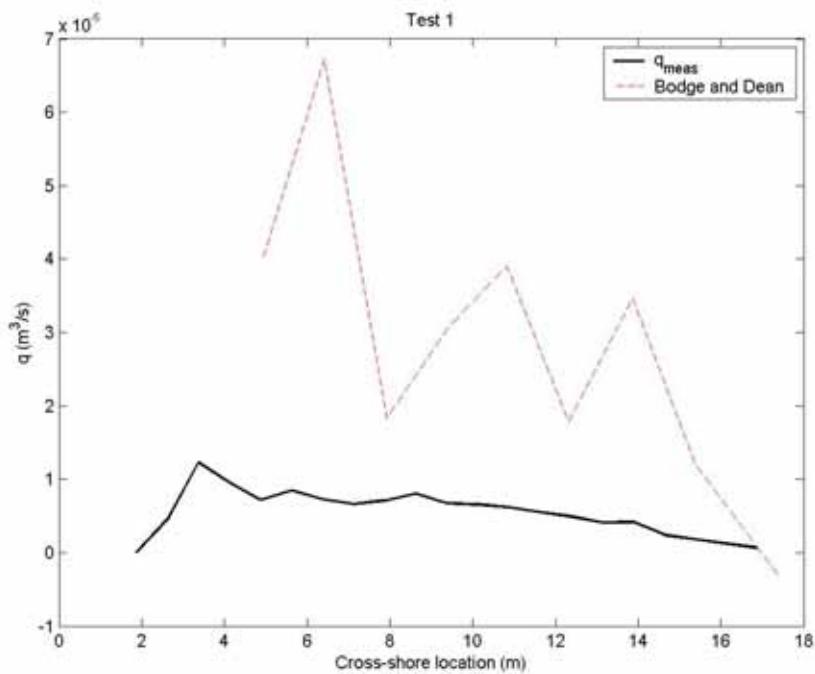
Figure 6-6. Bodge and Dean (1987) estimates compared to Test 1 measurements
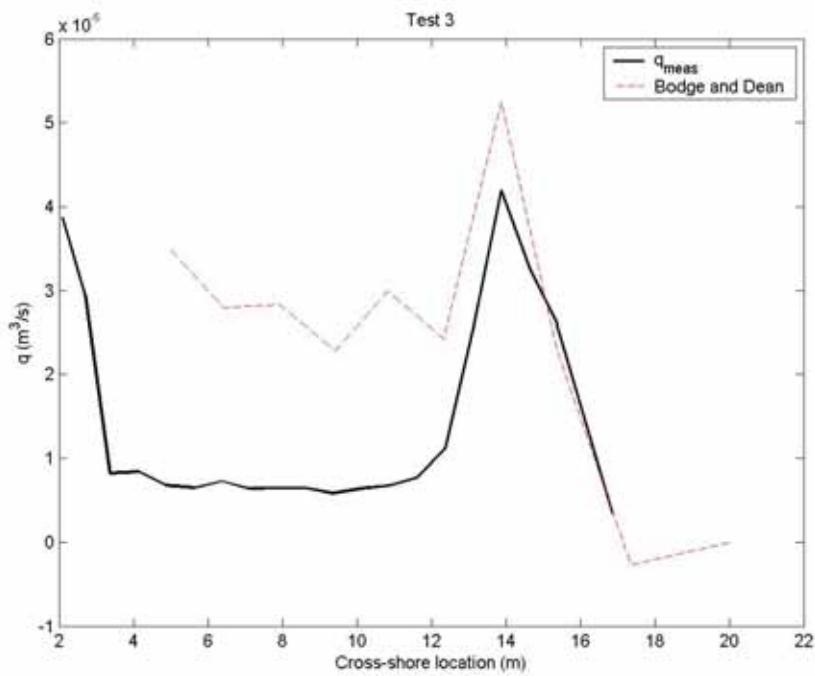
Figure 6-7. Bodge and Dean (1987) estimates compared to Test 3 measurements
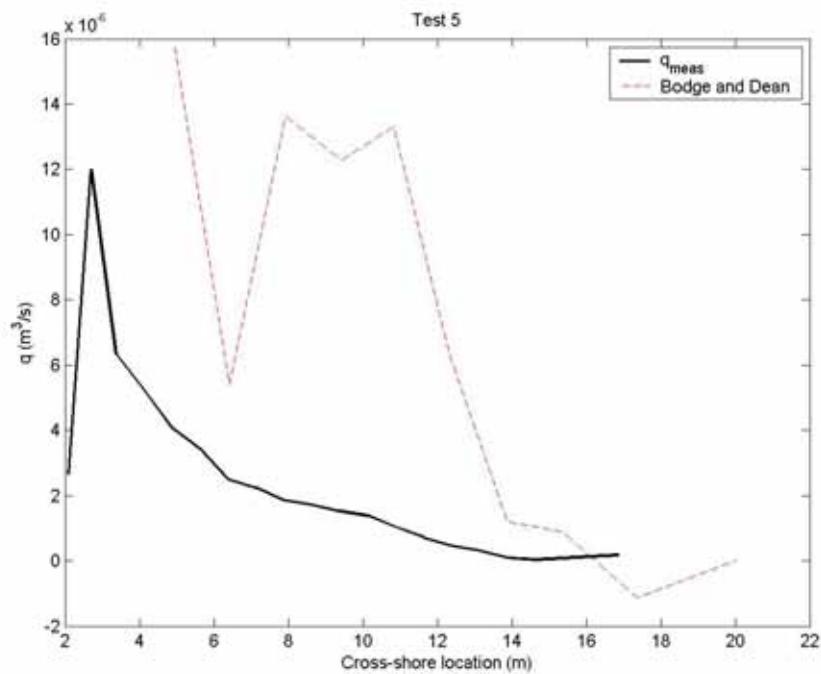
Figure 6-8. Bodge and Dean (1987) estimates compared to Test 5 measurements
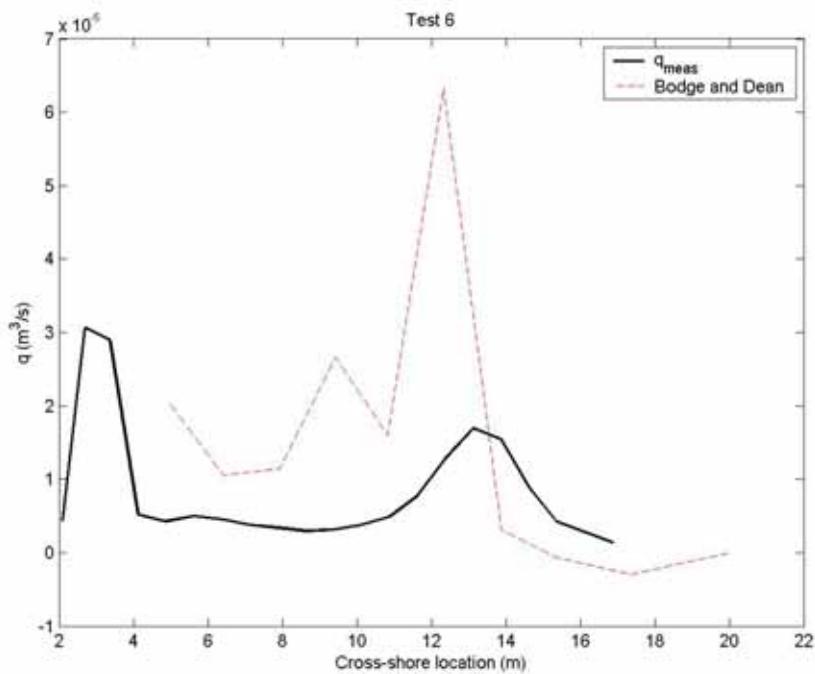
Figure 6-9. Bodge and Dean (1987) estimates compared to Test 6 measurements
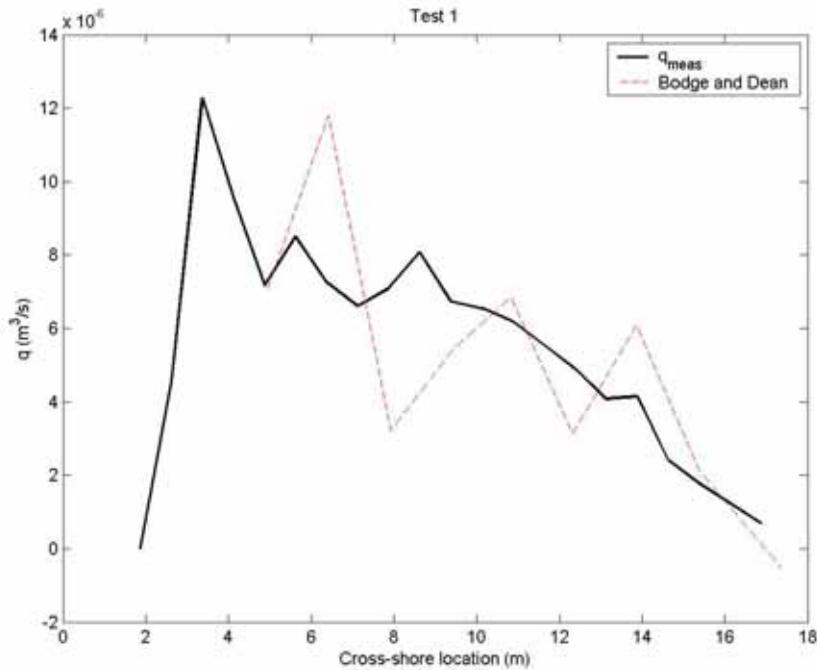
Figure 6-10. Bodge and Dean (1987) estimates compared to Test 1 measurements (k_q = 0.01)

transport rates. The model estimated a peak in transport near breaking of the Test 3

plunging waves test (Figure 6-11). However, all predictions underestimated the

measurements. Estimates with Test 5 were slightly overpredicted, although the model

predicted the general trend of the measurements (Figure 6-12). In general, estimates

were good for Test 6 waves (Figure 6-13). A peak in transport near breaking was

predicted, although the measurements were underestimated.

Reducing the coefficient k_q to 0.01 improved predictions with the Bodge and Dean

(1987) model that excluded the slope term. Predictions were similar to the original

model that included the slope term and k_q = 0.057. In addition, dropping the slope term
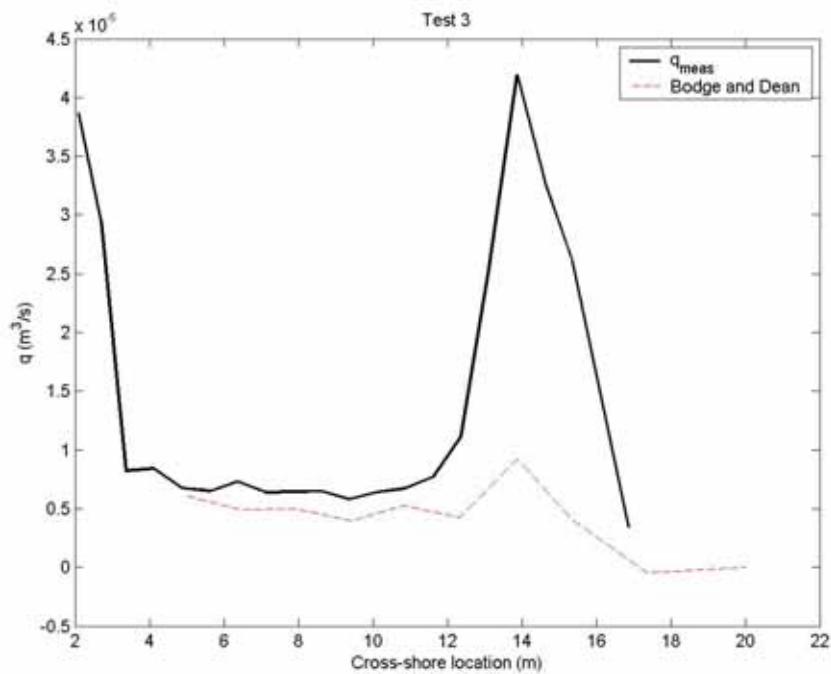
Figure 6-11. Bodge and Dean (1987) estimates compared to Test 3 measurements ($k_q = 0.01$)
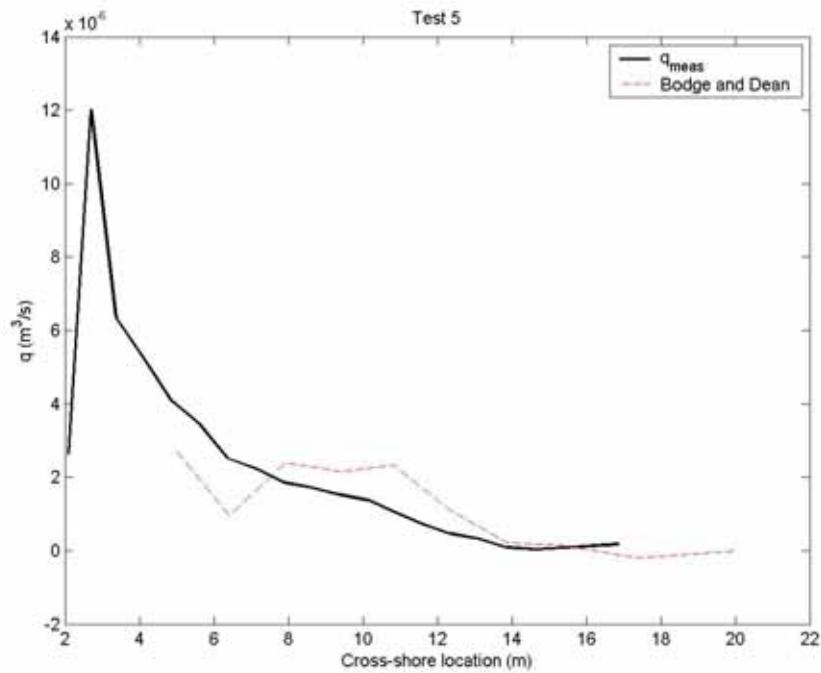
Figure 6-12. Bodge and Dean (1987) estimates compared to Test 5 measurements ($k_q = 0.01$)
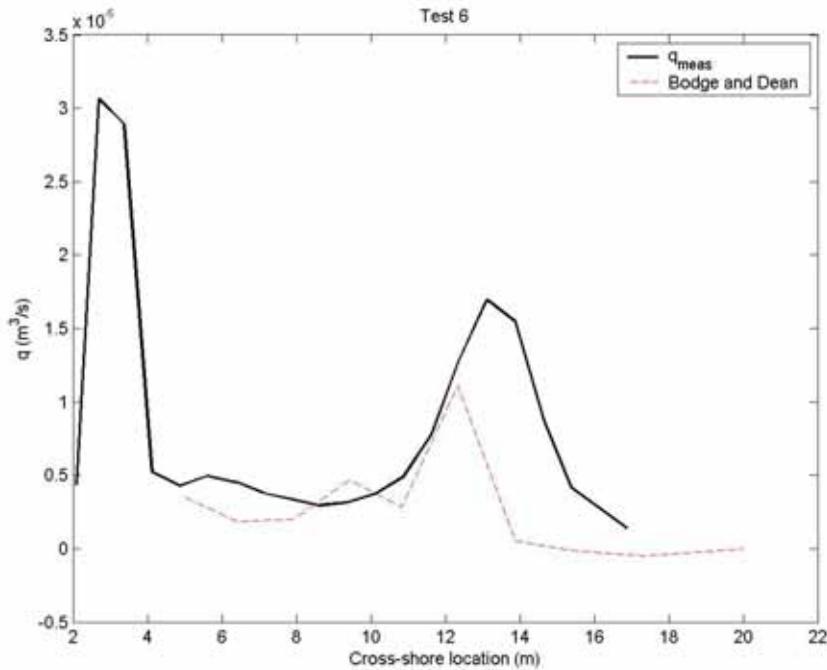
Figure 6-13. Bodge and Dean (1987) estimates compared to Test 6 measurements ($k_q = 0.01$)

from the equation allowed peaks in transport to be estimate in the trough of breakpoint bars. However, the model was very sensitive to changes in energy flux.

Equation 2-51, the form of the equation suggested by Bodge (1989), was compared to field measurements. The model was applied to SIS 15 and SIS 19 transects with the recommended field value of the coefficient, $k_q = 0.48$, Figures 6-14 and 6-15, respectively. Predictions greatly overestimated measurements by an order of magnitude for both transects. The model also was applied with the coefficient k_q reduced to 0.04 (Figures 6-16 and 6-17). Estimates of longshore transport were improved; however, the figures illustrate the sensitivity of the equation to change in energy flux.
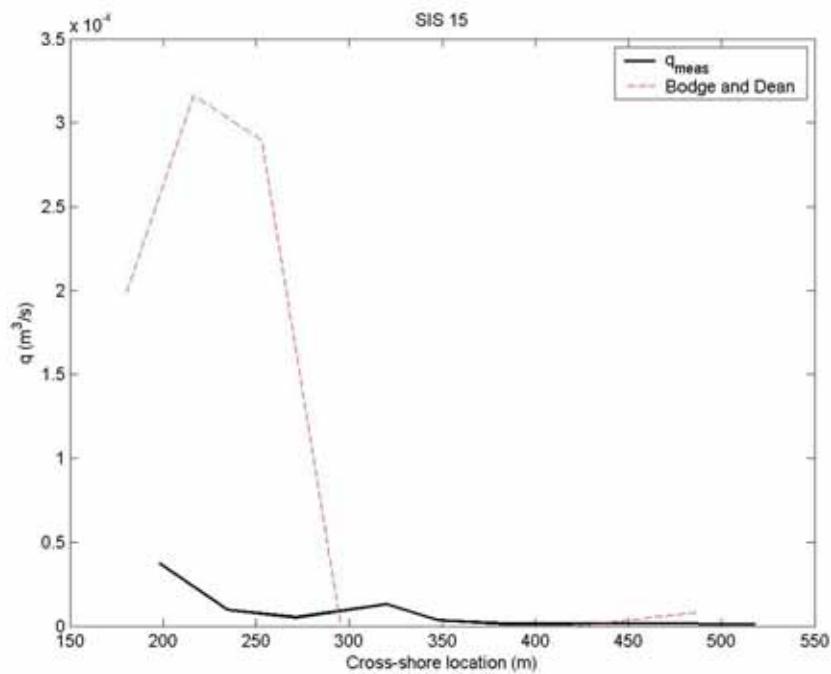
Figure 6-14. Bodge and Dean (1987) estimates compared to SIS 15 measurements
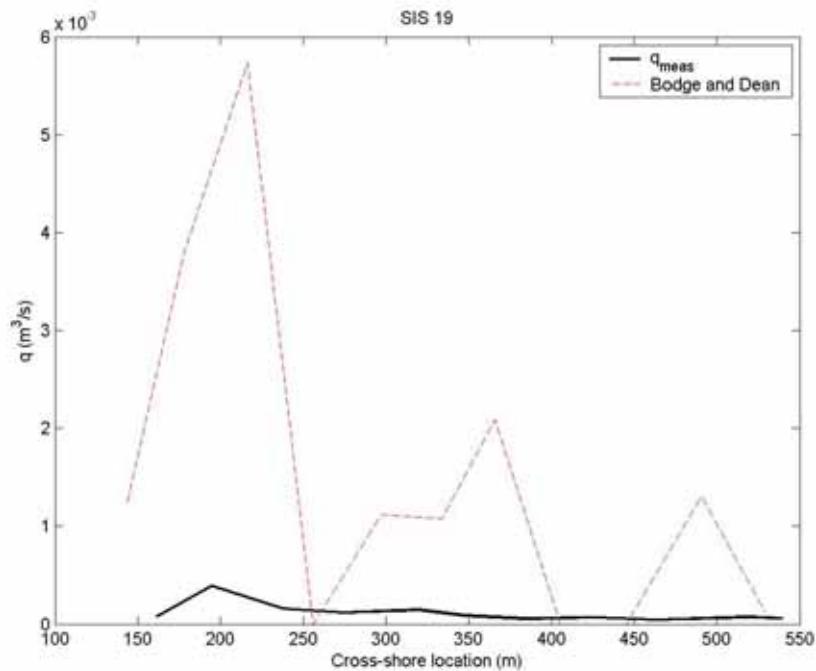
Figure 6-15. Bodge and Dean (1987) estimates compared to SIS 19 measurements
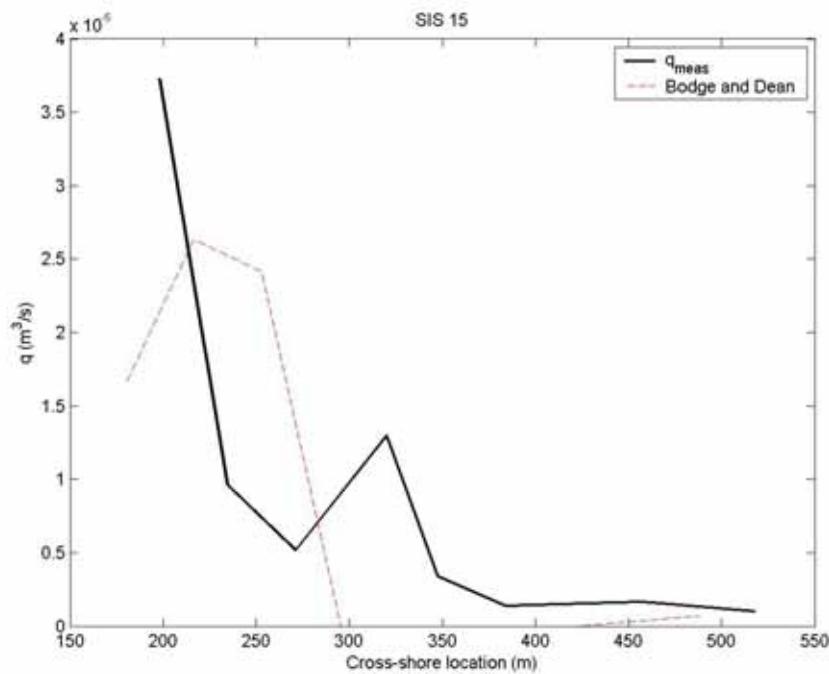
Figure 6-16. Bodge and Dean (1987) estimates compared to SIS 15 measurements ($k_q = 0.04$)
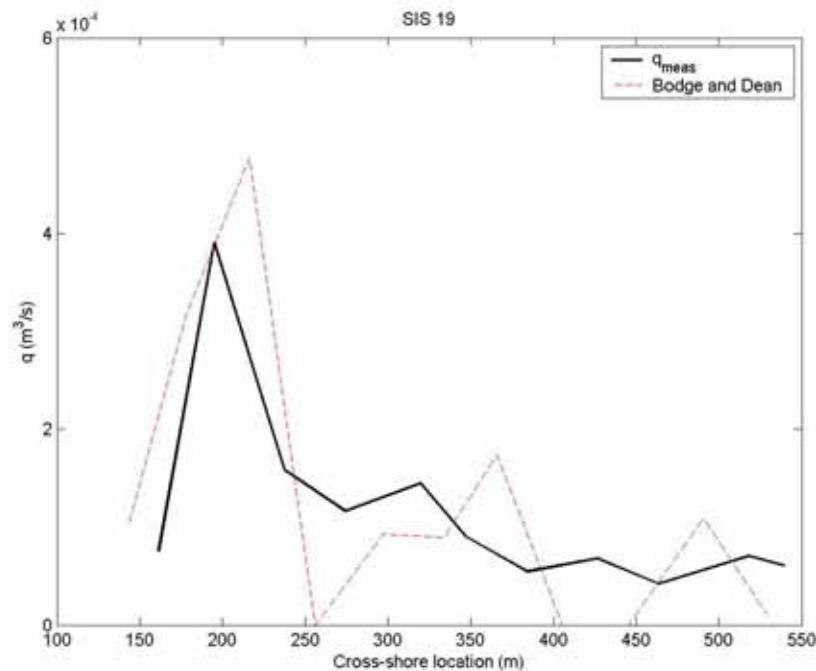
Figure 6-17. Bodge and Dean (1987) estimates compared to SIS 19 measurements ($k_q = 0.04$)

Watanabe (1992) Model

The Watanabe (1992) model, Equation 2-53, is based on the exceedance of the critical shear stress by the averaged bottom shear stress due to waves and currents. The model was applied to the LSTF tests with the coefficient $A = 2.0$. Transport was predicted for only the most shoreward ADV location for Test 1 conditions (Figure 6-18) because the time-averaged bottom shear stress only exceeded critical shear at that location. A similar result occurred if the equation was compared to Test 3 measurements (Figure 6-19). No transport was predicted for Test 5 and Test 6. The model failed when comparing to the laboratory data because it only estimates transport where the time-averaged bottom shear stress exceeds the critical shear. Adjustment of the coefficient
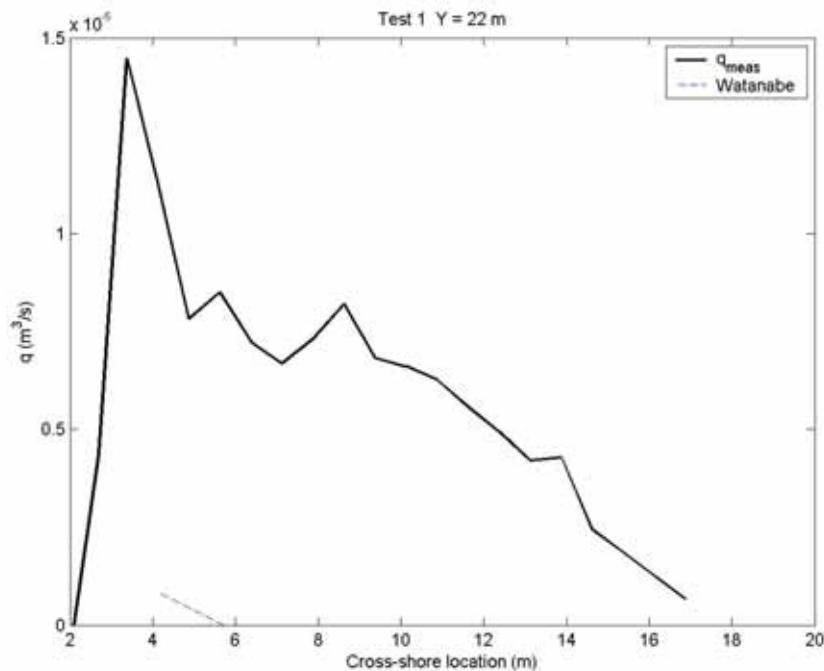
Figure 6-18. Watanabe (1992) estimates compared to Test 1 measurements
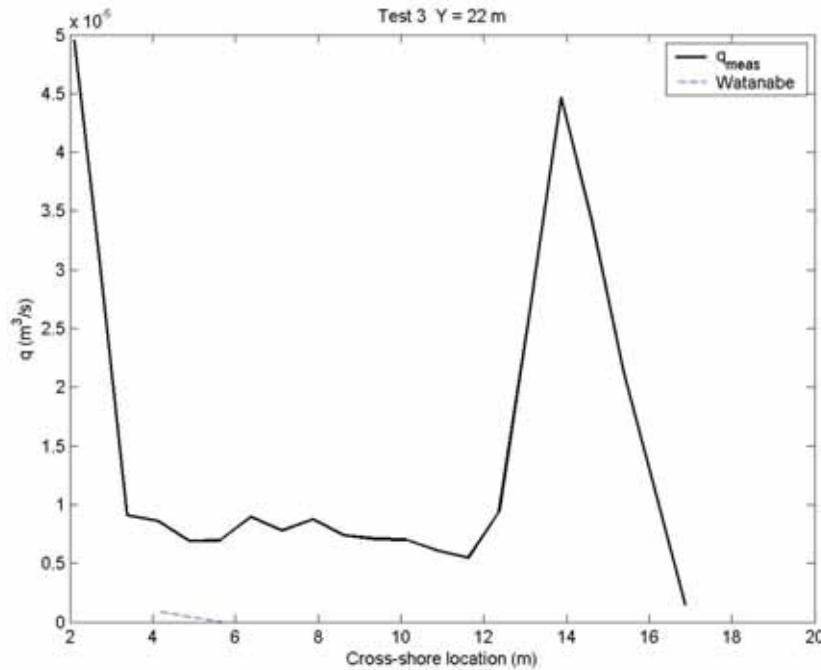
Figure 6-19. Watanabe (1992) estimates compared to Test 3 measurements

will not produce estimates where critical shear stress is not exceeded by the time-averaged bottom shear stress. For example, A was increased to 30 and compared to Test 1 measurements (Figure 6-20). The model estimated the measurement at the shoreward-most ADV, which was the only location the model predicted transport.

Bottom shear stresses are much greater in the field; therefore, the Watanabe (1992) model should perform better when applied to the SIS data. In contrast to the laboratory data, the model estimated transport at all cross-shore locations for SIS 15 and SIS 19, shown in Figures 6-21 and 6-22, respectively. However, the equation overestimated measurements of both transects by an order of magnitude. Reducing the coefficient to $A = 0.25$ improved estimates with SIS 15 (Figure 6-23). The form of the distribution
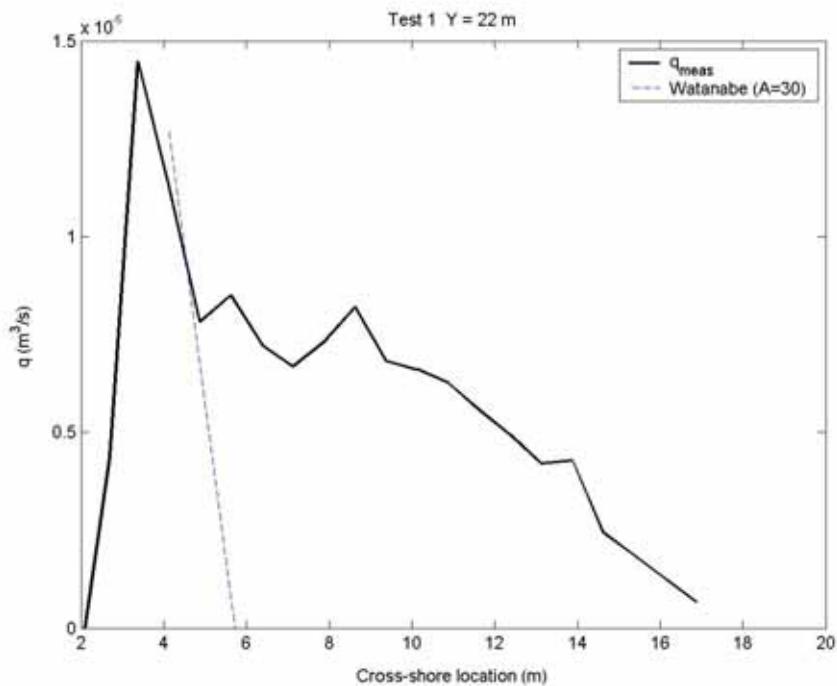
Figure 6-20. Watanabe (1992) estimates compared to Test 1 measurements ($A = 30$)
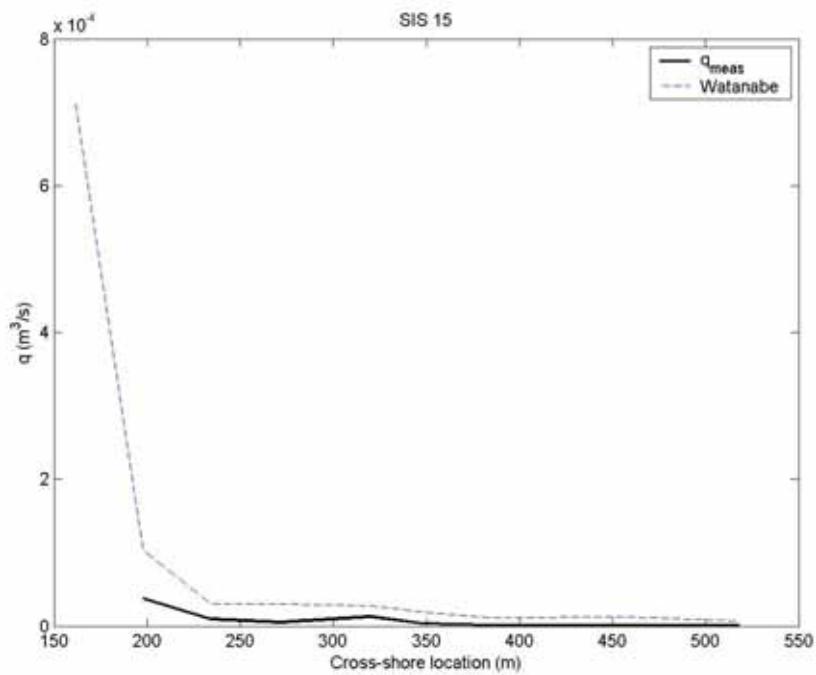
Figure 6-21. Watanabe (1992) estimates compared to SIS 15 measurements
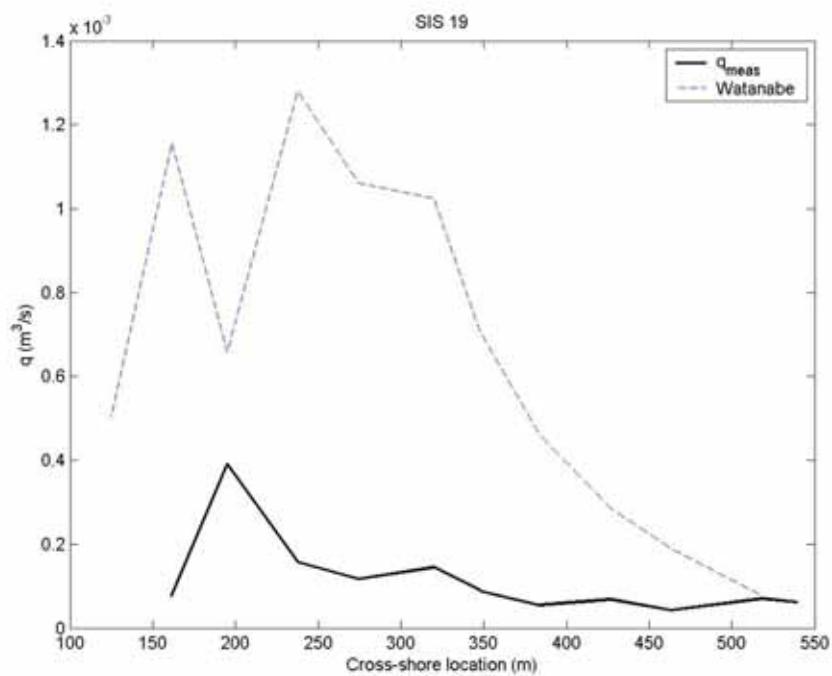
Figure 6-22. Watanabe (1992) estimates compared to SIS 19 measurements
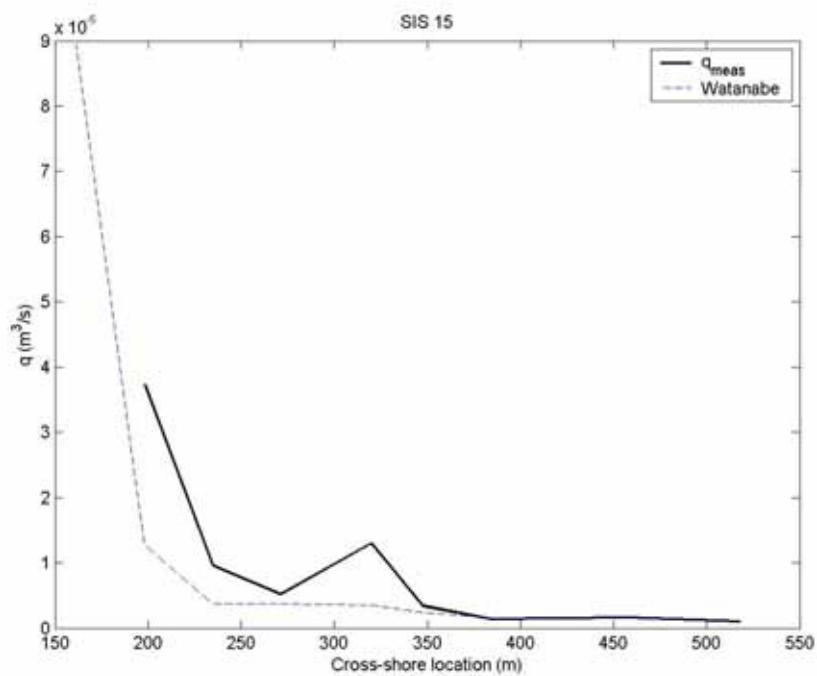
Figure 6-23. Watanabe (1992) estimates compared to SIS 15 measurements ($A = 0.25$)

was modeled well, but the formula underpredicted measurements shoreward of

X = 350 m. The model predicted the distribution of SIS 19 measurements well

(Figure 6-24). However, the equation did not model the peak in transport at breaking

and showed a decrease in transport at the location.
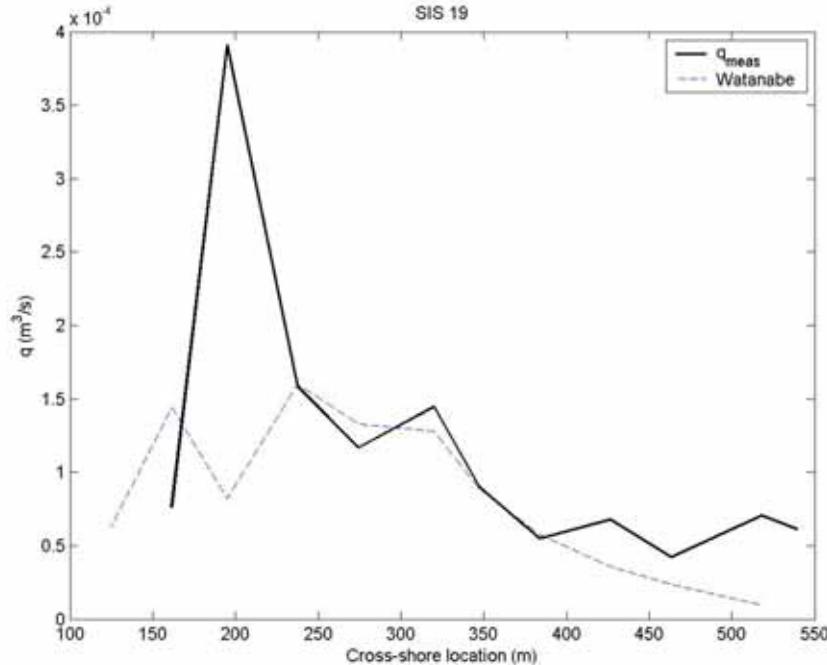
Figure 6-24. Watanabe (1992) estimates compared to SIS 19 measurements (*A* = 0.25)

The Watanabe (1992) model estimated the field data generally well if the coefficient

A was reduced to 0.25. However, it did not model the peak in transport observed at

breaking for SIS 19. The time-averaged bottom shear stress computed from the

laboratory data did not exceed the critical shear stress, which caused the model to fail in

predicting transport. The Watanabe model shows the capability of reproducing the

general trend of the field data, but because of its failure to predict the transport

measurements in the laboratory, it appears that application of the mean value of bottom shear stress should not be used in equations involving critical shear stress for laboratory applications. More generally, this observation indicates there is a substantial scaling distortion for small-scale and even mid-scale laboratory experiments, where the bottom shear stress based on mean currents rarely exceeds the critical value for sediment motion. Therefore, one would expect relatively substantial bedload transport, perhaps by saltation, as compared to suspended sediment transport, in contrast to the opposite situation expected in the field (Dean 1985; Madsen et al. 2003).

Van Rijn (1993) Model

In addition to hydrodynamic forcing conditions, application of the Van Rijn (1993) model requires knowledge of the grain size distribution, bed forms, and dimensions of the bed forms, i.e., ripple height and length, to compute roughness coefficients. Predictions of the Van Rijn model compared to the Test 1 measurements are shown in Figure 6-25. The model overestimated measurements offshore of X = 9 m and underestimated measurements between X = 7 m and X = 9 m. Measurements in the swash zone were slightly overpredicted. With exception of the underestimated points, the model predicted the general form of the distribution. Estimates generally compared well to the Test 3 measurements (Figure 6-26), although the peak in transport near breaking was underestimated. Also included in the plot is a point, denoted by a circle, which shows estimated transport rate using a rippled bed form to calculate bed
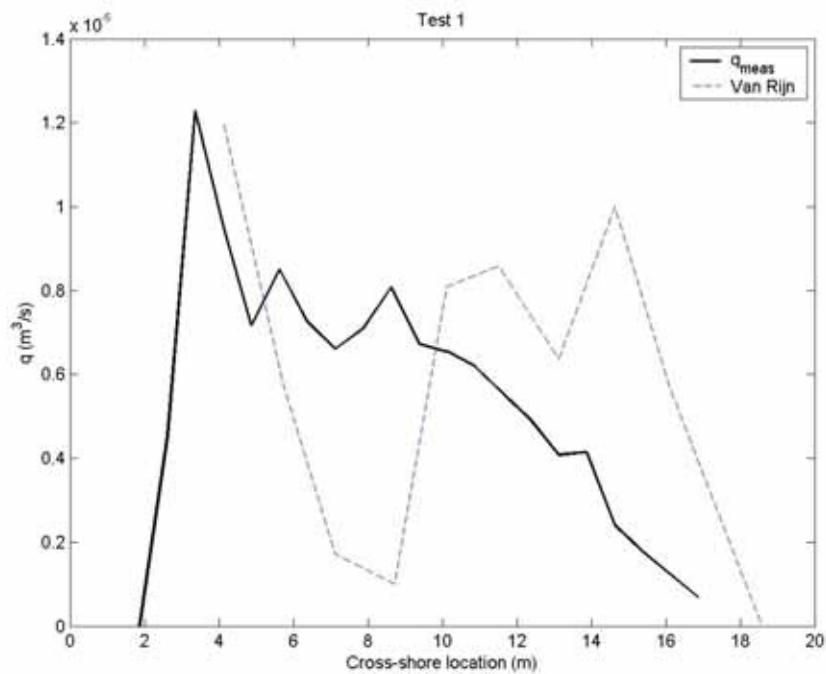
Figure 6-25. Van Rijn (1993) estimates compared to Test 1 measurements
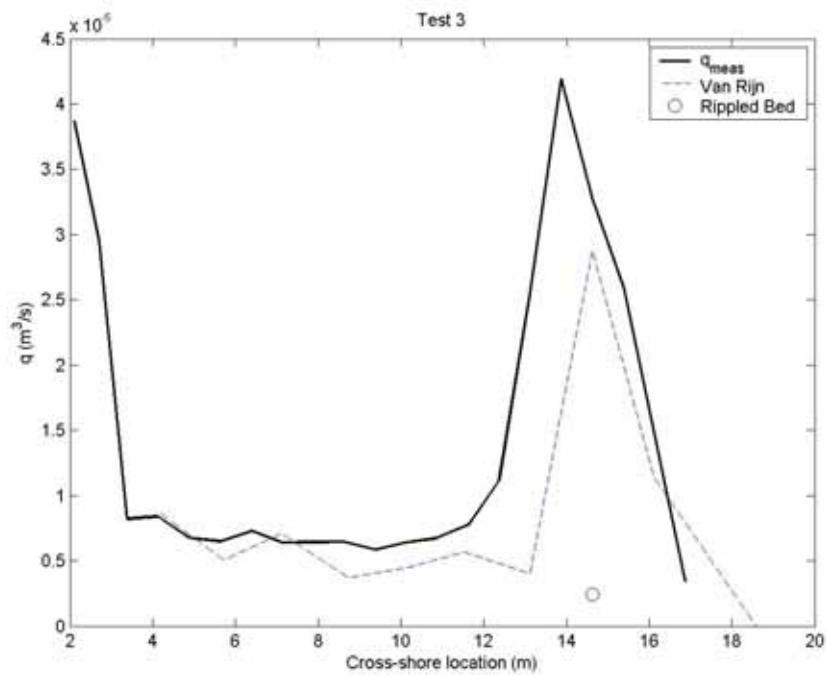
Figure 6-26. Van Rijn (1993) estimates compared to Test 3 measurements

roughness at the Test 3 breakpoint bar. Rippled bed forms were present at all locations

in the LSTF tests, with the exception of where sheet flow occurred: the swash zone of

each test and in the trough of the Test 3 breakpoint bar. If a rippled bed form was

assumed for all cross-shore locations, the peak in transport near breaking would be

greatly underestimated and not correctly simulated. This illustrates the requirement of

understanding the local littoral processes to achieve accurate results when applying

the Van Rijn model. The model estimated the trend of the Test 5 distribution, but

overpredicted measured transport at most cross-shore locations (Figure 6-27). Test 6

estimates were lower than measurements (Figure 6-28), although the model predicted a

broad peak in transport near breaking.
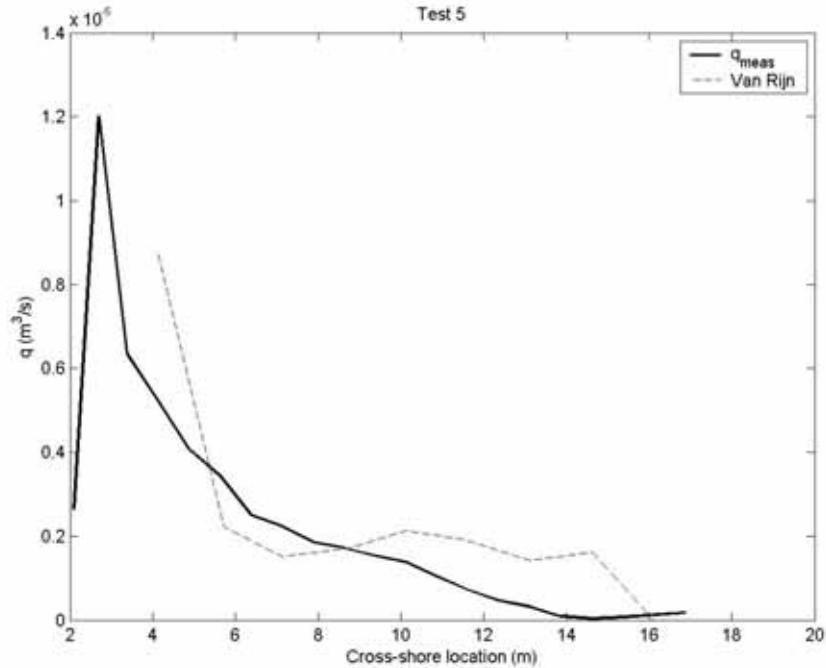
Figure 6-27. Van Rijn (1993) estimates compared to Test 5 measurements
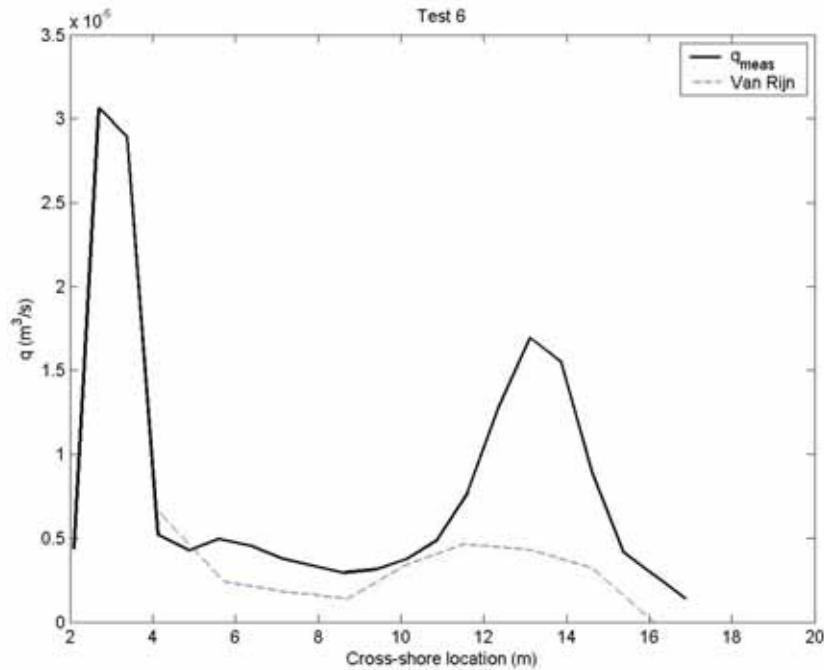
Figure 6-28. Van Rijn (1993) estimates compared to Test 6 measurements

Results of the Van Rijn (1993) model greatly overestimated SIS 15 and SIS 19 field

measurements (Figures 6-29 and 6-30, respectively). Although there are no explicit

empirical coefficients to adjust, the results were reduced by a factor of 50 to compare the

predicted distribution of sediment transport with measurements. The reduction produced

slightly underestimated results when compared to SIS 15, but the form of the distribution

was predicted well (Figure 6-31). The model also predicted the distribution of SIS 19

measurements well, although estimates were slightly higher than measurements

(Figure 6-32). The peak in transport near breaking was significantly lower than the

measurement and located slightly offshore.
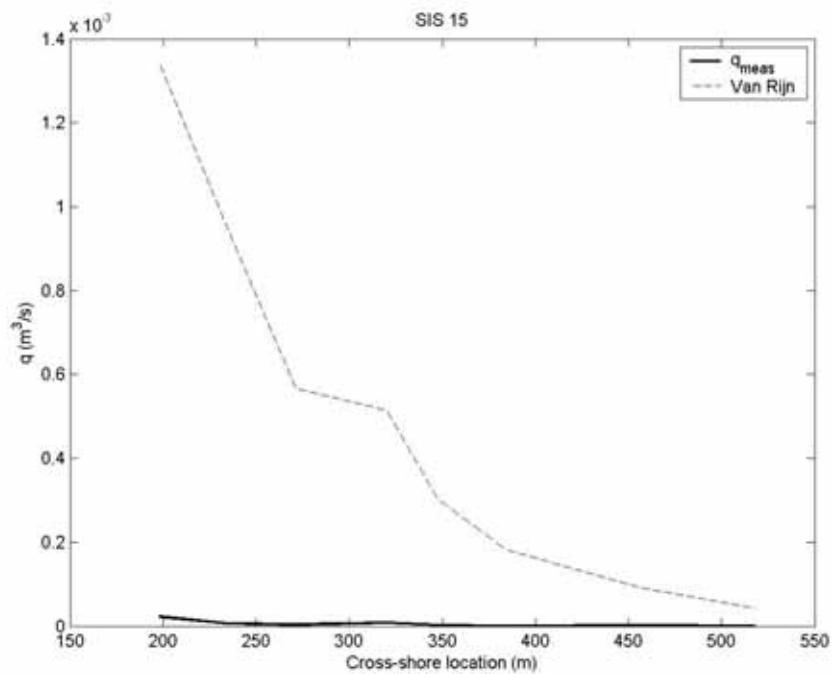
Figure 6-29. Van Rijn (1993) estimates compared to SIS 15 measurements
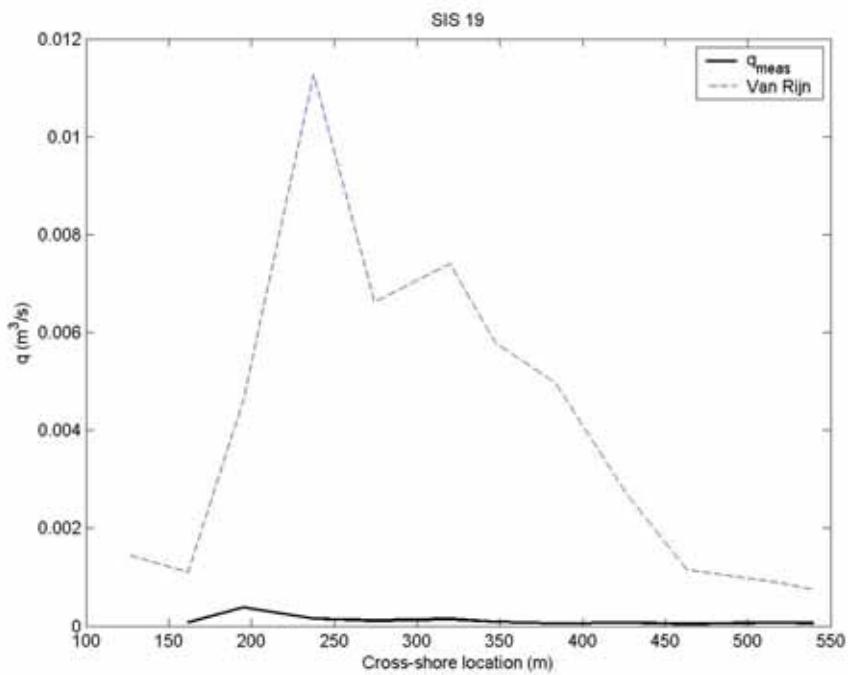
Figure 6-30. Van Rijn (1993) estimates compared to SIS 19 measurements
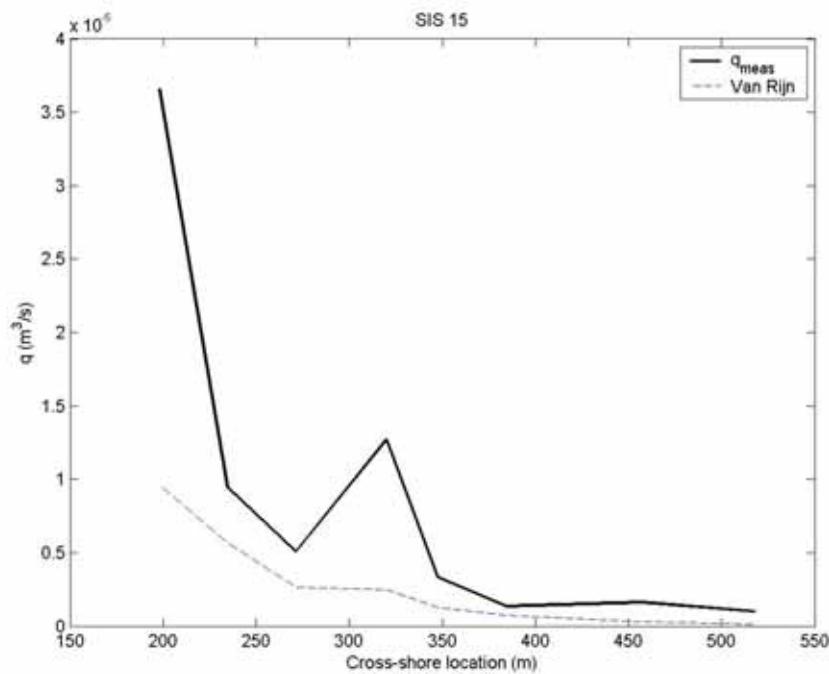
Figure 6-31. Van Rijn (1993) estimates reduced by 50 compared to SIS 15 measurements
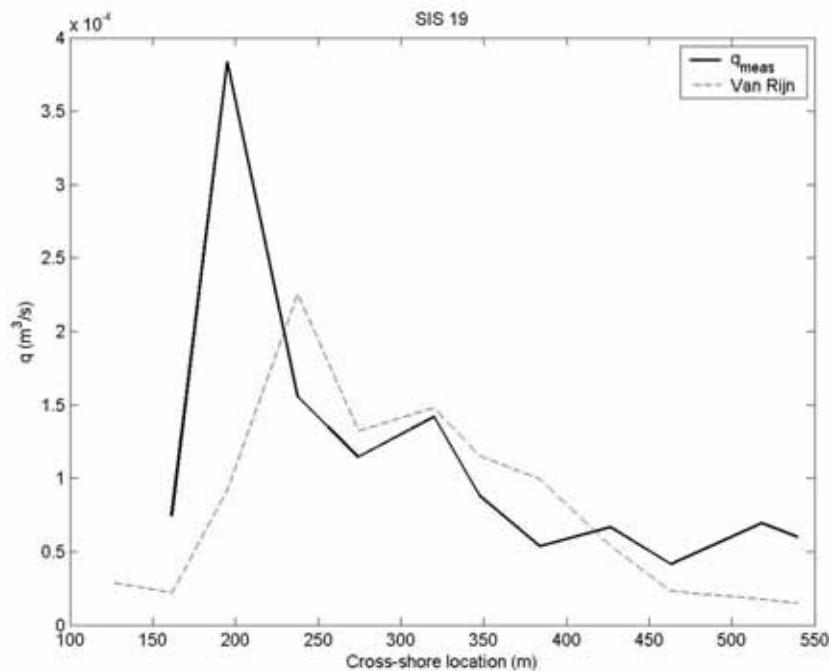
Figure 6-32. Van Rijn (1993) estimates reduced by 50 compared to SIS 19 measurements

The Van Rijn (1993) model predicted LSTF laboratory sediment transport distribution well, but greatly overpredicted field measurements of the SIS. However, the model predicted the form of longshore sediment distribution well, and reducing the field estimates by 50 gave reasonable estimates.

Summary of Distribution Models

The Bodge and Dean (1987) energetics model was sensitive to fluctuations in energy dissipation and often predicted peaks in transport that were not present in the data, an observation noted by Smith and Wang (2001). Because the equation is based on energy dissipation, no transport is predicted if waves shoal. If the slope term is included in the equation, transport cannot be predicted at the trough of a breakpoint bar, where bottom slope is negative between the bar crest and trough.

The Watanabe (1992) equation predicted transport for only one cross-shore location in two of the LSTF tests, and gave no transport at any location for the other two tests. The time-averaged bottom stress did not exceed the critical shear stress at the majority cross-shore locations, resulting in no transport estimates. Therefore, time averaged bottom stresses are evidently not adequate for a model that involves critical shear stress or critical velocity for inception of sediment motion. The model estimated the field data well if the empirical coefficient was reduced by a factor of 8 from 2.0 to 0.25. The distribution was estimated well, but the model did not predict the peak in transport near breaking with transect SIS 19.

The Van Rijn (1993) model estimated the laboratory data well, but overestimated the field data by a factor of approximately 50. The model estimated the distribution of the field data, but underestimated the peak near the breakpoint of SIS 19. The model is comprehensive, and the input requires detailed information of the bed at each cross-shore location to produce accurate estimates.

Each of the selected models examined has shortcomings. Comparison of the Bodge and Dean (1987) model to laboratory and field data indicates that energetics models are sensitive to energy dissipation. The Van Rijn (1993) model is complex and requires information on many parameters. Accurate estimates cannot be made quickly with the Van Rijn model. The main disadvantage of the Watanabe (1992) model is that it applies a time-averaged bottom shear stress in excess of the critical shear to compute longshore sediment transport. A more appropriate model would incorporate the fluctuations in bottom shear to predict transport, and this type of model will be discussed in the following chapter. However, the Watanabe model is theoretically correct in incorporating a critical shear stress for inception of sediment motion. In fact, such an assumption, from a theoretical point of view, is implied in all sediment transport formulas.

CHAPTER VII

NEW LONGSHORE SEDIMENT TRANSPORT MODELS

Introduction

The predictive models evaluated in Chapter VI did not perform well in comparisons to high-quality laboratory and field data. Therefore, an examination of transport mechanics from a more basic approach was warranted, and this work is described in this chapter.

Improvements to modeling the cross-shore distribution of longshore sediment flux, leading to new types of predictive formulas, were based on the premise that transported sediment is first mobilized by the total shear stress acting on the bottom and then transported by the current at that location. Madsen (1991) stated that any model of sediment response to fluid forces that relies on the mean turbulent flow characteristics is limited to be conceptual. The shear stress, including the turbulent component together with the mean value, can be calculated from the wave orbital velocity measured with the ADVs installed in the LSTF and EMCMs deployed in the SIS. The concept of including the turbulent component was motivated by the findings of Kraus et al. (1988), who demonstrated that trends in prediction of the local longshore sediment transport rate in the surf zone improved by including the dissipation by waves and standard deviation in the longshore current velocity, both of which increase turbulent fluctuations in the water and on the bed.

The first step in developing the transport models was to determine if shear stresses

computed from the wave orbital velocities would produce a distribution representative of

the distribution of longshore sediment flux. Figure 7-1 shows the standard deviation of

cross-shore wave orbital velocity $\sigma(u)$ measured at the one-third depth from the bottom

for each of the LSTF tests. The distribution of $\sigma(u)$ has a similar shape to longshore

sediment transport rate (Figure 4-53). The larger fluctuations in u associated with the

plunging wave tests, Test 3 and Test 6, correspond to the peaks in sediment flux

observed near breaking for those tests. This comparison indicates that fluctuations in

orbital velocities, or turbulence, lead to an increase in mobilized sediment, which then
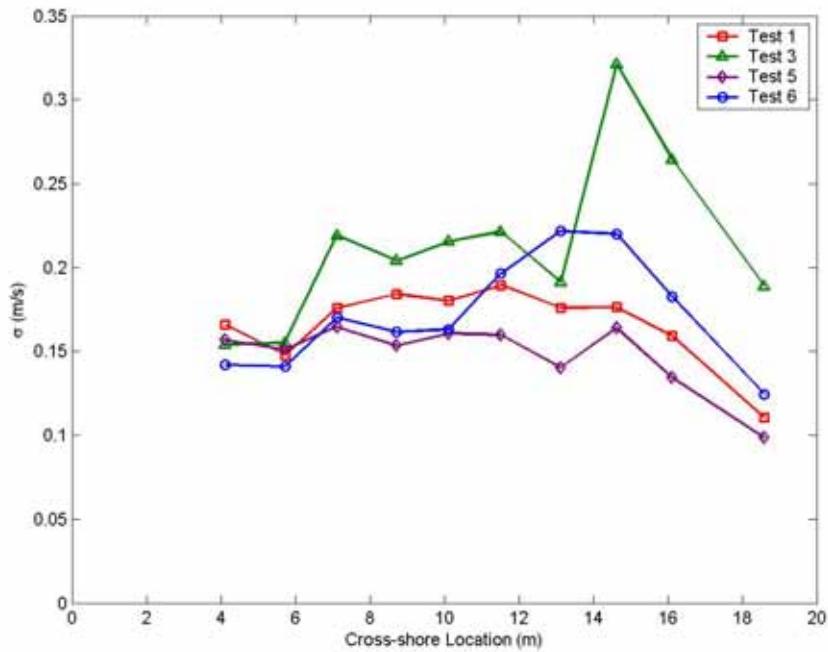
Figure 7-1. Standard deviation of cross-shore component of wave orbital velocities

can be transported by the longshore current. This chapter describes models developed based on shear stresses computed from the time series of the LSTF ADVs, which includes the turbulent components of the orbital velocities. The models are tested against both the laboratory data and the field data collected with the SIS.

Definitions

Development of the models assumes that the velocity records analyzed describe a stationary process, which implies that there is no systematic change in the mean or variance of the record if it is divided into smaller records. To test this assumption, the velocity record of Test 1, Case 1, Y = 22 m was divided into quarters, and the cross-shore orbital velocities were calculated. The mean and standard deviation for each quarter segment are listed in Table 7-1. The mean and standard deviation of the entire record is defined as U and $\sigma(u)$, respectively, and the subscripts 1 through 4 denote the statistic for each respective quarter segment. Some variability is present, but the values are similar, and a systematic trend is not evident. A small amount of variability is expected because the wave trains were random.

The total cross-shore component of velocity can be written:

$$u(t) = U + u'(t) \tag{7-1}$$

where U = mean of $u(t)$, and $u'(t)$ is the turbulent or random component. For a random Gaussian process:

$$\langle u'(t) \rangle = \frac{1}{T} \int_0^T u'(t)\, dt = 0 \qquad (7\text{-}2)$$

Table 7-1. Mean and standard deviation of u for Test 1, Case 1, Y = 22 m

ADV	U (m/s)	U_1 (m/s)	U_2 (m/s)	U_3 (m/s)	U_4 (m/s)	$\sigma(u)$ (m/s)	$\sigma(u)_1$ (m/s)	$\sigma(u)_2$ (m/s)	$\sigma(u)_3$ (m/s)	$\sigma(u)_4$ (m/s)
1	0.050	0.059	0.054	0.053	0.044	0.166	0.167	0.164	0.166	0.166
2	0.045	0.055	0.040	0.046	0.040	0.148	0.156	0.138	0.139	0.150
3	0.068	0.073	0.063	0.070	0.069	0.176	0.191	0.166	0.164	0.177
4	0.067	0.069	0.065	0.071	0.065	0.184	0.174	0.189	0.185	0.185
5	0.047	0.048	0.034	0.055	0.053	0.180	0.173	0.178	0.188	0.180
6	0.055	0.057	0.043	0.069	0.053	0.189	0.186	0.179	0.204	0.189
7	0.053	0.047	0.040	0.063	0.060	0.176	0.167	0.169	0.186	0.177
8	0.040	0.038	0.023	0.048	0.043	0.176	0.164	0.165	0.187	0.179
9	0.031	0.020	0.012	0.045	0.029	0.159	0.142	0.154	0.178	0.159
10	0.006	0.020	0.015	0.012	0.010	0.111	0.099	0.112	0.125	0.108

where T is the averaging interval that is taken as the wave period for monochromatic waves, and the triangular brackets denote a time average. For random waves of many periods, T can be taken as the time length of the record, assuming a record encompassing many waves, but retaining stationarity. A small bias may exist because of wave non-linearity, undertow, and mass transport, as well as periodic and turbulent motions in nature or in the laboratory basin. Equation 7-2 is a standard assumption in dealing with fluid turbulence.

Similarly, the total longshore current velocity can be written as:

$$v(t) = V + v'(t) \tag{7-3}$$

where V is the time mean of $v(t)$, and $v'(t)$ is the turbulent component. For a random

Gaussian process:

$$\langle v'(t) \rangle = \frac{1}{T} \int_0^T v'(t)\, dt = 0 \tag{7-4}$$

Transport Rate Formulas

Several transport formulas will be investigated, which can be expressed through the

concept of:

$$q(t) = ST(t) \times TR(t) \tag{7-5}$$

where $q(t)$ is the time-dependent transport rate per unit length perpendicular to the

transport, ST is a stirring function that mobilizes the sediment, and TR is a transporting

function that moves the sediment (Kraus and Horikawa 1990). All of these quantities

are functions of time, t. A critical shear stress or critical velocity will enter into either

the Stirring Function or the Transporting Function, depending on the particular formula.

Equation 7-5 must be averaged over the time record, with the average taken over the

full expression, although the averages of each quantity on the right may be of interest in

examining the physical processes of stirring and transport. For example, one model is

the time-mean of longshore transport rate:

$$q_y = K \left\langle \left(ST(t) - \tau_{cr} \right) \left(TR_y(t) \right) \right\rangle \tag{7-6}$$

where K = empirical parameter that may involve several dimensional quantities,

depending on the particular stirring function, $ST(t)$ and transporting function $TR_y(t)$. The

critical shear stress for inception of sand movement τ_{cr} is, based on the definition of the

Shields parameter:

$$\tau_{cr} = \left(\rho_s - \rho_w\right) g d_{50} \theta_{cr} \tag{7-7}$$

in which ρ_w is density water (1,000 kg/m^3 for the LSTF), ρ_s is density of sand (2,650

kg/m^3), g is acceleration due to gravity (9.806 m/sec^2); d_{50} is median grain size of sand

(0.00015 m for LSTF sand); and θ_{cr} is the critical Shields parameter for sediment

motion, taken to be 0.08 here. For the LSTF sand, Equation 7-7 gives τ_{cr} = 0.12 kg

m/sec^2/m^2 = 0.12 N/ m^2.

Power Expression

   Power law transport formulas have a long tradition in river transport and in coastal

transport calculations. A power law implies that water velocity cubed is the dominant

process, signifying a relation to the power of the water movement. This is generally

called a Meyer-Peter and Muller formula (Meyer-Peter and Muller 1948), and we will

adopt the Watanabe (1987) version that has found common applicability in the coastal

community.

   The total shear stress exerted by the water on the sand bottom is:

$$\vec{\tau}_{tot}(t) = \hat{x}\,\tau_x + \hat{y}\,\tau_y \tag{7-8}$$

where the components are:

$$\tau_x(t) = \frac{\rho_w c_f}{2} u(t)^2 = \frac{\rho_w c_f}{2} \left(U + u'(t)\right)^2$$
$$= \frac{\rho_w c_f}{2} \left(U^2 + 2u'(t)U + u'(t)^2\right)$$

(7-9)

and

$$\tau_y(t) = \frac{\rho_w c_f}{2} v(t)^2 = \frac{\rho_w c_f}{2} \left(V + v'(t)\right)^2$$
$$= \frac{\rho_w c_f}{2} \left(V^2 + 2v'(t)V + v'(t)^2\right)$$

(7-10)

in which c_f is the bottom friction coefficient with value on order of 0.005. Equations 7-9 and 7-10 must be evaluated numerically.

The stirring function at a given time, $ST(t)$, is for a Meyer-Peter and Muller velocity cubed sediment transport power law:

$$ST(t) = \left|\vec{\tau}_{tot}(t)\right| = \sqrt{\tau_x^2(t) + \tau_y^2(t)}$$

(7-11)

The time average of this quantity over the record is:

$$\langle ST \rangle = \langle \vec{\tau}_{tot}(t) \rangle = \frac{1}{N} \sum_1^N \sqrt{\tau_x^2(t) + \tau_y^2(t)}$$

(7-12)

where N is the number of measurements in the velocity record producing the shear stresses. The stirring function is the same for both the longshore and cross-shore components of transport, because any fluid motion that disturbs the bed will stir the sand.

For ease of reading, the explicit time-dependence notation (t) will be dropped if writing u' and v' and most other quantities. The prime necessarily means time dependent, unless we take a mean or standard deviation over the record.

For the longshore transport rate, the transporting function is:

$$TR_y(t) = V + v' \tag{7-13}$$

The time average of this is:

$$\langle TR_y(t) \rangle = V + \langle v' \rangle = V \tag{7-14}$$

because $\langle v' \rangle = 0$. In other words, the mean of the transporting function is simply the mean velocity. A similar expression for the cross-shore component is:

$$TR_x(t) = U + u' \tag{7-15}$$

which should be small, at least in a depth-averaged sense, because $U = 0$ as a depth average.

For the Watanabe (1987) version of the power law formula, the time-dependent longshore transport is:

$$q_y(t) = K\left(ST(t) - \tau_{cr}\right)TR_y(t)$$

$$= K\left(\sqrt{\tau_x^2(t) + \tau_y^2(t)} - \tau_{cr}\right)(V + v') \text{ for } ST(t) > \tau_{cr} \tag{7-16}$$

$$\text{and}$$

$$= 0 \text{ for } ST(t) \leq \tau_{cr}$$

in which the coefficient K is given by:

$$K = \frac{\alpha}{\rho_w g} \qquad (7\text{-}17)$$

where α is a dimensionless empirical coefficient on order 0.1. Therefore, $K = 1.0 \times 10^{-5}$

for LSTF conditions.

The time average longshore transport rate over the record is:

$$q_y = \frac{1}{N} \sum_1^N q_y(t) \qquad (7\text{-}18)$$

The units of q_y are ("units of" denoted with braces):

$$\left[q_y \right] = [K \times \tau \times V] = \frac{1}{\dfrac{kg}{m^3}\dfrac{m}{sec^2}} \times kg\,\frac{m}{sec^2}\frac{1}{m^2} \times \frac{m}{sec}$$
$$= \frac{m^3}{sec} \qquad (7\text{-}19)$$

To compare data to the proposed model, the measured velocity must be sampled at a

sufficiently high rate. LSTF electronic instruments, including the ADVs, were sampled

at 20 Hz, which is expected to adequately capture and represent random fluctuations of

the wave orbital velocity. For waves at the peak periods of 1.5 and 3.0 sec, 30 and 60

shear stresses, respectively, would be computed in one wave period.

The ADV records contained the total velocity components $u(t)$ and $v(t)$. Fluctuations

of these quantities were determined from the mean of the records and by Equations 7-1

and 7-3:

$$u'(t) = u(t) - U \qquad\qquad (7\text{-}20)$$

$$v'(t) = v(t) - V \qquad\qquad (7\text{-}21)$$

The majority of velocity measurements were collected one-third of the depth from the bottom. Although it would be more pertinent to consider only orbital velocities collected near the bottom, such data sets are lacking; no measurements were taken near the bottom for Test 6 and only one case was conducted with near-bottom measurements for the other three tests. Additionally, the sand bottom was mobile, meaning that velocity measurements near the bottom would be more affected by the small changes in depth and are, in any case, difficult to make in setting instrument elevations many times through the surf zone. Therefore, the one-third depth measurements were adopted for all comparisons for consistency between cases.

The time series of $\vec{\tau}_{tot}$ was calculated via Equation 7-12 for Test 1, Case 3, spilling waves at Y = 22k m. The results are plotted in Figures 7-2 through 7-5, for ADVs 10, 7, 4, and 1, respectively. Critical shear stress also is plotted as a dashed line in the figures. At ADV 10, the most offshore ADV at X = 18.6 m, shear stress regularly exceeded τ_{cr} but often did not (Figure 7-2). This result indicates that the sand in the LSTF for this location was only occasionally mobilized for transport, so the transport rate is expected to be small. The magnitudes of total shear stress were much higher at ADVs 7 and 4, X = 13.13 m and X = 8.73 m, respectively, and transport rates would be expected to be greater at these cross-shore locations. Figure 7-5 shows that shear stress magnitudes
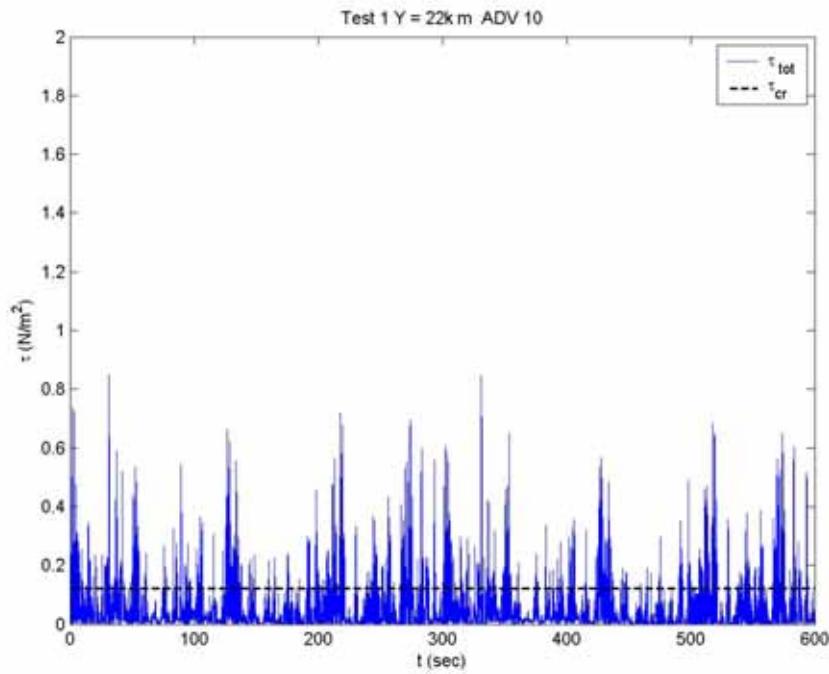
Figure 7-2. Time history of τ_{tot} at ADV 10, Test 1 Case 1, Y = 22 m
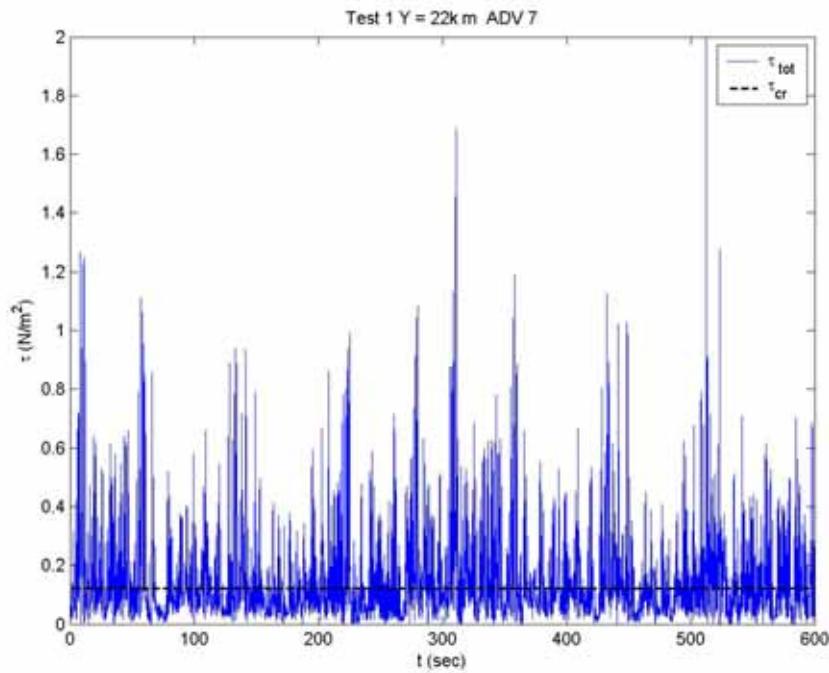
Figure 7-3. Time history of τ_{tot} at ADV 7, Test 1 Case 1, Y = 22 m
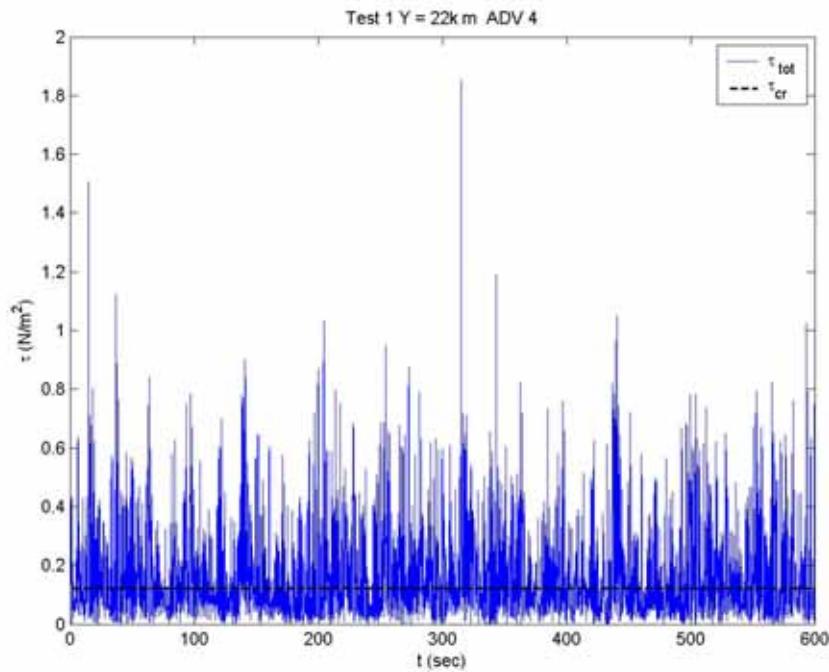
Figure 7-4. Time history of τ_{tot} at ADV 4, Test 1 Case 1, Y = 22 m
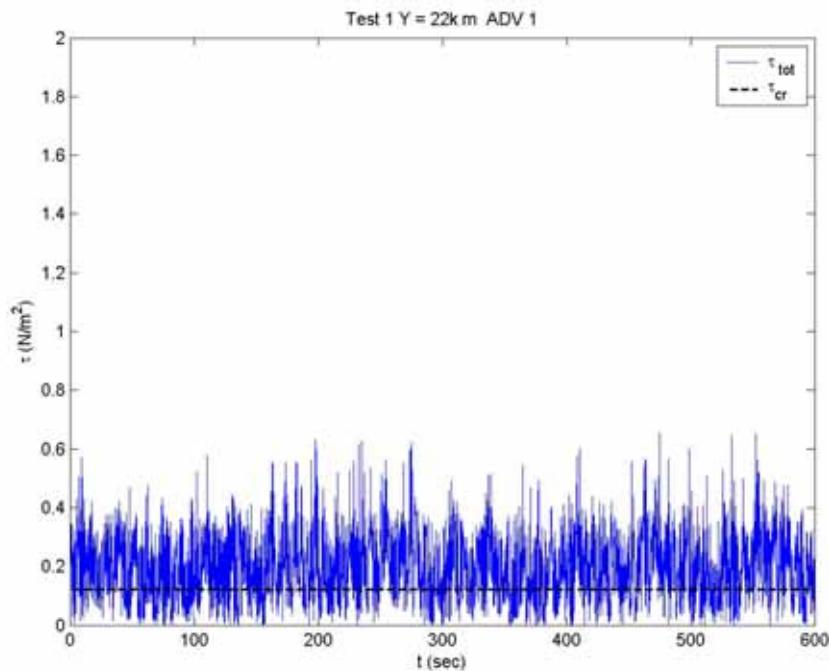
Figure 7-5. Time history of τ_{tot} at ADV 1, Test 1 Case 1, Y = 22 m

were smaller at ADV 1, X = 4.13 m, than ADVs 4 and 7, but τ_{cr} was exceeded more frequently, i.e., sand was mobilized to be transported more frequently at ADV 1 than at the other locations shown. This calculated greater mobilization correlates to the cross-shore distribution of sediment flux observed for this case (Figure 4-17).

The original Watanabe (1992) model included only the mean shear stress in the longshore transport equation. The equation predicted no transport at most of the cross-shore locations because the shear stress did not exceed the critical shear stress (Figures 6-18 and 6-19). However, Figures 7-2 through 7-5 show that the total velocity components, which include the turbulent components u' and v', produce a shear stress that frequently exceeds the critical shear. Therefore, accounting for turbulence appears to be essential for reproducing longshore sediment transport measurements in the surf zone under different types of breaking waves.

Comparison to LSTF Data

Model 1

Predicted transport rates using Equation 7-16 were compared to LSTF data for $ST(t) > \tau_{cr}$, and $q(t) = 0$, if the stirring coefficient was less than τ_{cr}. It was found that predicted transport rates followed the trend of the measurements if a coefficient was applied to Equation 7-16 as:

$$q_{y1} = f_1 q_y \qquad\qquad (7\text{-}22)$$

where q_y is calculated longshore sand transport rates using Equations 7-16 and 7-18, and f_1 is a coefficient equal to 40. The coefficient f_1 and subsequent coefficients were chosen as those that best described the transport rate measurements from all four test cases.

Predicted longshore transport rates for Test 1, Case 1, between transects Y = 18 m and Y =30 m are shown with measured values in Figure 7-6 (erroneous ADV results were omitted). Predicted rates were lower than measured values, but the shape of the distribution was similar to measured transport rates (q_{meas}) in the surf zone. In the swash zone, predictions showed an increase in transport, whereas measurements generally decreased in the swash zone.

Test 1, Case 2, predictions are shown in Figure 7-7. Several ADVs were omitted because of erroneous results; however, predictions for valid measurements were similar in quality to those of Test 1, Case 1. Both measurements and predictions show increased transport in the swash zone, which was not the case for Test 1, Case 1, where predictions increased, and q_{meas} decreased in the swash zone

One transect was obtained in which ADV measurements were acquired at the one-third depth for Test 1, Case 3. Predictions from Y = 22K, shown in Figure 7-8, were slightly smaller, but similar to the two other Test 1 cases. The predicted values showed the same trend as measurements in general, including an increase in transport in the swash zone

Predictions of Test 1, Case 1, longshore transport rates were similar to predictions of the other two cases; however, q_{meas} differs between Test 1, Case 1, and the subsequent cases. As mentioned in Chapter IV, the downdrift boundary was not adjusted in the
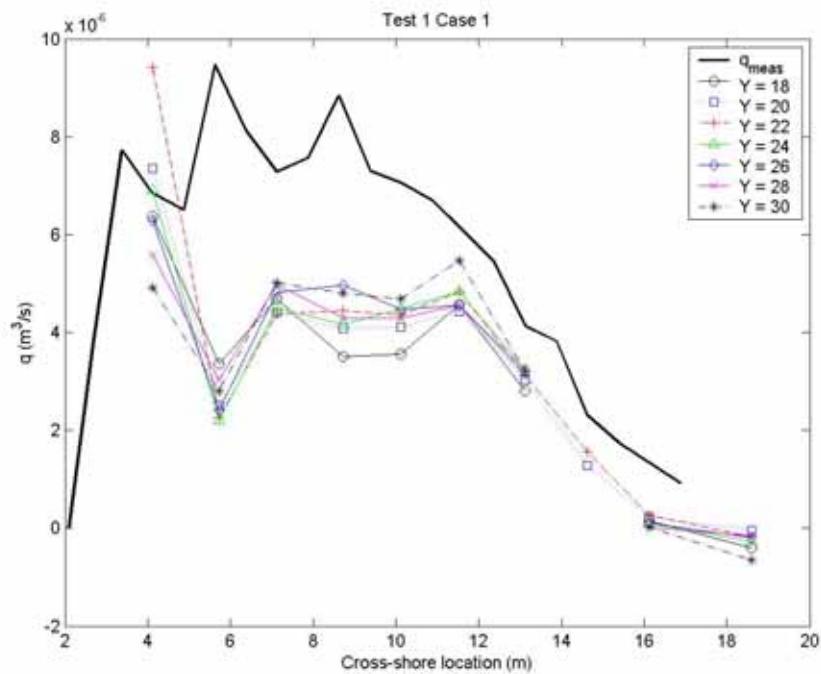
Figure 7-6. Model 1 longshore transport rate estimates compared to Test 1, Case 1, measurements
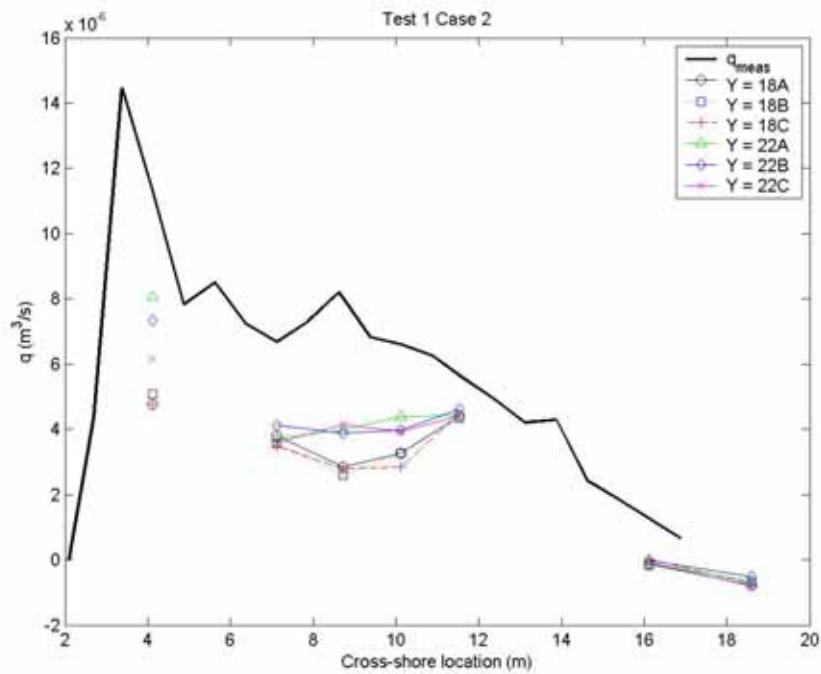
Figure 7-7. Model 1 longshore transport rate estimates compared to Test 1, Case 2, measurements
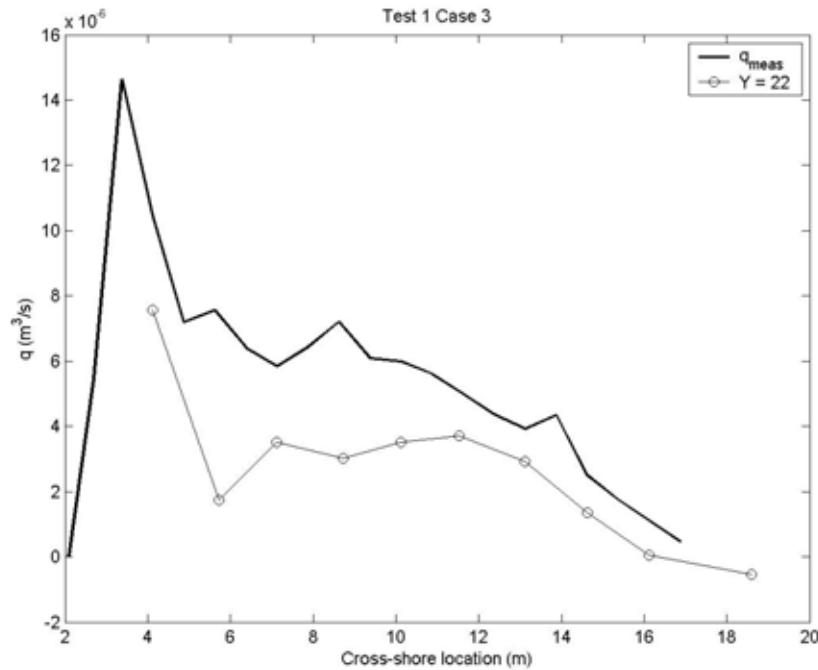
Figure 7-8. Model 1 longshore transport rate estimates compared to Test 1, Case 3, measurements

swash zone vicinity during Test 1, Case 1, which may be the source of this discrepancy. For this reason, it is judged that the swash zone transport measurements for Test 1, Case 1, are erroneous, and subsequent comparisons with Test 1, Case 1, predictions are made with Test 1, Case 3, longshore sand flux measurements.

Figure 7-9 shows predicted transport rates of Test 3, Case 1. The predicted distribution of longshore transport had the same general form of longshore transport measurements; a peak in transport occurred near the breakpoint, and transport was fairly uniform through the surf zone. However, predicted transport near the breakpoint was much smaller than the measurements. Predicted rates were slightly greater than the measured rates in the inner surf zone.
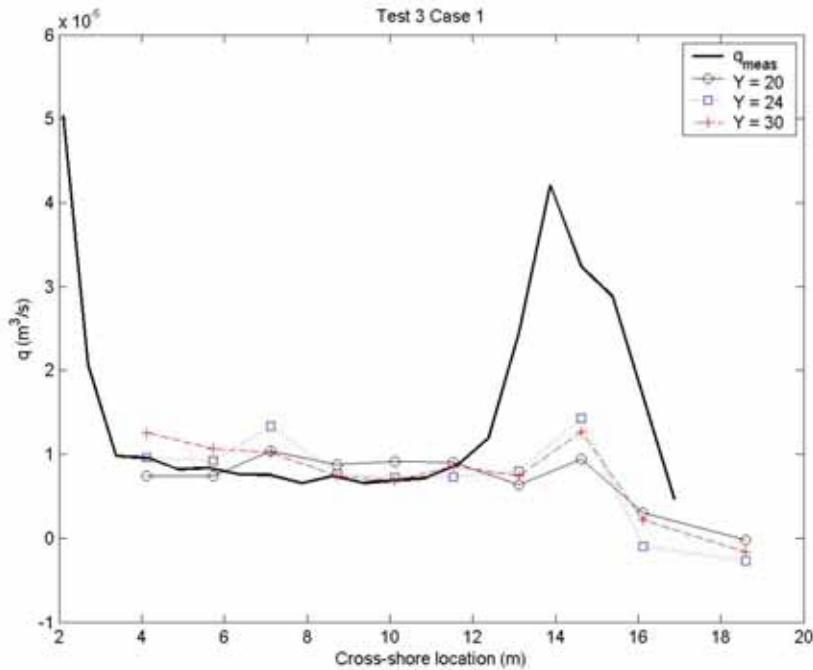
Figure 7-9. Model 1 longshore transport rate estimates compared to Test 3, Case 1, measurements

No velocity measurements were taken at the one-third depth for Test 3, Case 2.

Estimates of longshore transport rates for Test 3, Case 3, were similar to predictions

using Test 3, Case 1, data (Figure 7-10). The model showed a peak near the breakpoint

that was significantly smaller than the measurements; however, predicted transport rates

in the surf zone shoreward of breaking matched the measurements well.

Longshore sediment transport rate estimates of Test 5, Case 1, are shown in

Figure 7-11. The predictions matched measurements well through the outer surf zone,

but underpredicted the measurements in the inner surf zone. However, predictions

showed an increase in transport in the swash zone, which agreed with the trend of the

measurements. Similar results are shown for Test 5, Case 2 (Figure 7-12).
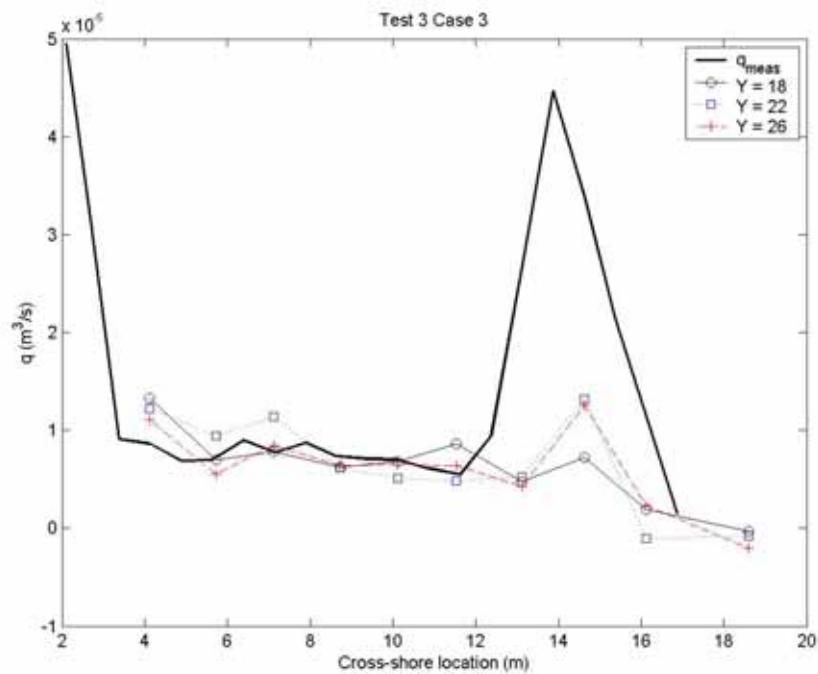
Figure 7-10. Model 1 longshore transport rate estimates compared to Test 3, Case 3, measurements
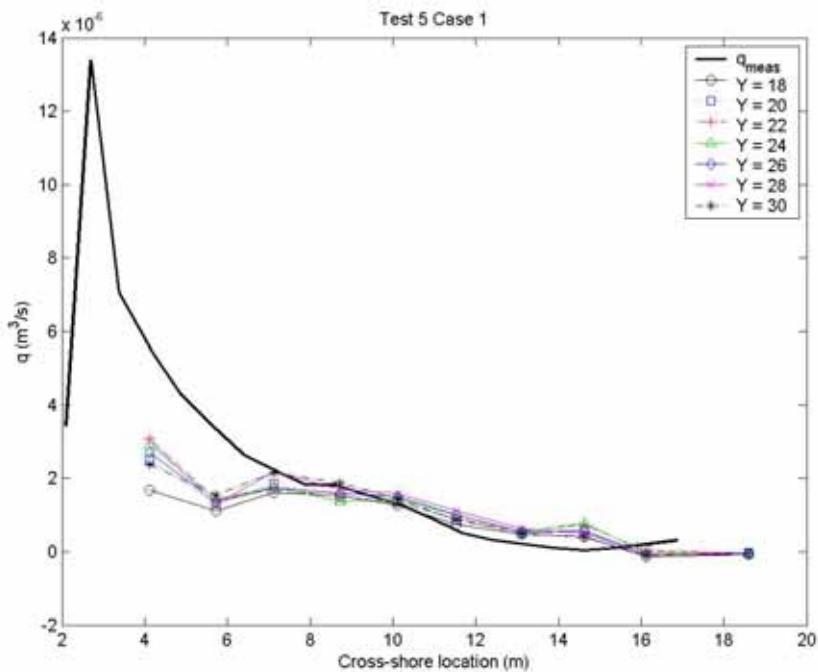

Figure 7-11. Model 1 longshore transport rate estimates compared to Test 5, Case 1, measurements
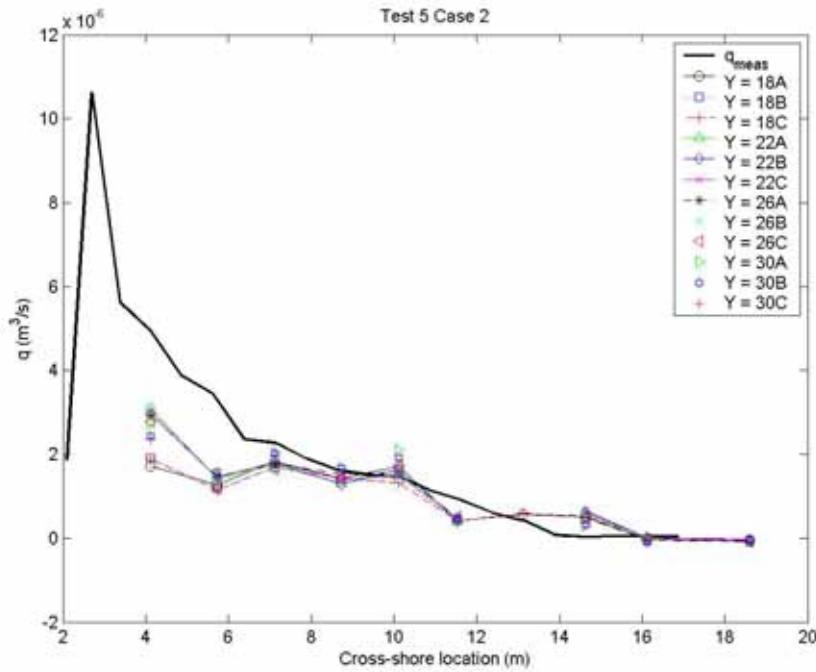
Figure 7-12. Model 1 longshore transport rate estimates compared to Test 5, Case 2, measurements

One transect was performed during Test 5, Case 3, with measurements obtained at the one-third depth. Estimates of the transport rate were slightly greater than measured transport rates and the estimates obtained for Test 5, Case 1 and Case 2, but swash zone predictions were predicted well (Figure 7-13).

Predicted Test 6, Case 1, transport rates underestimated measurements, but the distribution had a similar shape to measured values (Figure 7-14). The peak in transport near breaking was underpredicted significantly for the Test 6 plunging breakers, as was the result for the Test 3 plunging breakers.

In summary, estimates of longshore sand transport with Model 1 gave the general shape of the measured cross-shore distribution. For plunging waves, predictions showed
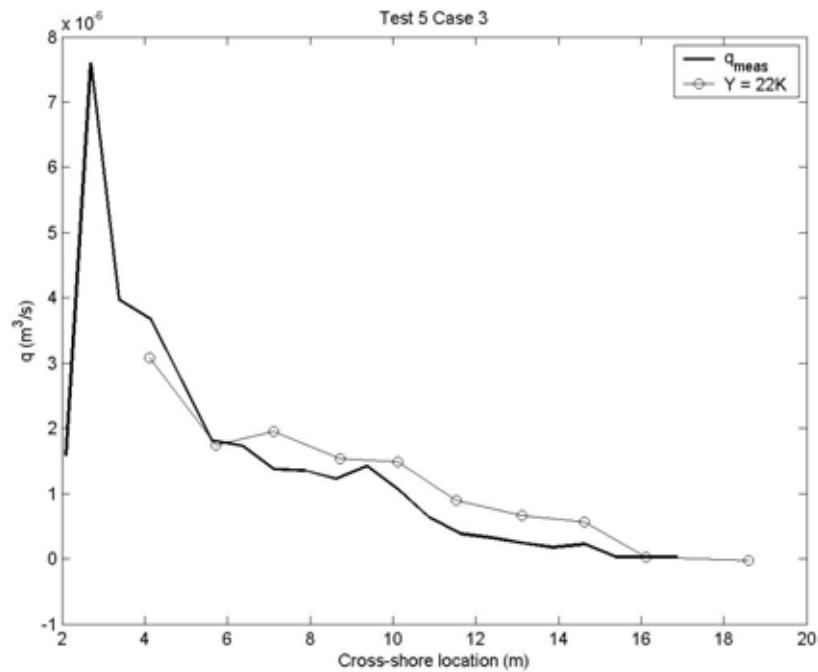
Figure 7-13. Model 1 longshore transport rate estimates compared to Test 5, Case 3, measurements
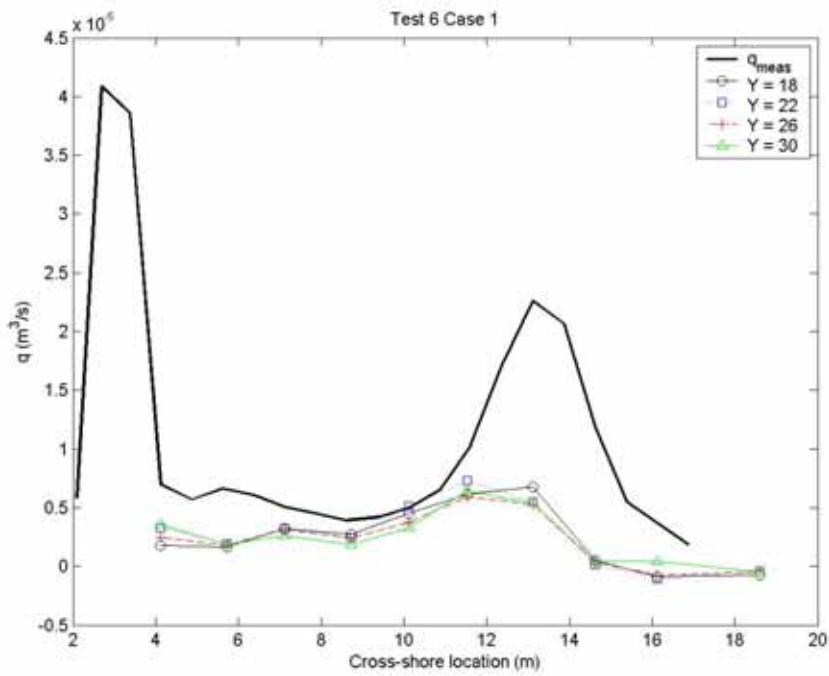
Figure 7-14. Model 1 longshore transport rate estimates compared to Test 6 measurements

a peak in transport near the breakpoint, but the estimated rates were greatly underpredicted. Shoreward of breaking, the model predicted longshore transport rates well with Test 3 waves, but overpredicted Test 6 waves. Estimates predicted Test 5 transport rates well, but Test 1 estimates underpredicted the measurements for a given test condition.

The results showed that individual transects of each wave condition gave similar predictions. Because results did not differ significantly between transects, it was determined that measurements at one representative transect were sufficient to compare to the model calculations.

Model 2

Model 1 predicted the general shape of the cross-shore distribution of longshore sediment transport. However it did not well estimate transport near the breakpoint that is associated with the plunging breaker tests. The Model 1 equation was modified in an attempt to better predict transport at breaking, as:

$$q_{y2}(t) = f_2\left(p(t) - u_{cr}\right) TR_y(t) \text{ for } p(t) > u_{cr}$$
$$\text{and} \tag{7-23}$$
$$q_{y2}(t) = 0 \text{ for } p(t) \le u_{cr}$$

where f_2 is a coefficient set to 0.001, u_{cr} is the critical shear velocity for initiation of sediment motion defined as:

$$u_{cr} = \sqrt{\frac{\tau_{cr}}{\rho}} \tag{7-24}$$

and $p(t)$ is the magnitude of orbital velocity fluctuations given by:

$$p(t) = \sqrt{u'(t)^2 + v'(t)^2} \tag{7-25}$$

The average longshore transport rate over the time record was calculated as:

$$q_{y2} = \frac{1}{N}\sum_{1}^{N} q_{y2}(t) \tag{7-26}$$

Predictions of longshore sediment transport rates, q_{y2}, with Test 1 measurements are shown in Figure 7-15. Although the model overestimated the measurements in the mid-surf zone, Model 2 generally predicted transport rates well, including in the swash zone. Estimates of Test 3 transport rates agreed well with the measurements shoreward of breaking (Figure 7-16). Although the model produced a peak in transport near the break point, transport rates were again significantly underpredicted in the breaking region. Test 5 predictions overestimated measurements throughout the surf zone (Figure 7-17). However, the shape of the estimated distribution followed the measurements through the surf zone and swash zones. Figure 7-18 shows that estimates with Test 6 conditions predicted measured values well in the surf zone with a peak in transport near breaking. Nevertheless, estimated transport rates near the break point were much less than measured rates and the peak was shifted shoreward of the observed transport peak.

In summary, Model 2 generally predicted longshore transport rates in the surf zone well shoreward of the break point for the four LSTF tests. However, the model did not improve estimates of the transport rates near the break point for the plunging breaker tests.
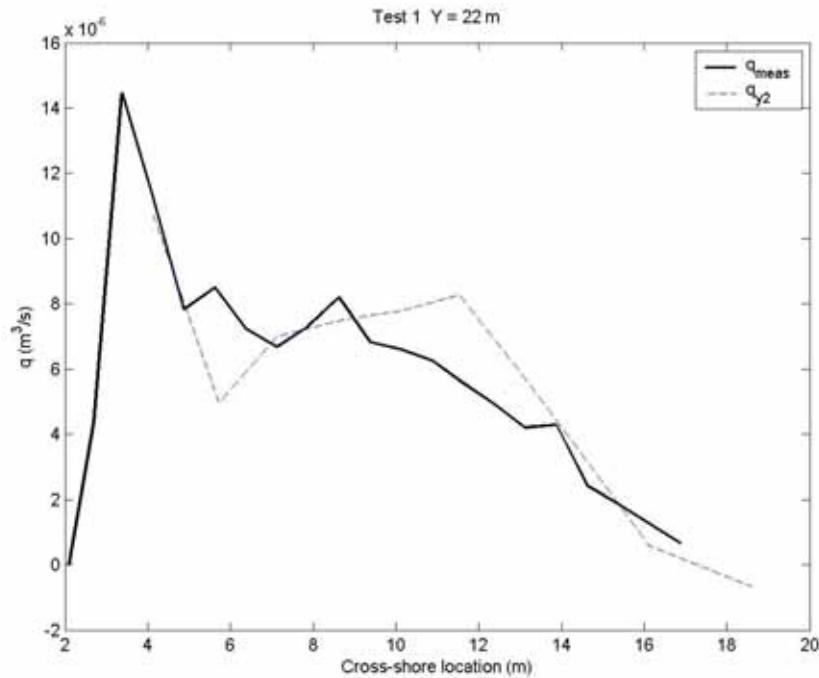
Figure 7-15. Model 2 longshore transport rate estimates compared to Test 1 measurements
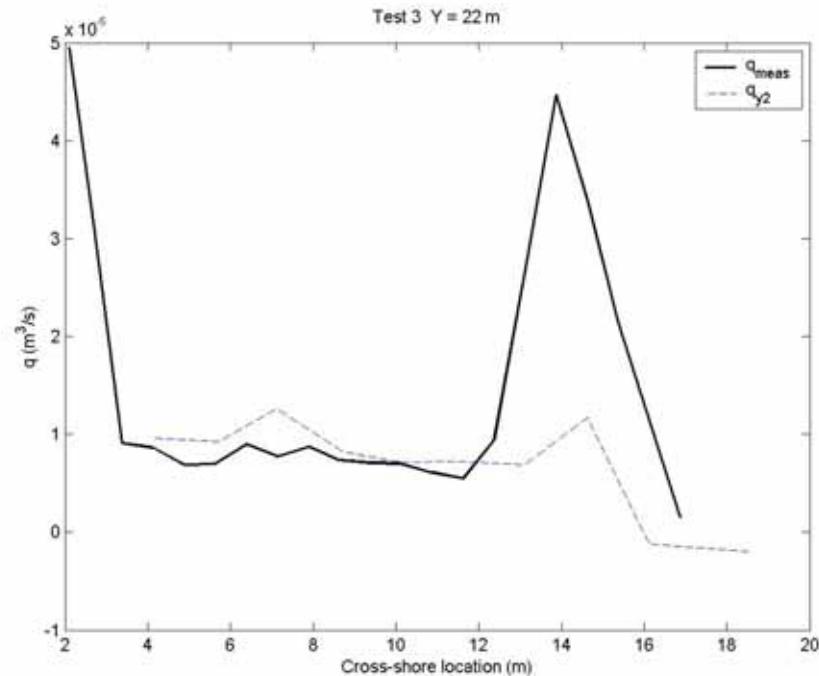
Figure 7-16. Model 2 longshore transport rate estimates compared to Test 3 measurements
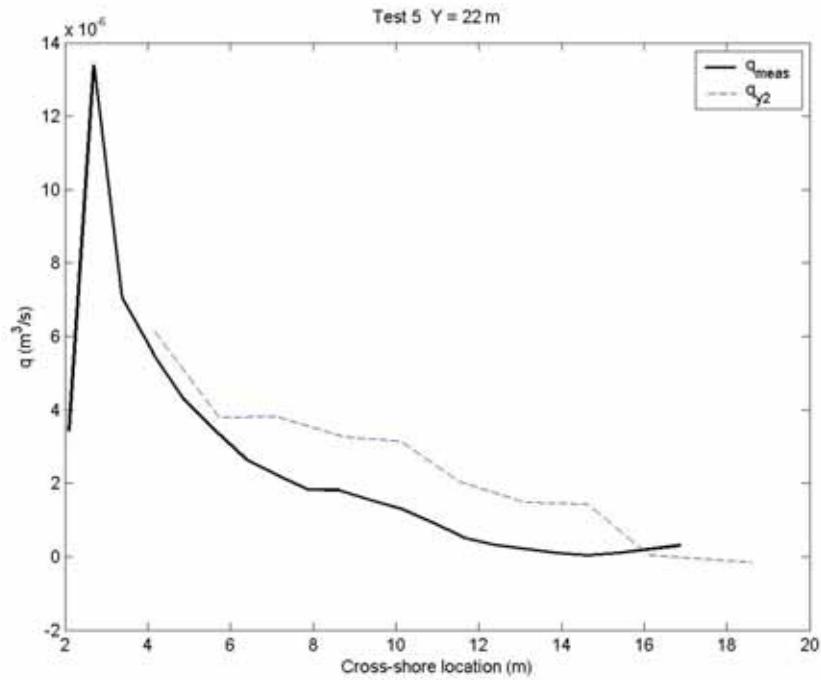
Figure 7-17. Model 2 longshore transport rate estimates compared to Test 5 measurements
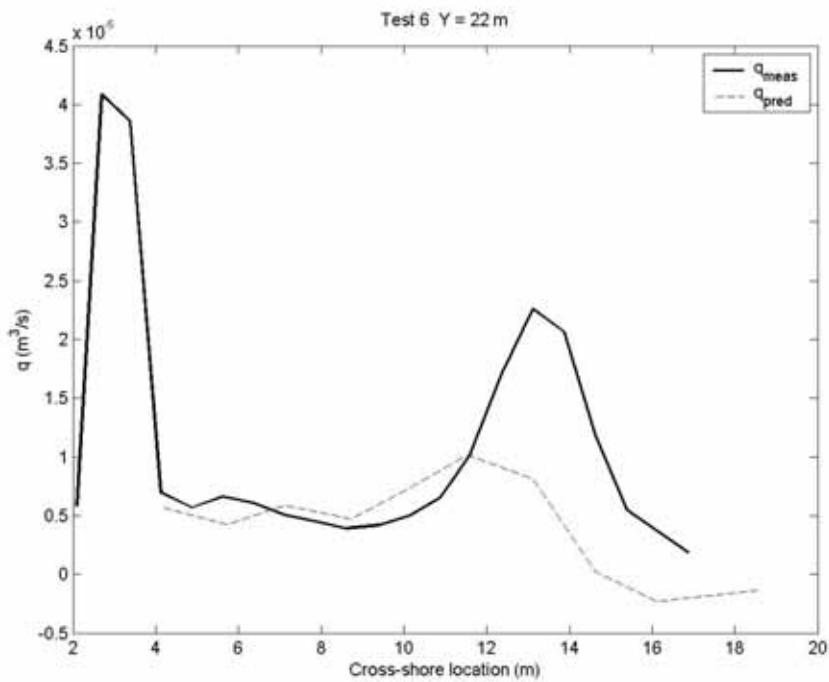
Figure 7-18. Model 2 longshore transport rate estimates compared to Test 6 measurements

Model 3

   A third model was considered by modifying the calculation of $\vec{\tau}_{tot}$. The revised

stirring function was calculated as:

$$\langle ST \rangle = \langle \vec{\tau}_{tot}(t) \rangle = \frac{\rho c_f}{2} \sqrt{U^2 + u'(t)^2}$$
(7-27)

which emphasizes the role of cross-shore velocity in stirring sediment.

Model 3 was of the form:

$$q_{y3}(t) = f_3 K \left(\vec{\tau}_{tot}(t) - \tau_{cr} \right) TR_y(t) \ \text{ for } \vec{\tau}_{tot}(t) > \tau_{cr}$$
$$\text{and}$$
$$q_{y3}(t) = 0 \ \text{ for } \vec{\tau}_{tot}(t) \le \tau_{cr}$$
(7-28)

where f_3 is an empirical coefficient set to 10. The time averaged longshore transport rate

for Model 3 was calculated as:

$$q_{y3} = \frac{1}{N} \sum_{1}^{N} q_{y3}(t)$$
(7-29)

   Results using Model 3 with Test 1 conditions were similar to Model 2 results

(Figure 7-19). Estimated transport rates agreed with the measurements, although they

were slightly greater in the mid surf zone. Model 3 predicted Test 3 transport rates well

shoreward of breaking, but estimates were significantly smaller near breaking

(Figure 7-20). Estimated transport rates overpredicted measurements of Test 5

conditions, but the shape of the distribution was predicted well (Figure 7-21). Transport

rates were estimated well shoreward of breaking with Test 6 conditions (Figure 7-22).
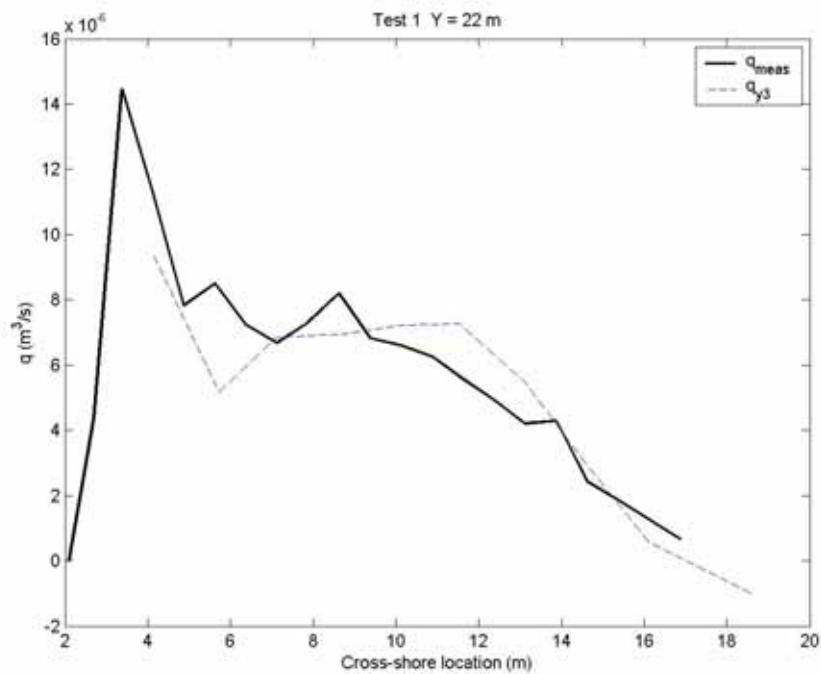
Figure 7-19. Model 3 longshore transport rate estimates compared to Test 1 measurements
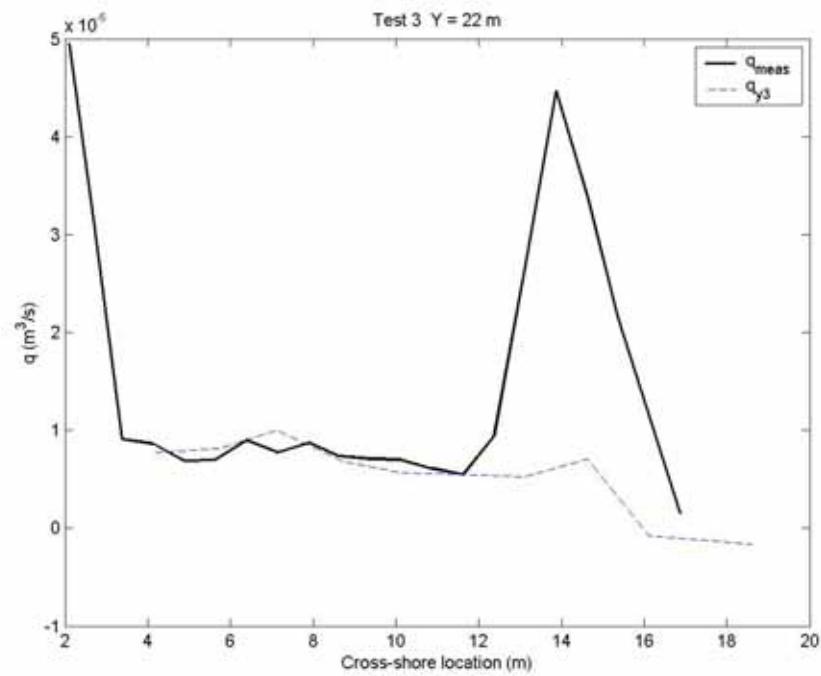
Figure 7-20. Model 3 longshore transport rate estimates compared to Test 3 measurements
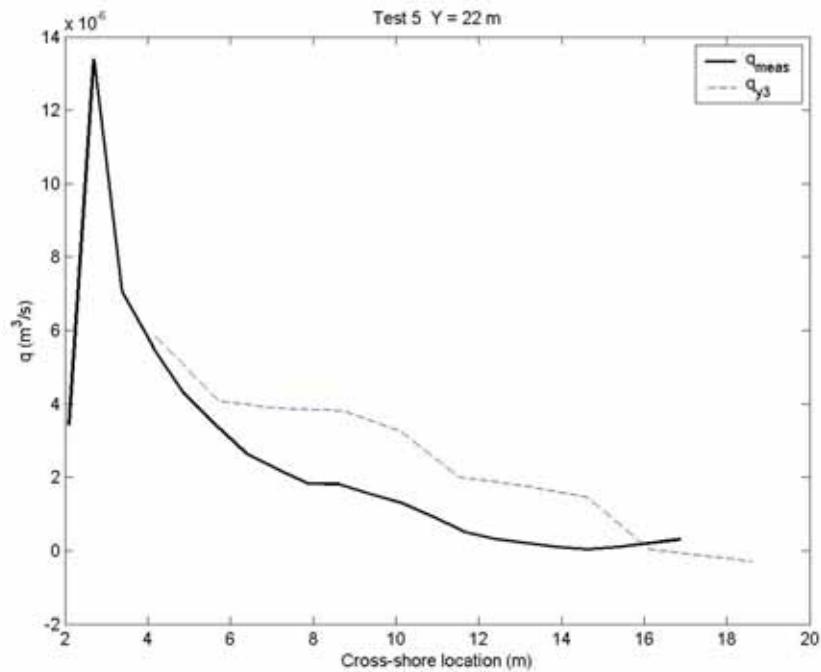
Figure 7-21. Model 3 longshore transport rate estimates compared to Test 5 measurements
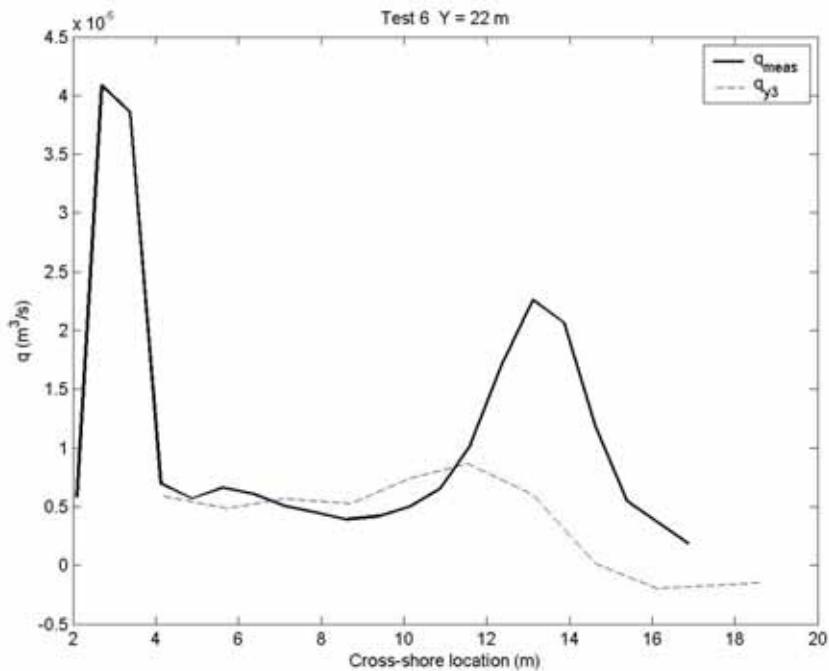

Figure 7-22. Model 3 longshore transport rate estimates compared to Test 6 measurements

However, estimated transport near breaking was less and shifted shoreward of the measured values.

In summary, results using Model 3 were similar to Model 2. Transport in the inner surf zone was estimated well. However, the longshore transport rate near the plunging break point was still underpredicted by this model.

Model 4

Models 1 through 3 gave reasonable estimates of longshore sand flux with the exception of transport rates at the break point for the plunging wave tests. The general form of the stirring function times transporting function concept appears to be valid; however, an additional term must evidently be added to capture rates near plunging wave breaking. It was observed during the plunging wave experiments that sediment remained in suspension at the trough of the breakpoint bar for the duration of the tests. The plunging waves distributed sediment throughout the water column, and sand entrained in the upper water column had a longer distance to settle to the bed – a time longer than several wave periods. Subsequent waves would redistribute the suspended sand through the water column. Therefore, sand entrained into the water column by a single plunging wave would continue to be transported during several subsequent waves. Model 4 was formulated with an additional term to account for events that cause sand to be suspended through the water column and increase the transport rate near the break point of plunging waves. The suspension term, $s(t)$, was defined as:

$$s(t) = \left(u'(t)^2 + v'(t)^2 \right)^{k_4}$$ (7-30)

where k_4 is an empirical exponent set to 1. Model 4 was therefore defined as:

$$q_{y4}(t) = f_4 K \left(\vec{\tau}_{tot}(t) - \tau_{cr} \right) \left(s(t) \right) TR_y(t) \text{ for } \vec{\tau}_{tot}(t) > \tau_{cr}$$

and (7-31)

$$q_{y4}(t) = 0 \text{ for } \vec{\tau}_{tot}(t) < \tau_{cr}$$

where f_4 is an empirical coefficient equal to 500, and $\vec{\tau}_{tot}$ was calculated using

Equation 7-12. The average transport rate over the time record was calculated as:

$$q_{y4} = \frac{1}{N} \sum_{1}^{N} q_{y4}(t)$$ (7-32)

Results of Model 4 with Test 1 conditions are shown in Figure 7-23. Estimates

compared well to measured values offshore of X = 12 m, but underpredicted

measurements inshore of this location. Test 3 estimates were slightly greater than

measurements shoreward of breaking (Figure 7-24). The estimated peak at the break

point agreed with the magnitude of measured transport, although it was located slightly

offshore of the measured peak. The apparent discrepancy in locations of the peaks is

such that the measured peak occurs at a sand trap located between ADVs. If ADV

measurements were available at the same cross-shoe location of the trap, predicted and

measured peak locations might agree more closely. However, because the magnitudes

of the peaks agree with the presently applied coefficients, it is anticipated that the

estimated transport rate would overpredict measurement rates. Model 4 predicted Test 5

transport generally well (Figure 7-25). Estimates were slightly smaller in the inner surf
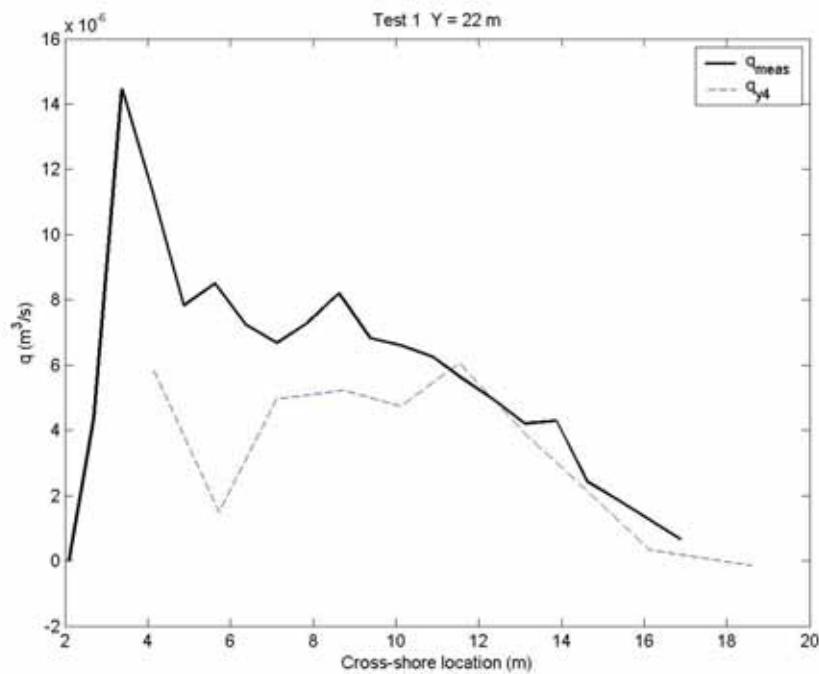
Figure 7-23. Model 4 longshore transport rate estimates compared to Test 1 measurements
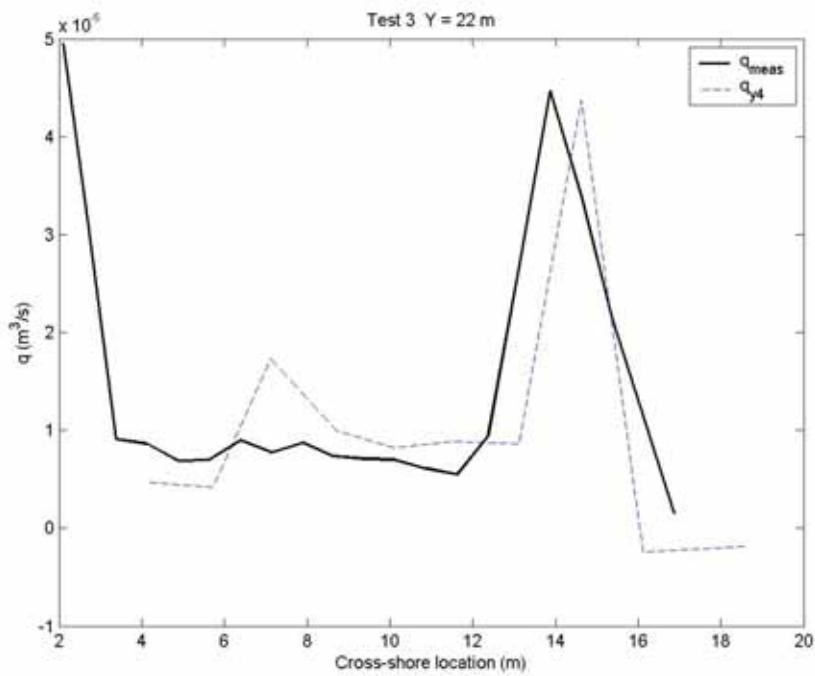

Figure 7-24. Model 4 longshore transport rate estimates compared to Test 3 measurements
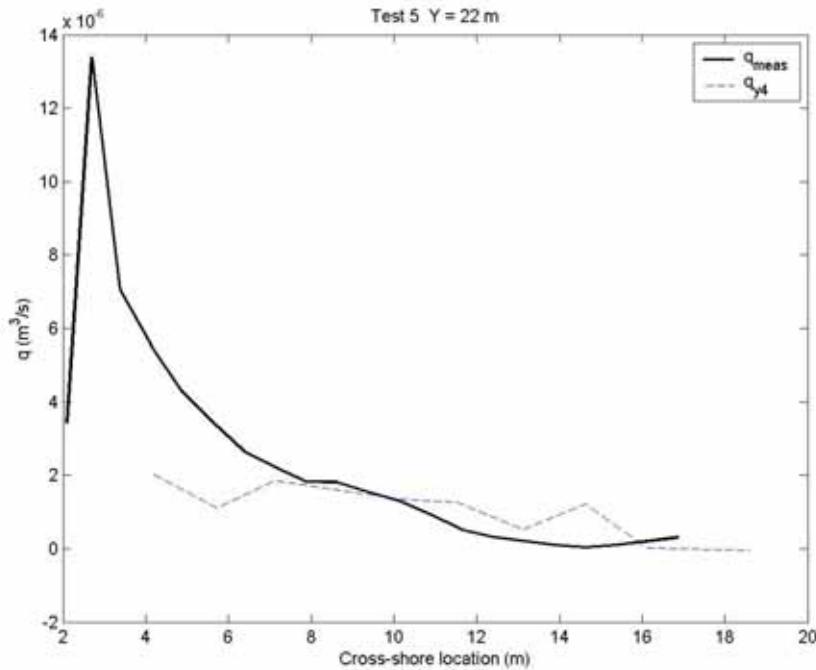
Figure 7-25. Model 4 longshore transport rate estimates compared to Test 5 measurements

and swash zone, and the overall distribution had a flatter profile than q_{meas}. Transport at

the Test 6 break point was underpredicted, but the rate was improved over previous

models (Figure 7-26). Estimates were slightly smaller than measured transport rates

shoreward of breaking.

In summary, estimates of longshore transport rate at the break point of the plunging

cases were improved using Model 4. Predicted distributions had a generally flatter

profile than measured transport rates, and q_{y4} underestimated measurements in the inner

surf and swash zones for the spilling breaker cases.
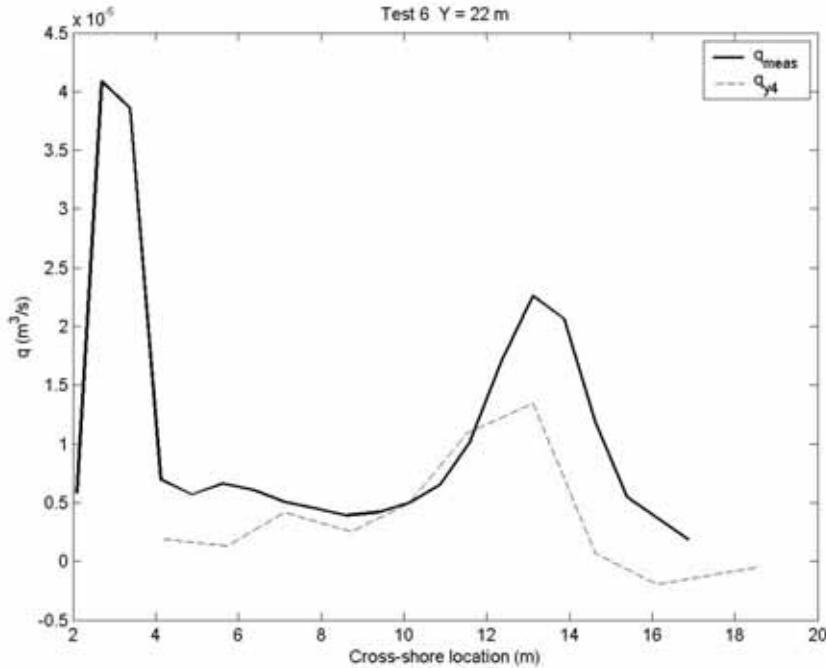
Figure 7-26. Model 4 longshore transport rate estimates compared to Test 6 measurements

Model 5

Inclusion of $s(t)$ in Model 4 improved estimates near the break point for the plunging breaker cases. Model 5 was devised to improve estimates in the inner surf zone, particularly for spilling wave cases. Model 5 included the suspension term added to the elements of Model 1:

$$q_{y5}(t) = \left(f_{b5} K \left(\vec{\tau}_{tot}(t) - \tau_{cr} \right) + f_{s5} \left(u'(t)^2 + v'(t)^2 \right)^{k_5} \right) TR_y(t) \text{ for } \vec{\tau}_{tot}(t) > \tau_{cr}$$

$$\text{and} \qquad\qquad (7\text{-}33)$$

$$q_{y5}(t) = 0 \text{ for } \vec{\tau}_{tot}(t) < \tau_{cr}$$

where $f_{b5} = 10$, $f_{s5} = 0.0175$, and $k_5 = 2$ are all empirical coefficients. The time-averaged transport rate over the record was calculated by:

$$q_{y5} = \frac{1}{N} \sum_{1}^{N} q_{y5}(t) \qquad (7\text{-}34)$$

Estimates of Test 1 longshore sand transport rates were improved using Model 5 (Figure 7-27). Model 5 estimated transport rates near breaking for Test 3 well, but predicted rates were significantly greater through the surf zone (Figure 7-28). As was observed with the Model 4 estimates, the location of the peak in measured transport occurred between ADV locations, which resulted in a discrepancy in location of the peaks between estimated and measured longshore transport rates. Figure 7-29 shows predicted transport rates of Test 5 using Model 5. The predictions were judged to be good overall, with estimates slightly greater than measurements in the surf zone, and slightly lower in the swash zone.

In summary, estimates with Test 6 conditions gave good general agreement with measurements (Figure 7-30). The estimated peak in transport near breaking with Test 6 waves was lower than q_{meas}, and the location of peak transport was shifted shoreward. However, estimates with Model 5 show closest agreement to transport near the break point than the previous models applied for Test 6.

Model 6

Model 6 consisted of a modified suspension term:

$$s(t) = f_{s6} \left[\frac{\left(u'(t)^2 + v'(t)^2 \right)}{\left(U^2 + V^2 \right)} \right]^{k_6} \quad \text{for } U \neq 0 \text{ and } V \neq 0$$

$$\text{and} \qquad (7\text{-}35)$$

$$s(t) = 0 \text{ for } U = 0 \text{ or } V = 0$$
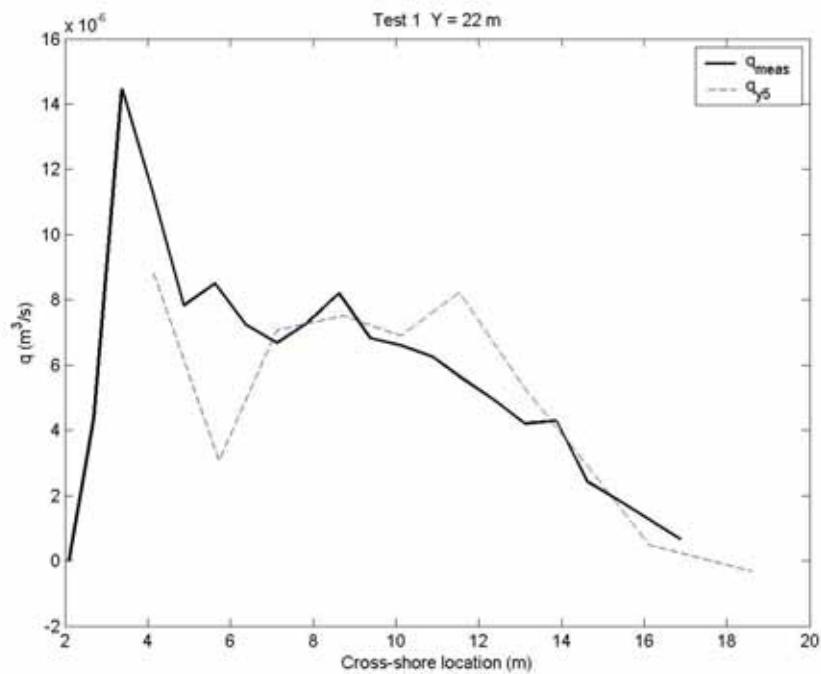
Figure 7-27. Model 5 longshore transport rate estimates compared to Test 1 measurements
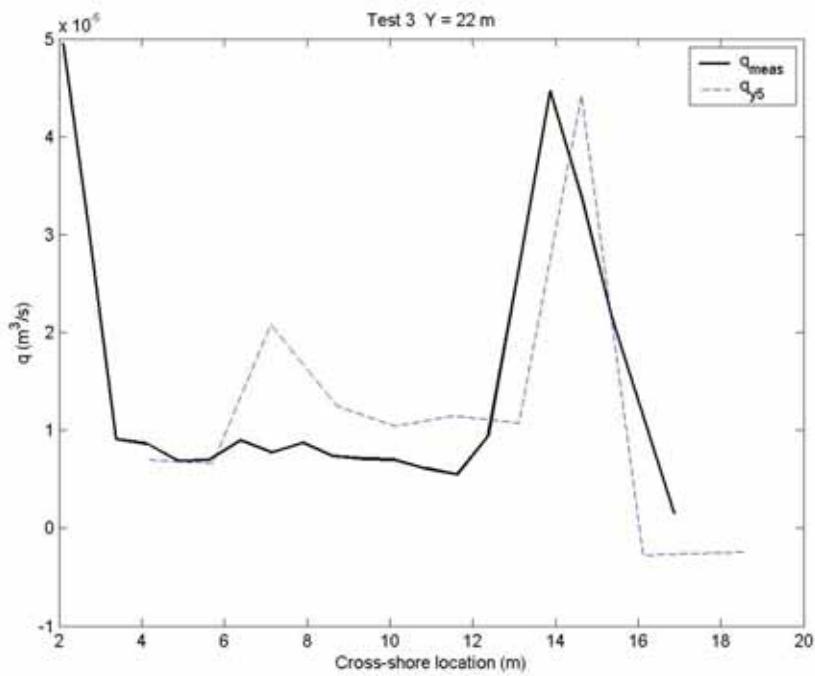
Figure 7-28. Model 5 longshore transport rate estimates compared to Test 3 measurements
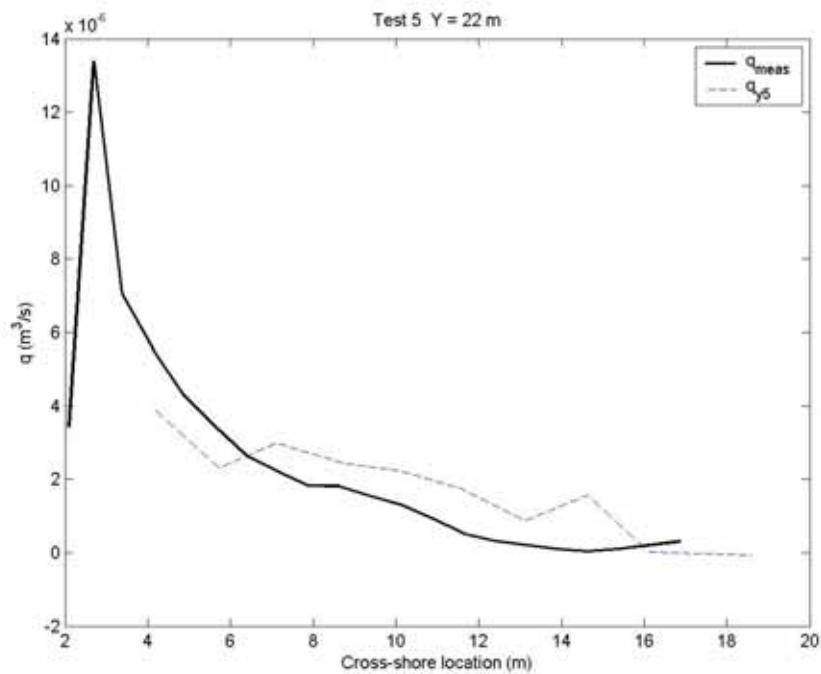
Figure 7-29. Model 5 longshore transport rate estimates compared to Test 5 measurements
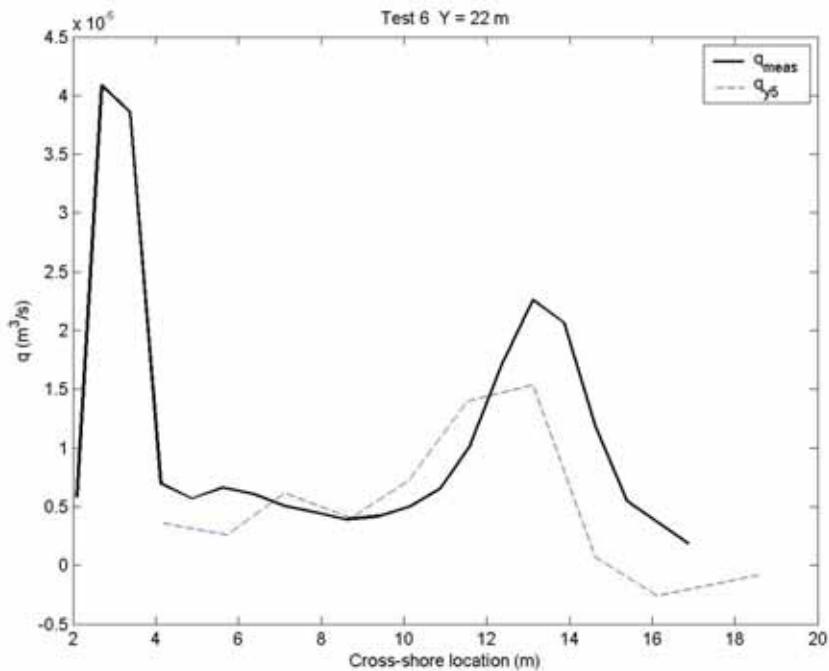
Figure 7-30. Model 5 longshore transport rate estimates compared to Test 6 measurements

in which the coefficients $f_{s6} = 0.25$ and $k_6 = 1$. Time-dependent transport rates were

calculated by:

$$q_{y6}(t) = f_6 K \left[\left(\vec{\tau}_{tot}(t) - \tau_{cr} \right)\left(1 + s(t) \right) TR_y(t) \right] \text{ for } \vec{\tau}_{tot}(t) > \tau_{cr}$$

$$\text{and} \qquad (7\text{-}36)$$

$$q_{y6}(t) = 0 \text{ for } \vec{\tau}_{tot}(t) < \tau_{cr}$$

where f_6 was set to 20. Estimated time-averaged transport rates were calculated from:

$$q_{y6} = \frac{1}{N} \sum_{1}^{N} q_{y6}(t) \qquad (7\text{-}37)$$

Model 6 gave a flatter cross-shore distribution of longshore transport rates with

Test 1 (Figure 7-31). Estimates were much smaller than q_{meas} through most of the surf

zone and slightly greater in the offshore region of the model. Results for Test 3 are

shown in Figure 7-32. The model overestimated the peak in transport near the break

point, but estimates shoreward of breaking agreed well with the measurements.

Estimates of Test 5 transport rates were significantly overpredicted, with exception of

the swash zone, which was underestimated (Figure 7-33). Additionally, previous models

in this chapter followed the increasing trend of longshore sediment flux through the surf

zone, but Model 6 showed no increasing trend. Model 6 estimated the distribution of

Test 6 waves well, including the location of the transport peak near breaking

(Figure 7-34).
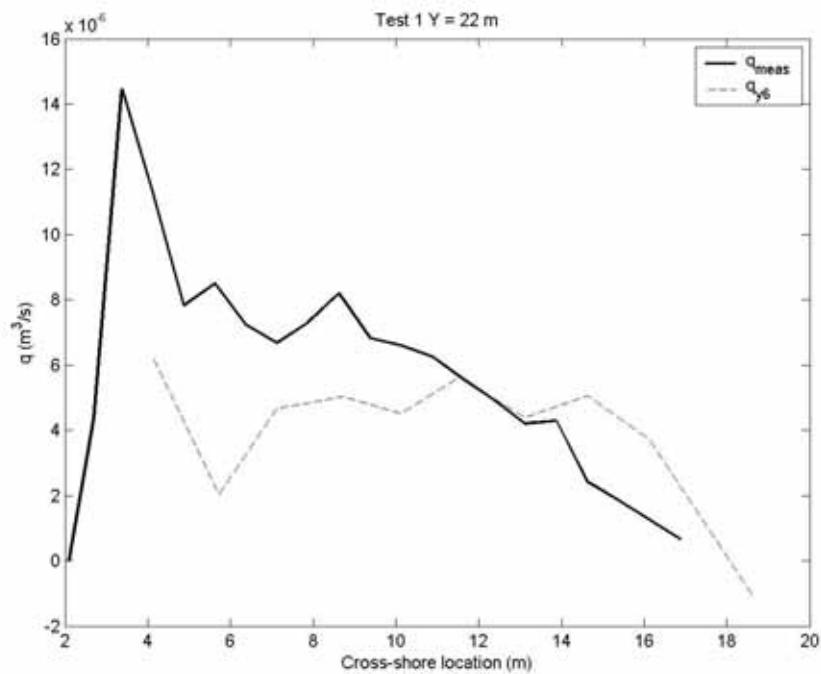
Figure 7-31. Model 6 longshore transport rate estimates compared to Test 1 measurements
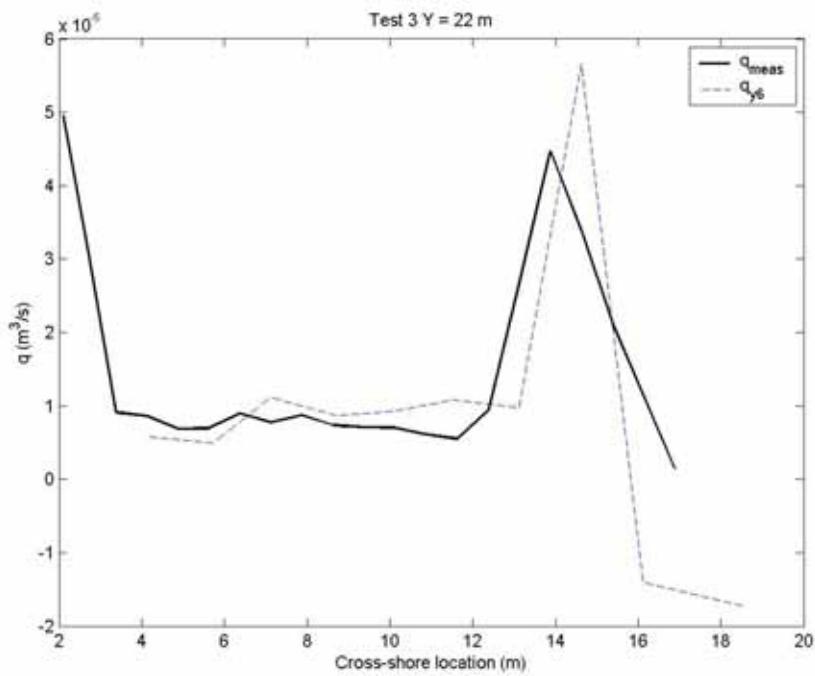
Figure 7-32. Model 6 longshore transport rate estimates compared to Test 3 measurements
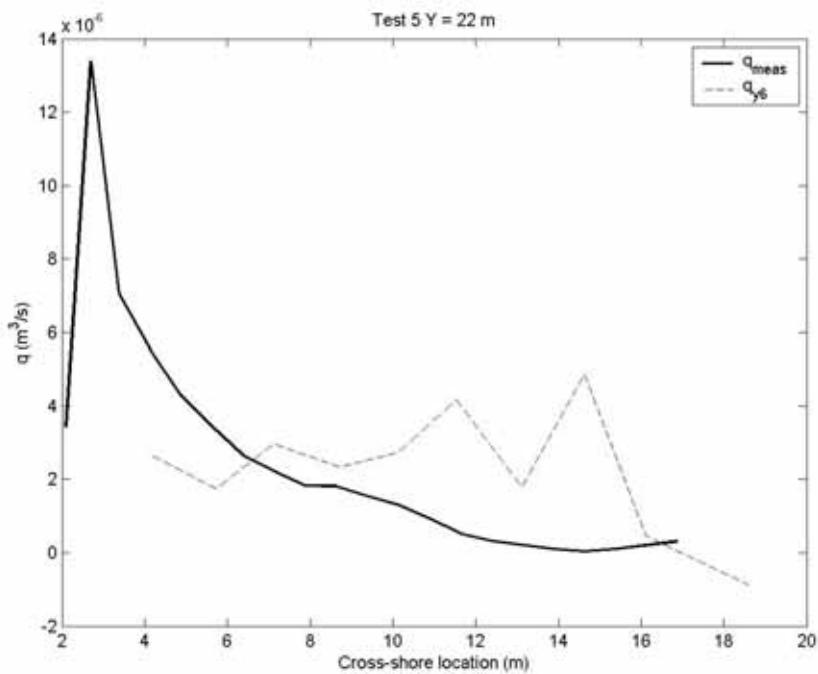
Figure 7-33. Model 6 longshore transport rate estimates compared to Test 5 measurements
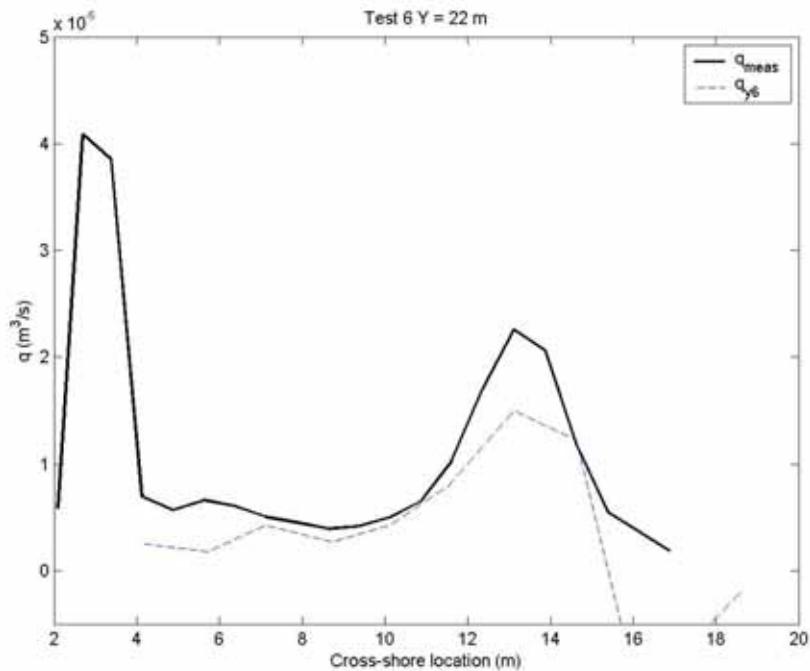
Figure 7-34. Model 6 longshore transport rate estimates compared to Test 6 measurements

In summary, Model 6 did not predict transport rates for the spilling cases well. Good agreement was found shoreward of breaking with Test 3 conditions, but the peak in transport near the breakpoint was overpredicted. The model performed well in predicting the Test 6 cross-shore distribution of sand flux.

Model 7

Model 7 included the product of the stirring function and sum of the transport function and suspension term:

$$q_{y7}(t) = f_7 K \left(\vec{\tau}_{tot}(t) - \tau_{cr} \right) \left(TR_y + s(t) \right) \text{ for } \vec{\tau}_{tot}(t) > \tau_{cr}$$
$$\text{and} \tag{7-38}$$
$$q_{y7}(t) = 0 \text{ for } \vec{\tau}_{tot}(t) < \tau_{cr}$$

where $f_7 = 20$. The suspension term was of the same form as used previously, but with different coefficients:

$$s(t) = f_{s7} \left(u'(t)^2 + v'(t)^2 \right)^{k_7} \text{ for } U \neq 0 \text{ and } V \neq 0$$
$$\text{and} \tag{7-39}$$
$$s(t) = 0 \text{ for } U = 0 \text{ or } V = 0$$

where f_{s7} was set to 1.0 and k_7 equaled 0.5. The transport rate averaged over the time record was calculated by:

$$q_{y7} = \frac{1}{N} \sum_{1}^{N} q_{y7}(t) \tag{7-40}$$

Model 7 followed the measured cross-shore distribution shape of Test 1 well (Figure 7-35). The model overpredicted q_{meas} offshore of X = 11.5 m, but predicted the
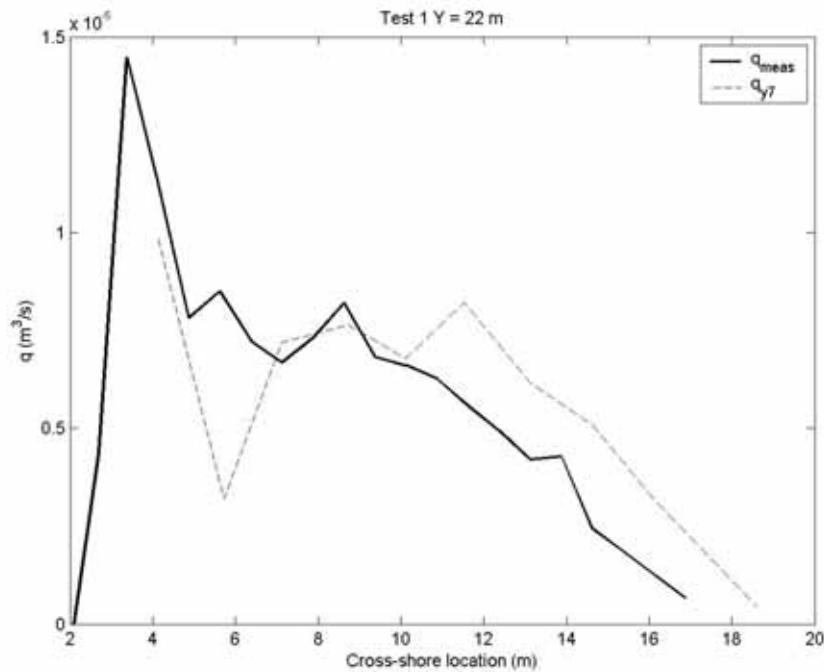
Figure 7-35. Model 7 longshore transport rate estimates compared to Test 1 measurements

inner surf and swash zones well with exception to estimates at X =5.7 m. Figure 7-36

shows estimates of Test 3, which agreed well with the magnitude of measured transport

near the break point. Predictions overestimated the measurements shoreward of

breaking, however. Test 5 transport measurements were significantly overpredicted

offshore of X = 5.7 m by Model 7 (Figure 7-37). Model 7 estimated the measured cross-

shore distribution of Test 6 sediment flux well (Figure 7-38). The peak in transport near

breaking was underpredicted, but the estimated distribution shoreward of breaking

agreed well with q_{meas}.
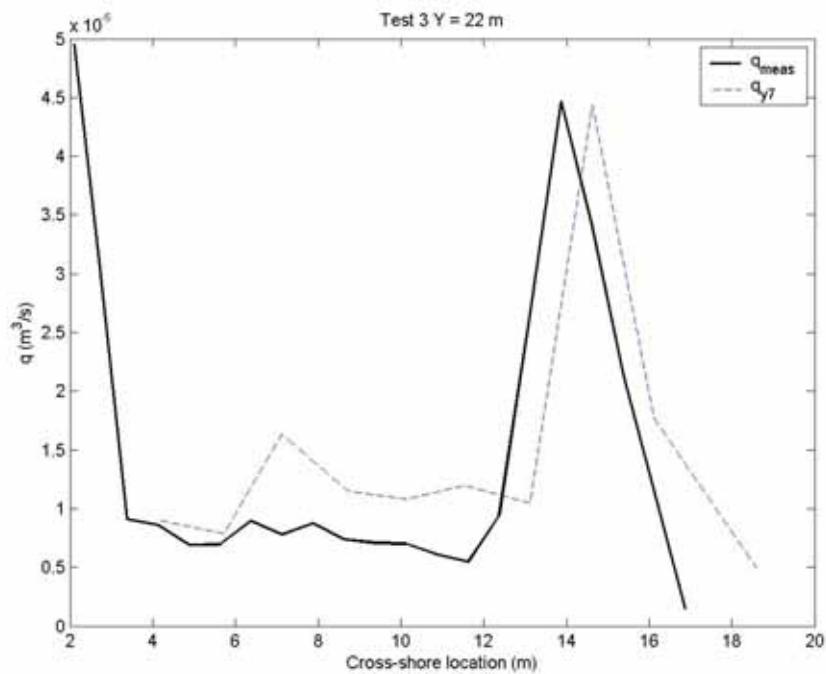
Figure 7-36. Model 7 longshore transport rate estimates compared to Test 3 measurements
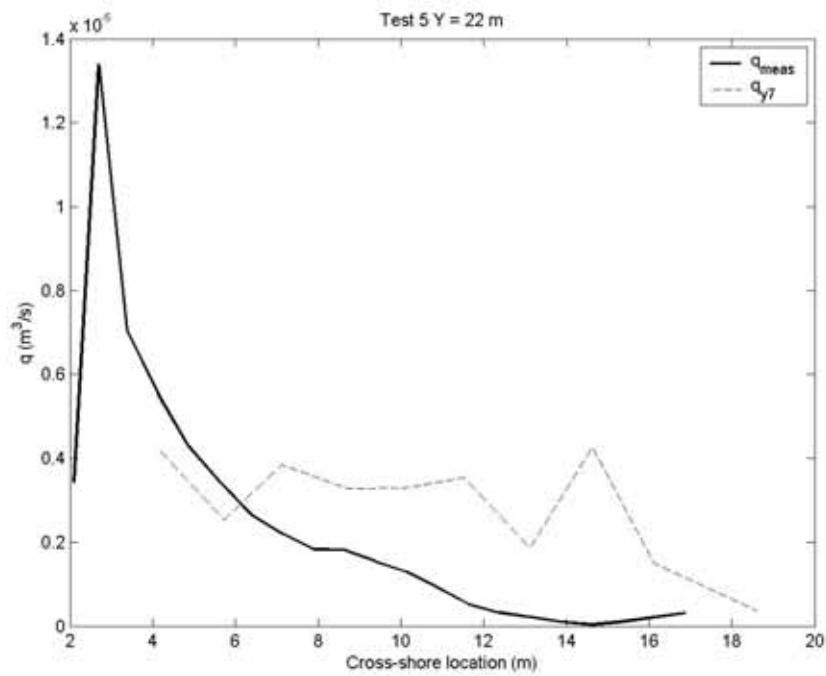
Figure 7-37. Model 7 longshore transport rate estimates compared to Test 5 measurements
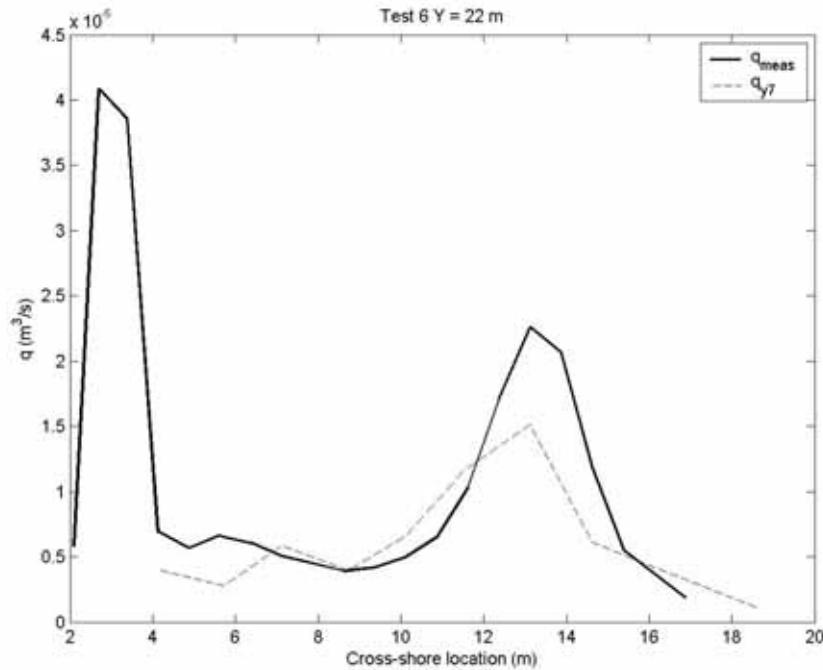
Figure 7-38. Model 7 longshore transport rate estimates compared to Test 6 measurements

Summary of LSTF comparisons

Model 1 gave similar results for the different transects of each test. Therefore, one representative transect for each test was considered to be sufficient for comparison with subsequent models.

The basic form of Equation 7-16, which entered Models 1 through 3, generally estimated longshore sediment transport rates well for spilling breaker cases. The equation predicted transport well shoreward of breaking for the plunging breaker cases. At breaking, the model indicated a peak in transport, but underpredicted the measurements. Inclusion of s(t) (Models 4 through 7) improved transport predictions for

the plunging breaker cases. The magnitude of sand flux at breaking was predicted well for Test 3, but the flux was underpredicted with Test 6 waves.

Comparison to Field (SIS) Data

Models 4, 5, and 7 gave the best overall representation of measured transport rates for the LSTF data (and considerably better predictions than other formulas discussed in Chapter VI). Therefore, these models were selected for comparison to field measurements. Although the LSTF experiments were conducted at a relatively large scale, wave heights in the field typically are much greater, especially during storms when wave heights can be more than an order of magnitude greater.

The models were compared to SIS Transects 15 and 19. The time series of $\vec{\tau}_{tot}(t)$ computed from SIS 15 orbital velocities is shown in Figures 7-39 to 7-42 for stations X = 518 m, 347 m, 234 m and 198 m, respectively. The computed critical shear stress (Equation 7-7) using $d_{50} = 0.15$ mm also is plotted. The figures show increasing shear stress as the waves transform across the surf zone, which corresponds to the magnitude of longshore sediment flux. Shear stresses are an order greater than observed in the LSTF, and almost all shear stresses exceed τ_{cr}.
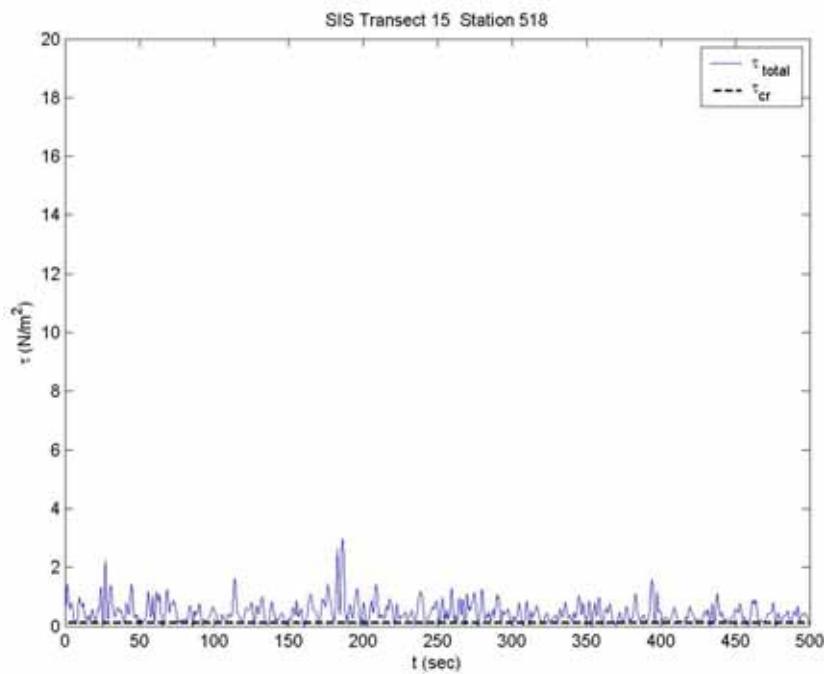
Figure 7-39. Time history of τ_{tot} at Station 518, SIS Transect 15
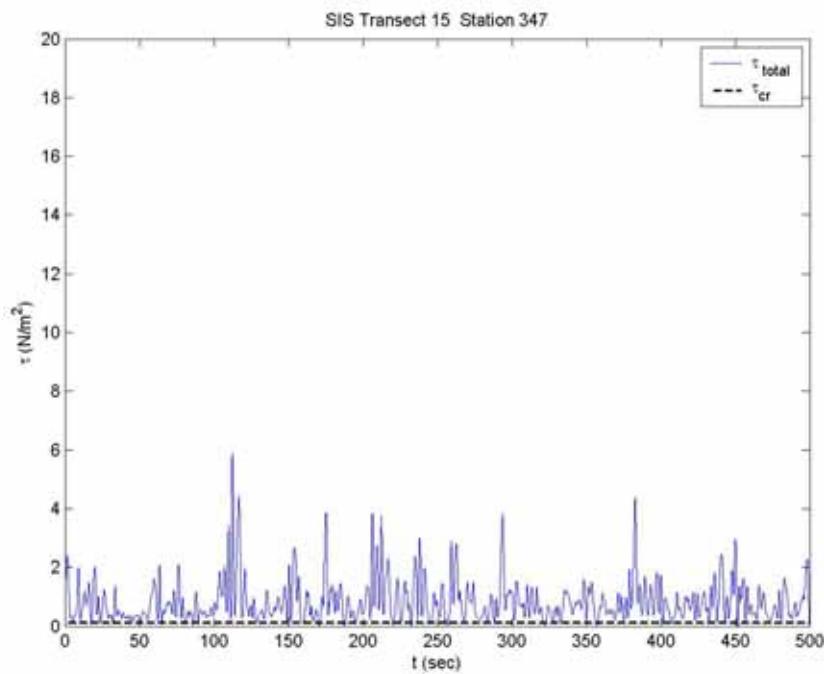
Figure 7-40. Time history of τ_{tot} at Station 347, SIS Transect 15
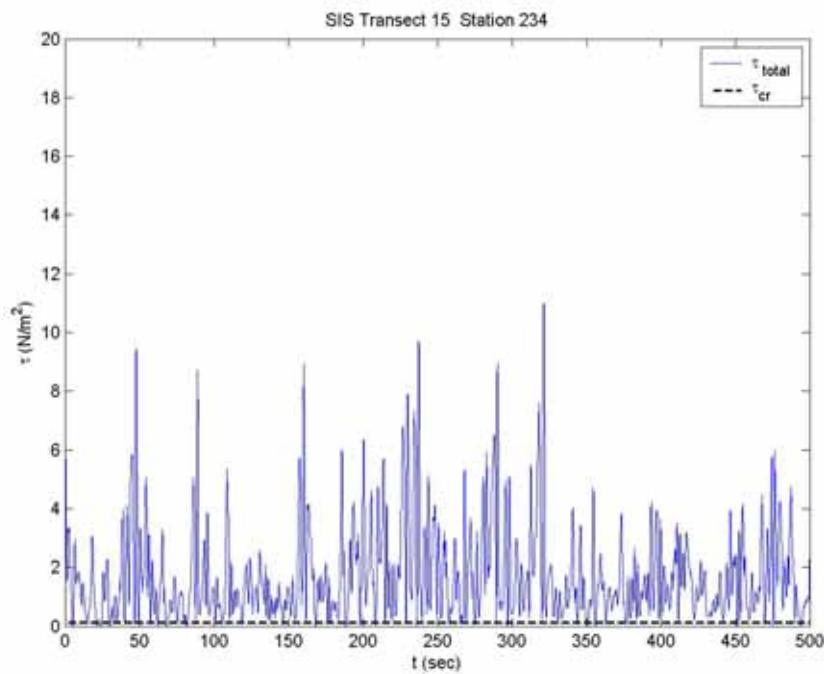
Figure 7-41. Time history of τ_{tot} at Station 234, SIS Transect 15
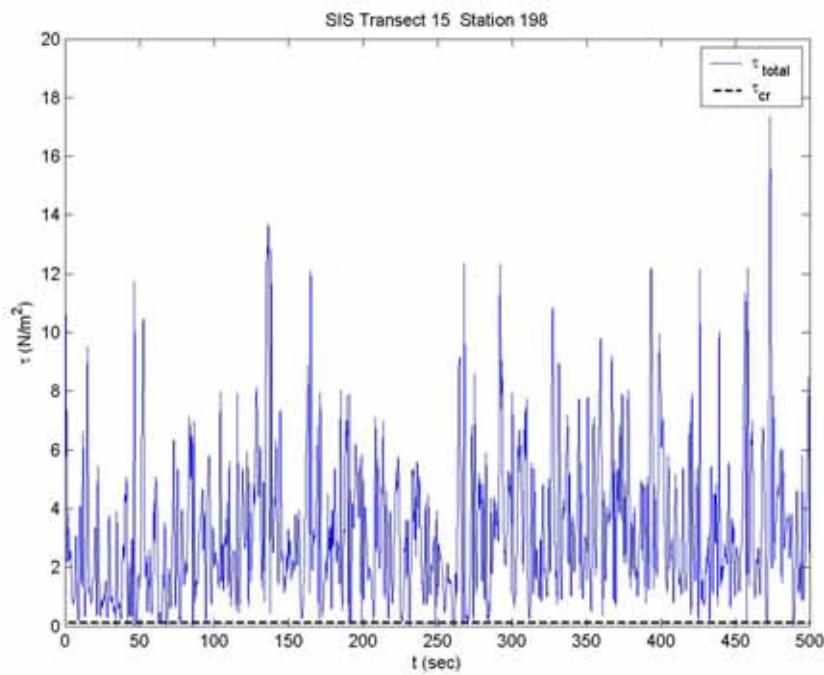
Figure 7-42. Time history of τ_{tot} at Station 198, SIS Transect 15

Model 4

Estimates of SIS 15 longshore transport rates using Model 4 (Equations 7-31

and 7-32) were compared to measurements with coefficient values $k_4 = 1$ and $f_4 = 3.5$

(Figure 7-43). The model estimated both the shape of the distribution and the magnitude

of sediment flux well. Predicted rates were slightly greater in the swash zone. The

model underestimated the peak in measured transport at $X = 320$ m; however, this

measurement is believed to be erroneous.

Model 4 also predicted the SIS 19 measurements well (Figure 7-44). The model

replicated the cross-shore distribution of sediment flux, but slightly overestimated

measurements in the surf zone and underestimated the peak transport at $X = 195$ m.
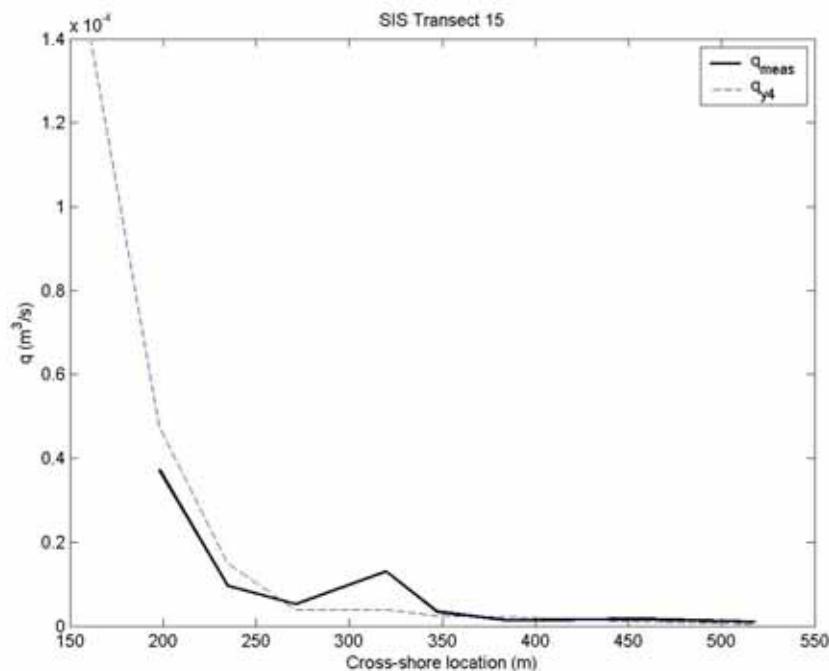
Figure 7-43. Model 4 longshore transport rate estimates compared to SIS 15 measurements
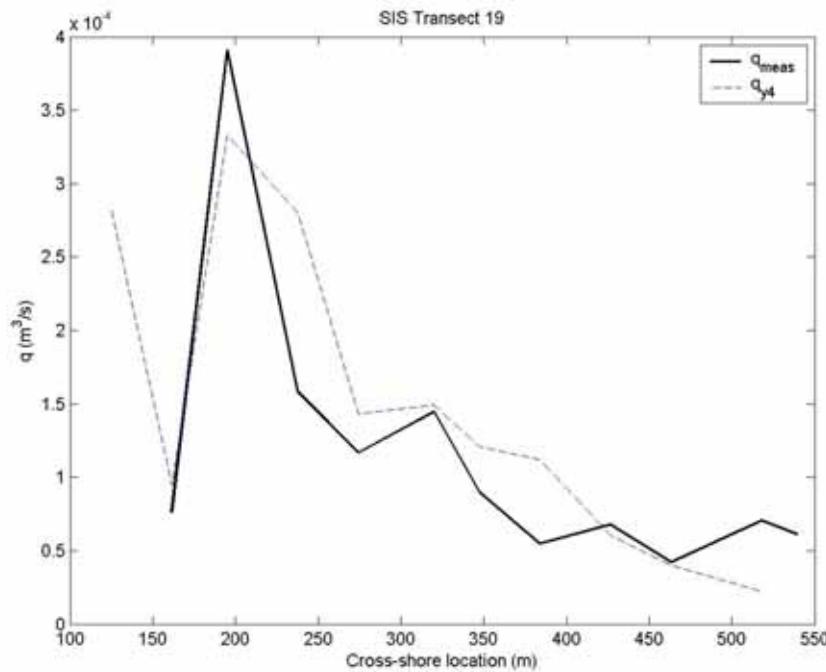
Figure 7-44. Model 4 longshore transport rate estimates compared to SIS 19 measurements

Model 5

Model 5 (Equations 7-33 and 7-34) estimates of SIS 15 data are shown in

Figure 7-45 using coefficient values $f_{b5} = 10$, $f_{s5} = 1.75e-4$, and $k_5 = 2$. Predictions

agreed with the shape of the observed cross-shore distribution; however, the model gave

greater estimates than measurements inshore of Station X = 271 m.

The model predicted sediment flux well for SIS 19 measurements, and estimates

equaled the measured transport peak (Figure 7-46).
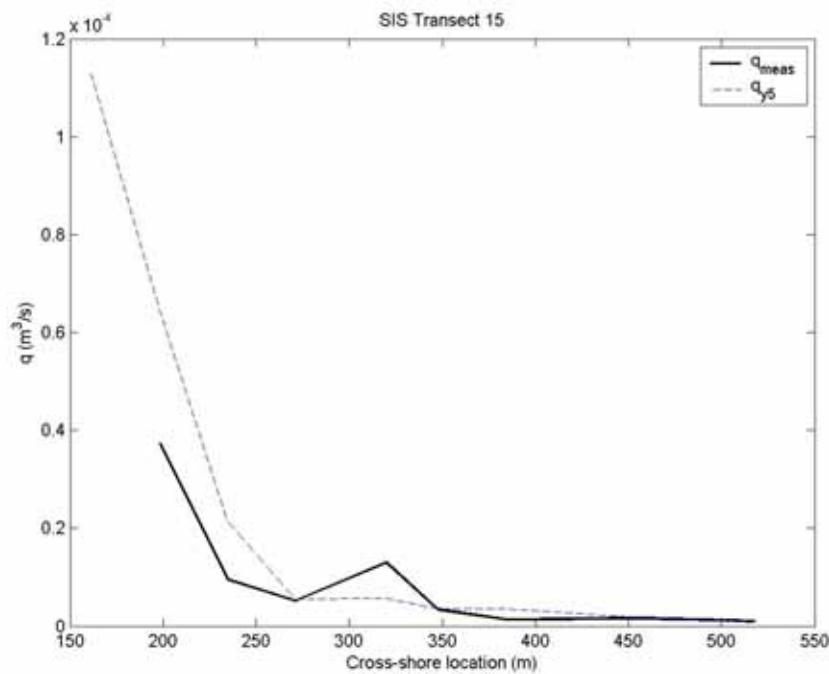
Figure 7-45. Model 5 longshore transport rate estimates compared to SIS 15 measurements
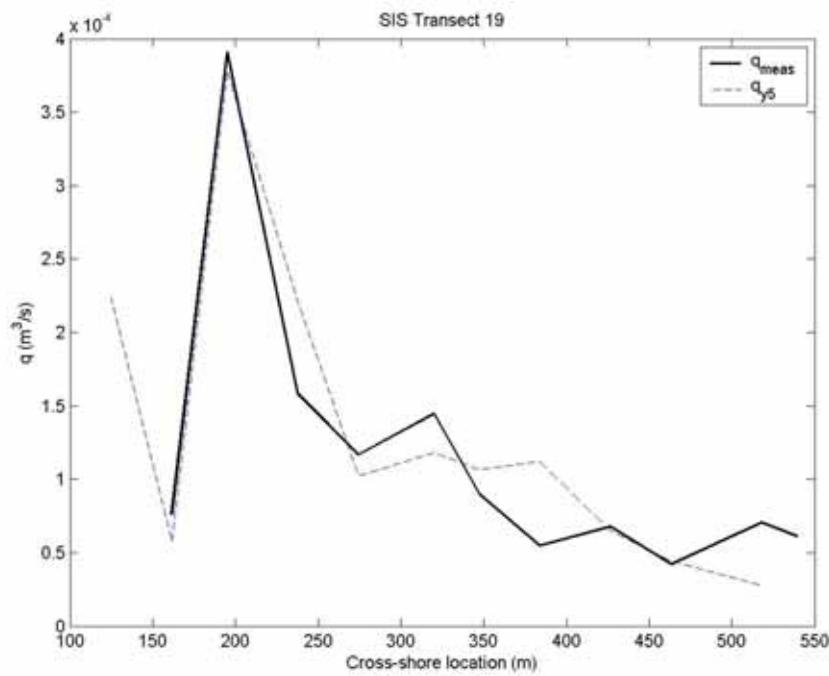
Figure 7-46. Model 5 longshore transport rate estimates compared to SIS 19 measurements

Model 7

Model 7 (Equations 7-38 and 7-40) results with coefficient values $f_7 = 1$, $f_{s7} = 1$, and $k_7 = 0.5$ did not estimate SIS 15 measurements as well as Models 4 and 5 (Figure 7-47). The shape of the estimated distribution corresponded to measurements; however, the model overestimated transport in the inner surf zone of SIS 15 measurements.

Calculation of SIS 19 transport was estimated well at most of the cross-shore locations (Figure 7-48), with exception of the peak in transport near breaking at $X = 195$ m, which was underpredicted.
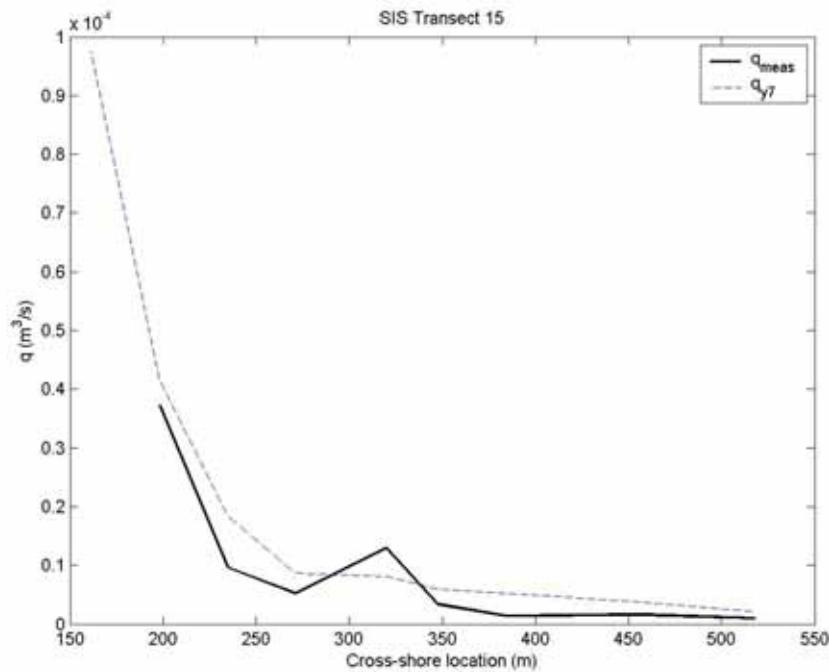

Figure 7-47. Model 7 longshore transport rate estimates compared to SIS 15 measurements
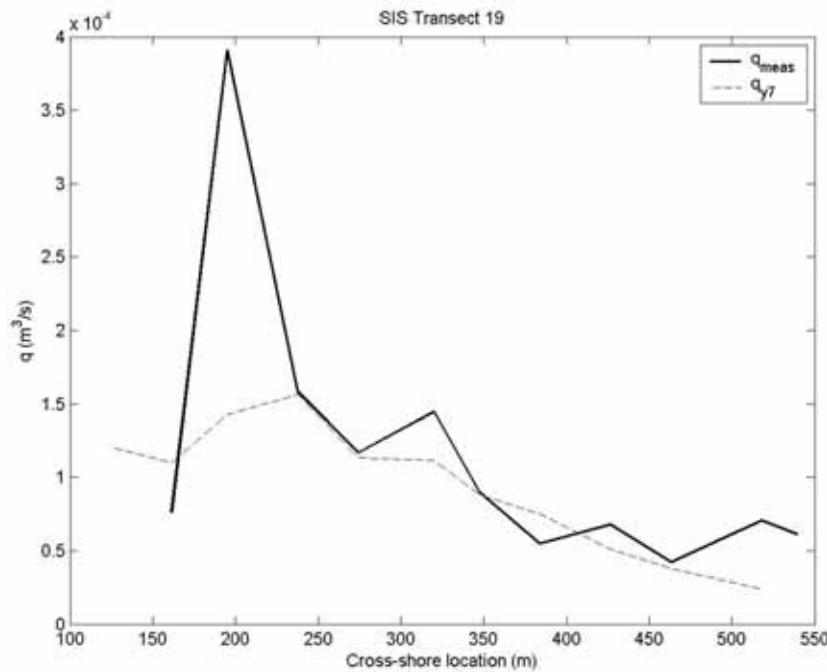
Figure 7-48. Model 7 longshore transport rate estimates compared to SIS 19 measurements

Summary

The predictive models developed and explored in this chapter were based on Equation 7-16, a conceptual model that involves the product of a sediment stirring function and a transporting function. Estimates using the basic form of the equation gave good results except near breaking with plunging waves. A suspension term included in Models 4 through 7 improved predictions near the plunging wave break point. Models 4, 5 and 7 gave the best overall estimate of the LSTF cross-shore distribution of sediment flux, and were compared to SIS field data obtained at the FRF. A summary of model comparisons is described in the following paragraphs.

The distribution of longshore sediment transport for the spilling wave cases increased as waves transformed across the beach, i.e., transport increased closer to shore. Model 4 predictions with Tests 1 and 5 gave a gentler slope to the cross-shore distribution. Test 1 measurements were underpredicted in the inner surf and swash zones, and Test 5 transport rates were overpredicted in the outer surf zone and slightly underpredicted in the inner surf zone. Model 5 estimated Test 1 measurements well, except at the ADV 2 location, where sediment flux was underpredicted. Estimates of Test 5 were slightly overpredicted for most of the surf zone; however, the shape of the distribution was described well with Model 5. Model 7 overestimated transport with the spilling wave cases through most of the surf zone. Models 4, 5, and 7 gave similar estimates for Test 3 conditions. The peak in transport magnitude near breaking compared well with measurements, but estimates shoreward of breaking were overpredicted. Models 4, 5, and 7 underpredicted the peak in transport near breaking associated with Test 6. However, the models estimated transport shoreward of breaking well and predicted the shape of longshore transport distribution well.

Model 4 gave excellent estimates of longshore sediment transport for SIS 15 data, and predicted SIS 19 measurements well. Model 5 gave better results for the SIS 19 transport measurements than Model 4, and predicted the SIS 15 measurements well, but longshore transport in the inner surf zone was overestimated. Model 7 estimated transport well at the majority of cross-shore locations for both SIS cases. However, transport was overpredicted in the inner surf zone of SIS 15 and the peak in transport

near breaking of SIS 19 was underpredicted. Additionally, Model 7 did not replicate the peak in transport near breaking of SIS 19 well.

Models 4, 5, and 7 all compared well to LSTF data, and none of the three produced results significantly better than any other. Models 4 and 5 gave good estimates for the field data of the SIS.

Each model included one or more empirical coefficients, values of which were not optimized for best results for a single test condition, but visually determined to give the best overall performance of the model. One set of coefficients was determined for the LSTF tests, and another set was determined for the SIS measurements for a particular model. The coefficients associated with the LSTF data are 1 to 2 orders of magnitude greater than those related to the SIS data. Critical shear stress is included in the equations, which accounts for sediment mobilization. However, transport under lower wave conditions of physical models is primarily through bedload transport, whereas transport in the field, particularly storm conditions, is dominated by suspended load transport (Komar 1978; Dean 1985; Madsen et al. 2003). There is a scale effect in the suspension process in the LSTF; suspended sediment associated with wave conditions in the LSTF does not properly scale to field measurements. Additional field data with a differing wave climate should be used to properly optimize the coefficients.

Swash zone transport was not addressed with the models because hydrodynamic data were not available from the LSTF or SIS measurements, although the LSTF experiments include swash sediment transport data. However, the models presented are capable of estimating swash zone transport if swash zone hydrodynamics are available for input.

A key finding of the present study is that it is essential to include the turbulent component of the orbital velocity in predictive sediment transport rate equations. The equations include the critical shear stress, and bottom shear stress calculated from mean velocities rarely exceed critical value for sediment motion for low energy conditions or for sediments with a large grain size. Figures 6-18 and 6-19 illustrate that the Watanabe (1992) equation, which is based on mean bottom shear stress, predicts no sediment transport for most of the LSTF cross-shore locations. Also, mean values of the longshore current and cross-shore current do not contain significant information on the wave breaking process, which determines in great part the amount and vertical extent of turbulence produced. Therefore, it is concluded that turbulence modeling must be included in future hydrodynamic simulations aimed at providing forcing information for calculating longshore sediment transport.

CHAPTER VIII

SUMMARY AND CONCLUSIONS

This study was conducted to develop and verify an improved method to determine the cross-shore distribution of longshore sediment transport. Mid-scale laboratory experiments were performed in the LSTF to measure longshore transport rate and nearshore hydrodynamics in a controlled environment. Field measurements from the FRF were included in comparisons of existing longshore transport equations and in the development of new transport models. This chapter summarizes the tests performed and the findings of the research.

Laboratory and Field Measurements

Four irregular wave conditions were generated in the LSTF with the purpose of obtaining longshore sediment transport rates for different breaker types. All wave conditions were generated at a 0.9 m water depth and with an incident wave angle of 10 deg from shore normal. Waves and currents were generally steady and uniform during the tests. Two of the wave conditions produced spilling-type breakers (Tests 1 and 5) and two produced plunging-type breakers (Tests 3 and 6). The wave conditions were grouped by energy level; Tests 1 and 3 had similar incident wave heights and are

referred to as higher energy conditions, and Tests 5 and 6 are referred to as lower energy conditions.

Three distinct zones of longshore sediment flux were observed; the incipient breaking zone, inner surf zone, and swash zone. At incipient breaking, a substantial peak in transport occurred for the plunging wave tests, which was not observed in the spilling wave tests. Kana (1977) and Wang et al. (2002) found that sediment concentration was higher under plunging waves than spilling waves. Turbulence associated with spilling breakers is contained close to the surface in the bore. However, the jet associated with the plunging waves penetrates deep into the water column, impacts the bed, and causes sand to be suspended and transported by the longshore current.

In the inner surf zone, wave energy is saturated, and wave height is strongly controlled by depth, independent of period. Test 1 and Test 3 have similar wave height (energies) and similar sediment flux in the inner surf zone. Wave height and sediment flux for Test 5 and Test 6 are smaller in the inner surf zone than for the higher energy cases. The results imply that sediment flux in the inner surf zone is dominated by wave height and independent of period.

A transport peak was present in the swash zone for all tests, and swash zone transport has a dependence on wave period. Swash zone transport is much greater for the longer period tests. This result is consistent with the Hunt (1959) formula, in which runup is directly proportional to wave period. Swash zone transport accounted for a third of the total transport for the higher energy tests (Tests 1 and 3), and 40 to 60

percent of the total transport of the lower energy tests (Tests 5 and 6). This result agrees with the findings of Elfrink and Baldock (2002) who found that the relative contribution of swash zone transport was greater during calm conditions than during storms. Although swash zone transport measurements are difficult to obtain in the field, the results indicate that the swash zone contribution is significant, and it is necessary to include swash zone transport to obtain accurate measurements of the total longshore sediment transport.

Field data from the Field Research Facility in Duck, NC, were compared to selected available predictive formulas and to new models developed as part of this study. Data from two SIS transects, SIS 15 and 19, were obtained during a northeaster storm on 18 and 19 October 1997. The SIS data are similar to LSTF data in that measurements of wave height, current, and sediment transport are made at several cross-shore locations.

Comparison Between Selected Available Models to the Laboratory and Field Data

Selected models from the literature were compared to measured transport rates from the LSTF and SIS. Comparisons were made with total load equations and with distributed load equations.

Total Load Models

The CERC formula, which is based on energy flux, overestimated both laboratory and field data with the recommended *K*-value of 0.39. When compared to the laboratory

tests, the CERC formula overestimated transport of the spilling breakers by a factor of 8 for Test 1 and nearly 7 for Test 5. Overestimates were greater than a factor of 3 for both plunging wave tests. The CERC formula produced similar estimates for Test 1 and Test 3 because they have similar breaking waves, although measured transport rates were nearly 3 times greater for Test 3 (plunging) than Test 1 (spilling). However, if *K* was calibrated and applied to similar breaker types, the CERC formula gave excellent results.

The models of Bailard (1984) and Ozhan (1982) also overestimated laboratory and field measurements. The Bailard model was developed from field and laboratory data to estimate the CERC coefficient *K* based on sediment fall speed. The Ozhan model, based on laboratory data, used deepwater wave steepness to estimate the *K* coefficient.

The Kamphuis (1991) and Madsen et al. (2003) equations gave more consistent results for the laboratory and field data. In addition to breaker height and angle, the Kamphuis equation includes wave period, beach slope, and sediment grain size. The Kamphuis equation is appealing because it includes wave height, wave period and beach slope; factors that determine the breaker type. The Madsen et al. equation was based on physically realistic, but simple, numerical models of surf zone hydrodynamics and sediment transport processes. The coefficients Madsen et al. gave for the equation are preliminary, but gave acceptable results.

Distributed Load Models

The energetics model of Bodge and Dean (1987) was sensitive to fluctuations in energy dissipation and often predicted peaks in sediment transport that were not present in the data. The original form of the equation, which included a slope term, was compared to the LSTF data. The equation estimated the longshore transport trend well for the spilling breaker tests, but underpredicted measurements of the plunging breaker tests. Because of the slope term, no transport is estimated if the water depth increases shoreward. Therefore, no transport was predicted in the trough of the breakpoint bar formed by the plunging waves of Test 3. Bodge (1989) later suggested the slope term be omitted from the equation. When compared to measurements, the suggested form of the Bodge and Dean model overpredicted both the laboratory and field transport rates. The model gave better estimates if the recommended value of the coefficient k_q was reduced from 0.057 to 0.01 for the LSTF data and from 0.48 to 0.04 for the SIS data.

The Watanabe (1992) equation is based on time-averaged bottom stress. The averaged bottom stress of the laboratory waves exceeded the critical shear stress at only one cross-shore location for Test 1 and Test 3, and it did not exceed critical shear stress at any location for Test 5 and Test 6. As a result no transport was predicted for the majority of the cross-shore locations. Time-averaged bottom stresses are not adequate for a model that includes critical shear stress or critical velocity for inception of sediment motion. The Watanabe equation estimated the SIS transport rates well if the empirical coefficient was reduced from 2.0 to 0.25; however, it did not predict the peak in transport near breaking with transect SIS 19.

The Van Rijn (1993) model is comprehensive and requires hydrodynamic data and information on the bedforms and grain sizes at each cross-shore location. The model estimated the LSTF distributed transport rates well, but overestimated the SIS transport rates by a factor of 50.

New Longshore Transport Models

New models were developed based on the principle that transported sediment is first mobilized by the total shear stress acting on the bottom and transported by the current at that location. The shear stress, including the turbulent component and the mean value, were calculated from the wave orbital velocity measured with the LSTF ADVs and SIS EMCMs.

Seven models were developed, and all were based on the power law expression. The Watanabe (1987) form was adopted as the basis of all the models. Each model was first compared to LSTF data. Models 1 through 3 gave good results, but underpredicted the peak in transport near the breakpoint of the plunging wave cases. It was observed during the LSTF tests that sediment in the trough of the breakpoint bar stayed in suspension over the duration of the entire tests. Therefore, a suspension term was included in Models 4 through 7, which improved estimates near the plunging wave break point.

Models 4, 5 and 7 gave the best overall estimates of the distribution of longshore sediment transport and were compared to SIS data obtained at the FRF. Model 4 gave excellent estimates of sediment flux for SIS 15 data and predicted SIS 19 measurements

well. Model 5 predicted SIS 19 transport rates very well, but SIS 15 transport rates were overestimated transport the inner surf zone. Model 7 overestimated transport in the inner surf zone of SIS 15 measurements. Model 7 predicted transport at most of the SIS 19 cross-shore locations well, but it did not replicate the peak in transport near breaking.

Each model included at least one empirical coefficient that was visually determined to give the best overall performance of the model. One set of coefficients was described for the LSTF tests and one for the SIS measurements for a particular model. The laboratory coefficients were 1 to 2 orders of magnitude greater than the field coefficients. The difference was attributed to a scale effect in the suspension process in the LSTF. Transport under lower wave conditions associated with physical models is primarily through bedload transport, whereas transport under higher wave conditions found in the field is dominated by suspended load transport. It was determined that the model coefficients should be optimized with additional field data.

A key finding of this research is that it is essential to include the turbulent component of the orbital velocity in predictive sediment transport equations. Mean velocities rarely exceed the critical value for incipient sediment motion for low energy conditions or for sediments with a large grain size. Additionally, breaker type was found to be an important variable in the amount of sediment transport that occurs at a location. Plunging breakers produce greater turbulence throughout the water column whereas turbulence associated with spilling breakers remains near the surface in the bore. Mean

values of the longshore and cross-shore current do not provide information on the wave

breaking process, which determines the amount of turbulence produced.

REFERENCES

Ahrens, J.P., and Titus, M.F. 1985. Wave runup formulas for smooth slopes, Journal of Waterway, Port, Coastal & Ocean Engineering, ASCE, 111, 998-1019.

Bagnold, R.A., 1963. Beach and nearshore processes Part I: Mechanisms of marine sedimentation, in The Sea: Ideas and Observations, 3, M. N. Hill (ed.), Interscience, New York, 507-528.

Bailard, J.A., 1984. A simplified model for longshore sediment transport, Proceedings of the 19th International Conference on Coastal Engineering, ASCE, 1454-1470.

Bailard, J.A., and Inman, D.L., 1981. An energetics bedload model for a plane sloping beach: local transport, Journal of Geophysical Research, 86, 2035-2043.

Battjes, J.A., 1974. Surf similarity, Proceedings of the 14th International Conference on Coastal Engineering, ASCE, 466-480.

Battjes, J.A., and Janssen, J.P.F.M., 1978. Energy loss and setup due to breaking of random waves, Proceedings of the 16th International Conference on Coastal Engineering, ASCE, 569-587.

Bijker, E.W., 1967. Some considerations about scales for coastal models with movable bed, Delft Hydraulics Laboratory, Publication 50, Delft, The Netherlands.

Bodge, K.R., 1989. A literature review of the distribution of longshore sediment transport across the surf zone, Journal of Coastal Research, 5(2), 307-328.

Bodge, K.R. and Dean, R.G., 1987. Short-term impoundment of longshore transport, Proceedings of Coastal Sediments '87, 468-483.

Bouws, E., Gunther, H., Rosenthal, W., and Vincent, C.L., 1985. Similarity of the wind wave spectrum in finite depth water. 1. Spectral form, Journal of Geophysical Research, 90(C1), 975–986.

Brown, C.B., 1950. Sediment transportation, in Engineering Hydraulics, H. Rouse (ed.), Wiley, New York, 1039p.

Bruno, R.O., Dean, R.G., and Gable, C.G., 1980. Longshore transport evaluations at a detached breakwater, Proceedings of the 17th International Conference on Coastal Engineering, ASCE, 1203-1222.

Bruno, R.O, and Gable, C.G., 1976. Longshore transport at a total littoral barrier, Proceedings of the 15th International Conference on Coastal Engineering, ASCE, 1453-1475.

Bruun, P., 1954. Coast erosion and the development of beach profiles. Technical Memorandum No. 44, Beach Erosion Board, Washington, D.C.

Caldwell, J., 1956. Wave action and sand movement near Anaheim Bay, California, U.S. Army Corps of Engineers, Beach Erosion Board, Tech. Mem. No. 68, Washington D.C.

Coastal Engineering Manual, 2002. Engineer Manual 1110-2-1100, U.S. Army Corps of Engineers, Washington D.C.

Dally, W.R., Dean, R.G., and Dalrymple, R.A., 1984. A model for breaker decay on beaches, Proceedings of the 19th International Conference on Coastal Engineering, ASCE, 82-98.

Dean, R.G., 1977. Equilibrium beach profiles: U.S. Atlantic and Gulf coasts. Ocean Engineering Report No. 12, Department of Civil Engineering, University of Delaware, Newark, DE.

Dean, R.G., 1985. Physical modeling of littoral process, in Physical Modelling in Coastal Engineering, R. A. Dalrymple (ed.), A. A. Balkema, Rotterdam, The Netherlands, 119-139.

Dean, R.G., 1989. Measuring longshore sediment transport with traps, in Nearshore Sediment Transport, R.J. Seymour (ed.), Plenum Press, New York, pp. 313-337.

Dean, R.G., Berek, E.P, Gable, C.G., and Seymour, R.J., 1982. Longshore transport determined by an efficient trap, Proceedings of the 18th International Conference on Coastal Engineering, ASCE, 954-968.

Dean, R.G. and Dalrymple, R.A., 1991. Water Wave Mechanics for Engineers and Scientists, World Scientific, Singapore, 353p.

del Valle, R., Medina, R., and Losada, M.A. 1993. Dependence of coefficient *K* on grain size, Technical Note No. 3062, Journal of Waterway, Port, Coastal, and Ocean Engineering, 119 (5) 568-574.

Downing, J.P., Sternberg, R.W., and Lister, C.R.B. 1981. New instrumentation for investigation for sediment suspension in the shallow marine environment, Marine Geology, 42, 19-34.

Einstein, H.A., 1950. The bed load function for sediment transportation in open channel flow, Technical Bulletin No. 1026, U.S. Department of Agriculture, Washington, D.C.

Einstein, H.A., 1972. A basic description of sediment transport on beaches, in Waves on Beaches, R.E. Meyer (ed.), Academic Press, New York, 29-34.

Elfrink, B. and Baldock, T., 2002. Hydrodynamics and sediment transport in the swash zone: a review and perspectives, Coastal Engineering, 45, 149-167.

Fowler, J.E., Rosati, J.D., Hamilton, D.G., and Smith, J.M., 1995. Development of a large-scale laboratory facility for longshore sediment transport research. The CERCular, CERC-95-2, U.S. Army Engineer Waterways Experiment Station, Vicksburg, MS.

Frijlink, H.C., 1952. Discussion des formules de debit solide de Kalinske, Einstein de Meyer-Peter et Mueller copte tenue des mesures recentes de transport dans les rivieres Neerlandaises, 2me Journal Hydraulique Societe Hydraulique de France, Grenoble, 98-103.

Galvin, C.J., 1968. Breaker type classifications of three laboratory beaches, Journal of Geophysical Research, 73, 3651-3659.

Garcez Faria, A.F., Thornton, E.B., Stanton, T.P., Soares, C.V., and Lippmann, T.C., 1998. Vertical profiles of longshore currents and related bed shear stress and bottom roughness, Journal of Geophysical Research, 103, C2, 3217-3232.

Hallermeier, R. J., 1981. Terminal settling velocity of commonly occurring sand grains, Sedimentology, 28, 859-865.

Hamilton, D.G., and Ebersole, B.A., 2001. Establishing uniform longshore currents in a large-scale laboratory facility, Coastal Engineering, 42, 199-218.

Hamilton, D.G., Ebersole, B.A., Smith, E.R., and Wang, P., 2001. Development of a large-scale laboratory facility for sediment transport study. Technical Report ERDC/CHL TR-01-22, U.S. Army Engineer Waterways Experiment Station, Vicksburg, MS.

Hughes, S.A., 2004. Estimation of wave runup on smooth, impermeable slopes using the wave momentum flux parameter. Coastal Engineering, 51, 1085-1104.

Hunt, I. A., 1959. Design of seawalls and breakwaters, Journal of the Waterways and Harbors Division, ASCE, 85(WW3), 123-152.

Inman, D.L., and Bagnold, R.A., 1963. Beach and nearshore processes Part II: Littoral processes, in The Sea: Ideas and Observations, 3, M.N. Hill (ed.), Interscience, New York, 529-553.

Inman, D.L., Zampol, J.A., White, T.E., Hanes, B.W., Waldorf, B.W., and Kastens, K.A., 1980. Field measurements of sand motion in the surf zone. Proceedings of the 17th International Conference on Coastal Engineering, ASCE, 1215-1234.

Johnson, B.D., 2003. Model for the computation of time-steady nearshore currents, ERDC/CHL CHETN-VI-39, U. S. Army Engineer Research and Development Center, Vicksburg, MS.

Johnson, B.D., and Smith, J.M., 2005. Longshore current forcing by irregular waves, Journal of Geophysical Research, 110, C06006, doi:10.1029/2004JC002336.

Johnson, J.W., 1952. Sand transport by littoral currents, Institute of Engineering Research, Wave Research Laboratory, University of California at Berkeley, T.R. Series 3, Issue 338.

Jonsson, I.G., 1966. Wave boundary layers and friction factors, Proceedings of the 10th International Conference on Coastal Engineering, ASCE, 127-148.

Kamphuis, J.W., 1991. Alongshore sediment transport rate. Journal of Waterways, Port, Coastal and Ocean Engineering, ASCE, 117(6), 624-641.

Kamphuis, J.W., 2002. Alongshore transport of sand, Proceedings of the 28th International Conference on Coastal Engineering, ASCE, 2478-2490.

Kamphuis, J.W. Davies, M.H. Nairn, R.B., and Sayao, O.J., 1986. Calculation of littoral sand transport rate, Coastal Engineering, 10, 1-21.

Kamphuis, J.W. and Readshaw, J.S., 1978. A model study of alongshore sediment transport rate, Proceedings of the International Conference on Coastal Engineering, ASCE press, 1656-1674.

Kana, T.W., 1976. A new apparatus for collecting simultaneous water samples in the surf zone, Journal of Sedimentology Petrology, 46, 1031-1034.

Kana, T.K., 1977. Suspended sediment transport at Price Inlet, S.C., Proceedings of Coastal Sediments '77, 366-382.

Komar, P.D., 1971. The mechanics of sand transport on beaches, Journal Geophysical Research, 76(3), 713-721.

Komar, P.D., 1975. Longshore currents and sand transport on beaches, Proceedings, Civil Engineering in the Oceans/III, ASCE, 1, 333-354.

Komar, P.D., 1977. Beach sand transport: distribution and total drift, Journal Waterway, Port, Coastal and Ocean Engineering, ASCE, 103(WW2), 225-239.

Komar, P.D., 1978. Relative quantities of suspension versus bed-load transport on beaches, Journal of Sedimentary Petrology, 48 (3) 921-932.

Komar, P.D., 1988. Environmental controls on littoral sand transport, Proceedings of the 21st International Conference on Coastal Engineering, ASCE, 1238-1252.

Komar, P.D., 1998. Beach Processes and Sedimentation. Prentice-Hall, Upper Saddle River, NJ, 544p.

Komar, P.D. and Inman, D.L., 1970. Longshore sand transport on beaches, Journal of Geophysical Research, 75(30), 5514-5527.

Kraus, N.C., 1987. Application of portable traps for obtaining point measurements of sediment transport rates in the surf zone, Journal of Coastal Research, 3(2), 139-152.

Kraus, N.C., and Dean, J.L., 1987. Distributions of the longshore sediment transport rate measured by trap, Proceedings of Coastal Sediments '87, ASCE, 881-896.

Kraus, N.C.; Gingerich, K.J., And Rosati, J.D., 1988. Toward an improved empirical formula for longshore sand transport, Proceedings of the 21st International Conference on Coastal Engineering, ASCE, 1183-1196.

Kraus, N.C. and Horikawa, K., 1990. Nearshore sediment transport. in The Sea: Ocean Engineering Science, Part B, B. LeMehaute and D.M. Hanes (eds.), John Wiley and Sons, New York, 775-813.

Kraus, N.C., Isobe, M., Igarashi, H., Sasaki, T.O., and Horikawa, K., 1982. Field experiments on longshore transport in the surf zone, Proceedings of the 18th International Conference on Coastal Engineering, ASCE, 969-988.

Kraus, N.C. and Larson, M., 1991. NMLONG: Numerical model for simulating the longshore current – Report 1: model development and tests. Technical Report DRP-91-1, U.S. Army Engineer Waterways Experiment Station, Vicksburg, MS.

Kraus, N. C., Lohrmann, R. A., and Cabrera, R., 1994. New acoustic meter for measuring 3D laboratory flows, Journal of Hydraulic Engineering, 120(3), 406–412.

Krumbein, W.C., 1944. Shore currents and sand movement on a model beach, U.S. Army Corps of Engineers, Beach Erosion Board, Technical Memorandum No. 7, Washington D.C.

Madsen, O.S., 1978. An analytical model of longshore sediment transport, Proceedings, workshop on coastal sediment transport; January, 1977, Department of Civil Engineering and Sea Grant College Program, University of Delaware, Newark, DE.

Madsen, O.S., 1991. Mechanics of cohesionless sediment transport in coastal waters, Proceedings of Coastal Sediments '91, 15-27.

Madsen, O.S., and Grant, W.D., 1976. Quantitative description of sediment transport by waves, Proceedings of 15th International Conference on Coastal Engineering, ASCE, 1093-1112.

Madsen, O.S., Tajima, Y, and Ebersole, B.A., 2003. Longshore sediment transport: a realistic order-of-magnitude estimate, Proceedings of Coastal Sediments '03, CD-ROM, World Scientific Corporation and East Meets West Productions, Corpus Christi, TX, ISBN 981-238-422-7.

McCowan, J., 1891. On the solitary wave, Philosophical Magazine, 5th Series, 32 (194), 45-58.

Meyer-Peter, E. and Muller, R., 1948. Formulas for bed-load transport, Proceedings of the 2nd Meeting of the International Association for Hydraulic Structures, IAHR, 39-64.

Miller, H.C., 1998. Comparison of storm longshore transport rates to predictions, Proceedings of the 26th International Conference on Coastal Engineering, ASCE, 2954-2967.

Miller, H.C., 1999. Field measurements of longshore sediment transport during storms, Coastal Engineering, 36, 301-321.

Nordstrom, K.F., 1992. Estuarine Beaches. Elsevier Applied Science, London, 225 pp.

Ozhan, E., 1982. Laboratory study of breaker type effect on longshore sand transport, in Proceedings, Euromech 156: Mechanics of Sediment Transport; July, 1982, B.M. Sumer and A. Muler, (ed.), A. A. Balkema, Rotterdam, The Netherlands.

Patrick, D.A. and Wiegel, R.L., 1957. Amphibian tractors in the surf. Proceedings of the First Conference on Ships and Waves, The Engineering Foundation Council on Wave Research and the American Society of Naval Architects and Marine Engineers, 397-422.

Puleo, J.A., Holland, K.T., Kooney, T.N., and Sallenger, Jr., A.H., 2000. Field observations of swash zone flow patterns and 3D morphodynamics, Proceedings of the 27th International Conference on Coastal Engineering, ASCE, 637-650.

Putrevu, U. and Svendsen, I. A., 1999. Three-dimensional dispersion of momentum in wave-induced nearshore currents. European Journal of Mechanics B/Fluids, 83-101.

Rattanapitikon, W. and Shibayama, T., 2000. Verification and modification of breaker height formulas, Coastal Engineering Journal, 42 (4), 389-406.

Sauvage de Saint Marc, G., and Vincent, G., 1954. Transport littoral formation de fleches et de tombolos, Proceedings of the 5th International Conference on Coastal Engineering, ASCE, 296-328.

Savage, R.P., 1962. Laboratory determination of littoral transport rates, Journal of Waterway, Port, Coastal and Ocean Engineering, ASCE, 88, No. WW2, 69-92.

Saville, T., 1950. Model study of sand transport along an infinitely long, straight beach, Trans., American Geophysical Union, 31 (4), 555-565.

Sawaragi, T. and Deguchi I., 1978. Distribution of sand transport rate across the surf zone, Proceedings of the 16th International Conference on Coastal Engineering, ASCE, 1596-1613.

Schoonees, J.S. and Theron, A.K., 1993. Review of the field data base for longshore sediment transport, Coastal Engineering, 19, 1-25.

Schoonees, J.S. and Theron, A.K., 1996. Improvement of the most accurate longshore transport formula, Proceedings of the 25th International Conference on Coastal Engineering, ASCE, 3652-3665.

Shay, E.A., and Johnson, J.W., 1951. Model studies on the movement of sand transported by wave action along a straight beach, Issue 7, Series 14, Inst. Of Engineering Research, Univ. of California, Berkeley, CA.

Shore Protection Manual, 1984. 4th ed., 2 Vol, U.S. Army Waterways Experiment Station, U.S. Government Printing Office, Washington, D.C.

Smith, E.R. and Kraus, N.C., 1991. Laboratory study of wave-breaking over bars and artificial reefs, Journal of Waterway, Port, Coastal and Ocean Engineering, ASCE, 117, 307-325.

Smith, E.R. and Wang, P., 2001. Longshore sediment transport as a function of energy dissipation, Waves 2001, ASCE, 1218-1227.

Smith, E.R., Wang, P., and Zhang, J., 2003. Evaluation of the CERC formula using large-scale model data, Proceedings of Coastal Sediments '03, CD-ROM, World Scientific Corporation and East Meets West Productions, Corpus Christi, TX, ISBN 981-238-422-7.

Stauble, D.K., 1992, Long-term profile and sediment morphodynamics: Field Research Facility case history, US Army Corps of Engineers, Coastal & Hydraulics Laboratory, TR-CERC-92-7, Vicksburg, MS.

Tajima, Y. and Madsen, O.S., 2005. Waves, currents, and sediment transport in the surf zone along long, straight beaches, Contract Report ERDC/CHL CR-05-1, Coastal and Hydraulics Laboratory, U.S Army Engineering and Research Development Center, Vicksburg, MS.

USACE, 1966. Shore Protection, Planning and Design, Tech Rep. 4 (3rd ed.), Coastal Engineering Research Center, U.S. Army Engineer Waterways Experiment Station, Vicksburg, MS.

Van Rijn, L.C., 1993. Principles of Sediment Transport in Rivers, Estuaries and Coastal Seas. Aqua Publications, Amsterdam, The Netherlands.

Van Wellen, E., Baldock, T., Chadwick, A., and Simmonds, D., 2000. STRAND – a model for longshore sediment transport in the swash zone, Proceedings of the 27th International Conference on Coastal Engineering, ASCE, 3139-3150.

Visser, P.J., 1991. Laboratory measurements of uniform longshore currents. Coastal Engineering, 15, 563-593.

Walton, T. L., 1979. Littoral sand transport on beaches, PhD. Dissertation, University of Florida, Gainesville, FL.

Walton, T. L., and Chiu, T., 1979. A review of analytical techniques to solve the sand transport equation and some simplified solutions, Proceedings of Coastal Structures '79, ASCE, 809-837.

Wang, P., 1998. Longshore sediment flux in the water column and across the surf zone. Journal of Waterway, Port, Coastal & Ocean Engineering, ASCE, 124, 108-117.

Wang, P. and Kraus, N.C., 1999. Longshore sediment transport rate measured by short-term impoundment. Journal of Waterway, Port, Coastal and Ocean Engineering, ASCE, 125, 118-126.

Wang, P., Kraus, N.C., and Davis, R.A., Jr., 1998. Total rate of longshore sediment transport in the surf zone: field measurements and empirical predictions. Journal of Coastal Research, 14(1), 269-283.

Wang, P., Smith, E.R., and Ebersole, B.A., 2002. Large-scale laboratory measurements of longshore sediment transport under spilling and plunging breakers, Journal of Coastal Research, 18, 118-135.

Watanabe, A., 1987. Three-dimensional numerical model for beach evolution, Proceedings of Coastal Sediments '87, ASCE, 802-818.

Watanabe, A., 1992. Total rate and distribution of longshore sand transport, Proceedings of the 23rd International Coastal Engineering Conference, ASCE, 2528-2541.

Watts, G.M., 1953. A study of sand movement at South Lake Worth Inlet, Florida, U.S. Army Corps of Engineers, Beach Erosion Board, Tech Mem. No. 42, Washington D.C.

Weggel, J.R., 1972. Maximum breaker height, Journal of the Waterways, Harbors and Coastal Engineering Division, ASCE, 98, WW4, 529-548.

REPORT DOCUMENTATION PAGE			*Form Approved* *OMB No. 0704-0188*

Public reporting burden for this collection of information is estimated to average 1 hour per response, including the time for reviewing instructions, searching existing data sources, gathering and maintaining the data needed, and completing and reviewing this collection of information. Send comments regarding this burden estimate or any other aspect of this collection of information, including suggestions for reducing this burden to Department of Defense, Washington Headquarters Services, Directorate for Information Operations and Reports (0704-0188), 1215 Jefferson Davis Highway, Suite 1204, Arlington, VA 22202-4302. Respondents should be aware that notwithstanding any other provision of law, no person shall be subject to any penalty for failing to comply with a collection of information if it does not display a currently valid OMB control number. **PLEASE DO NOT RETURN YOUR FORM TO THE ABOVE ADDRESS.**

1. REPORT DATE *(DD-MM-YYYY)* September 2006	2. REPORT TYPE Final report	3. DATES COVERED *(From - To)*

4. TITLE AND SUBTITLE Longshore Sediment Transport Rate Calculated Incorporating Wave Orbital Velocity Fluctuations	5a. CONTRACT NUMBER
	5b. GRANT NUMBER
	5c. PROGRAM ELEMENT NUMBER
6. AUTHOR(S) Ernest R. Smith	5d. PROJECT NUMBER
	5e. TASK NUMBER
	5f. WORK UNIT NUMBER

7. PERFORMING ORGANIZATION NAME(S) AND ADDRESS(ES) Coastal and Hydraulics Laboratory U.S. Army Engineer Research and Development Center 3909 Halls Ferry Road Vicksburg, MS 39180-6199	8. PERFORMING ORGANIZATION REPORT NUMBER ERDC/CHL TR-06-18

9. SPONSORING / MONITORING AGENCY NAME(S) AND ADDRESS(ES) U.S. Army Corps of Engineers Washington, DC 20314-1000	10. SPONSOR/MONITOR'S ACRONYM(S)
	11. SPONSOR/MONITOR'S REPORT NUMBER(S)

12. DISTRIBUTION / AVAILABILITY STATEMENT

Approved for public release; distribution is unlimited.

13. SUPPLEMENTARY NOTES

14. ABSTRACT

Laboratory experiments were performed to study and improve longshore sediment transport rate predictions. Measured total longshore transport in the laboratory was approximately three times greater for plunging breakers than spilling breakers. Three distinct zones of longshore transport were observed across the surf zone: incipient breaker zone, inner surf zone, and swash zone. Transport at incipient breaking was influenced by breaker type; inner surf zone transport was dominated by wave height, independent of wave period; and swash zone transport was dependent on wave period.

Selected predictive formulas to compute total load and distributed load transport were compared to laboratory and field data. Equations by Kamphuis (1991) and Madsen et al. (2003) gave consistent total sediment transport estimates for both laboratory and field data. Additionally, the CERC formula predicted measurements well if calibrated and applied to similar breaker types. Each of the distributed load models had shortcomings. The energetics model of Bodge and Dean (1987) was sensitive to fluctuations in energy dissipation and often predicted transport peaks that were not present in the data. The Watanabe (1992) equation, based on time-averaged bottom stress, predicted no transport at most laboratory locations. The Van Rijn (1993) model was comprehensive and required hydrodynamic, bedform, and sediment data. The model estimated the laboratory cross-shore distribution well, but greatly overestimated field transport. (Continued)

15. SUBJECT TERMS CERC Formula Large-Scale Sediment Transport Facility	Longshore Currents Longshore Sediment Transport Physical Modeling	Surf Zone Processes Wave Breaking

16. SECURITY CLASSIFICATION OF:			17. LIMITATION OF ABSTRACT	18. NUMBER OF PAGES	19a. NAME OF RESPONSIBLE PERSON Ernest R. Smith
a. REPORT UNCLASSIFIED	b. ABSTRACT UNCLASSIFIED	c. THIS PAGE UNCLASSIFIED		232	19b. TELEPHONE NUMBER *(include area code)* (601) 634-4030

14. (Concluded)

Seven models were developed in this study based on the principle that transported sediment is mobilized by the total shear stress acting on the bottom and transported by the current at that location. Shear stress, including the turbulent component, was calculated from the wave orbital velocity. Models 1 through 3 gave good estimates of the transport distribution, but underpredicted the transport peak near the plunging wave breakpoint. A suspension term was included in Models 4 through 7, which improved estimates near breaking for plunging breakers. Models 4, 5, and 7 also compared well to the field measurements.

It was concluded that breaker type is an important variable in determining the amount of transport that occurs at a location. Lastly, inclusion of the turbulent component of the orbital velocity is vital in predictive sediment transport equations.